Analysis of
the mitochondrial unfolded protein response
in *Caenorhabditis elegans*

DISSERTATION ZUR ERLANGUNG DES DOKTORGRADES DER NATURWISSENSCHAFTEN
DOCTOR RERUM NATURALIUM (DR. RER. NAT.) AN DER FAKULTÄT FÜR BIOLOGIE DER
LUDWIG-MAXIMILIANS-UNIVERSITÄT MÜNCHEN

Vorgelegt von
Fabian Thomas Köhler
München, 09. Juli 2020

1. Gutachter: Prof. Dr. Barbara Conradt

2. Gutachter: Prof. Dr. Christof Osman

Tag der Abgabe: 09.07.2020

Tag der mündlichen Prüfung: 19.11.2020

Eidesstattliche Versicherung

Ich versichere hiermit an Eides statt, dass die vorgelegte Dissertation von mir selbständig und ohne unerlaubte Hilfe angefertigt ist.

Fabian Köhler (München, den 09.07.2020)

Erklärung

Hiermit erkläre ich, dass die Dissertation nicht ganz oder in wesentlichen Teilen einer anderen Prüfungskommission vorgelegt worden ist. Ich habe mich nicht anderweitig einer Doktorprüfung ohne Erfolg unterzogen.

Fabian Köhler (München, den 09.07.2020)

Contents

Abbreviations

ΔΨm	mitochondrial membrane potential
ABC	ATP-binding cassette
ADP	adenosine diphosphate
Akt	protein kinase B
AMP	adenosine monophosphate
AMPK	AMP-activated protein kinase
ATG	autophagy-related
ATP	adenosine triphosphate
BH3	Bcl-2 homology 3
bZIP	basic leucine zipper
CCCP	carbonyl cyanide *m*-chlorophenylhydrazone
CoA	coenzyme A
COX	cytochrome *c* oxidase
DNA	deoxyribonucleic acid
E. coli	*Escherichia coli*
ER	endoplasmic reticulum
ESCRT	endosomal sorting complex required for transport
FAO	fatty acid β-oxidation
gf	gain-of-function
GO	gene ontology
GTPase	guanosine triphosphatase
IIS	insulin/IGF-1-like signaling
ILV	intralumenal vesicle
IMS	intermembrane space
ISR	integrated stress response
KFERQ	lysine-phenylalanine-glutamate-arginine-glutamine
lf	loss-of-function
LIR	LC3-interacting region
mm	millimeter
MRC	mitochondrial respiratory chain
mRNA	messenger RNA
mtDNA	mitochondrial DNA

MTS	mitochondrial targeting sequence
MVB	multivesicular body
NLS	nuclear localization signal
OXPHOS	oxidative phosphorylation
PE	phosphatidylethanolamine
PI3K	phosphoinositide 3-kinase
RNA	ribonucleic acid
RNAi	RNA interference
ROS	reactive oxygen species
rRNA	ribosomal RNA
SUMO	small ubiquitin-like modifier
TCA	tricarboxylic acid
TG	triacylglycerol
TIM	translocase of the inner membrane
TOM	translocase of the outer membrane
µm	micrometer
uORF	upstream open reading frame
UPR^{mt}	mitochondrial unfolded protein response
UPS	ubiquitin-proteasome system

List of Publications

Köhler, F.*, Müller-Rischart, A.K.*, Conradt, B., and Rolland, S.G. (2015). The loss of *LRPPRC* function induces the mitochondrial unfolded protein response. Aging *7*, 701-712. https://doi.org/10.18632/aging.100812

Haeussler, S.*, **Köhler, F.***, Witting, M., Premm, M.F., Rolland, S.G., Fischer, C., Chauve, L., Casanueva, O., and Conradt, B. (2020). Autophagy compensates for defects in mitochondrial dynamics. PLoS Genetics *16*, e1008638. https://doi.org/10.1371/journal.pgen.1008638

* contributed equally

Declaration of Contribution

In this dissertation, I present the results of my doctoral research, which I conducted from May 2014 to December 2019 under the supervision of Prof. Dr. Barbara Conradt. The results are presented in two chapters. Chapter I has been published in *Aging (Albany NY)* and chapter II has been published in *PLoS Genetics*. All the work of these two chapters is the result of collaborations with other scientists.

Chapter I:

Köhler, F.*, Müller-Rischart, A.K.*, Conradt, B., and Rolland, S.G. (2015). The loss of *LRPPRC* function induces the mitochondrial unfolded protein response. Aging *7*, 701-712.

* contributed equally

Author Contributions: FK, AKM-R and SGR designed and conducted the experiments and wrote the paper. B.C. designed the experiments and wrote the paper.

FK and SGR contributed the *C. elegans* data (Figures 3, 4, S3, S4, S5) and AKM-R contributed the cell culture data (Figures 1, 2, S1, S2).

Fabian Köhler Dr. Anne Kathrin Müller-Rischart Prof. Dr. Barbara Conradt

Chapter II:

Haeussler, S.*, **Köhler, F.***, Witting, M., Premm, M.F., Rolland, S.G., Fischer, C., Chauve, L., Casanueva, O., and Conradt, B. (2020). Autophagy compensates for defects in mitochondrial dynamics. PLoS Genetics *16*, e1008638.

* contributed equally

Author Contributions: SH, FK and MW designed and conducted the experiments and wrote the paper. BC designed the experiments and wrote the paper. LC designed and conducted the experiments. SGR and OC designed the experiments. MFP conducted the experiments and CF wrote a script for image analysis.

SH performed the primary and secondary UPR^{mt} suppressor screen(s) and FK performed the autophagy screen. Data from SH is presented in Figures 1, 2, 4A, 4D, 4E, 5A-5F, 6C, 6D, S1A-S1E, S2A, S3B, S6A, S6B, S6D and Table S1. Data from FK is presented in Figures 3, 4A, 4B, 4C, 5G-5I, 6A, 6B, S2B, S3A, S5, S6C, S6D, S7 and Table S1. SH prepared *C. elegans* samples for lipid profiling and the execution of the mass spectrometry and subsequent analysis was performed by MW (Figures 7, S8, S9 and Table S2). Figure S4 was provided by CF and data for Figure S1F and Table S3 were provided by LC.

Fabian Köhler Simon Häußler Prof. Dr. Barbara Conradt

Summary

Maintaining a functional and healthy pool of mitochondria is critical for cellular homeostasis. This is ensured by the action of several quality control and stress response pathways. One of these pathways is the mitochondrial unfolded protein response (UPR^{mt}), which is activated upon perturbation of mitochondrial proteostasis and specifically leads to increased expression of mitochondrial chaperones and proteases. Since the mitochondrial proteome is encoded by the mitochondrial as well as the nuclear genome, a high coordination of mitochondrial and nuclear gene expression is required.

In chapter I it is shown that the inactivation of *LRPPRC* in mammalian cells results in an imbalance between mitochondria- and nuclear-encoded subunits of complex IV. This imbalance is counteracted by the activation of the UPR^{mt}, which consequently helps to restore mitochondrial proteostasis. Interestingly, this response is conserved since the inactivation of the *LRPPRC*-like gene *mma-1* in *C. elegans* also induces the UPR^{mt} in this species.

Chapter II describes a more global aspect of UPR^{mt} regulation in *C. elegans*. In particular, the data indicates that the induction of autophagy, which is another cellular quality control mechanism, leads to the suppression of UPR^{mt} in response to a block in mitochondrial fission or fusion. Noteworthy, increased autophagic flux does not restore mitochondrial morphology but rather increases mitochondrial membrane potential and thereby suppresses UPR^{mt}. Moreover, lipid profiling in mutants with a block in mitochondrial fusion revealed increased levels of specific triacylglycerols (TGs), which is partially reverted by the induction of autophagy. This suggests that the breakdown of these TGs fuels mitochondrial metabolism and thereby increases mitochondrial membrane potential, which consequently leads to the suppression of UPR^{mt}.

Taken together, this study shows that the mitonuclear protein imbalance upon knock-down of *LRPPRC* is counteracted by the activation of UPR^{mt}. Moreover, a so far unknown functional connection between UPR^{mt} and autophagy has been established. Thus, these findings provide novel insights into how UPR^{mt} is affected by changes in metabolism.

1 Introduction

1.1 *Caenorhabditis elegans*

The simple metazoan *Caenorhabditis elegans* (*C. elegans*) has been introduced into scientific research in the early 1960s by Sydney Brenner. Since then, the small (~1 mm) free-living nematode has been extensively used as a model organism for basic research especially in the field of animal development and programmed cell death. One key feature of *C. elegans* is its entirely mapped and invariant cell lineage (Sulston et al., 1983; Sulston and Horvitz, 1977). This makes cell fate prediction for every single cell as well as manipulation of individual cell lineages during development possible. In addition, the establishment of the RNA interference (RNAi) technique (Fire et al., 1998) made *C. elegans* an organism in which large-scale genetic screens can easily be performed.

C. elegans has two natural sexes: hermaphrodites (XX) and males (XO). Hermaphrodites can either self-fertilize or mate with a male to produce offspring. The natural incidence of males after self-fertilization is very low (~0.2%) since this requires a spontaneous loss of the X-chromosome at meiosis (Hodgkin et al., 1979; Hodgkin and Doniach, 1997). However, the frequency of males can be increased upon incubation (~3 to 6 hours) at higher temperatures (~30°C).

Importantly, *C. elegans* harbors several advantages that make it well suitable for daily laboratory use. First, *C. elegans* can be cultured and maintained on agar plates with *E. coli* as food source. Second, *C. elegans* has a short temperature-dependent life cycle and strains can be frozen at -80°C for long-term storage. Furthermore, transgenic animals can be generated by microinjection of DNA into the gonad and its transparency enables *in vivo* microscopy analysis, which is of particular relevance when examining fluorescently labeled proteins or, for example, organelles like mitochondria that can specifically be stained with fluorescent dyes.

Altogether, *C. elegans* is a powerful model organism that is used to study various fundamental biological processes. Since 38% of *C. elegans* genes have orthologs in mammals (Shaye and Greenwald, 2011), this research will also contribute to acquire more knowledge of how diseases in higher organisms are regulated and how they can be fought against.

1.2 Mitochondria

Mitochondria are organelles with an average size in diameter of 0.5 – 1 µm and found in most eukaryotic cells (except mature red blood cells). They are often referred to as the 'powerhouse of the cell' since one of their key function is the generation of adenosine triphosphate (ATP). In mammalian somatic cells, the number of mitochondria per cell primarily depends on the energy demand of the different cell types and varies considerably, ranging from about eighty to a several thousand (Kukat et al., 2011; Robin and Wong, 1988; reviewed in Bogenhagen, 2012).

According to the endosymbiotic theory, mitochondria most likely evolved from an aerobic bacterial progenitor that was ingested by a primitive early eukaryotic cell. This explains why mitochondria are enclosed by a double membrane, the inner and outer mitochondrial membrane, making them distinct from all other non-nuclear organelles. The presence of the two membranes consequently also leads to the creation of two compartments in the mitochondria: the intermembrane space (IMS), which reflects the region between the inner and outer mitochondrial membrane, and the mitochondrial matrix, which describes the space enclosed by the inner membrane (Figure 1). The double membrane nature of the mitochondria was already described in the early 1950s by George Palade and Fritiof Sjöstrand by using electron microscopy analysis (Palade, 1952, 1953; Sjostrand, 1953). Interestingly, these studies additionally revealed the occurrence of inner membrane invaginations that project into the mitochondrial matrix and these inner membrane folds are known as 'cristae' (Figure 1). Cristae are vital for mitochondria's role in ATP production because they lead to an increased surface area of the inner mitochondrial membrane. This is of importance since the mitochondrial respiratory chain complexes are all embedded in the inner mitochondrial membrane. Hence, an increased inner membrane surface area results in a higher competence of energy production.

Another characteristic of mitochondria that can be explained by endosymbiotic theory is the presence of its own genome, the mitochondrial DNA (mtDNA). The mtDNA is found in the mitochondrial matrix (Figure 1) and one mitochondrion usually contains between 1 and 15 copies of mtDNA (Kukat et al., 2011; Robin and Wong, 1988; Satoh and Kuroiwa, 1991; Wiesner et al., 1992). It encodes for only a small subset of all mitochondrial proteins as the nuclear DNA encodes for the vast majority of proteins composing the mitochondrial proteome. Specifically, the mtDNA in *C. elegans*, which is 13,794 nucleotides in length, encodes for 12 protein subunits of the mitochondrial respiratory chain, 2 ribosomal RNAs and 22 transfer RNAs (Okimoto et al., 1992).

Mitochondria fulfill many more tasks in the cell besides their role in energy production. They, for example, function in the absorption and storage of calcium ions to regulate intracellular calcium homeostasis (reviewed in Giorgi et al., 2018; Rizzuto et al., 2012). In addition, mitochondria play a critical role in regulating programmed cell death (reviewed in Bock and Tait, 2020) and signaling via reactive oxygen species (ROS) (reviewed in Shadel and Horvath, 2015). Furthermore, mitochondria are known to contribute to the immune response (reviewed in Breda et al., 2019) and to be involved in phospholipid synthesis as well as in the assembly of iron-sulfur clusters (reviewed in Braymer and Lill, 2017; Tatsuta and Langer, 2017). Due to its importance in cellular homeostasis, it is therefore not surprising that mitochondria have been associated with many human diseases like diabetes, Alzheimer's or Parkinson's (reviewed in Billingsley et al., 2018; Kwak et al., 2010; Perez Ortiz and Swerdlow, 2019).

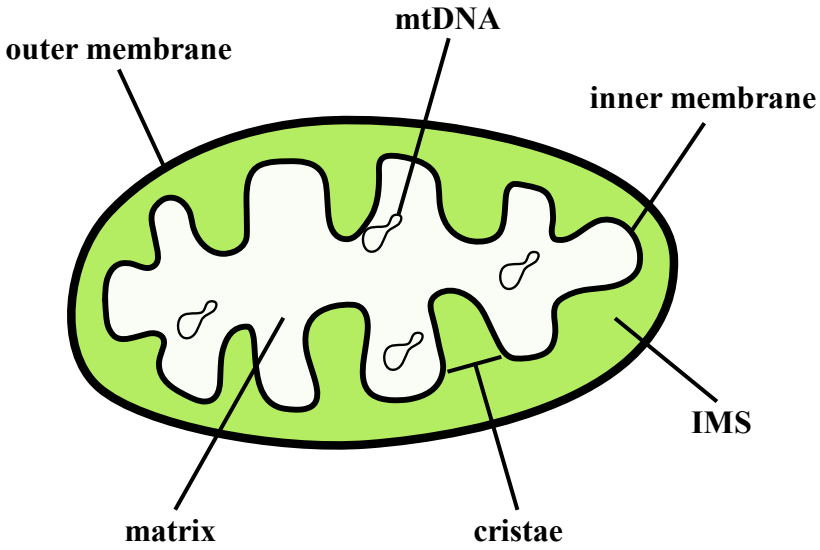

Figure 1. Mitochondria structure. Basic schematic of the main structural features of mitochondria. Figure modified based on (Labieniec-Watala et al., 2012).

1.2.1 Mitochondrial dynamics

In textbooks, mitochondria are usually illustrated as kidney bean-shaped and static organelles. In fact, mitochondria display varying morphologies among different cell types and are often organized in highly connected networks. Moreover, mitochondria are very dynamic organelles that frequently undergo fusion and fission events, which is referred to as 'mitochondrial dynamics'. The balance of fusion and fission is adjusted by the cell in response to various stimuli and a balanced rate of fusion and fission events is important for maintaining mitochondrial function and, hence, cellular homeostasis (reviewed in Youle and van der Bliek,

2012). Upon energy demand, mitochondrial hyperfusion can, for example, lead to a higher rate of oxidative phosphorylation (Rossignol et al., 2004; Tondera et al., 2009). Furthermore, mitochondrial fusion results in the mixing of contents between mitochondria, which can serve as a complementation mechanism in order to fight the accumulation of misfolded proteins and mutated mtDNAs (Chen et al., 2005; Ono et al., 2001). If severe damage in mitochondria persist and cannot be restored, mitochondrial fission ensures the separation of these mitochondria from the network and the subsequent activation of mitophagy, a selective form of autophagy, finally leads to their elimination (reviewed in Palikaras et al., 2018; Pickles et al., 2018). In addition, mitochondrial fission is crucial for the proper partitioning of mitochondria during mitosis (Taguchi et al., 2007) and it has also been shown that mitochondria undergo excessive fission during apoptosis (Frank et al., 2001; Jagasia et al., 2005). Interestingly, blocking either mitochondrial fusion or fission has been shown to have implications in neurodegenerative diseases, underlining the importance of mitochondrial dynamics with respect to organismal health (Guo et al., 2013; Zuchner et al., 2004).

1.2.1.1 Mitochondrial fusion

Mitochondrial fusion and fission are both regulated by dynamin-related GTPases, several of them being highly conserved between yeast, worms, flies and mammals (reviewed in Hoppins et al., 2007). The first mitochondrial fusion gene identified was *fuzzy onions* (*fzo*) in *Drosophila melanogaster*, which was named after the aberrant appearance of mitochondria during spermatogenesis in the respective mutant (Hales and Fuller, 1997). Fzo belongs to the mitofusin (Mfn) class of proteins and members of this protein family have been shown to be embedded in the outer mitochondrial membrane (reviewed in Chan, 2012; Mozdy and Shaw, 2003). Moreover, mitofusins are known to mediate the tethering and fusion of mitochondria through their auto-oligomerization between opposing outer mitochondrial membranes (Figure 2) (Koshiba et al., 2004; Meeusen et al., 2004). Interestingly, the GTPase activity is crucial for the fusion process since defects in its domain lead to tethered but not fused mitochondria (Chen et al., 2003; Hales and Fuller, 1997; Hermann et al., 1998). Although both the N-terminal and C-terminal domain of metazoan mitofusins were initially thought to face the cytosol, a recent study provided evidence that the C-terminal domain localizes to the IMS (Mattie et al., 2018). This is of particular interest because the same study showed that the C-terminal domain is essential for the fusogenic function, suggesting that interactions in the IMS are key for the oligomerization of mitofusins and, hence, for their ability to mediate mitochondrial fusion.

Noteworthy, mammals possess two mitofusins, Mfn1 and Mfn2. Although they share ~80% sequence similarity, both proteins are required for efficient mitochondrial fusion and mitochondria only have residual fusion activity upon depletion of one of them (Chen et al., 2003; Zorzano and Pich, 2006). Remarkably, the lack of either Mfn1 or Mfn2 results in a disparate mitochondrial phenotype. While cells lacking Mfn1 show highly fragmented mitochondria of small size, cells lacking Mfn2 display bigger mitochondrial fragments that tend to form aggregates (Chen et al., 2003). This is in line with findings that Mfn1 has a higher fusion and GTPase activity as compared to Mfn2 (Chen et al., 2003; Ishihara et al., 2004). In addition, it was shown that mitochondrial fusion is completely blocked in Mfn1/2 double knock-out cells (Chen et al., 2003). These results suggest that Mfn1 and Mfn2 function differently in regulating the mitochondrial fusion process. However, it also has been shown that mitochondria lacking Mfn1 can, at least to some extent, fuse with mitochondria lacking Mfn2, indicating that both mitofusins have at least partially redundant functions with respect to their competence in assisting mitochondrial fusion (Chen et al., 2005). Interestingly, Mfn2 has also been shown to be involved in the control of mitochondrial membrane potential as well as in the oxidation of glucose, pyruvate and fatty acids – all independent of its fusogenic function (Bach et al., 2003; Pich et al., 2005). It is worth mentioning that, in contrast to mammals, *C. elegans* only contains one mitofusin ortholog, FZO-1, and, as expected, its loss results in highly fragmented mitochondria (Breckenridge et al., 2008; Ichishita et al., 2008).

After fusion of the outer mitochondrial membranes, it also requires the fusion of the inner mitochondrial membranes to complete the mitochondrial fusion process. In mammals, this is achieved by another dynamin-related GTPase called OPA1 (Figure 2). First evidence for its role in regulating mitochondrial dynamics arose from its homolog in yeast, Mgm1, which was initially shown to be essential for mitochondrial fusion and later demonstrated to be specifically implicated in the tethering and fusion of the inner mitochondrial membranes (Meeusen et al., 2006; Wong et al., 2000; Wong et al., 2003). The *C. elegans* homolog of OPA1/Mgm1 is named EAT-3 and was already found in 1993 during a screen for eating defective mutants (Avery, 1993). However it still lasted 15 years until its function in mitochondrial fusion was assessed (Kanazawa et al., 2008). OPA1, as well as Mgm1 and EAT-3, exists in two major isoforms (long and short) that are generated through proteolytic cleavage in the mitochondria (Chaudhari and Kipreos, 2017; Griparic et al., 2007; Herlan et al., 2003; McQuibban et al., 2003; Olichon et al., 2007). While the long isoform is integral in the inner mitochondrial membrane, its cleavage results in a short isoform that lacks the transmembrane domain. This more soluble isoform localizes to the intermembrane space. Interestingly, it has been proposed that both

isoforms are needed for efficient mitochondrial fusion (Griparic et al., 2007; Herlan et al., 2003; Mishra et al., 2014; Song et al., 2007). However, recent data from mammalian cells suggests that the short isoform of OPA1 rather facilitates mitochondrial fragmentation (Anand et al., 2014; Wai et al., 2015). It will require further research in order to shed more light on the functions of the different isoforms of OPA1/Mgm1/EAT-3 with respect to their role in mitochondrial dynamics.

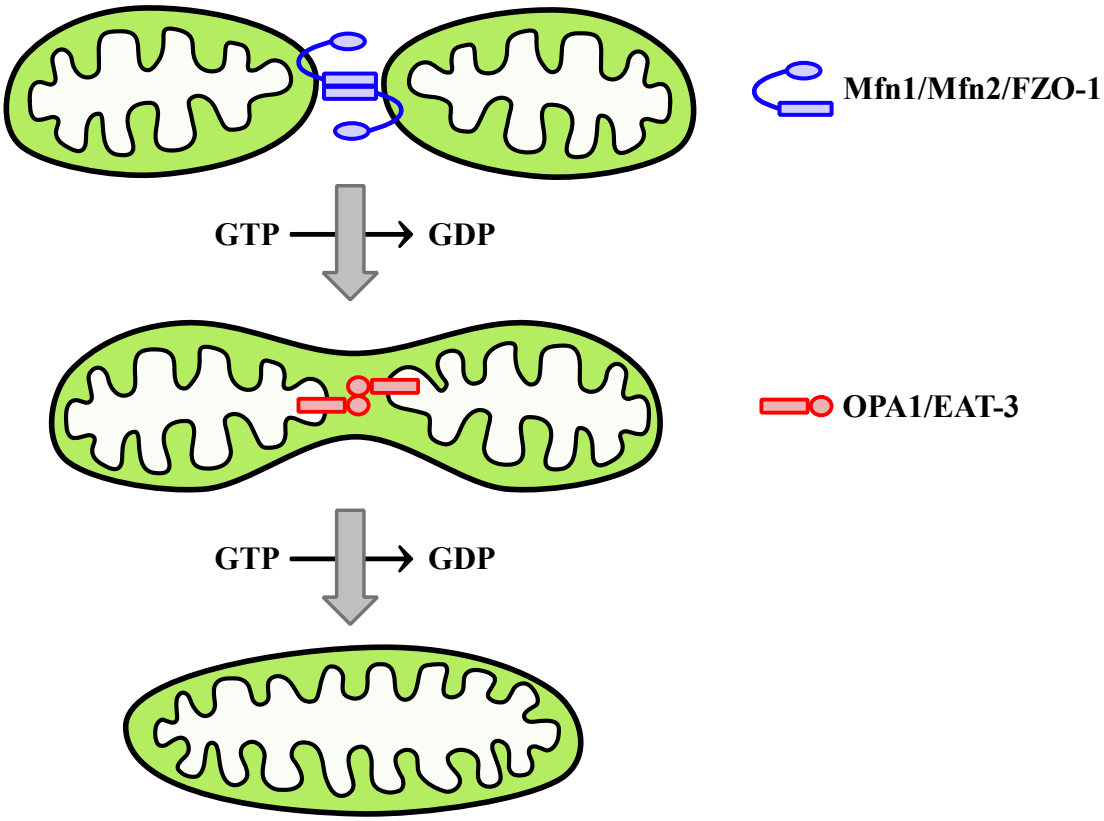

Figure 2. Schematic representation of mitochondrial fusion. Fusion of the outer mitochondrial membranes is mediated by mitofusins (Mfn1/Mfn2/FZO-1) and fusion of the inner mitochondrial membranes is mediated by OPA1/EAT-3. Both steps are dependent on GTP hydrolysis. Figure modified based on (Mishra and Chan, 2016).

Besides their task in controlling mitochondrial fusion, OPA1, Mgm1 and EAT-3 have also been shown to be involved in the regulation and maintenance of mitochondrial cristae structure since cristae were highly disorganized and shortened upon loss of these proteins (Frezza et al., 2006; Kanazawa et al., 2008; Meeusen et al., 2006; Olichon et al., 2003). Remarkably, a recent study revealed that mitochondria also display aberrant cristae in the absence of FZO-1 in *C. elegans* (Byrne et al., 2019), indicating that mitofusins may also be important for mitochondrial cristae formation and/or maintenance.

1.2.1.2 Mitochondrial fission

In 1999, both the yeast dynamin-related GTPase Dnm1 and its homolog in *C. elegans*, DRP-1, were found to be required for mitochondrial fission because their depletion led to highly elongated and interconnected mitochondria (Bleazard et al., 1999; Labrousse et al., 1999; Sesaki and Jensen, 1999). Two years later, this was also established for the mammalian homolog Drp1 (Smirnova et al., 2001). Drp1 is a primarily cytosolic-localized protein that can be recruited to the outer mitochondrial membrane where it oligomerizes and forms spirals around the membrane to drive its constriction in a GTP-dependent manner (reviewed in Kraus and Ryan, 2017). The exact mechanism of how Drp1 is recruited to its target membrane is still under investigation, yet several outer mitochondrial membrane receptors have been shown to assist in the recruitment of Drp1 in mammalian cells. These receptors are Mff, MIEF1 and MIEF2 (with MIEF1 and MIEF2 being largely redundant in function) (Gandre-Babbe and van der Bliek, 2008; Loson et al., 2013; Otera et al., 2010; Palmer et al., 2011). Remarkably, Mff and MIEF1/2 can independently recruit Drp1 to the mitochondrial surface (Loson et al., 2013; Palmer et al., 2013). *C. elegans* has two Mff homologs, MFF-1 and MFF-2, while MIEF1 and MIEF2 homologs are absent. Nevertheless, there may be additional receptors in *C. elegans* that aid in DRP-1 recruitment given that the defects in the mitochondrial network upon lack of both MFF-1 and MFF-2 is less severe than in *drp-1* mutants (Shen et al., 2014). Noteworthy, the anti-apoptotic Bcl-2 family protein CED-9 can also act as a receptor for DRP-1 in *C. elegans* since it has been shown to interact with and recruit DRP-1 upon binding of the pro-apoptotic BH3-only protein EGL-1 in order to promote mitochondrial fission (Lu et al., 2011). A similar function may be fulfilled by mammalian Bcl-2 family members as some of them have also been implicated in the regulation of mitochondrial dynamics (reviewed in Autret and Martin, 2010). In yeast, Dnm1 recruitment is known to be dependent on a different receptor protein called fission factor 1 (Fis1) (Mozdy et al., 2000). Despite the presence of Fis1 homologs in mammals and *C. elegans*, it has been shown that they are not required for mitochondrial fission in these organisms (Osellame et al., 2016; Otera et al., 2010; Shen et al., 2014).

Interestingly, there is emerging evidence that the ER and the actin network are also key players in the process of mitochondrial fission and start to act even before Drp1 comes into play. Specifically, it has been proposed that the ER localizes to future fission sites to promote and control curvature induction as well as the initial constriction of the membrane (Figure 3) (Friedman et al., 2011; Korobova et al., 2013). This Drp1-independent process is thought to rely on ER-associated actin and requires the formin protein INF2 as well as the spire protein

Spire1C for stimulation of actin polymerization, thereby generating the force for membrane constriction (Korobova et al., 2014; Korobova et al., 2013; Manor et al., 2015). Moreover, myosin-II has also been suggested to be implicated in this process (Hatch et al., 2014; Korobova et al., 2014). In a second step, Drp1 may then assemble on the sites that were pre-constricted by the ER to further promote the constriction and scission of the membrane with the help of actin fibers.

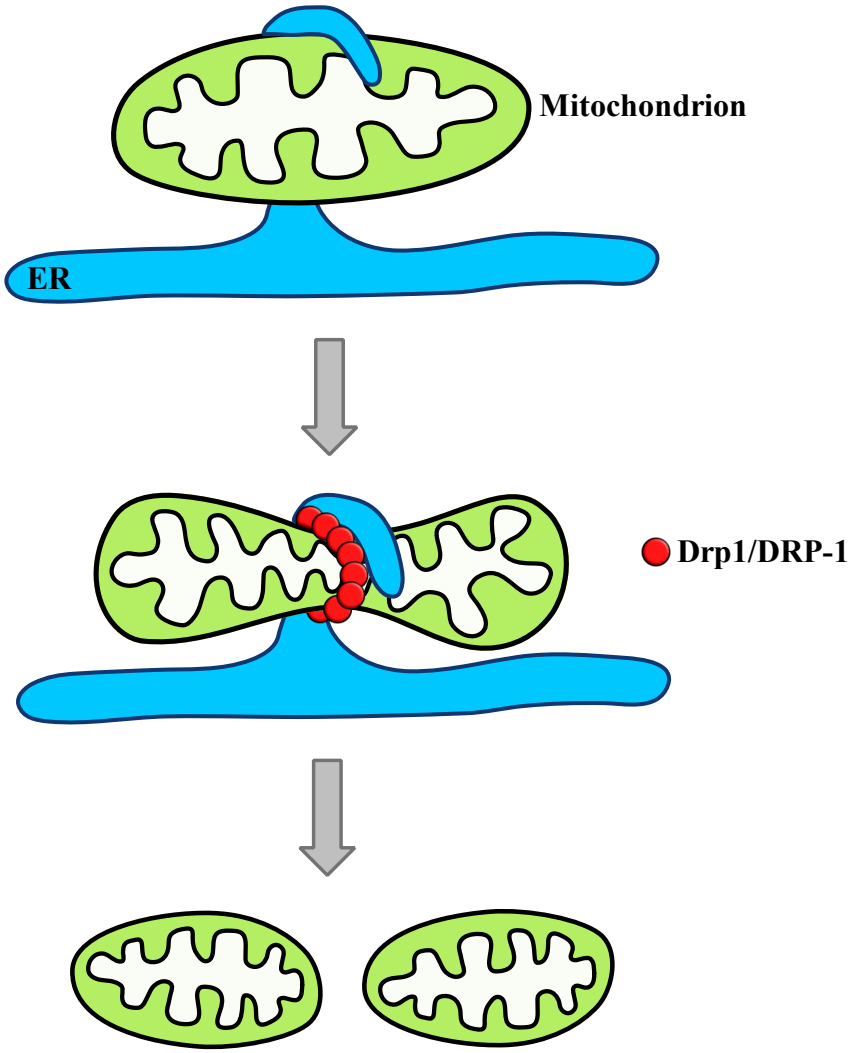

Figure 3. Proposed model of mitochondrial fission. The ER localizes to future sites of mitochondrial fission to promote mitochondrial constriction. Next, Drp1/DRP-1 oligomerizes on pre-constricted sites and forms spirals around the membrane in order to further drive its constriction, thereby facilitating mitochondrial fission. Figure modified based on (Nezich and Youle, 2013).

1.2.2 Oxidative phosphorylation

Most of the cell's ATP is generated inside mitochondria via oxidative phosphorylation (OXPHOS). Two important mitochondrial metabolic pathways that directly feed into OXPHOS

are fatty acid β-oxidation (FAO) and the tricarboxylic acid (TCA) cycle. The final products of FAO are NADH, $FADH_2$ and acetyl-CoA (reviewed in Houten et al., 2016). Whereas the electron carriers NADH and $FADH_2$ can directly be used for ATP production by OXPHOS, acetyl-CoA enters the TCA cycle. In the TCA cycle, acetyl-CoA is oxidized in a series of reactions resulting in the generation of further molecules of NADH and $FADH_2$ (reviewed in Akram, 2014). Noteworthy, the central metabolic intermediate acetyl-CoA is not only fueled into the TCA cycle by FAO but also by other metabolic pathways that degrade carbohydrates or proteins. During OXPHOS, the electrons deriving from NADH and $FADH_2$ are then, through a series of sequential redox reactions, transferred between the mitochondrial respiratory chain (MRC) complexes I – IV (Figure 4) (reviewed in Rich and Marechal, 2010; Sousa et al., 2018; van der Bliek et al., 2017) (see below). Herein, molecular oxygen serves as the final electron acceptor, resulting in its reduction to water. Importantly, the electron transport among the MRCs is coupled to the transfer of protons from the mitochondrial matrix into the IMS. This leads to the establishment of an electrochemical gradient across the inner mitochondrial membrane, which is harnessed by the final OXPHOS complex, ATP synthase (complex V), to catalyze the synthesis of ATP through phosphorylation of ADP (Figure 4).

As mentioned above, five protein complexes are crucial for OXPHOS and the proper stoichiometric assembly of these multi-subunit complexes requires a high coordination between mitochondrial and nuclear gene expression since their proteins are encoded by both mtDNA and nuclear DNA. The MRC complex I (NADH dehydrogenase) is the largest of the five complexes and represents the entry point for electrons from NADH into the OXPHOS system (reviewed in Hirst, 2005). Specifically, via a series of redox reactions, two electrons are transferred from NADH to the electron acceptor ubiquinone, resulting in the formation of its reduced form, ubiquinol. Besides electron transfer, complex I additionally translocates four protons from the mitochondrial matrix into the IMS. Complex II (succinate dehydrogenase) is the smallest complex and consists of only four subunits, all of which are encoded by the nuclear DNA (reviewed in Cecchini, 2003). It functions in parallel with complex I to serve as a second entry site for electrons. Notably, complex II is not only an OXPHOS constituent but also a component of the TCA cycle where it catalyzes the oxidation of succinate to fumarate, thereby producing the electron carrier $FADH_2$. The electrons from $FADH_2$ are then utilized by complex II for reduction of ubiquinone to ubiquinol, though no further protons are translocated. Noteworthy, $FADH_2$ can also be directed into complex II by FAO (see above). Next, the ubiquinol produced by complex I or II freely diffuses within the inner mitochondrial membrane and is subsequently used by complex III (cytochrome bc_1 complex) for electron transfer to

cytochrome *c* via the Rieske protein, whereby the oxidation of one molecule ubiquinol leads to the reduction of two molecules cytochrome *c* (reviewed in Berry et al., 2000). More precisely, it is the iron in the heme group of cytochrome *c* that serves as the electron acceptor in this case. Importantly, the electron transfer mediated by complex III is also accompanied by the translocation of four protons into the IMS. The reduced cytochrome *c* molecules are then utilized by complex IV (cytochrome *c* oxidase or COX) in order to finally transfer the electrons (originating from NADH or $FADH_2$) to oxygen, thereby generating water (reviewed in Calhoun et al., 1994; Yoshikawa et al., 2006). For this step, four molecules of reduced cytochrome *c* are needed, and four further protons are in total translocated across the inner mitochondrial membrane. Ultimately, proton flow through the ATP synthase back along the electrochemical gradient, which has been established by complexes I – IV, provides the energy to drive the phosphorylation of ADP to ATP (reviewed in Junge and Nelson, 2015).

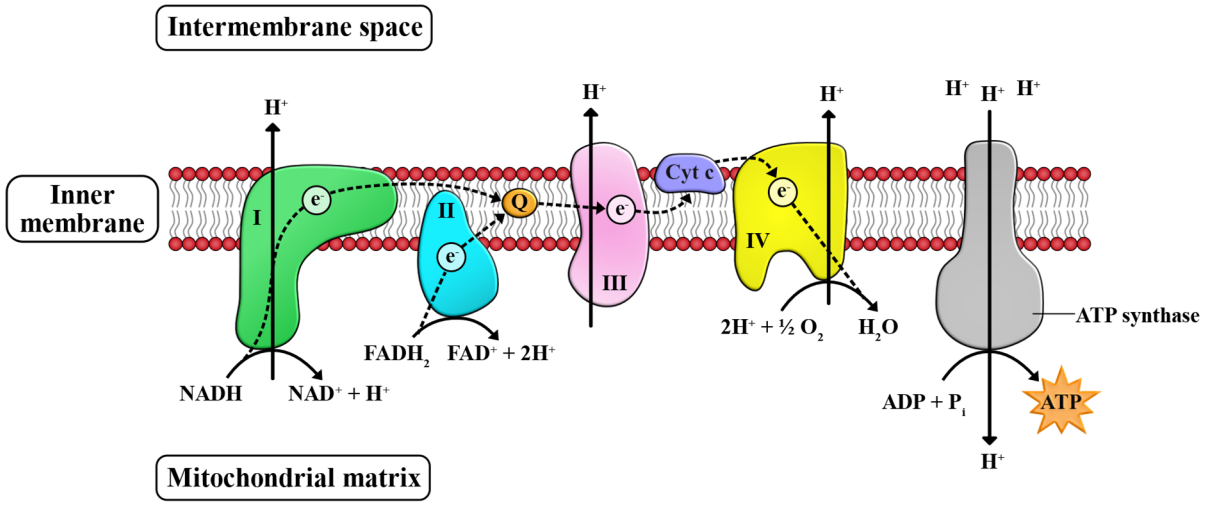

Figure 4. Schematic overview of oxidative phosphorylation. Electrons (e^-) deriving from NADH and $FADH_2$ are transferred between the mitochondrial respiratory chain complexes I – IV and ultimately used to reduce molecular oxygen to water. The electrochemical gradient that has been established by the action of the four complexes is then harnessed by the ATP synthase in order to generate ATP. Figure modified based on (Benard et al., 2011).

1.2.3 LRPPRC

The French Canadian Leigh Syndrome is an early-onset neurodegenerative disease that is caused by mutations in the *LRPPRC* (leucine-rich pentatricopeptide repeat containing) gene and associated with impaired complex IV activity (Mootha et al., 2003). LRPPRC is primarily found in mitochondria and plays an important role in the regulation of mitochondrial mRNA metabolism (Cooper et al., 2006; Mili and Pinol-Roma, 2003; Ruzzenente et al., 2012;

Sasarman et al., 2010; Sterky et al., 2010). For that purpose, LRPPRC functions in a complex with the stem-loop RNA-binding protein SLIRP (Sasarman et al., 2010). The LRPPRC-SLIRP complex acts as an ATP-independent RNA chaperone and is able to locally relax the secondary structure of mitochondrial mRNAs in order to facilitate their polyadenylation and translation (Siira et al., 2017). More precisely, the LRPPRC-SLIRP complex not only promotes polyadenylation of mRNAs by stimulating mitochondrial poly(A) polymerase (mtPAP) activity but also stabilizes polyadenylated mRNAs in general (Chujo et al., 2012; Ruzzenente et al., 2012). How exactly the LRPPRC-SLIRP complex controls mitochondrial translation is unclear, however, its inactivation has been shown to be detrimental for efficient mRNA translation and potentially also influences rRNA maturation (Lagouge et al., 2015; Ruzzenente et al., 2012; Siira et al., 2017). Although it has been initially proposed that LRPPRC depletion only affects the stability of specific COX mRNAs (Xu et al., 2004), it is now evident that LRPPRC acts globally on all mitochondrial mRNAs, with the exception of MT-ND6 (Ruzzenente et al., 2012; Siira et al., 2017). However, the mRNAs encoding for COX subunits seem to be more sensitive to the loss of LRPPRC as compared to all other mitochondrial mRNAs since they are found to be disproportionally decreased (Ruzzenente et al., 2012; Sasarman et al., 2010). This may account for the specific impairment of complex IV in patients suffering from French Canadian Leigh Syndrome. Furthermore, it was shown that reduced LRPPRC levels in mammalian cells, or reduced levels of the LRPPRC-like protein MMA-1 in *C. elegans*, result in mitochondrial hyperfusion in order to compensate for decreased complex IV activity by maintaining mitochondrial ATP production (Rolland et al., 2013). However, this response is of transient nature since prolonged knock-down of *LRPPRC* ultimately leads to mitochondrial fragmentation, decreased ATP levels and collapse of cellular function (Rolland et al., 2013). Consistently, fibroblasts from patients with French Canadian Leigh Syndrome have also been shown to display fragmented mitochondria (Sasarman et al., 2010). Moreover, it is worth mentioning that LRPPRC has additionally been implicated in several other diseases like cancer, Parkinson's and neurofibromatosis type I (Arun et al., 2013; Gaweda-Walerych et al., 2016; Jiang et al., 2014; Li et al., 2014; Tian et al., 2012).

1.2.4 The mitochondrial unfolded protein response

The mitochondrial proteome is composed of more than 1000 proteins (Rhee et al., 2013). Nearly all these proteins are encoded by the nuclear DNA and synthesized in the cytosol. Hence, they need to be imported into mitochondria via the TIM/TOM complexes (reviewed in Chacinska et

al., 2009) and folded within the organelle. The folding of both mitochondrially translated and imported proteins is achieved by molecular chaperones like mtHSP70 and HSP60 (Cheng et al., 1989; Mizzen et al., 1989). Interestingly, mtHSP70 does not only function in protein folding but also plays an essential role at the mitochondrial import channel where it facilitates the import of proteins by interacting with the TIM complex (D'Silva et al., 2003; Gaume et al., 1998; Voisine et al., 1999). Damaged or misfolded proteins are degraded by mitochondrial proteases, such as ClpXP or LONP1, to ensure the maintenance of mitochondrial protein homeostasis (Bota and Davies, 2002; Desautels and Goldberg, 1982; Kang et al., 2002; Wang et al., 1993). Once unfolded and/or misfolded proteins in the mitochondrial matrix start to accumulate, a retrograde quality control signaling pathway referred to as the 'mitochondrial unfolded protein response' (UPR^{mt}) is activated (reviewed in Naresh and Haynes, 2019). This promotes the transcriptional upregulation of nuclear genes encoding for mitochondrial protective proteins (like the aforementioned chaperones and proteases) in order to re-establish mitochondrial proteostasis.

The first evidence for the existence of such a mitochondria-specific stress response pathway was provided in mammalian cells upon depletion of mtDNA by exposure to ethidium bromide (Martinus et al., 1996). Because the overexpression of a misfolding-prone mitochondrial-targeted protein had been shown to result in a similar response, this pathway was named UPR^{mt} (Zhao et al., 2002). Since then, much has been learned about UPR^{mt} and its molecular regulation through extensive studies in *C. elegans*. Specifically, UPR^{mt} in *C. elegans* is mediated by the bZIP transcription factor ATFS-1 (activating transcription factor associated with stress-1), which possesses both an N-terminal mitochondrial targeting sequence (MTS) and a C-terminal nuclear localization signal (NLS) (Haynes et al., 2010; Nargund et al., 2012). In the absence of mitochondrial stress, ATFS-1 is imported into the mitochondrial matrix where it is degraded by the LONP-1 protease (Nargund et al., 2012). However, upon activation of the UPR^{mt}, mitochondrial protein import is generally compromised, which leads to the accumulation of ATFS-1 in the cytosol and its subsequent import into the nucleus (Nargund et al., 2012). Once in the nucleus, ATFS-1 then promotes the expression of several stress response genes like chaperones (e.g., *hsp-6*, *hsp-60*) and proteases (e.g., *clpp-1*) (Nargund et al., 2012). Interestingly, this transcriptional activation is also tightly regulated by chromatin remodeling and requires the proteins LIN-65, MET-2, JMJD-1.2 and JMJD-3.1 (Merkwirth et al., 2016; Tian et al., 2016). While LIN-65 in conjunction with the histone methyltransferase MET-2 mediates the condensation of global chromatin (Tian et al., 2016), the two histone demethylases JMJD-1.2 and JMJD-3.1 act to specifically open the chromatin structure of UPR^{mt} target genes

(Merkwirth et al., 2016). Two additional proteins that participate in chromatin remodeling and UPR^{mt} activation are DVE-1 and UBL-5 (Benedetti et al., 2006; Haynes et al., 2007; Tian et al., 2016). Both the homeobox transcription factor DVE-1 and the small ubiquitin-like protein UBL-5 normally localize to the cytoplasm but translocate into the nucleus upon disruption of mitochondrial protein homeostasis (Benedetti et al., 2006; Haynes et al., 2007). In the nucleus, DVE-1 and UBL-5 form a complex and bind to UPR^{mt} gene promoters that have been made accessible by JMJD-1.2 and JMJD-3.1 to further promote remodeling of chromatin (Benedetti et al., 2006; Haynes et al., 2007; Tian et al., 2016). This keeps the respective genes in a transcription-competent state, which thereby facilitates binding of ATFS-1 and, hence, activation of UPR^{mt} (Tian et al., 2016). Another layer of complexity in this regard has recently been added since it was shown that also the SUMO peptidase ULP-4 is required for UPR^{mt} activation (Gao et al., 2019). More precisely, ULP-4 deSUMOylates DVE-1 in the cytoplasm to enable its import into the nucleus (Gao et al., 2019). Furthermore, ULP-4-dependent deSUMOylation also increases the stability and the transcriptional activity of ATFS-1 (Gao et al., 2019).

As outlined above, the nuclear localization of ATFS-1 is key for UPR^{mt} activation and requires hampered mitochondrial protein import. Initially, this impaired mitochondrial protein import has been proposed to be caused by the release of short peptides from mitochondria into the cytoplasm (Haynes et al., 2010). This was based on studies showing that the mitochondrial matrix protease CLPP-1 and the inner membrane-spanning ABC (ATP-binding cassette) transporter HAF-1 are required for proper UPR^{mt} activation (Haynes et al., 2010; Nargund et al., 2012). CLPP-1 is known to cleave unfolded proteins into small peptides and it has been proposed that these peptides are subsequently transported across the inner membrane via HAF-1 (Haynes et al., 2010; Nargund et al., 2012). The peptides are then thought to further diffuse across the outer mitochondrial membrane through porins or the TOM complex and this peptide efflux into the cytoplasm has been proposed to act as the signal that triggers UPR^{mt} by blocking mitochondrial import (via an unknown mechanism) (Haynes et al., 2010). However, a recent study provided evidence that it is rather a decrease of mitochondrial membrane potential that acts as the signal for UPR^{mt} activation (Rolland et al., 2019). Since mitochondrial membrane potential is intimately linked to mitochondrial import (Martin et al., 1991; reviewed in Kulawiak et al., 2013; Zorova et al., 2018), changes in the mitochondrial membrane potential can therefore regulate the import efficiency of ATFS-1 (Figure 5). In particular, mitochondrial import also depends on the net charge of the MTS of a protein (reviewed in Hartl et al., 1989) and a drop in mitochondrial membrane potential greatly decreases the import of ATFS-1 due to

its relatively 'weak' MTS whereas proteins with a 'strong' MTS (e.g., HSP-60) are still imported (Rolland et al., 2019). Thus, the MTS of ATFS-1 acts as a sensor for reduced mitochondrial membrane potential.

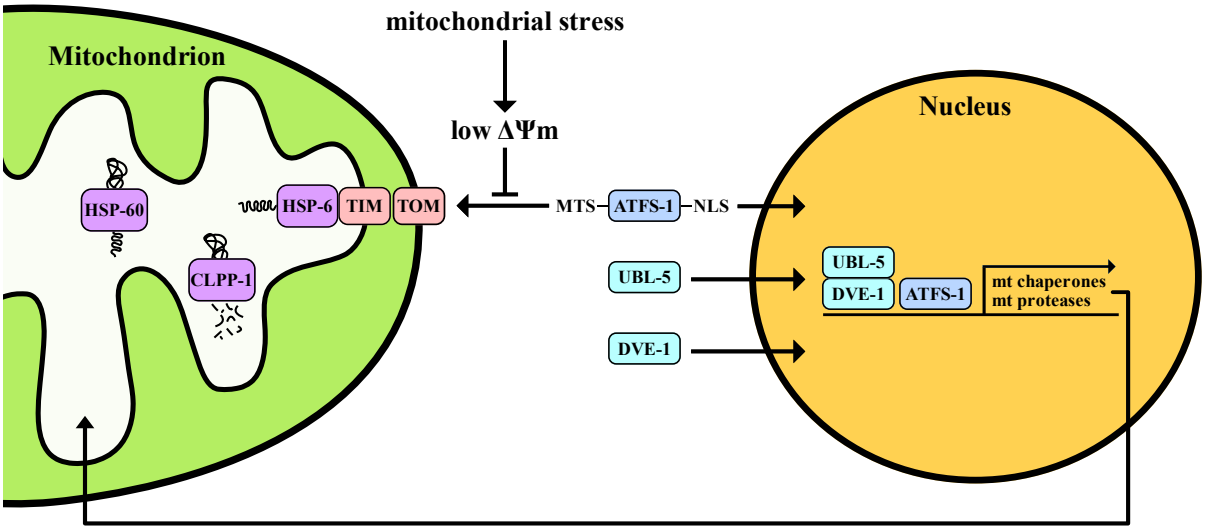

Figure 5. Schematic representation of UPR^{mt} signaling in *C. elegans*. Mitochondrial stress leads to decreased mitochondrial membrane potential (ΔΨm) and thereby to impaired import of ATFS-1. Hence, ATFS-1 is imported into the nucleus where it cooperates with DVE-1 and UBL-5 in order to drive the expression of mitochondrial stress response genes like chaperones (e.g., *hsp-6*, *hsp-60*) and proteases (e.g., *clpp-1*), which ideally results in the reconstitution of mitochondrial homeostasis. Figure modified based on (Jovaisaite et al., 2014).

Numerous genes have been shown to induce UPR^{mt} when inactivated. Among them are, for example, all the three GTPases (*fzo-1*, *eat-3* and *drp-1*) that regulate mitochondrial dynamics (Kim and Sieburth, 2018; Zhang et al., 2018). In addition, the depletion of SPG-7, which is a subunit of the mitochondrial *m*-AAA protease complex, has been exploited for studying the UPR^{mt} (Benedetti et al., 2006; Haynes et al., 2007; Haynes et al., 2010; Lin et al., 2016; Nargund et al., 2015; Shao et al., 2016). Moreover, blocking mitochondrial translation by using doxycycline as well as the knock-down of mitochondrial respiratory chain components was shown to activate the UPR^{mt} in *C. elegans* (Benedetti et al., 2006; Durieux et al., 2011; Houtkooper et al., 2013; Yoneda et al., 2004).

The UPR^{mt} in mammalian cells is not as well understood, but it has been shown that the pathway is at least partially conserved (reviewed in Melber and Haynes, 2018; Naresh and Haynes, 2019). For instance, it has been shown that the bZIP transcription factor ATF5 shares similarities with ATFS-1 because it also harbors both a MTS and a NLS and its import into mitochondria is similarly regulated (Fiorese et al., 2016). In line with this, ATF5 was shown to

be able to regulate UPR^{mt} in worms lacking ATFS-1 (Fiorese et al., 2016). Nevertheless, the regulation of UPR^{mt} is thought to be more complex as compared to in *C. elegans* since two additional bZIP transcription factors, ATF4 and CHOP, have been shown to be required for UPR^{mt} induction in mammals (Chung et al., 2017; Fusakio et al., 2016; Horibe and Hoogenraad, 2007; Quiros et al., 2017). The exact function of the three transcription factors with respect to their roles in UPR^{mt} activation stills needs to be determined. Importantly, UPR^{mt} in mammalian cells is tightly connected to the integrated stress response (ISR), which is a common adaptive eukaryotic signaling pathway that drives the expression of stress response genes in order to restore cellular homeostasis (reviewed in Pakos-Zebrucka et al., 2016). The ISR is stimulated following diverse cellular stressors such as amino acid starvation, ER stress, mitochondrial stress or viral infection (Quiros et al., 2017; reviewed in Pakos-Zebrucka et al., 2016). Evidence indicates that mitochondrial dysfunction activates the ISR via the cytoplasmic kinase GCN2 (Martinez-Reyes et al., 2012; Michel et al., 2015; Wang et al., 2016). More accurately, GCN2 phosphorylates the translation initiation factor eIF2α, which results in inhibition of general protein synthesis while translation of mRNAs harboring upstream open reading frames (uORFs) is preferentially initiated (reviewed in Barbosa et al., 2013; Dever, 2002; Hinnebusch et al., 2016; Young and Wek, 2016). Interestingly, among the mRNAs that are preferentially translated upon phosphorylation of eIF2α are the mRNAs of all three transcription factors (ATF4, ATF5 and CHOP) that are required for UPR^{mt} since they all harbor uORFs (Jousse et al., 2001; Lu et al., 2004; Teske et al., 2013; Vattem and Wek, 2004; Zhou et al., 2008). Thus, the activation of the ISR is a prerequisite for UPR^{mt} induction in mammalian cells. However, this seems not be conserved in *C. elegans* as neither GCN-2 (the homolog of mammalian GCN2) nor phosphorylation of eIF2α is required for UPR^{mt} activation in this organism (Baker et al., 2012; Rolland et al., 2019).

1.3 Autophagy

Autophagy (cellular ‘self-eating’) is the process of lysosomal degradation and recycling of cytoplasmic constituents, long-lived proteins or dysfunctional organelles (reviewed in Levine and Klionsky, 2004; Mizushima, 2007). It was first described in the 1960s (De Duve and Wattiaux, 1966) and has been extensively studied during the past decades (reviewed in Galluzzi et al., 2017). Three different types of autophagy can be distinguished: macroautophagy, microautophagy and chaperone-mediated autophagy. Microautophagy is the least understood

type and involves the uptake of cytoplasmic cargo into the lysosome through invagination or protrusion of the lysosomal membrane (reviewed in Mijaljica et al., 2011). Chaperone-mediated autophagy is a very selective form of autophagy and only involves cytosolic proteins that contain a KFERQ-like motif (Dice, 1990). These substrates are recognized and unfolded by specific chaperones, subsequently translocated across the lysosomal membrane and finally degraded within the lysosomal lumen (reviewed in Cuervo and Wong, 2014).

1.3.1 Macroautophagy

Macroautophagy (hereafter referred to as 'autophagy') is mediated by a cellular component called 'autophagosome' (Figure 6). More specifically, the induction of autophagy results in the establishment of a double-membrane structure called the 'phagophore', which elongates and ultimately engulfs the autophagic cargo by closure of the membrane structure, thereby giving rise to an autophagosome. The fusion of the autophagosome with a lysosome then leads to formation of an autolysosome, in which the engulfed cargo is finally degraded by acidic lysosomal hydrolases (reviewed in Feng et al., 2014; Mizushima, 2007; Nakatogawa et al., 2009).

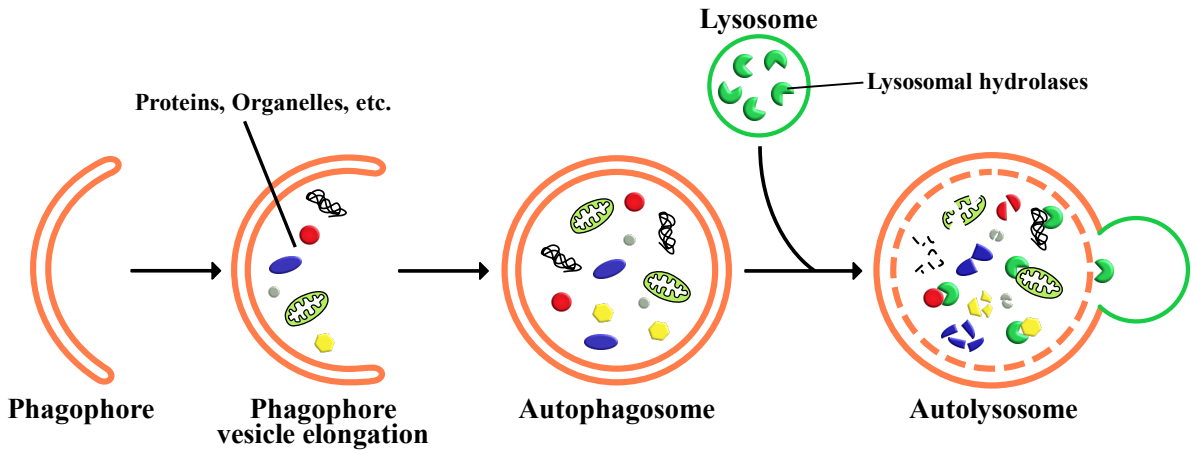

Figure 6. Schematic model of the autophagy process. Upon induction of autophagy, a double-membrane structure named phagophore forms. The phagophore elongates and completely engulfs the autophagic cargo upon closure, thereby resulting in an autophagosome. Degradation of the autophagic cargo is then finally mediated by lysosomal hydrolases in the autolysosome, which derives from the fusion of the autophagosome with a lysosome. Figure modified based on (Melendez and Levine, 2009).

Importantly, studies in mammalian systems have shown that autophagosomes can, prior to fusion with lysosomes, also fuse with early and late endosomes to form an intermediate hybrid

organelle known as ‘amphisome’ (Berg et al., 1998; Gordon and Seglen, 1988; Tooze et al., 1990).

Seminal insights into the molecular basis of the autophagic machinery were initially gained by studies in *Saccharomyces cerevisiae* with the discovery of several autophagy-related (*ATG*) genes, many of them being conserved from yeast to humans (Harding et al., 1995; Klionsky et al., 2003; Thumm et al., 1994; Tsukada and Ohsumi, 1993; reviewed in Galluzzi et al., 2017). One of these genes is *ATG1* and its homolog in *C. elegans* and mammals is *unc-51* and *ULK* (*unc-51-like kinase*), respectively. The serine/threonine kinase Atg1/UNC-51/ULK is part of a complex that is required for initiation of phagophore assembly and the kinase TOR/LET-363/mTOR acts a key regulator of autophagy since it generally represses this complex (reviewed in Galluzzi et al., 2017; Palmisano and Melendez, 2019). However, in case of nutrient deprivation, TOR/LET-363/mTOR is inhibited, which in turn leads to de-repression of the Atg1/UNC-51/ULK initiation complex and thereby to induction of autophagy (reviewed in Galluzzi et al., 2017; Palmisano and Melendez, 2019). In addition to TOR/LET-363/mTOR, the AMP-activated protein kinase (AMPK) signaling pathway plays an important role in regulating autophagy because it is also involved in nutrient sensing and was found to be able to inhibit TOR/LET-363/mTOR activity and/or to directly activate the Atg1/UNC-51/ULK complex (Egan et al., 2011; Gwinn et al., 2008; Inoki et al., 2002; Kim et al., 2011; Lee et al., 2010). Interestingly, the membrane source for phagophore assembly is still under debate, but for mammalian phagophores it has been shown that they usually form near ER-mitochondria contact site-associated structures called omegasomes (Axe et al., 2008; Hayashi-Nishino et al., 2009; Yla-Anttila et al., 2009).

The commonly utilized autophagy marker in *C. elegans* is GFP::LGG-1. LGG-1 is homologous to yeast Atg8, which is a ubiquitin-like protein that is conjugated to phosphatidylethanolamine (PE) in the forming autophagosome and found on the inner as well as on the outer autophagosomal membrane (Ichimura et al., 2000; Kirisako et al., 1999). Although the exact function of Atg8 is still under investigation, it has been shown that Atg8 is involved in phagophore expansion and maturation of the autophagosome since Atg8 levels directly correlate with autophagosome size (Xie et al., 2008). Noteworthy, Atg8 is delipidated and released from the outer membrane during late stages of autophagy while the PE-conjugated Atg8 in the inner membrane is eventually degraded along with the autophagic cargo (Huang et al., 2000; Kirisako et al., 2000; Nair et al., 2012). Whereas only one Atg8 protein is present in yeast, several orthologs of Atg8 have been described in mammalian systems. They can be sub-

divided into the LC3 and GABARAP families, but little is known about the exact function or redundancy of each ortholog with respect to their biological roles in regulating autophagosome biogenesis (reviewed in Lee and Lee, 2016; Slobodkin and Elazar, 2013). Interestingly, the two Atg8 orthologs in *C. elegans*, LGG-1 and LGG-2, are both not only implicated in autophagosome formation but also play a crucial role in autophagosome-lysosome fusion and recent evidence indicates that this holds true for mammalian Atg8 family proteins as well (Manil-Segalen et al., 2014; Nguyen et al., 2016b; Wu et al., 2015).

One well-known function of Atg8-like proteins is that they mediate the selective removal of autophagic cargo. This is achieved by interaction with specific autophagy receptors like the mammalian p62/SQSTM1 (hereafter referred to as 'p62'), which recognizes and binds to ubiquitinylated protein aggregates in order to deliver them into growing phagophores for subsequent degradation (Bjorkoy et al., 2005; Pankiv et al., 2007). Notably, the binding of p62 to Atg8 family proteins in the phagophore is facilitated by a basic hydrophobic LC3-interacting region (LIR) motif that is common to all selective autophagy receptors (reviewed in Johansen and Lamark, 2011; Rogov et al., 2014). Since p62 itself is an autophagic substrate, increased levels of p62 are generally indicative of impaired autophagy (reviewed in Klionsky et al., 2016). This also applies to the *C. elegans* p62 homolog SQST-1, which is selectively degraded by autophagy during embryogenesis (Tian et al., 2010) and, hence, routinely used as a tool in order to check for hampered autophagy (reviewed in Chen et al., 2017; Zhang et al., 2015).

Remarkably, autophagy genes have been shown to be required for health- and lifespan extension under certain conditions in several organisms, however, how exactly autophagy affects this beneficial outcome remains largely enigmatic (reviewed in Hansen et al., 2018). Furthermore, defects in the autophagic machinery have been linked to several human pathologies like cancer, myopathies, aging, neurodegeneration and metabolic diseases (reviewed in Choi et al., 2013; Saha et al., 2018).

1.3.2 Mitophagy

Mitophagy is a selective form of autophagy that specifically degrades mitochondria and the most well-characterized stress-induced mitophagy pathway is the PINK1/Parkin-mediated pathway (Figure 7). Interestingly, mutations in both PINK1 and Parkin have been shown to be implicated in early-onset Parkinson's disease (Kitada et al., 1998; Valente et al., 2004). In the absence of mitochondrial stress, PINK1 is imported into the inner mitochondrial membrane via

the TOM/TIM complexes and cleaved by the PARL protease (Jin et al., 2010). Next, cleaved PINK1 translocates back into the cytosol where it is degraded by the proteasome (Lin and Kang, 2008; Yamano and Youle, 2013). However, upon dissipation of the mitochondrial membrane potential, PINK1 import into mitochondria is compromised, resulting in the accumulation of PINK1 on the mitochondrial surface (Jin et al., 2010; Narendra et al., 2010). The auto-phosphorylation of accumulated PINK1 then leads to activation of its kinase domain, which results in phosphorylation of several PINK1 substrates such as ubiquitin and this subsequently promotes the recruitment of the E3 ubiquitin ligase Parkin from the cytosol to damaged mitochondria (Kane et al., 2014; Okatsu et al., 2012; Shlevkov et al., 2016). Through phosphorylation by PINK1, Parkin is activated and eventually mediates polyubiquitination of its substrates on the outer mitochondrial membrane (Kane et al., 2014; Kondapalli et al., 2012; Koyano et al., 2014). Noteworthy, this entails a positive feedback loop since polyubiquitination of mitochondrial surface proteins by Parkin in turn provides additional substrates for PINK1 phosphorylation and, hence, further drives the recruitment of Parkin molecules to damaged mitochondria (Ordureau et al., 2014). Finally, cytosolic autophagy receptors recognize and interact with ubiquitinated mitochondria to convey their incorporation into the autophagosomal degradation pathway (Lazarou et al., 2015).

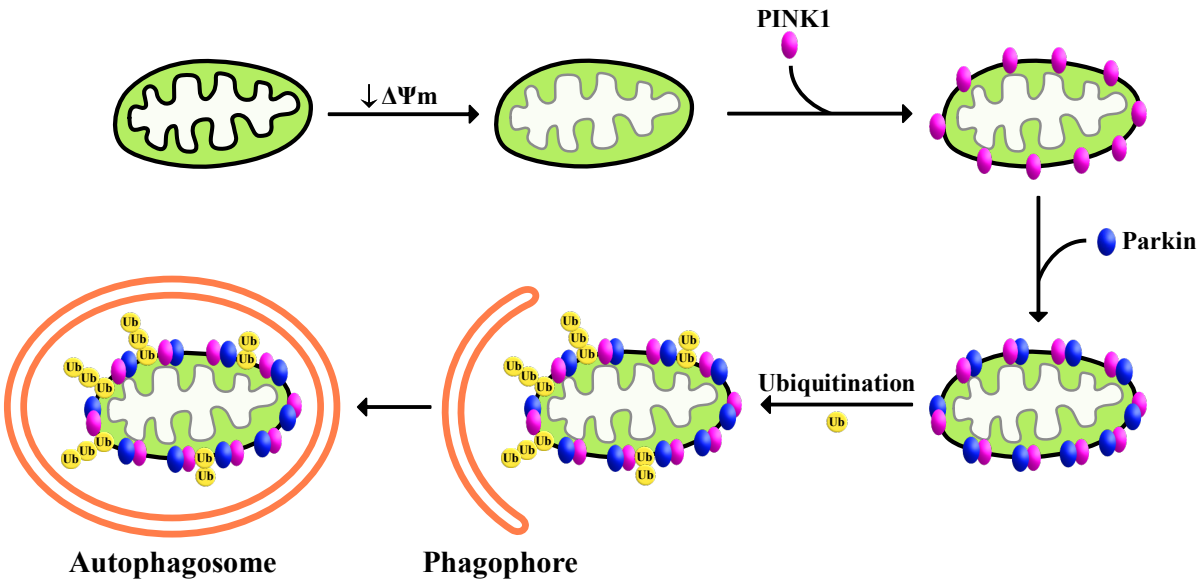

Figure 7. Schematic model of PINK1/Parkin-mediated mitophagy. PINK1 accumulates on depolarized mitochondria and subsequent Parkin recruitment results in ubiquitination of outer mitochondrial membrane proteins, which ultimately leads to the engulfment of damaged mitochondria into autophagosomes. Figure modified based on (Wang et al., 2019).

Remarkably, besides the PINK1/Parkin-mediated pathway, there also exists receptor-mediated mitophagy pathways that specifically act in response to various stimuli such as hypoxia or developmental cues (reviewed in Chakravorty et al., 2019; Palikaras et al., 2018). Three of those receptors are the outer mitochondrial membrane proteins BNIP3, NIX and FUNDC1 and all of them promote mitophagy by direct interaction with the autophagic machinery in a PINK1/Parkin-independent manner (reviewed in Liu et al., 2014a; Nguyen et al., 2016a; Villa et al., 2018). However, a crosstalk between the PINK1/Parkin-mediated pathway and receptor-mediated pathways likely occurs since, for example, both BNIP3 and NIX have been shown to be able to regulate Parkin recruitment (Ding et al., 2010; Lee et al., 2011).

In nematodes, mitophagy is not well-studied as compared to in mammalian systems, however, homologs of mammalian mitophagy genes have been identified. For instance, the *C. elegans* homologs of PINK1 and Parkin are PINK-1 and PDR-1, respectively, and both have been demonstrated to be crucial for selective removal of mitochondria under stress conditions (Cummins et al., 2019; Fang et al., 2019; Ryu et al., 2016). This also holds true for DCT-1, which is the nematode homolog of BNIP3 and NIX (Fang et al., 2019; Ryu et al., 2016). Furthermore, it has recently been shown that the loss of FNDC-1 (the *C. elegans* FUNDC1 homolog) impairs the elimination of paternal mitochondria (Lim et al., 2019).

1.4 ESCRT

The Endosomal Sorting Complex Required for Transport (ESCRT) is an evolutionary conserved machinery that mediates a specific membrane remodeling reaction, which involves membrane bending and abscission away from the cytosol (reviewed in Gatta and Carlton, 2019; Vietri et al., 2020). It has first been identified in the pathway of multivesicular body (MVB) formation during endocytosis, in which ESCRT facilitates the sorting of ubiquitinated membrane proteins into small intralumenal vesicles (ILVs) (Katzmann et al., 2001). Since then, ESCRT has also been implicated in many other cellular processes such as cytokinetic abscission, virus budding, neuron pruning, plasma membrane repair and nuclear pore quality control (Carlton and Martin-Serrano, 2007; Issman-Zecharya and Schuldiner, 2014; Jimenez et al., 2014; Webster et al., 2014). The ESCRT is composed of five different subcomplexes (ESCRT-0, -I, -II, -III and the AAA-ATPase VPS4) whereby ESCRT-III in conjunction with VPS4 acts as the functional key component in regulating membrane remodeling and scission

while ESCRT-0, -I and -II generally facilitate the targeted recruitment of ESCRT-III and VPS4 (reviewed in Gatta and Carlton, 2019; Vietri et al., 2020).

Interestingly, ESCRT has also been implicated in autophagy. In mammalian cells and flies, depletion of ESCRT components leads to defects in the autophagic process and it has initially been suggested that this is due to impaired fusion of autophagosomes with lysosomes (Filimonenko et al., 2007; Lee et al., 2007; Rusten et al., 2007; Tamai et al., 2007). More recent data from yeast and mammals, however, indicate that ESCRT is rather required for the sealing of phagophores (Takahashi et al., 2018; Zhen et al., 2019; Zhou et al., 2019). Hence, the autophagy impairment upon loss of ESCRT is most likely due to accumulation of unsealed phagophores. Surprisingly, studies in *C. elegans* showed that ESCRT depletion does not block but induce autophagy (Djeddi et al., 2012; Guo et al., 2014) and it has been proposed that this is an indirect pro-survival mechanism in response to enlarged endosomes (Djeddi et al., 2012). Furthermore, ESCRT has recently also been suggested to facilitate endosomal sequestration of mitochondria in an autophagy-independent mitochondrial clearance pathway in mouse embryonic fibroblasts (Hammerling et al., 2017).

2 Chapter I – The loss of *LRPPRC* function induces the mitochondrial unfolded protein response

Köhler, F.*, Müller-Rischart, A.K.*, Conradt, B., and Rolland, S.G. (2015). Aging *7*, 701-712. https://doi.org/10.18632/aging.100812

* contributed equally

www.impactaging.com AGING, September 2015, Vol 7 N 9

Research Paper

The loss of *LRPPRC* function induces the mitochondrial unfolded protein response

Fabian Köhler [1*], Anne Kathrin Müller-Rischart [1*], Barbara Conradt [1], and Stéphane Guy Rolland [1]

[1] *Center for Integrated Protein Science, Fakultät für Biologie, Ludwig-Maximilians-Universität München, 82152 Planegg-Martinsried, Germany*

** Equally contributed to the work*

Key words: *Mitochondrial stress response, UPR^{mt}, mitochondrial hyperfusion, mma-1, LRPPRC*

Received: *06/02/15; Accepted: 09/12/15; Published: 09/26/15*

Correspondence to: *Barbara Conradt, PhD; Stéphane Rolland, PhD;* ***E-mail:*** *conradt@bio.lmu.de; rolland@bio.lmu.de*

Abstract: The inactivation of the *LRPPRC* gene, which has previously been associated with the neurodegenerative French Canadian Leigh Syndrome, results in a decrease in the production of mitochondria-encoded subunits of complex IV, thereby causing a reduction in complex IV activity. Previously we have shown that reducing complex IV activity triggers a compensatory and conserved mitochondrial hyperfusion response. We now demonstrate that *LRPPRC* knock-down in mammalian cells leads to an imbalance between mitochondria-encoded and nuclear-encoded subunits of complex IV and that this imbalance triggers the mitochondrial unfolded protein response (UPR^{mt}). The inactivation of the *LRPPRC*-like gene *mma-1* in *C. elegans* also induces UPR^{mt}, which demonstrates that this response is conserved. Furthermore, we provide evidence that mitochondrial hyperfusion and UPR^{mt} are coordinated but mediated by genetically distinct pathways. We propose that in the context of *LRPPRC mma-1* knock-down, mitochondrial hyperfusion helps to transiently maintain mitochondrial ATP production while UPR^{mt} participates in the restoration of mitochondrial proteostasis. Mitochondrial proteostasis is not only critical in pathophysiology but also during aging, as proteotoxic stress has been shown to increase with age. Therefore, we speculate that the coordination of these two mitochondrial stress responses plays a more global role in mitochondrial proteostasis.

INTRODUCTION

Mitochondria are essential eukaryotic organelles that participate in processes such as cellular energy production, cell signaling and apoptosis [1-3]. The production of cellular energy by mitochondria produces as a byproduct reactive oxygen species (ROS). While the effect of ROS on the accumulation of mutations in the mitochondrial genome is still under debate, ROS have been shown to promote protein oxidation and consequently misfolding and/or unfolding of these proteins inside mitochondria [4,5]. The resulting proteotoxic stress has been shown to increase with age and to participate in several age-related disorders, such as neurodegenerative diseases [6]. To maintain mitochondrial proteostasis and, hence, mitochondrial function, it is important that damaged proteins are eliminated by mitochondrial proteases and that mitochondrial chaperones assist in the folding of nascent proteins. Another challenge that mitochondria face is the fact that the assembly of complexes of the Electron Transport Chain (ETC) in the inner mitochondrial membrane (IMM) requires a proper stoichiometric ratio of their subunits. Hence, misfolding of one subunit of an ETC complex results in the failure to assemble the entire complex. Consequently, the other subunits will accumulate in the mitochondrial matrix and thereby compromise mitochondrial proteostasis. Finally, ETC components are encoded by the mitochondrial and the nuclear genome. In order to maintain their respective stoichiometric ratios, the expression of mitochondrial and nuclear encoded proteins therefore has to be properly coordinated [7].

Several mitochondrial stress response pathways that maintain mitochondrial function have been described. One or more of these pathways are activated, depending on the extent to which mitochondrial proteostasis is compromised or mitochondria are damaged. For example, severely damaged mitochondria, which have irremediably lost their membrane potential, are eliminated from the functional mitochondrial network by mitochondrial-specific autophagy (mitophagy) (see for review [8]). The accumulation of unfolded or misfolded mitochondrial proteins activates the mitochondrial unfolded protein response (UPR^{mt}). This response leads to the increased production and import into mitochondria of chaperones (such as HSP60 and HSP70) and proteases (such as ClpP), which help misfolded proteins to fold properly or cause their degradation, respectively (see for review [9]). Finally, the mitochondrial hyperfusion response has recently been described in mammalian cells and in *C. elegans*. Various forms of stress, such as a decrease in complex IV activity, the inhibition of cytosolic protein synthesis or starvation, induce mitochondrial hyperfusion in order to maintain mitochondrial ATP production [10-12].

The human *LRPPRC* gene encodes a leucine-rich pentatricopeptide repeat containing protein that is imported into mitochondria and that is mutated in patients with French Canadian Leigh Syndrome, a neurodegenerative disorder associated with complex IV deficiency [13]. Inside the mitochondrial matrix, the LRPPRC protein is part of a ribonucleoprotein complex that post-transcriptionally controls the expression of specific mitochondrial mRNAs such as the mRNA coding for COX I, a component of complex IV [14,15]. We have previously shown that reducing *LRPPRC* function in mammalian tissue culture cells or reducing the function of the *LRPPRC*-like gene *mma-1* (*mma*, mitochondrial morphology-abnormal) in *C. elegans* leads to a decrease in the level of COX I and, consequently, a decrease in complex IV activity [11]. This decrease in complex IV activity is compensated by an evolutionarily conserved mitochondrial hyperfusion response [11]. COX I is one of three mitochondria-encoded subunits of complex IV. The remaining 11 subunits in mammals and 6 subunits in *C. elegans* are nuclear-encoded [16,17]. Therefore, we hypothesized that the reduction of COX I protein level upon *LRPPRC mma-1* knock-down might cause an imbalance between nuclear- and mitochondria-encoded subunits and, hence, trigger UPR^{mt}. Here we report that in addition to triggering a mitochondrial hyperfusion response, *LRPPRC mma-1* knock-down also triggers UPR^{mt} in both mammalian cell cultures and *C. elegans*. We propose that these two responses act together to maintain and restore mitochondrial function, in response to decreased complex IV activity.

RESULTS

LRPPRC siRNA leads to an imbalance between mitochondria-encoded and nuclear-encoded subunits of complex IV and triggers UPR^{mt}

Inactivation of *LRPPRC* results in a decrease in the production of mitochondria-encoded subunits of complex IV [11,14,15]. We reasoned that this decrease may lead to an imbalance between mitochondria-encoded and nuclear-encoded subunits of this complex and thereby trigger UPR^{mt}. To test this hypothesis, we inactivated *LRPPRC* in SH-SY5Y cells using small interfering RNA (siRNA) and quantified the level of COX I protein (a mitochondria-encoded subunit of complex IV) and the level of COX IV protein (a nuclear-encoded subunit of complex IV). As shown in Figure 1A, the level of COX I protein decreases after 3 days of *LRPPRC* siRNA (down to 50% of the level in control siRNA cells). In contrast, the level of COX IV protein remains stable, resulting in an imbalance between COX I and COX IV subunits with ~1.8 times more COX IV subunits than COX I subunits upon *LRPPRC* siRNA.

In order to test whether this imbalance triggers UPR^{mt}, we measured the levels of the mitochondrial chaperones HSP60 and HSP70 as well as the mitochondrial protease ClpP. We observed that 3 days of *LRPPRC* siRNA triggers a ~3-fold increase in the level of endogenous HSP70 protein (Figure 1B; n=3; p=0.0473 by one sample t-test), a ~1.3-fold increase in the level of endogenous HSP60 protein (Figure 1B; n=3; p=0.178 by one sample t-test) and a ~2.3-fold increase in the level of the endogenous mitochondrial protease ClpP (Figure 1B; n=3; p=0.0202 by one sample t-test). Similar results were observed using HEK293T cells (Figure S1). Based on these results, we conclude that the imbalance between nuclear- and mitochondria-encoded subunits of complex IV caused by *LRPPRC* siRNA triggers UPR^{mt}.

The transient activation of UPR^{mt} by *LRPPRC* siRNA correlates with the restoration of the balance between complex IV subunits

In order to test the effect of the induction of UPR^{mt} upon *LRPPRC* siRNA on the balance between nuclear- and mitochondria-encoded complex IV subunits, we performed a time course experiment. The imbalance between COX I and COX IV is first observed after 3 days of *LRPPRC* siRNA (Figure 2A). This time point

also corresponds to the highest level of induction of HSP70 and ClpP (Figure 2B). After 5 days of *LRPPRC* siRNA, the level of COX IV protein decreases (down to 50% of the level in control siRNA cells), restoring the balance between COX I and COX IV subunits (Figure 2A). This time point coincides with a decrease of the levels of HSP70 and ClpP back to the levels measured in control cells (Figure 2B). A similar transient activation of UPR^{mt} was observed in HEK293T cells (Figure S1). Therefore, the transient activation of UPR^{mt} correlates with the restoration of mitochondrial proteostasis in the context of *LRPPRC* siRNA.

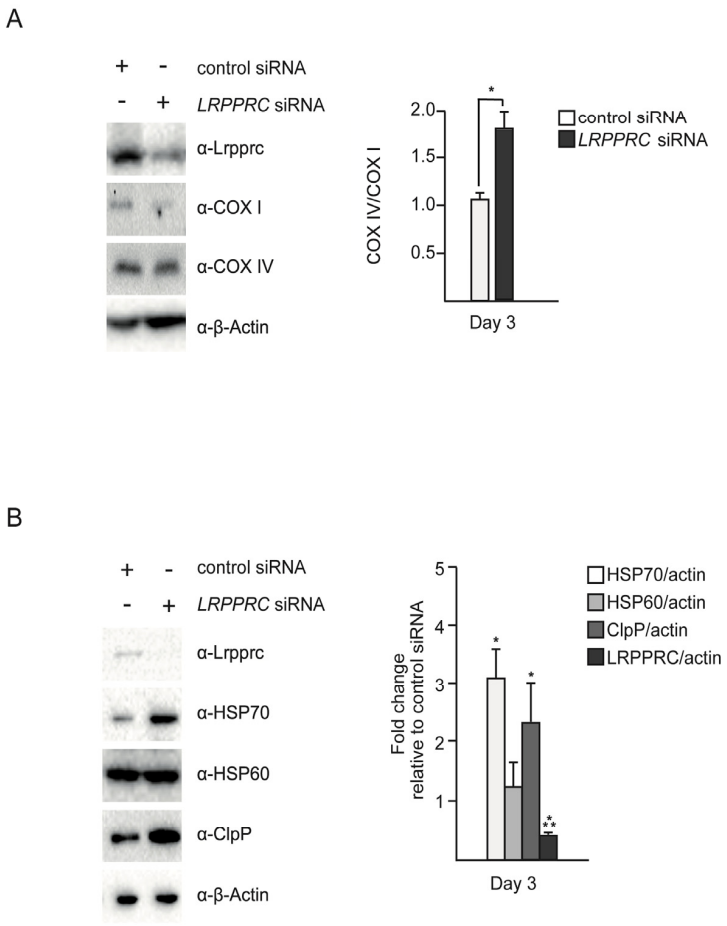

Figure 1. Silencing of *LRPPRC* leads to an imbalance between mitochondria-encoded and nuclear-encoded subunits of complex IV and triggers UPR^{mt}. SH-SY5Y cells were treated with control or *LRPPRC* siRNA for three days and transferred for 24 hours to low glucose medium (5 mM) to enhance oxidative phosphorylation. (**A**) Total protein extracts were analyzed by Western using anti-LRPPRC, anti-COX I, anti-COX IV and anti-β-Actin antibodies. COX IV/COX I ratios are indicated. (**B**) The same protein extracts as in panel **A** were also analyzed by Western using anti-LRPPRC, anti-HSP70, anti-HSP60, anti-ClpP and anti-β-Actin antibodies. Ratios relative to the control siRNA are indicated. (For all panels, quantifications are based on data from three independent experiments; average values are shown and error bars indicate s.d.; * p≤0.05, *** p≤0.001 by one way ANOVA for panel **A** and one sample t-test for panel **B**).

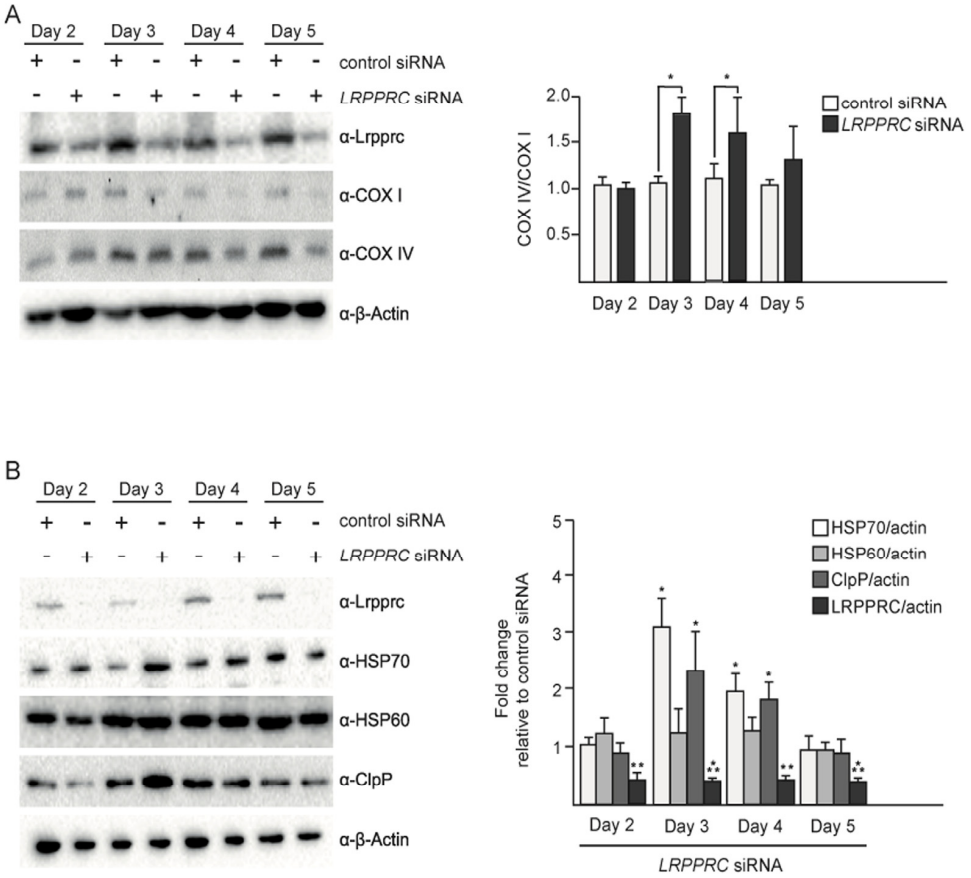

Figure 2. Upon *LRPPRC* siRNA-induced UPR^{mt}, mitochondrial proteostasis is restored. UPR^{mt} in SH-SY5Y cells treated with control or *LRPPRC* siRNA for 2, 3, 4 or 5 days and transferred for 24 hours in low glucose medium. (**A**) Total protein extracts were analyzed by Western using anti-LRPPRC, anti-COX I, anti-COX IV and anti-β-Actin antibodies. COX IV/COX I ratios are indicated. (**B**) The same protein extracts as in panel A were also analyzed by Western using anti-LRPPRC, anti-HSP70, anti-HSP60, anti-ClpP and anti-β-Actin antibodies. Ratios relative to the control siRNA are indicated. (For all panels, quantifications are based on data from three independent experiments; average values are shown and error bars indicate s.d.; * p≤0.05, ** p≤0.01, *** p≤0.001 by one way ANOVA for panel **A** and one sample t-test for panel **B**).

UPR^{mt} and mitochondrial hyperfusion are transient responses to *LRPPRC* siRNA that follow similar kinetics

We have previously shown that mitochondrial hyperfusion is a transient response, which peaks at 3 days of *LRPPRC* siRNA (Figure S2; day 3: 50% of cells have hyperfused mitochondria, 32% have tubular mitochondria and 18% have fragmented mitochondria). After 4 or 5 days of inactivation, the population of cells that display hyperfused mitochondria decreases while the population of cells that display fragmented mitochondria increases (Figure S2; day 5: 35% of cells have hyperfused mitochondria, 45% have tubular mitochondria and 28% have fragmented mitochondria). Similarly, we observed that the induction of UPR^{mt} is at its maximum at 3 days of *LRPPRC* siRNA, in both SH-SY5Y cells and HEK293T cells (Figure 2B, Figure S1). After 4 and 5 days of inactivation, the UPR^{mt} decreases in both cell lines (Figure 2B, Figure S1B). Hence, in mammalian cell culture, UPR^{mt} and the mitochondrial hyperfusion response both are transient and follow similar kinetics.

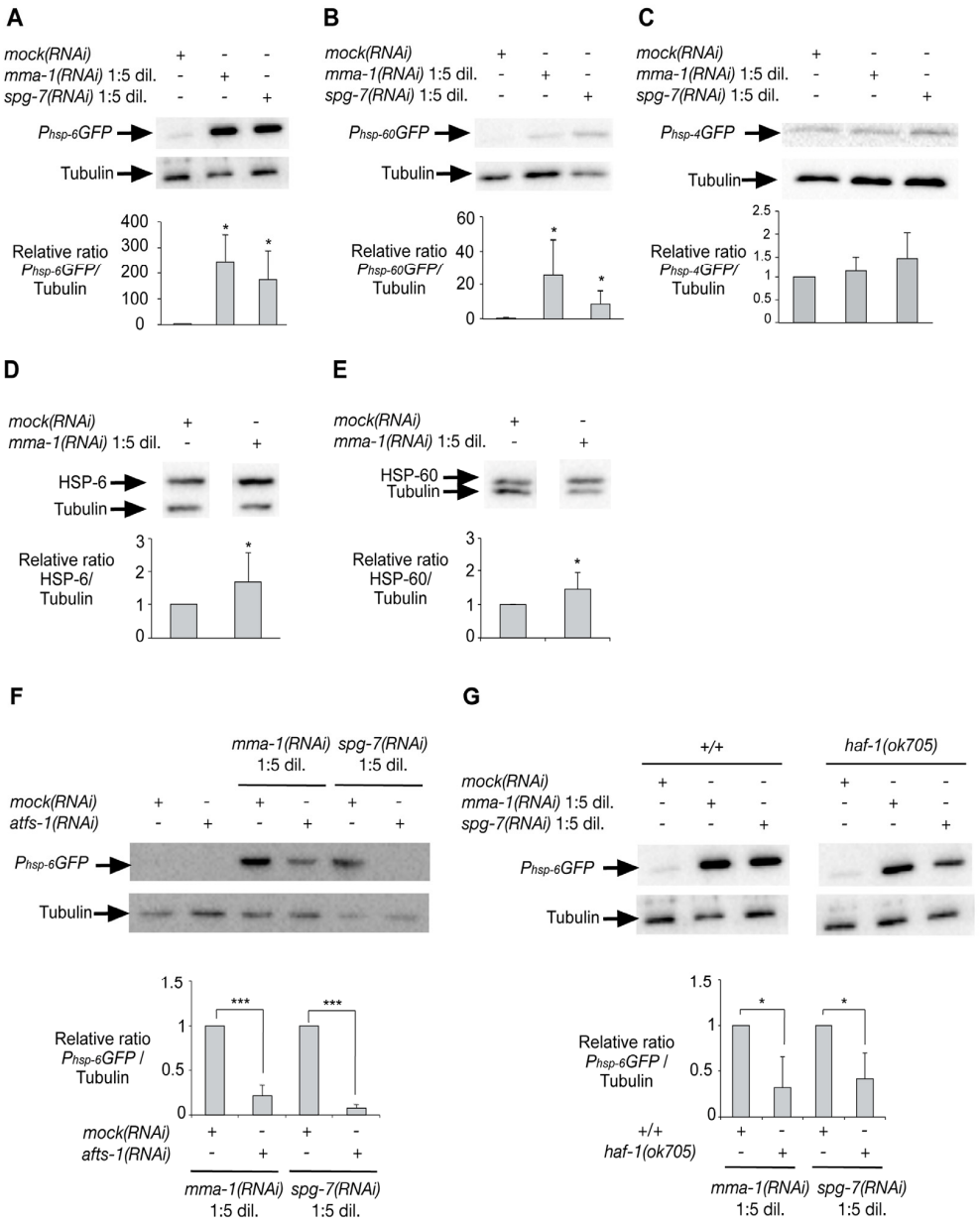

Figure 3. Inactivation of *mma-1* by RNAi in *C. elegans* induces ATFS-1-dependent UPR^{mt}. Western analysis of (**A**) $P_{hsp\text{-}6}$*GFP* (mitochondrial Hsp70), (**B**) $P_{hsp\text{-}60}$*GFP* (mitochondrial Hsp60) or (**C**) $P_{hsp\text{-}4}$*GFP* (ER BiP) reporter strains treated with *mock(RNAi)*, *mma-1(RNAi)* 1:5 dil. (diluted 1:5 (v/v) with *mock(RNAi)*) or *spg-7(RNAi)* 1:5 dil. (diluted 1:5 (v/v) with *mock(RNAi)*). Ratios of $P_{hsp\text{-}6}$*GFP*/Tubulin, $P_{hsp\text{-}60}$*GFP*/Tubulin and $P_{hsp\text{-}4}$*GFP*/Tubulin relative to the *mock(RNAi)* treated animals are indicated (n=5 for $P_{hsp\text{-}6}$*GFP* + *mma-1(RNAi)*; n=7 for $P_{hsp\text{-}6}$*GFP* + *spg-7(RNAi)*; n=6 for $P_{hsp\text{-}60}$*GFP* + *mma-1(RNAi)*; n=9 for $P_{hsp\text{-}60}$*GFP* + *spg-1(RNAi)*; n=5 for $P_{hsp\text{-}4}$*GFP*). Western analysis of the effect of *mma-1(RNAi)* on endogenous (**D**) HSP-6 or (**E**) HSP-60 protein level. Ratios of HSP-6/Tubulin and HSP-60/Tubulin relative to the *mock(RNAi)* treated animals are indicated (n=8 for HSP-6 and n=10 for HSP-60). (**F**) Western analysis of the effect of ATFS-1 on *mma-1(RNAi)*-induced UPR^{mt}. *mma-1(RNAi)* or *spg-7(RNAi)* were diluted either with *mock(RNAi)* or *atfs-1(RNAi)*. Relative ratios of $P_{hsp\text{-}6}$*GFP*/Tubulin are indicated (n=7 for *mma-1(RNAi)* and n=10 for *spg-7(RNAi)*). (**G**) Western analysis of the effect of HAF-1 on *mma-1(RNAi)*-induced UPR^{mt}. Wild-type $P_{hsp\text{-}6}$*GFP* reporter strain (+/+) or $P_{hsp\text{-}6}$*GFP* reporter strain carrying the *haf-1*(*ok705*) loss-of-function mutation were analyzed. The relative ratios of $P_{hsp\text{-}6}$*GFP*/Tubulin are indicated (n=5 for *mma-1(RNAi)* and n=6 for *spg-7(RNAi)*) (For all panels, average values are shown and error bars indicate s.d.; * p≤0.05, ** p≤0.01, *** p≤0.001 by one sample t-test).

Inactivation of the *LRPPRC*-like gene *mma-1* in *C. elegans* also induces UPR^{mt}

In order to address whether the induction of UPR^{mt} in response to *LRPPRC* siRNA is conserved, we inactivated the *LRPPRC*-like gene *mma-1* in *C. elegans*. We used the transcriptional reporters $P_{hsp-6}GFP$, $P_{hsp-60}GFP$ and $P_{hsp-4}GFP$ to monitor the expression of the genes encoding the mitochondrial HSP70 chaperone (*hsp-6*), the mitochondrial HSP60 chaperone (*hsp-60*) or the endoplasmic reticulum (ER) chaperone BiP (*hsp-4*), respectively [18]. We reduced *mma-1* function using RNA-mediated interference (RNAi) by feeding [19]. Specifically, we grew L4 larvae of the reporter strains on RNAi plates seeded with an *Escherichia coli* strain expressing double-strand RNA (dsRNA) of *mma-1*. The plates were seeded with *mma-1(RNAi)* bacteria diluted 1:5 (v/v) with *mock(RNAi)* bacteria; hereafter referred to as '*mma-1(RNAi)* 1:5 dil.'. The expression of the reporters was analyzed four days later in the F1 generation. Using these conditions, the level of MMA-1 protein is reduced by ~40% (see below, Figure S4). As shown in Figure 3, the $P_{hsp-6}GFP$ reporter is strongly up-regulated in response to *mma-1(RNAi)* (on average ~200-fold compared to *mock(RNAi)*; Figure 3A; n=5; p=0.037 by one sample t-test). $P_{hsp-60}GFP$ expression was also increased in *mma-1(RNAi)* animals compared to *mock(RNAi)* animals, albeit to a lesser extent (Figure 3B; n=9; p=0.011 by one sample t-test). Finally, *mma-1* knock-down did not affect the expression of the ER chaperone *hsp-4* (Figure 3C; n=5; p=0.36 by one sample t-test). We also tested the effect of reducing the activity of the *C. elegans* homolog of paraplegin *spg-7*, which has previously been shown to induce UPR^{mt} [18]. Using the RNAi conditions described above, the inactivation of *spg-7* induces a strong up-regulation of the $P_{hsp-6}GFP$ reporter and a weak up-regulation of the $P_{hsp-60}GFP$ reporter but has no effect on the expression of the $P_{hsp-4}GFP$ reporter (Figure 3).

In order to confirm the effect of *mma-1(RNAi)* on the expression of *hsp-6* and *hsp-60* at the levels of endogenous HSP-6 and HSP-60 protein, we used a mouse monoclonal anti-HSP-60 antibody [20] and generated rabbit polyclonal anti-HSP-6 antibodies. We confirmed that the anti-HSP-6 antibodies specifically recognize HSP-6 (Figure S3). Using these antibodies we found that the inactivation of *mma-1* by RNAi leads to a ~1.7-fold increase in the level of endogenous HSP-6 protein (Figure 3D; n=8; p=0.024 by one sample t-test). In addition, we found that *mma-1(RNAi)* induces a ~1.4-fold increase in the level of endogenous HSP-60 protein (Figure 3E; n=10; p=0.022 by one sample t-test). The discrepancy between the level of induction for endogenous proteins (~1.4-fold and ~1.7-fold for HSP-60 and HSP-6, respectively) and for transcriptional reporters (~20-fold and ~200-fold for $P_{hsp-60}GFP$ and $P_{hsp-6}GFP$, respectively) is most likely due to the copy number of the $P_{hsp-6}GFP$ and $P_{hsp-60}GFP$ transgenes integrated in the genome of the reporter strains; however, we cannot exclude that this discrepancy is also caused by post-transcriptional regulations of *hsp-6* and/or *hsp-60* expression. Based on these results we conclude that *mma-1(RNAi)* induces UPR^{mt} and the transcriptional up-regulation of the *hsp-6* and *hsp-60* genes, which results in a significant increase in the level of endogenous HSP-6 and HSP-60 protein.

***mma-1(RNAi)*-induced up-regulation of *hsp-6* transcription is dependent on ATFS-1 and HAF-1**

In *C. elegans*, UPR^{mt} is dependent on the peptide exporter HAF-1 as well as the bZip transcription factor ATFS-1 [21,22]. Consistent with previous studies [22], we confirmed that the inactivation of *atfs-1* by RNAi suppresses the up-regulation of the $P_{hsp-6}GFP$ reporter induced by *spg-7(RNAi)* (Figure 3F; n=7; p=0.0001 by one sample t-test). Furthermore, we found that *mma-1(RNAi)*-induced UPR^{mt} is suppressed by *atfs-1(RNAi)* as well (Figure 3F; n=10; p=0.0001 by one sample t-test). To rule out that the effects observed are due to differences in RNAi efficiency, we quantified the knock-down of *mma-1* using anti-MMA-1 antibodies [11]. As shown in Figure S4A, the efficiency of *mma-1(RNAi)* in *atfs-1(RNAi)* animals is similar to that in wild-type animals (reduction by ~40% on average). Hence, the *mma-1(RNAi)*-induced up-regulation of *hsp-6* transcription is dependent on ATFS-1. In contrast, the *haf-1* loss-of-function mutation *ok705* only partially suppresses the up-regulation of $P_{hsp-6}GFP$ in response to *mma-1(RNAi)* (Figure 3G; n=5; p=0.0217 by one sample t-test). We observed a similar result for *spg-7(RNAi)*-induced $P_{hsp-6}GFP$ up-regulation (Figure 3G; n=6; p=0.017 by one sample t-test). We confirmed that the effects observed were not due to differences in the efficiency of *mma-1(RNAi)* (Figure S4B). Therefore, *mma-1(RNAi)* induces UPR^{mt} in a manner that is dependent on the bZip transcription factor ATFS-1 and that is partially dependent on the peptide exporter HAF-1.

Strong depletion of MMA-1 protein leads to both mitochondrial hyperfusion and UPR^{mt} induction whereas mild depletion of MMA-1 protein only leads to UPR^{mt}

When growing animals on 'non-diluted' *mma-1(RNAi)* plates, we achieved on average an ~80% reduction in the level of MMA-1 protein (Figure 4A; *mma-1(RNAi)*). Under these conditions, as previously reported, animals

exhibit hyperfused mitochondria in body wall muscle cells (76%; Figure 4A; n=17; two independent experiments) [11]. These animals also show a stronger UPR^{mt} as reflected by the up-regulation of the $P_{hsp-6}GFP$ reporter (on average ~600-fold compared to *mock(RNAi)* animals; Figure 4A). When reducing the level of MMA-1 protein by only 40% (*mma-1(RNAi)* 1:5 dil.), the $P_{hsp-6}GFP$ reporter is still up-regulated (on average 200-fold compared to *mock(RNAi)* animals; Figure 4A); however, these animals do not exhibit mitochondrial hyperfusion (6%; Figure 4A; n=16; two independent experiments). Hence, mild depletion of MMA-1 protein leads to the activation of the UPR^{mt} pathway and strong depletion of MMA-1 protein additionally leads to the activation of the mitochondrial hyperfusion response pathway.

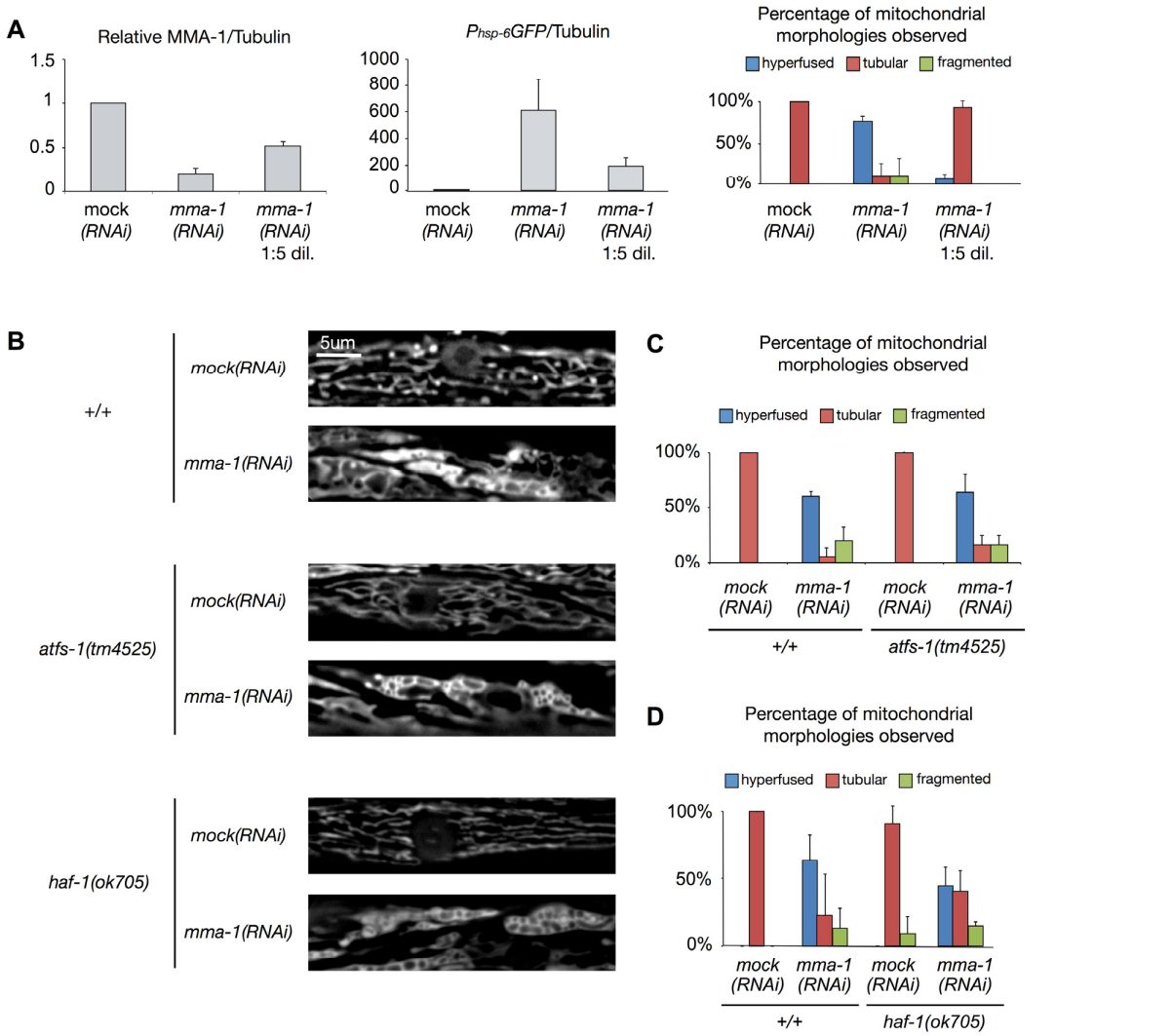

Figure 4. *mma-1(RNAi)*-induced mitochondrial hyperfusion is not dependent on ATFS-1 or HAF-1. (**A**) Strong depletion of MMA-1 protein (*mma-1(RNAi)*) leads to both mitochondrial hyperfusion and UPR^{mt} response whereas mild depletion of MMA-1 protein (*mma-1(RNAi)* 1:5 dil.) only leads to UPR^{mt}. Average relative ratios of MMA-1/Tubulin and $P_{hsp-6}GFP$/Tubulin are indicated. Mitochondrial morphology in body wall muscles was assessed in L4 larvae of the F1 generation. Percentage of animals showing fragmented, tubular or hyperfused mitochondria are indicated (n>10 for each condition; average values are shown and error bars indicate s.d.). (**B**) Fluorescence microscopy analysis of wild-type $P_{myo-3}mitoGFP$ reporter strain (+/+) or $P_{myo-3}mitoGFP$ reporter strain carrying the *haf-1(ok705)* mutation or *atfs-1(tm4525)* mutation. (**C-D**) Quantification of the different mitochondrial morphologies observed (at least 15 animals were analyzed for each condition; two independent experiments were performed for panel **C**; three independent experiments were performed for panel **D**; average values are shown and error bars indicate s.d.).

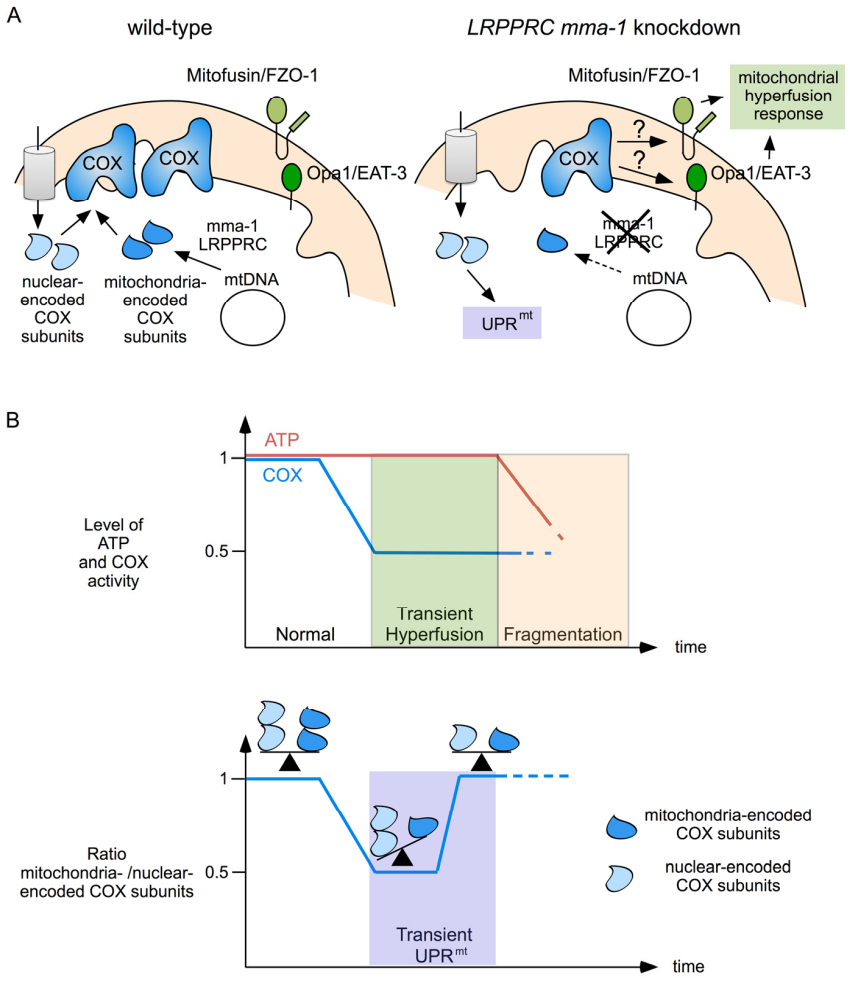

Figure 5. Mitochondrial hyperfusion and UPR^{mt} act together to protect mitochondrial function. (**A**) Complex IV of the ETC is composed of mitochondria-encoded and nuclear-encoded subunits. Upon *LRPPRC mma-1* RNAi, the level of mitochondria-encoded subunits decreases, leading to a reduction in complex IV activity, which triggers the mitochondrial hyperfusion response and an accumulation of unassembled nuclear-encoded subunits, which triggers UPR^{mt}. (**B**) While mitochondrial hyperfusion helps to maintain ATP level in response to a reduction in complex IV activity [11], UPR^{mt} helps to restore the balance between mitochondria-encoded and nuclear-encoded subunits of this complex. Mitochondrial hyperfusion can only compensate for reduced complex IV activity for a limited time. Prolonged inactivation of *LRPPRC mma-1* eventually leads to mitochondrial fragmentation and drop in ATP level as previously shown [11].

mma-1(RNAi)-induced mitochondrial hyperfusion is independent of HAF-1 and ATFS-1

In order to test whether the mitochondrial hyperfusion response induced by the inactivation of *mma-1* is dependent on HAF-1 and ATFS-1, we used a transgene (*bcIs78* [$P_{myo\text{-}3}$*mitoGFP*]) that expresses mitochondrial matrix-targeted GFP in body wall muscles, which allows us to monitor steady-state mitochondrial morphology in these cells [11]. In an otherwise wild-type background, *mma-1(RNAi)* causes mitochondrial hyperfusion (64%, n=30, Figure 4B-D, three independent experiments) [11]. Similarly, *mma-1(RNAi)* causes mitochondrial hyperfusion in animals homozygous for the *atfs-1* loss-of-function mutation *tm4525* (67%, Figure 4B-C; n=19, two independent experiments). Finally, *mma-1(RNAi)* also causes mitochondrial hyperfusion in animals homozygous for the *haf-1* loss-of-function mutation *ok705* (45%; Figure 4B-D; n=33; three independent experiments). Compared to the response in the wild-type and *atfs-1*(*tm4525*) background, the response in the *haf-1*(*ok705*)

background is slightly reduced; however, the difference is not statistically significant (p=0.22 by Student t-test). Based on these results we conclude that *mma-1(RNAi)*-induced mitochondrial hyperfusion is independent of ATFS-1 and HAF-1.

ATFS-1-dependent UPR^{mt} is not essential for viability in response to *mma-1(RNAi)*

We previously showed that *mma-1(RNAi)* causes synthetic embryonic lethality and synthetic midlarval arrest in the *fzo-1(tm1133)* loss-of-function mutant background, indicating that mitochondrial hyperfusion is essential for viability in response to *mma-1(RNAi)* [11]. To test whether UPR^{mt} is also essential for viability in response to *mma-1(RNAi),* we inactivated *mma-1* in animals carrying a loss-of-function mutation in the *atfs-1* gene (*atfs-1(tm4525)*) [22]. We found that *mma-1(RNAi)* does not cause any obvious embryonic lethality or midlarval arrest in *atfs-1(tm4525)* mutant animals (Figure S5A). We also performed the experiment using double RNAi (*afts-1(RNAi)+mma-1(RNAi)*) and did not observe any obvious synthetic lethality or arrest (Figure S5B). This indicates that in response to *mma-1(RNAi),* mitochondrial hyperfusion is essential for viability while ATFS-1-dependent UPR^{mt} is not.

DISCUSSION

Depending on the type and the severity of the stress to which mitochondria are exposed, different mitochondrial stress responses (such as UPR^{mt}, mitochondrial hyperfusion or mitophagy) can be activated in order to protect mitochondrial function [23]. Here, we show that reducing *LRPPRC* or *mma-1* function leads to an evolutionary conserved co-activation of UPR^{mt} and mitochondrial hyperfusion. Depletion of LRPPRC or MMA-1 protein results in a decrease in the production of mitochondria-encoded subunits of complex IV and thereby causes a reduction of complex IV activity [11,14,15]. Depletion of LRPPRC or MMA-1 protein also leads to an imbalance between nuclear-encoded and mitochondria-encoded subunits of this complex. We show that the activation of the UPR^{mt} occurs when this balance and, hence mitochondrial proteostasis, is disrupted (Figure 2; day 3 of *LRPPRC* siRNA). This finding suggests that the accumulation of unassembled complex IV subunits is most likely the signal that triggers UPR^{mt}. Furthermore, our data indicate that UPR^{mt} is transiently activated until mitochondrial proteostasis is restored (Figure 2; day 5 of *LRPPRC* siRNA). We, therefore, propose that the transient activation of UPR^{mt} participates in the restoration of mitochondrial proteostasis by either proteolytic degradation of unassembled subunits by ClpP or assisted folding of nascent subunits by HSP70. In addition, the response may also involve the down-regulation of the genes encoding nuclear-encoded subunits of complex IV.

Whereas UPR^{mt} and mitochondrial hyperfusion in response to *LRPPRC mma-1* RNAi follow similar kinetics, genetic experiments in *C. elegans* indicate that the pathways that mediate these two responses are distinct. Specifically, *LRPPRC mma-1* RNAi-induced UPR^{mt} is dependent on the previously described HAF-1, ATFS-1 pathway, whereas *LRPPRC mma-1* RNAi-induced mitochondrial hyperfusion is not. This notion is furthermore supported by the fact that in *C. elegans,* a mild depletion of MMA-1 protein activates only the UPR^{mt} pathway whereas a strong depletion of MMA-1 activates both pathways. The pathway through which a reduction in *LRPPRC mma-1* function induces mitochondrial hyperfusion remains to be elucidated. Similarly, the mechanism through which mitochondrial hyperfusion and UPR^{mt} are coordinated is currently unknown.

We propose that the mitochondrial hyperfusion response and UPR^{mt} act together to maintain and restore mitochondrial function (Figure 5). We have previously shown that mitochondrial hyperfusion helps to maintain cellular ATP levels despite a reduction in complex IV activity caused by *LRPPRC mma-1* RNAi [11]. We now propose that this transient compensation enables the cell to restore the balance between mitochondria-encoded and nuclear-encoded subunits of complex IV. However, as previously shown, prolonged inactivation of *LRPPRC mma-1* eventually leads to mitochondrial fragmentation, a drop in ATP level and the loss of cellular and organismal functions [11]. The two mitochondrial stress response pathways we unraveled are therefore likely to be important for the maintenance of mitochondrial function in response to moderate and short-term changes in mitochondrial proteostasis. Interestingly, UPR^{mt} as well as an 'elongation' of mitochondria are also induced in response to the infection of *C. elegans* by *Pseudomonas aeruginosa* [24]; however, how these two stress responses are induced in this context remains to be determined. In contrast, UPR^{mt} and mitochondrial hyperfusion may not protect against more drastic and long-term changes in mitochondrial proteostasis, such as in *C. elegans* in which *mma-1* has been chronically inactivated or in French Canadian Leigh Syndrome patients carrying mutations in the *LRPPRC* gene. In cell lines derived from these patients, mitochondria are fragmented [15], which indicates that the mitochondrial hyperfusion response has already failed. Whether UPR^{mt} is activated in these cell lines is currently unknown. In case it is

activated, it will be interesting to determine whether this pathway contributes to the pathophysiology of this neurodegenerative disorder, which has not been completely elucidated yet.

We previously showed that the mitochondrial hyperfusion response is essential for viability in response to *mma-1(RNAi)* [11]. In contrast, we present evidence that ATFS-1-dependent UPR^{mt} is not essential for viability upon inactivation of *mma-1*. Furthermore, we show that ATFS-1-dependent UPR^{mt} is also not essential for viability in response to *spg-7(RNAi)*. One possible explanation for this finding is the existence of an ATFS-1-independent UPR^{mt} pathway. Indeed, Haynes and co-workers have shown that while *spg-7(RNAi)* induces the up-regulation of 685 genes, 294 of these genes are still up-regulated in *atfs-1(tm4525)* mutant animals [22]. Hence, in the context of *mma-1* inactivation, the ATFS-1-independent UPR^{mt} in combination with the mitochondrial hyperfusion response may be sufficient for the completion of embryonic and larval development.

The effect of the activation of UPR^{mt} on aging remains controversial. While Houtkooper *et al* reported an extension of lifespan in response to the activation of UPR^{mt} [7], Bennett *et al* observed no clear correlation between UPR^{mt} and lifespan [25]. We and others have previously shown in *C. elegans* and in rat that mitochondrial fragmentation increases with age and that this fragmentation is accompanied with a loss of mitochondrial volume [26,27]. Interestingly, a recent study reports that fibroblasts isolated from long-lived human individuals exhibit hyperfused mitochondria [28]. While the genetic determinants resulting in this change in mitochondrial morphology remain unknown, the mitochondrial hyperfusion in the cells of these individuals has been shown to increase mitochondrial mass by preventing mitophagy [28]. Consequently, while the activity of their individual mitochondria decreases with age, the overall mitochondrial function of their cells is maintained, implicating a beneficial role of mitochondrial hyperfusion in aging [28]. In conclusion, a better understanding of UPR^{mt} and the mitochondrial hyperfusion response has not only the potential to increase our knowledge of how cells respond to mitochondrial stress under physiological and pathophysiogical conditions (i.e. French Canadian Leigh Syndrome) but also during aging.

MATERIALS AND METHODS

General *C. elegans* methods and strains. *C. elegans* strains were cultured as previously described [29]. Bristol N2 was used as the wild-type strain. Mutations used in this study were described by Riddle and co-workers [30] except: (LG IV) *haf-1*(*ok705*) (OMRF Knockout Group); (LG V) *atfs-1*(*tm4525*) (National BioResource Project). A summary of the transgenic lines is provided in Table S1.

C. elegans RNA interference. RNAi by feeding was performed as previously described [11] with the following modifications. RNAi plates containing 1 mM IPTG were inoculated with 50 µl of 0.5 OD_{600nm}/ml of concentrated *mma-1(RNAi)* or *spg-7(RNAi)* bacterial clones from the Ahringer library [31] or diluted 1:5 (v/v) with *mock(RNAi)* bacteria (HT115 bacteria transformed with the empty RNAi feeding vector pPD129.36) or *atfs-1(RNAi)* bacteria. 24 hours later, L4 larvae were inoculated on the RNAi plates and incubated at 20ºC for 4 days. Mitochondrial morphology in L4 larvae of the F1 generation was analyzed by fluorescent microscopy as described [32]. For protein analyses, mixed-stage populations of worms were harvested and analyzed as described below. For the analysis of the effect of RNAi on *C. elegans* development, three wild-type (+/+), three *atfs-1(tm4525)* and 15 *fzo-1(tm1133)* L4 animals (15 animals of the *fzo-1(tm1133)* genotype were used since the broodsize of these animals is smaller) were inoculated on *mock(RNAi)*, *mma-1(RNAi) or spg-7(RNAi)* plates and incubated at 20°C for 18 hours. For the double RNAi experiment, three wild-type L4 larvae were inoculated on *mock(RNAi)*, *atfs-1(RNAi)*, *mma-1(RNAi)* (diluted 1:5 with *mock(RNAi)* or *atfs-1(RNAi)*) *or spg-7(RNAi)* (diluted 1:5 with *mock(RNAi)* or *atfs-1(RNAi)*) plates and incubated at 20°C for 18 hours. The adults were then transferred onto freshly seeded RNAi plates and incubated for an additional three hours at 20°C. After removing the adults, the embryos laid during these three hours were counted. 24 hours later, the number of unhatched embryos was counted to determine the embryonic lethality. The number of animals that reached adulthood by day 5 and the number of animals that underwent a midlarval arrest were also counted.

Mammalian cell culture and transfection. SH-SY5Y cells were cultivated in DMEM:F12 supplemented with 15% FBS (Sigma), 1% non essential amino acids and 1% penicillin/streptomycin (Invitrogen); HEK293T cells were cultivated in DMEM supplemented with 10% FBS (Sigma) and 1% penicillin/streptomycin (Invitrogen); both cell lines were passaged twice a week and kept at 37°C with 5% CO_2. For RNA interference, cells were transfected reversely with control stealth siRNA medium GC or stealth siRNA oligos targeting *LRPPRC* using Lipofectamine RNAiMax in OPTI-MEM (Invitrogen). 24 hours after transfection, fresh

culture medium (25 mM glucose) was added. For the analysis of mitochondrial morphology, cells were kept in normal culture medium until harvested. For the analysis of UPR^{mt}, the normal culture medium was replaced with medium containing only 5 mM glucose 24 hours before analysis.

Protein analysis. Rabbit polyclonal anti–HSP-6 antibodies were generated using the antigenic peptide C^{472}QEAKTAEEPKKEQN (cysteine plus HSP-6 C-terminal sequence) by Thermo Fisher Scientific, as previously described [33] and used at 1:5000 for Western analysis. Worm protein extracts were subjected to SDS/PAGE and Western. To detect HSP-60, GFP and α-Tubulin, we used a mouse monoclonal antibody developed by Nonet and co-workers and available at DHSB [20] (1:2000), rabbit polyclonal antibodies from Abcam ab290 (1:2000) and a mouse monoclonal antibody from Abcam ab7291 (1:2000), respectively. Images were quantified using the ChemiDoc XRS+ System (Bio-Rad). The data presented are ratios relative to the *mock(RNAi)*. Only samples for which *mma-1* knock-down was at least 20% were used for the statistically analysis. Statistical analysis was performed by using one sample t-test. Normality of the data was assessed by Shapiro-Wilk Normality test.

SH-SY5Y and HEK293T cells were harvested with pre-warmed 1x Laemmli-sample buffer and boiled for 10 minutes at 95°C and then subjected to SDS/PAGE and Western. The following antibodies were used: mouse monoclonal anti-β-Actin (Sigma AC-15, 1:5000), mouse monoclonal anti-LRP130 (sc-166178, 1:1000), goat polyclonal anti-HSP60 (sc-1052, 1:2000), rabbit polyclonal anti mortalin/mitochondrial HSP70 (sc-13967, 1:1000), rabbit polyclonal anti-ClpP (sc-134496, 1:1000), goat polyclonal anti-COXI (sc-48143, 1:500) and goat polyclonal anti-COXIV (sc-69359, 1:1000) (With the exception of the anti-β-Actin, all the antibodies were provided from Santa Cruz Biotechnology).

Analysis of mitochondrial morphology in SH-SY5Y cells. Mitochondrial morphology was analyzed as previously described with the following modifications [11]. Cells grown on glass coverslips were fixed with PBS 3.7% PFA at 20°C for 10 minutes and permeabilized with PBS 0.2% Triton X-100 for 10 minutes at 20°C. The coverslips were blocked with PBS 5% BSA for 1 hour at 4°C and incubated overnight at 4°C in PBS 5% BSA with polyclonal anti-TOM20 antibodies (1:2000, Santa Cruz Biotechnology). After three washes with PBS, the coverslips were incubated with an Alexa555 goat anti-rabbit antibody (1:2000, Molecular Probes) in PBS 5% BSA for 2 hours at 20°C. After three washes with PBS, three washes with PBS 0.2% Tween and three washes with PBS, the glass coverslips were mounted on glass slides with MOWIOL 4-88 containing DAPI (Sigma). At least 300 cells per coverslip were counted in a blinded manner. Results are based on three independent experiments.

ACNOWLEDGMENTS

We thank Eric Lambie, Nikola Wagener, Tamara Mikeladze-Dvali, Nadin Memar and members of the B.C. laboratory for comments on the manuscript; N. Lebedeva, L. Jocham, and M. Schwarz for excellent technical support; S. Mitani (National BioResource Project, Tokyo, Japan) for *atfs-1(tm4525)*; and the *Caenorhabditis elegans* Genetics Center (supported by the National Institutes of Health National Center for Research Resources) for strains. The anti-HSP-60 antibody developed by Nonet, M.L., Hadwiger, G. and Dour, S was obtained from the Developmental Studies Hybridoma Bank (DSHB), created by the NICHD of the NIH and maintained at The University of Iowa, Department of Biology, Iowa City, IA 52242.

Funding

This work was funded by NIH grant GM076651 and CIPSM (to BC).

Conflict of interest statement

The authors declare that they have no conflict of interest.

REFERENCES

1. Blackstone NW. The impact of mitochondrial endosymbiosis on the evolution of calcium signaling. Cell calcium. 2015; 57:133-139.

2. Saraste M. Oxidative phosphorylation at the fin de siecle. Science. 1999; 283:1488-1493.

3. Wang C, and Youle RJ. The role of mitochondria in apoptosis. Annual review of genetics. 2009; 43:95-118.

4. Larsson NG. Somatic mitochondrial DNA mutations in mammalian aging. Annual review of biochemistry. 2010; 79:683-706.

5. Niforou K, Cheimonidou C, and Trougakos IP. Molecular chaperones and proteostasis regulation during redox imbalance. Redox biology. 2014; 2:323-332.

6. Jensen MB, and Jasper H. Mitochondrial proteostasis in the control of aging and longevity. Cell metabolism. 2014; 20:214-225.

7. Houtkooper RH, Mouchiroud L, Ryu D, Moullan N, Katsyuba E, Knott G, Williams RW, and Auwerx J. Mitonuclear protein imbalance as a conserved longevity mechanism. Nature. 2013; 497:451-457.

8. Narendra D, Walker JE, and Youle R. Mitochondrial quality control mediated by PINK1 and Parkin: links to parkinsonism. Cold Spring Harbor perspectives in biology. 2012; 4: a011338.
9. Pellegrino MW, Nargund AM, and Haynes CM. Signaling the mitochondrial unfolded protein response. Biochimica et biophysica acta. 2013; 1833:410-416.
10. Gomes LC, Di Benedetto G, and Scorrano L. During autophagy mitochondria elongate, are spared from degradation and sustain cell viability. Nature cell biology. 2011; 13:589-598.
11. Rolland SG, Motori E, Memar N, Hench J, Frank S, Winklhofer KF, and Conradt B. Impaired complex IV activity in response to loss of *LRPPRC* function can be compensated by mitochondrial hyperfusion. Proceedings of the National Academy of Sciences of the United States of America. 2013; 110:E2967-2976.
12. Tondera D, Grandemange S, Jourdain A, Karbowski M, Mattenberger Y, Herzig S, Da Cruz S, Clerc P, Raschke I, Merkwirth C, Ehses S, Krause F, Chan DC et al. SLP-2 is required for stress-induced mitochondrial hyperfusion. The EMBO journal. 2009; 28:1589-1600.
13. Mootha VK, Lepage P, Miller K, Bunkenborg J, Reich M, Hjerrild M, Delmonte T, Villeneuve A, Sladek R, Xu F, Mitchell GA, Morin C, Mann M, et al. Identification of a gene causing human cytochrome c oxidase deficiency by integrative genomics. Proceedings of the National Academy of Sciences of the United States of America. 2003; 100:605-610.
14. Ruzzenente B, Metodiev MD, Wredenberg A, Bratic A, Park CB, Camara Y, Milenkovic D, Zickermann V, Wibom R, Hultenby K, Erdjument-Bromage H, Tempst P, Brandt U, et al. LRPPRC is necessary for polyadenylation and coordination of translation of mitochondrial mRNAs. The EMBO journal. 2012; 31:443-456.
15. Sasarman F, Brunel-Guitton C, Antonicka H, Wai T, Shoubridge EA, and Consortium L. LRPPRC and SLIRP interact in a ribonucleoprotein complex that regulates posttranscriptional gene expression in mitochondria. Molecular biology of the cell. 2010; 21:1315-1323.
16. Balsa E, Marco R, Perales-Clemente E, Szklarczyk R, Calvo E, Landazuri MO, and Enriquez JA. NDUFA4 is a subunit of complex IV of the mammalian electron transport chain. Cell metabolism. 2012; 16:378-386.
17. Lemire B. Mitochondrial genetics. WormBook : the online review of *C. elegans* biology. 2005; 1-10
18. Yoneda T, Benedetti C, Urano F, Clark SG, Harding HP, and Ron D. Compartment-specific perturbation of protein handling activates genes encoding mitochondrial chaperones. Journal of cell science. 2004; 117:4055-4066.
19. Timmons L, Court DL, and Fire A. Ingestion of bacterially expressed dsRNAs can produce specific and potent genetic interference in *Caenorhabditis elegans*. Gene. 2001; 263:103-112.
20. Hadwiger G, Dour S, Arur S, Fox P, and Nonet ML. A monoclonal antibody toolkit for *C. elegans*. PloS one. 2010; 5:e10161.
21. Haynes CM, Yang Y, Blais SP, Neubert TA, and Ron D. The matrix peptide exporter HAF-1 signals a mitochondrial UPR by activating the transcription factor ZC376.7 in *C. elegans*. Molecular cell. 2010; 37:529-540.
22. Nargund, AM, Pellegrino MW, Fiorese CJ, Baker BM, and Haynes CM. Mitochondrial import efficiency of ATFS-1 regulates mitochondrial UPR activation. Science. 2012; 337:587-590.
23. Friedman JR, and Nunnari J. Mitochondrial form and function. Nature. 2014; 505:335-343.
24. Pellegrino MW, Nargund AM, Kirienko NV, Gillis R, Fiorese CJ, and Haynes CM. Mitochondrial UPR-regulated innate immunity provides resistance to pathogen infection. Nature. 2014; 516:414-417.
25. Bennett CF, Vander Wende H, Simko M, Klum S, Barfield S, Choi H, Pineda VV, Kaeberlein M Activation of the mitochondrial unfolded protein response does not predict longevity in *Caenorhabditis elegans*. Nature communications. 2014; 5:3483.
26. Regmi SG, Rolland SG, Conradt B. Age-dependent changes in mitochondrial morphology and volume are not predictors of lifespan. Aging. 2014; 6:118-130.
27. Iqbal S, Ostojic O, Singh K, Joseph AM, Hood DA. Expression of mitochondrial fission and fusion regulatory proteins in skeletal muscle during chronic use and disuse. Muscle & nerve. 2013; 48:963-970.
28. Sgarbi G, Matarrese P, Pinti M, Lanzarini C, Ascione B, Gibellini L, Dika E, Patrizi A, Tommasino C, Capri M, Cossarizza A, Baracca A, Lenaz G et al. Mitochondria hyperfusion and elevated autophagic activity are key mechanisms for cellular bioenergetic preservation in centenarians. Aging. 2014; 6:296-310.
29. Brenner S. The genetics of *Caenorhabditis elegans*. Genetics. 1974; 77:71-94.
30. Riddle DL, Blumenthal T, Meyer BJ, and Priess JR. Introduction to *C. elegans*. in *C. elegans II* (Riddle, D. L., Blumenthal, T., Meyer, B. J., and Priess, J. R. eds.), 2nd Ed., Cold Spring Harbor (NY). 1997.
31. Kamath RS, and Ahringer J. Genome-wide RNAi screening in *Caenorhabditis elegans*. Methods. 2003; 30:313-321.
32. Rolland SG, Lu Y, David CN, and Conradt B. The BCL-2-like protein CED-9 of *C. elegans* promotes FZO-1/Mfn1,2- and EAT-3/Opa1-dependent mitochondrial fusion. The Journal of cell biology. 2009; 186:525-540.
33. Yokoyama K, Fukumoto K, Murakami T, Harada S, Hosono R, Wadhwa R, Mitsui Y, and Ohkuma S. Extended longevity of *Caenorhabditis elegans* by knocking in extra copies of hsp70F, a homolog of *mot-2* (mortalin)/mthsp70/Grp75. FEBS letters. 2002; 516:53-57.

SUPPLEMENTARY INFORMATION

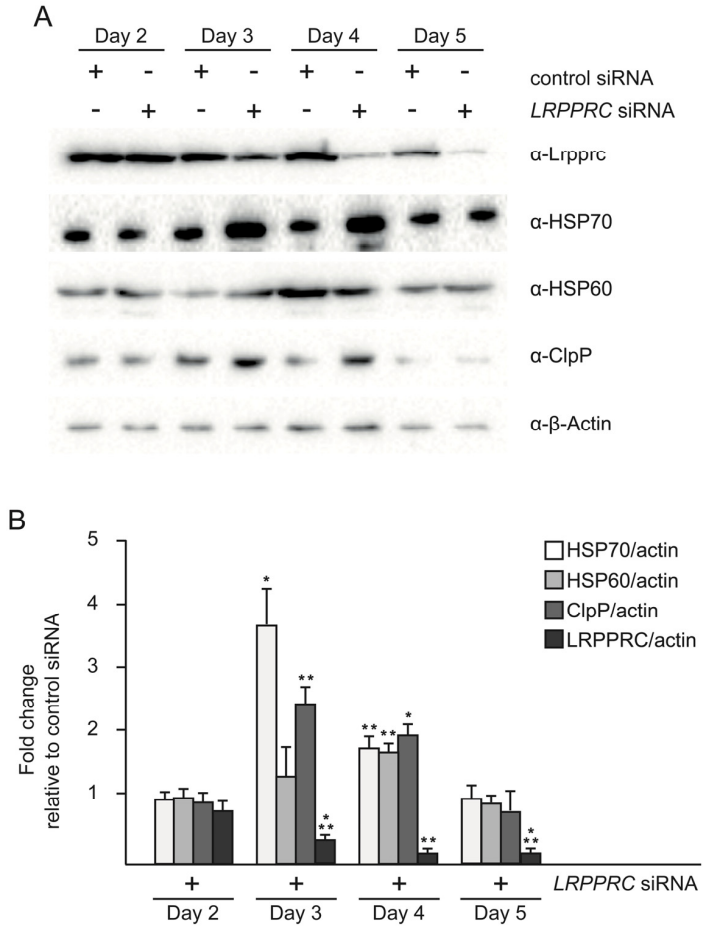

Figure S1. Silencing of *LRPPRC* also induces UPR^{mt} in HEK293T cells. UPR^{mt} in HEK293T cells treated with control or *LRPPRC* siRNA for 2, 3, 4 or 5 days and transferred for 24 hours into low glucose medium. Total protein extracts were then analyzed by Western using anti-LRPPRC, anti-HSP70, anti-HSP60, anti-ClpP and anti-β-Actin antibodies. Quantifications were performed on data from three independent experiments (For all panels, average values are shown and error bars indicate s.d.; * p≤0.05, ** p≤0.01 and *** p≤0.001 by one sample t-test).

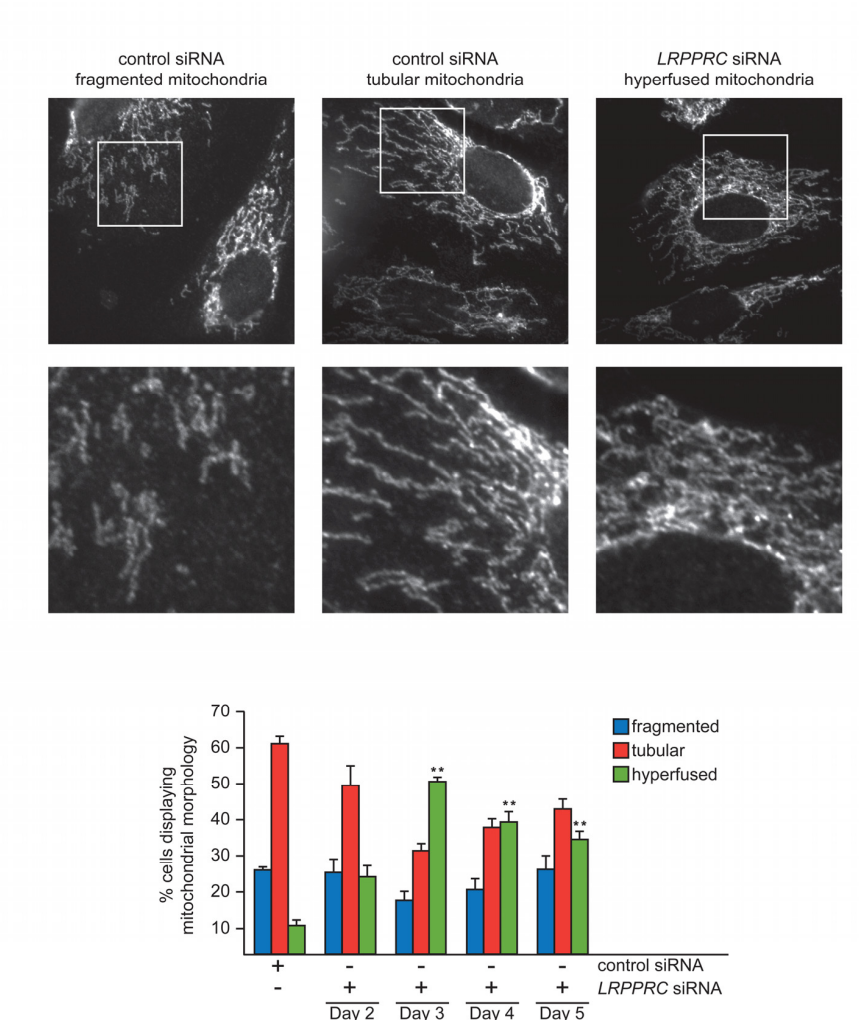

Figure S2. Silencing of *LRPPRC* induces mitochondrial hyperfusion in SH-SY5Y cells. Mitochondrial morphology of SH-SY5Y cells treated with control or *LRPPRC* siRNA for 2, 3, 4 or 5 days. Representative mitochondrial morphologies visualized using an anti-Tom20 antibody are indicated. Quantifications are based on data from three independent experiments. (n=300 cells per condition and experiment; average values are shown and error bars indicate s.d.; * p≤0.05, ** p≤0.01 and *** p≤0.001 by one way ANOVA).

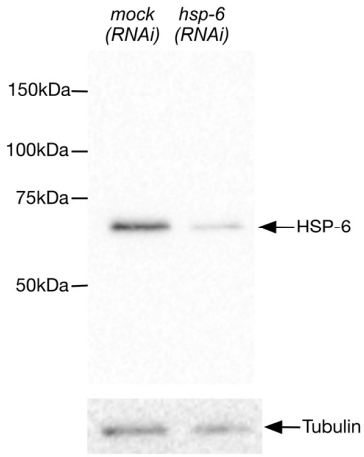

Figure S3. Rabbit polyclonal anti-HSP-6 antibodies recognize specifically *C. elegans* HSP-6 protein. L4 larvae of N2 (wild-type) were inoculated onto *mock(RNAi)* or *hsp-6(RNAi)* plates. 4 days later, animals of the F1 generation were lysed in Laemmli buffer and analyzed by Western using anti-HSP-6 and anti-Tubulin antibodies.

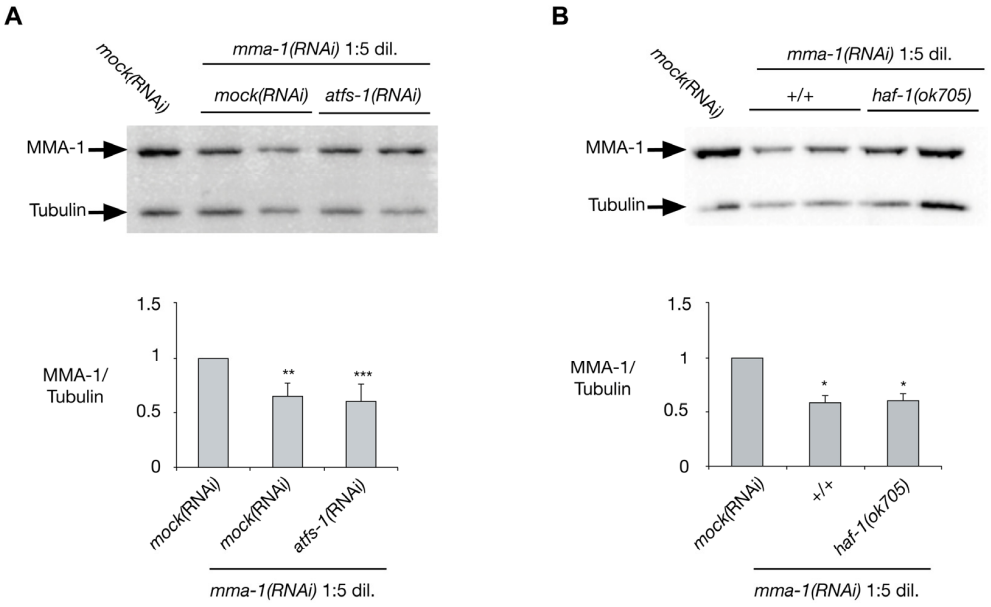

Figure S4. *atfs-1(RNAi)* and *haf-1(ok705)* do not affect *mma-1(RNAi)* efficiency. (A) L4 larvae of SJ4100 (*zcIs13 [P_{hsp-6}GFP]*) were inoculated onto *mock(RNAi)*, *mma-1(RNAi) or atfs-1+mma-1(RNAi)* plates. 4 days later, animals of the F1 generation were lysed in Laemmli buffer and analyzed by Western using anti-MMA-1 and anti-Tubulin antibodies. Ratios of MMA-1/Tubulin relative to the *mock(RNAi)* treated animals are indicated (n=5). **(B)** L4 larvae of SJ4100 (*zcIs13 [P_{hsp-6}GFP]*) or MD3550 (*haf-1(ok705); zcIs13[P_{hsp-6}GFP]*) were inoculated onto *mock(RNAi)* or *mma-1(RNAi)* plates. 4 days later, animals of the F1 generation were lysed in Laemmli buffer and analyzed by Western using anti-MMA-1 and anti-Tubulin antibodies. Ratios of MMA-1/Tubulin relative to the *mock(RNAi)* treated animals are indicated. (n=5). (For all panels, average values are shown and error bars indicate s.d.; * p≤0.05, ** p≤0.01 and *** p≤0.001 by one sample t-test).

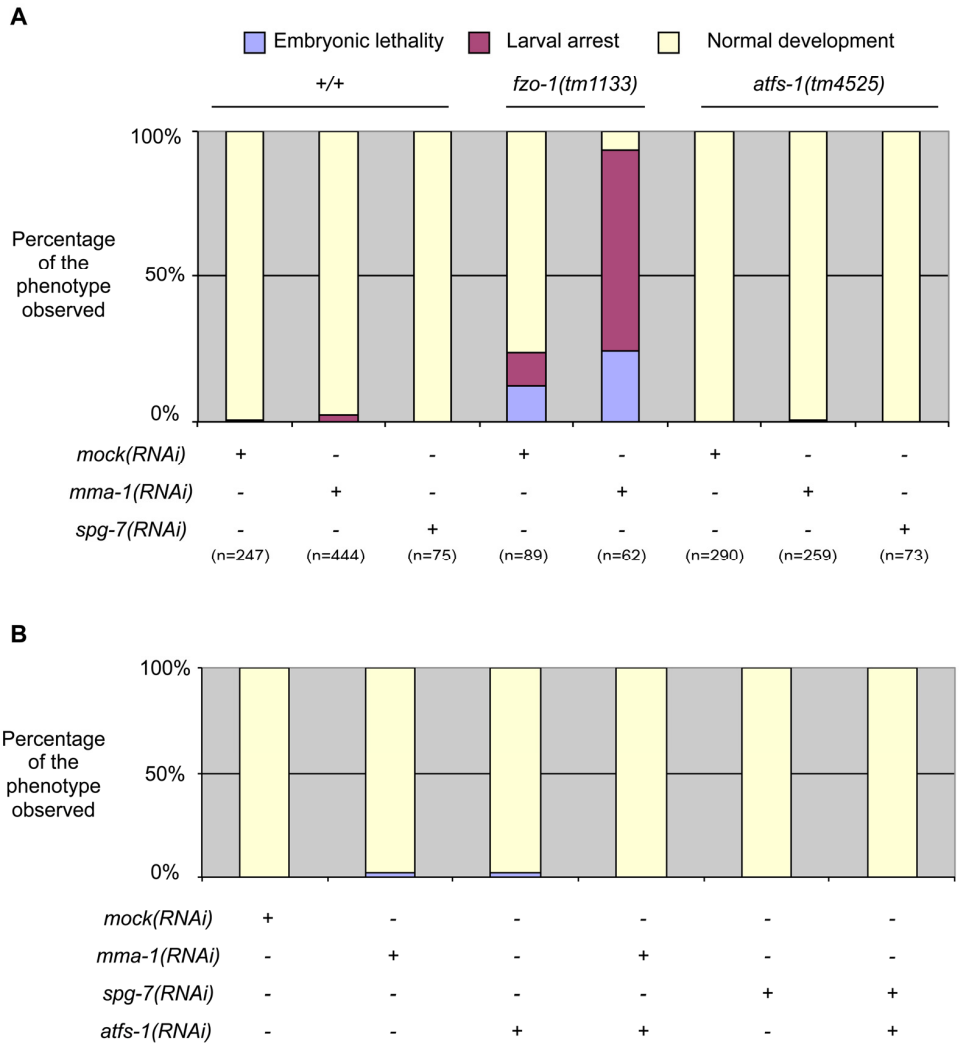

Figure S5. ATFS-1-dependent UPR^{mt} is not essential for viability in response to *mma-1*(*RNAi*). **(A)** Wild-type (+/+), *fzo-1(tm1133)* or *afts-1(tm4525)* L4 larvae were inoculated on *mock(RNAi)*, *mma-1(RNAi)* or *spg-7(RNAi)* plates. After 18 hours, a three hours lay off was performed onto new RNAi plates. The percentage of embryonic lethality, larval arrest as well as the percentage of animals developing into adults (normal development) was quantified in all conditions. **(B)** Wild-type L4 larvae were inoculated on *mock(RNAi)*, *atfs-1(RNAi)*, *mma-1(RNAi)* (diluted 1:5 with *mock(RNAi)* or *atfs-1(RNAi)*) or *spg-7(RNAi)* (diluted 1:5 with *mock(RNAi)* or *atfs-1(RNAi)*) plates. After 18 hours, a three hours lay off was performed onto new RNAi plates. The percentage of embryonic lethality, larval arrest as well as the percentage of animals developing into adults (normal development) was quantified in all conditions.

Table S1: List of the *C. elegans* transgenic lines used in this study.

Strain	Genotype	Reference
SJ4100	*zcIs13 V [P_{hsp-6}GFP]*	[18]
SJ4058	*zcIs9 V [P_{hsp-60}GFP]*	[18]
SJ4005	*zcIs4 V [P_{hsp-4}GFP]*	[18]
MD3550	*haf-1(ok705) IV ; zcIs13 V [P_{hsp-6}GFP]*	This study
MD3011	*bcIs78 I [P_{myo-3}mitoGFP]*	[11]
MD3572	*bcIs78 I [P_{myo-3}mitoGFP]; haf-1(ok705) IV*	This study
MD3573	*bcIs78 I [P_{myo-3}mitoGFP];atfs-1(tm4525) V*	This study

3 Chapter II – Autophagy compensates for defects in mitochondrial dynamics

Haeussler, S.*, **Köhler, F.***, Witting, M., Premm, M.F., Rolland, S.G., Fischer, C., Chauve, L., Casanueva, O., and Conradt, B. (2020). PLoS Genetics *16*, e1008638. https://doi.org/10.1371/journal.pgen.1008638

* contributed equally

PLOS GENETICS

RESEARCH ARTICLE

Autophagy compensates for defects in mitochondrial dynamics

Simon Haeussler[1☯], Fabian Köhler[1☯], Michael Witting[2,3], Madeleine F. Premm[1], Stéphane G. Rolland[1], Christian Fischer[1,4], Laetitia Chauve[5], Olivia Casanueva[5], Barbara Conradt[1,4,6]*

1 Faculty of Biology, Ludwig-Maximilians-University Munich, Munich, Germany, **2** Research Unit Analytical BioGeoChemistry, Helmholtz Zentrum München, Neuherberg, Germany, **3** Chair of Analytical Food Chemistry, Technische Universität München, Freising, Germany, **4** Center for Integrated Protein Science, Ludwig-Maximilians-University Munich, Planegg-Martinsried, Germany, **5** Epigenetics Programme, The Babraham Institute, Cambridge, United Kingdom, **6** Department of Cell and Developmental Biology, Division of Biosciences, University College London, London, United Kingdom

☯ These authors contributed equally to this work.
* b.conradt@ucl.ac.uk

OPEN ACCESS

Citation: Haeussler S, Köhler F, Witting M, Premm MF, Rolland SG, Fischer C, et al. (2020) Autophagy compensates for defects in mitochondrial dynamics. PLoS Genet 16(3): e1008638. https://doi.org/10.1371/journal.pgen.1008638

Editor: Gregory P. Copenhaver, The University of North Carolina at Chapel Hill, UNITED STATES

Received: June 18, 2019

Accepted: January 28, 2020

Published: March 19, 2020

Peer Review History: PLOS recognizes the benefits of transparency in the peer review process; therefore, we enable the publication of all of the content of peer review and author responses alongside final, published articles. The editorial history of this article is available here: https://doi.org/10.1371/journal.pgen.1008638

Data Availability Statement: All relevant data are within the manuscript and its Supporting Information files.

Funding: This work was supported by the Deutsche Forschungsgemeinschaft https://eur01.

Abstract

Compromising mitochondrial fusion or fission disrupts cellular homeostasis; however, the underlying mechanism(s) are not fully understood. The loss of *C. elegans fzo-1*^{MFN} results in mitochondrial fragmentation, decreased mitochondrial membrane potential and the induction of the mitochondrial unfolded protein response (UPR^{mt}). We performed a genome-wide RNAi screen for genes that when knocked-down suppress *fzo-1*^{MFN}(lf)-induced UPR^{mt}. Of the 299 genes identified, 143 encode negative regulators of autophagy, many of which have previously not been implicated in this cellular quality control mechanism. We present evidence that increased autophagic flux suppresses *fzo-1*^{MFN}(lf)-induced UPR^{mt} by increasing mitochondrial membrane potential rather than restoring mitochondrial morphology. Furthermore, we demonstrate that increased autophagic flux also suppresses UPR^{mt} induction in response to a block in mitochondrial fission, but not in response to the loss of *spg-7*^{AFG3L2}, which encodes a mitochondrial metalloprotease. Finally, we found that blocking mitochondrial fusion or fission leads to increased levels of certain types of triacylglycerols and that this is at least partially reverted by the induction of autophagy. We propose that the breakdown of these triacylglycerols through autophagy leads to elevated metabolic activity, thereby increasing mitochondrial membrane potential and restoring mitochondrial and cellular homeostasis.

Author summary

Various quality control mechanisms within the cell ensure mitochondrial homeostasis. Specifically, mitochondrial fission and fusion, the mitochondrial unfolded protein response (UPR^{mt}) and/or mitophagy are induced upon mitochondrial stress to maintain or restore mitochondrial homeostasis. How these different quality control mechanisms are coordinated and how they influence each other is currently not well understood.

safelinks.protection.outlook.com/?url=https%3A%2F%2Fwww.dfg.de%2Fen%2F&data=02%7C01%7C%7C381f38b59bcd4e9a567f08d7bba8aec2%7C1faf88fea9984c5b93c9210a11d9a5c2%7C0%7C0%7C637184205470464132&sdata=Eb4roXJqDx7UamjpWqYooqGw6RKzo5yD8jDFkLtapls%3D&reserved=0 (CO204/6-1, CO204/9-1 and EXC114 to BC). Some strains were provided by the CGC, which is funded by NIH Office of Research Infrastructure Programs https://eur01.safelinks.protection.outlook.com/?url=https%3A%2F%2Fwww.nih.gov%2F&data=02%7C01%7C%7C381f38b59bcd4e9a567f08d7bba8aec2%7C1faf88fea9984c5b93c9210a11d9a5c2%7C0%7C0%7C637184205470464132&sdata=LGLqn8cL5mhk9Xn6gWttZPV5hOmsiv%2Fi13%2BC6CDBYPU%3D&reserved=0 (P40 OD010440). The funders had no role in study design, data collection and analysis, decision to publish, or preparation of the manuscript.

Competing interests: The authors have declared that no competing interests exist.

Interestingly, the disruption of mitochondrial dynamics has recently been shown to induce UPR^{mt}. We performed a genome-wide RNAi screen for suppressors of UPR^{mt} induced by a block in mitochondrial fusion and found approximately half of the candidate genes identified to negatively regulate autophagy, a central quality control mechanism that adjusts cellular metabolism under conditions of stress. Furthermore, we found that induction of autophagy also suppresses UPR^{mt} induced by a block in mitochondrial fission. In addition, we demonstrate that defects in mitochondrial dynamics lead to changes in lipid metabolism, which can partially be reverted by the induction of autophagy. Taken together, our results suggest a so far unknown functional connection between UPR^{mt} and autophagy in animals with defects in mitochondrial dynamics.

Introduction

Mitochondrial dynamics plays an important role in the maintenance of mitochondrial function and, hence, cellular homeostasis [1]. Mitochondrial fission and fusion are both mediated by members of the family of dynamin-like guanosine triphosphatases (GTPases) [2]. In the nematode *Caenorhabditis elegans*, mitochondrial fission is facilitated by the cytosolic dynamin-like GTPase DRP-1^{DRP1}, which is recruited to mitochondria where it presumably forms constricting spirals as shown for its *Saccharomyces cerevisiae* counterpart Drp1 [3,4]. Conversely, fusion of the outer and inner mitochondrial membranes is carried out by the membrane-anchored dynamin-like GTPases FZO-1^{MFN} [5] and EAT-3^{OPA1} [6], respectively. The consequences with respect to mitochondrial function and cellular homeostasis of disrupting mitochondrial dynamics are not yet fully understood; however, it has recently been demonstrated that this activates a retrograde quality control signaling pathway referred to as the 'mitochondrial Unfolded Protein Response' (UPR^{mt}) [7,8]. In *C. elegans*, UPR^{mt} is activated upon mitochondrial stress, which leads to a decrease in mitochondrial membrane potential and the subsequent import into the nucleus of the 'Activating Transcription Factor associated with Stress 1' (ATFS-1^{ATF4,5}) [9,10]. ATFS-1^{ATF4,5} harbors both an N-terminal mitochondrial targeting sequence and a C-terminal nuclear localization sequence and is normally imported into mitochondria [11]. Upon mitochondrial stress, ATFS-1^{ATF4,5} is imported into the nucleus, where it cooperates with the proteins UBL-5^{UBL5} and DVE-1^{SATB1} to promote the transcription of genes that act to restore mitochondrial function and to adjust cellular metabolism [9,10,12,13]. Among these genes are the mitochondrial chaperone genes *hsp-6*^{mtHSP70} and *hsp-60*^{HSP60}, the transcriptional upregulation of which is commonly used to monitor UPR^{mt} activation [14].

Whereas UPR^{mt} is a quality control pathway that is activated upon mitochondrial stress, macro-autophagy (from now on referred to as 'autophagy') is a more general cellular quality control mechanism. Through autophagy, cytosolic constituents, long-lived proteins or dysfunctional organelles are degraded and recycled [15,16]. Upon the induction of autophagy, a double-membrane structure called 'phagophore' forms, which enlarges and eventually engulfs the cargo to form an 'autophagosome'. The autophagosome then fuses with a lysosome to form an 'autolysosome', in which the engulfed cargo is subsequently degraded by lysosomal hydrolases [16–18]. A key regulator of autophagy in *C. elegans* is the kinase LET-363^{mTOR} [19]. When cellular nutrients are abundant, LET-363^{mTOR} represses the 'induction complex', which includes UNC-51^{ULK}, a kinase that initiates autophagy [20–26].

Another vesicular process that targets cargo for degradation to the lysosome is endocytosis. The 'Endosomal Sorting Complex Required for Transport' (ESCRT) plays a critical role in

endocytosis [27,28]. The ESCRT is composed of five different subcomplexes (ESCRT-0, -I, -II, -III and the AAA-ATPase VPS4) and was originally identified because of its role in the formation of multivesicular bodies (MVBs), which enables ubiquitinated membrane proteins to be sorted into small intralumenal vesicles (ILVs) [29,30]. The ESCRT has since been shown to be required for a number of other cellular processes, such as cytokinesis and virus budding [27,31,32]. ESCRT activity has also been shown to affect autophagy. Studies in mammals and *Drosophila melanogaster* demonstrated that depleting ESCRT components results in a block in autophagy and that in these animals, the ESCRT is required for the fusion of endosomes with lysosomal compartments and also autophagosomes [33–36]. Moreover, ESCRT components have recently been shown to be involved in the closure of autophagosomes in mammals and yeast [37,38]. However, in *C. elegans*, the depletion of ESCRT components results in the induction of autophagy, which suggests that in this species, ESCRT function antagonizes or suppresses autophagy [39,40].

Whereas a functional connection between the ESCRT and autophagy has been established in yeast, nematodes, flies and mammals [33–40], functional connections between the ESCRT and UPR^{mt} or between autophagy and UPR^{mt} [40] have not been described or are poorly understood. In this study, we present evidence that in *C. elegans*, the ESCRT, autophagy and UPR^{mt} functionally interact. Specifically, we found that the induction of autophagy suppresses UPR^{mt} induced by a block in mitochondrial fusion or fission. Interestingly, lipid profiling revealed alterations in the lipidome of mutants defective in mitochondrial dynamics, and we present evidence that changes in the levels of certain types of triacylglycerols (TGs) in *fzo-1*^{MFN} mutants can be reverted by the induction of autophagy. We propose that through the breakdown of these triacylglycerols, the induction of autophagy leads to elevated metabolic activity, thereby increasing mitochondrial membrane potential and restoring mitochondrial and, hence, cellular homeostasis.

Results

In *C. elegans*, knock-down by RNA-mediated interference (RNAi) of genes encoding dynamin-like GTPases required for mitochondrial fusion (*fzo-1*^{MFN}, *eat-3*^{OPA1}) or mitochondrial fission (*drp-1*^{DRP1}) induces the 'mitochondrial Unfolded Protein Response' (UPR^{mt}) [7,8]. Using a multi-copy transgene of the transcriptional reporter P$_{hsp\text{-}6\ mtHSP70}$*gfp* (*zcIs13*) [14], we tested strong loss-of-function (lf) mutations of *fzo-1*^{MFN} and *drp-1*^{DRP1} (*fzo-1(tm1133)*, *drp-1 (tm1108)* (National BioResource Project)) and found that they induce UPR^{mt} to different degrees (S1A and S1C Fig). As a positive control, we used animals carrying a lf mutation of the gene *spg-7*^{AFG3L2} (*spg-7(ad2249)*), which encodes a mitochondrial metalloprotease required for mitochondrial function [41]. The *zcIs13* transgene shows very low baseline expression in wild-type animals and is widely used to monitor UPR^{mt} in *C. elegans* [7,9–14,42–44]. In the case of *fzo-1(tm1133)* animals, for example, its expression is induced more than 15-fold (S1C Fig). Furthermore, RNAi knock-down of *spg-7*^{AFG3L2} or genes encoding subunits of the electron transport chain (ETC), or treatments with drugs targeting the latter (e.g. antimycin) lead to strong induction of *zcIs13* expression [14,43]. This makes the *zcIs13* transgene suitable for high throughput, large-scale screens.

However, considering that *fzo-1(tm1133)* causes an increase in the amount of endogenous HSP-6^{mtHSP70} protein by only 1.44-fold (S1E Fig), the fold induction observed with the multi-copy *zcIs13* transgene may not reflect the physiological response with respect to UPR^{mt} induction by the loss of *fzo-1*^{MFN}. Furthermore, the *zcIs13* transgene exhibits large variability in expression between animals (inter-individual variability) (S1A Fig), which makes it difficult to obtain consistent results, especially when knocking-down genes using RNA-mediated

interference (RNAi). For this reason, we generated a single-copy transgene, *bcSi9* (integrated at a defined chromosomal location using MosSCI), of the transcriptional reporter $P_{hsp\text{-}6\ \mathrm{mtHSP70}}$*gfp*. As shown in S1B Fig, the *bcSi9* transgene shows low baseline expression and, in the case of *spg-7 (ad2249)* and *fzo-1(tm1133)*, an increase in expression of ~5-fold or ~4-fold, respectively (S1D Fig). Furthermore, compared to *fzo-1(tm1133)* animals carrying the multi-copy transgene *zcIs13*, *fzo-1(tm1133)* animals carrying the single-copy transgene *bcSi9* exhibit less inter-individual variability (S1A and S1B Fig). Similarly, *drp-1(tm1108)* animals carrying *bcSi9* show significantly less inter-individual variability compared to *drp-1(tm1108)* animals carrying the multi-copy transgene *zcIs13* (S1A and S1B Fig). Importantly, for all genotypes tested, we found that compared to the fold-induction observed with the multi-copy transgene *zcIs13*, the fold-induction observed with the single-copy transgene *bcSi9* correlated better with the fold-induction observed in the amount of endogenous HSP-6^{mtHSP70} protein (S1A–S1E Fig). Finally, to compare inter-individual variability of the expression of the two $P_{hsp\text{-}6\ \mathrm{mtHSP70}}$*gfp* transgenes *zcIs13* and *bcSi9* as well as the endogenous *hsp*-6^{mtHSP70} locus in a quantitative manner, we performed single-worm RT-qPCR experiments in synchronized populations of 36 individual animals and compared inter-individual variability in expression of *zcIs13*, *bcSi9* or the endogenous *hsp*-6^{mtHSP70} locus to those of loci with low (*hsp-1*$^{\mathrm{HSPA1L}}$), medium (*ttr-45*) or high (*nlp-29*) inter-individual variability in expression, respectively (S1F Fig). While the expression of the endogenous *hsp-6*$^{\mathrm{mtHSP70}}$ locus is not variable between individuals of a population, the expression of the multi-copy transgene *zcIs13* is highly variable in both a wild-type and *fzo-1(tm1133)* background (S1F Fig). Furthermore, the single-copy transgene *bcSi9* exhibits some inter-individual variability in expression, however, to a much lower degree than the transgene *zcIs13*. Therefore, based on these results, we decided to use the multi-copy transgene *zcIs13* for a genome-wide RNAi screen for suppressors of *fzo-1(tm1133)*-induced UPR$^{\mathrm{mt}}$ and the single-copy transgene *bcSi9* for subsequent analyses of candidates identified (see below).

Depletion of ESCRT components suppresses *fzo-1(tm1133)*-induced UPR$^{\mathrm{mt}}$

To identify genes that affect the induction of UPR$^{\mathrm{mt}}$ in response to a block in mitochondrial fusion, we performed a genome-wide RNAi screen using *fzo-1(tm1133)* animals carrying the multi-copy $P_{hsp\text{-}6\ \mathrm{mtHSP70}}$*gfp* transgene *zcIs13* (S1A Fig). To that end, we used an RNAi feeding library that covers approximately 87% of *C. elegans* protein coding genes [45] and analyzed animals of the F1 generation. Among the 299 suppressors identified, three genes, *vps-4*$^{\mathrm{VPS4}}$, *vps-20*$^{\mathrm{CHMP6}}$ and *vps-37*$^{\mathrm{VPS37}}$, encode components of the 'Endosomal Sorting Complex Required for Transport' (ESCRT) [27–30]. We analyzed the suppression of *fzo-1(tm1133)*-induced UPR$^{\mathrm{mt}}$ using the single-copy $P_{hsp\text{-}6\ \mathrm{mtHSP70}}$*gfp* transgene *bcSi9* and found that knockdown of *vps-4*$^{\mathrm{VPS4}}$ or *vps-20*$^{\mathrm{CHMP6}}$ by RNAi (referred to as '*vps-4(RNAi)*' or '*vps-20(RNAi)*') causes suppression by 39% or 23% on average, respectively (Fig 1A and 1C). *vps-37(RNAi)* does not result in a statistically significant suppression on average; however, some individual animals show strong suppression (see Fig 1A; *vps-37(RNAi)*; red arrowheads). As a positive control, we knocked-down the function of *atfs-1*$^{\mathrm{ATF4,5}}$ by RNAi, which results in suppression of *fzo-1(tm1133)*-induced UPR$^{\mathrm{mt}}$ by 54% on average. (In a wild-type background, *atfs-1 (RNAi)*, *vps-4(RNAi)* or *vps-20(RNAi)* suppresses baseline expression of the *bcSi9* transgene by 8%, 14% or 14%, respectively (S2A Fig).) To confirm the suppression of *fzo-1(tm1133)*-induced UPR$^{\mathrm{mt}}$ upon *ESCRT(RNAi)*, we used a multi-copy transgene *(zcIs9)* of a transcriptional reporter of the gene *hsp-60*$^{\mathrm{HSP60}}$ ($P_{hsp\text{-}60\ \mathrm{HSP60}}$*gfp)*, which is also transcriptionally upregulated in response to the induction of UPR$^{\mathrm{mt}}$ [14]. Using the $P_{hsp\text{-}60\ \mathrm{HSP60}}$*gfp* reporter, we found that *vps-37(RNAi)*, *vps-20(RNAi)* or *vps-4(RNAi)* suppresses by 34%, 41% or 33% on average, respectively (Fig 1B and 1D).

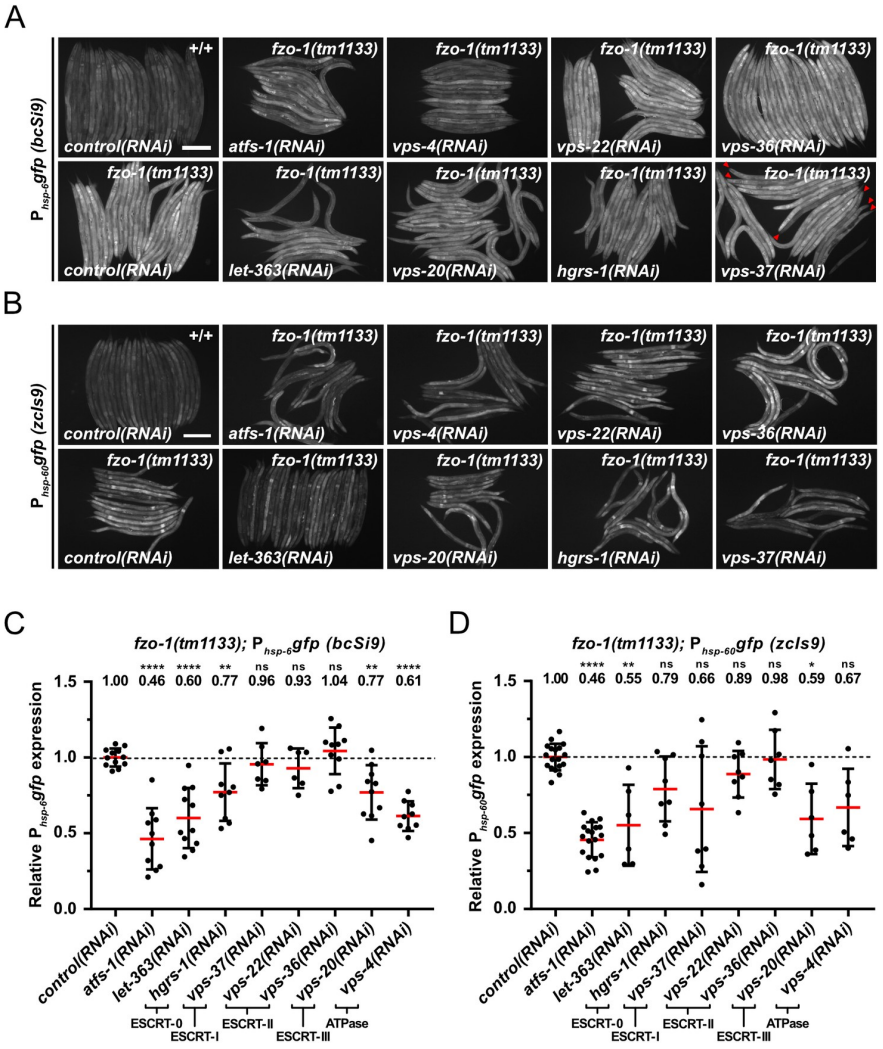

Fig 1. Depletion of ESCRT components and LET-363 suppresses *fzo-1(tm1133)*-induced UPR^{mt}. **(A)** Fluorescence images of L4 larvae expressing P$_{hsp-6}$*gfp (bcSi9)* in wild type (+/+) or *fzo-1(tm1133)*. L4 larvae were subjected to *control (RNAi)*, *atfs-1(RNAi)*, *vps-4(RNAi)*, *vps-20(RNAi)*, *vps-22(RNAi)*, *hgrs-1(RNAi)*, *vps-36(RNAi)*, *vps-37(RNAi)* or *let-363 (RNAi)* and the F1 generation was imaged. Red arrowheads indicate suppressed animals upon *vps-37(RNAi)*. Scale bar: 200 μm. **(B)** Fluorescence images of L4 larvae expressing P$_{hsp-60}$*gfp (zcIs9)* in wild type (+/+) or *fzo-1(tm1133)*. L4 larvae were subjected to *control(RNAi)*, *atfs-1(RNAi)*, *vps-4(RNAi)*, *vps-20(RNAi)*, *vps-22(RNAi)*, *hgrs-1(RNAi)*, *vps-36 (RNAi)*, *vps-37(RNAi)* or *let-363(RNAi)* and the F1 generation was imaged. Scale bar: 200 μm. **(C)** Quantifications of fluorescence images from panel A. After subtracting the mean fluorescence intensity of wild type (+/+) on *control (RNAi)*, the values were normalized to *fzo-1(tm1133)* on *control(RNAi)*. Each dot represents the quantification of fluorescence intensity of 15–20 L4 larvae. Values indicate means ± SD of at least 3 independent experiments in duplicates. $^{**}P<0.01$, $^{****}P<0.0001$ using one-way ANOVA with Dunnett's multiple comparison test to *control (RNAi)*. **(D)** Quantifications of fluorescence images from panel B. After subtracting the mean fluorescence intensity of wild type (+/+) on *control(RNAi)*, the values were normalized to *fzo-1(tm1133)* on *control(RNAi)*. Each dot represents the quantification of fluorescence intensity of 10–20 L4 larvae. Values indicate means ± SD of 3 independent experiments in duplicates. ns: not significant, $^{*}P<0.05$, $^{**}P<0.01$, $^{****}P<0.0001$ using Kruskal-Wallis test with Dunn's multiple comparison test to *control(RNAi)*.

https://doi.org/10.1371/journal.pgen.1008638.g001

To validate that the reduced P$_{hsp-6\ \mathrm{mtHSP70}}$*gfp (bcSi9)* and P$_{hsp-60\ \mathrm{HSP60}}$*gfp (zcIs9)* expression in *fzo-1(tm1133)* animals upon *ESCRT(RNAi)* is specific to the UPR^{mt} response, we tested a

transcriptional reporter, $P_{ges\text{-}1\ CES2}gfp$, that has a similar expression pattern as the two UPR^{mt} reporters. Depletion of ESCRT component VPS-4^{VPS4} or VPS-20^{CHMP6} does not result in suppression of the $P_{ges\text{-}1\ CES2}gfp$ reporter (Fig 2A and 2B), suggesting that ESCRT depletion does not cause degradation of cytosolic GFP *per se* but specifically suppresses the expression of the two UPR^{mt} reporters.

Since *vps-4*^{VPS4}, *vps-20*^{CHMP6} and *vps-37*^{VPS37} are part of different ESCRT subcomplexes (*vps-4*^{VPS4}—ATPase, *vps-20*^{CHMP6}—ESCRT-III, *vps-37*^{VPS37}—ESCRT-I) [27], we tested whether depletion of components of the two remaining ESCRT subcomplexes, ESCRT-0 and ESCRT-II, also suppresses *fzo-1(tm1133)*-induced UPR^{mt}. Using the $P_{hsp\text{-}6\ mtHSP70}gfp$ reporter *(bcSi9)*, we found that RNAi knock-down of *hgrs-1*^{HGS} (ESCRT-0) suppresses by 23% on average (Fig 1A and 1C). In contrast, RNAi knock-down of two genes encoding components of ESCRT-II, *vps-22*^{SNF8} and *vps-36*^{VPS36}, fails to suppress. Similarly, using the $P_{hsp\text{-}60\ HSP60}gfp$ reporter *(zcIs9)*, we found suppression by *hgrs-1(RNAi)* but not *vps-22(RNAi)* or *vps-36(RNAi)* (Fig 1B and 1D). Taken together, our results demonstrate that the depletion of components of ESCRT-0, -I, -III or VPS-4 ATPase can suppress *fzo-1(tm1133)*-induced UPR^{mt}.

Depletion of ESCRT components does not rescue the fragmented mitochondria phenotype in *fzo-1(tm1133)* animals but increases mitochondrial membrane potential

The loss of *fzo-1*^{MFN} function has a dramatic effect on steady-state mitochondrial morphology. This is easily detectable in *C. elegans* body wall muscles using a reporter that drives the expression of mitochondrial-matrix targeted GFP protein *(*$P_{myo\text{-}3\ MYH}gfp^{mt}$*)* [3,5,46]. In *control (RNAi)* animals, the mitochondria in body wall muscle cells are predominantly tubular (Fig 2C). In contrast, in *fzo-1(tm1133)* animals treated with *control(RNAi)*, the mitochondria are predominantly fragmented (referred to as 'fragmented mitochondria' phenotype). To determine whether the depletion of components of ESCRT-I or -III, or the depletion of the ATPase VPS-4^{VPS4} restores steady-state mitochondrial morphology, we analyzed mitochondrial morphology in *fzo-1(tm1133)* animals, in which *vps-4*^{VPS4}, *vps-20*^{CHMP6} or *vps-37*^{VPS37} had been knocked-down by RNAi. We found that knock-down of these genes has no effect on the fragmented mitochondria phenotype in body wall muscle cells of *fzo-1(tm1133)* animals (Fig 2C). Knock-down of *vps-4*^{VPS4}, *vps-20*^{CHMP6} or *vps-37*^{VPS37} in *fzo-1(tm1133)* animals also has no effect on mitochondrial morphology in hypodermal or intestinal cells (Fig 2E and S3B Fig). (ESCRT depletion has no effect on steady-state mitochondrial morphology in body wall muscle cells in a wild-type background (S3A Fig).)

Since we did not see a change in mitochondrial morphology in *fzo-1(tm1133)* animals upon *ESCRT(RNAi)*, we tested whether it affects mitochondrial membrane potential. Therefore, we stained larvae with TMRE (Tetramethylrhodamine ethyl ester), a membrane potential dependent dye that is commonly used in *C. elegans* to measure mitochondrial membrane potential in hypodermal cells [10,14]. To measure the intensity of TMRE signal, mitochondria in the fluorescent images were segmented using Fiji image software to generate a binary mask (S4 Fig). This mask, which includes all mitochondria of an image, was then used to measure TMRE fluorescence intensity per mitochondrial area in the raw image. Compared to wild type, TMRE fluorescence intensity per mitochondrial area was reduced by 63% in *fzo-1 (tm1133)* animals (Fig 2D). We found increased levels of TMRE fluorescence intensity per mitochondrial area in *fzo-1(tm1133)* animals upon *vps-4(RNAi)* (19%) or *vps-20(RNAi)* (33%), compared to *control(RNAi)* (Fig 2E and 2F). In contrast, ESCRT depletion in the wild-type background causes a reduction in TMRE fluorescence intensity per mitochondrial area by 24% upon *vps-4(RNAi)* or 18% upon *vps-20(RNAi)* (Fig 2G and 2H). Mitochondrial TMRE

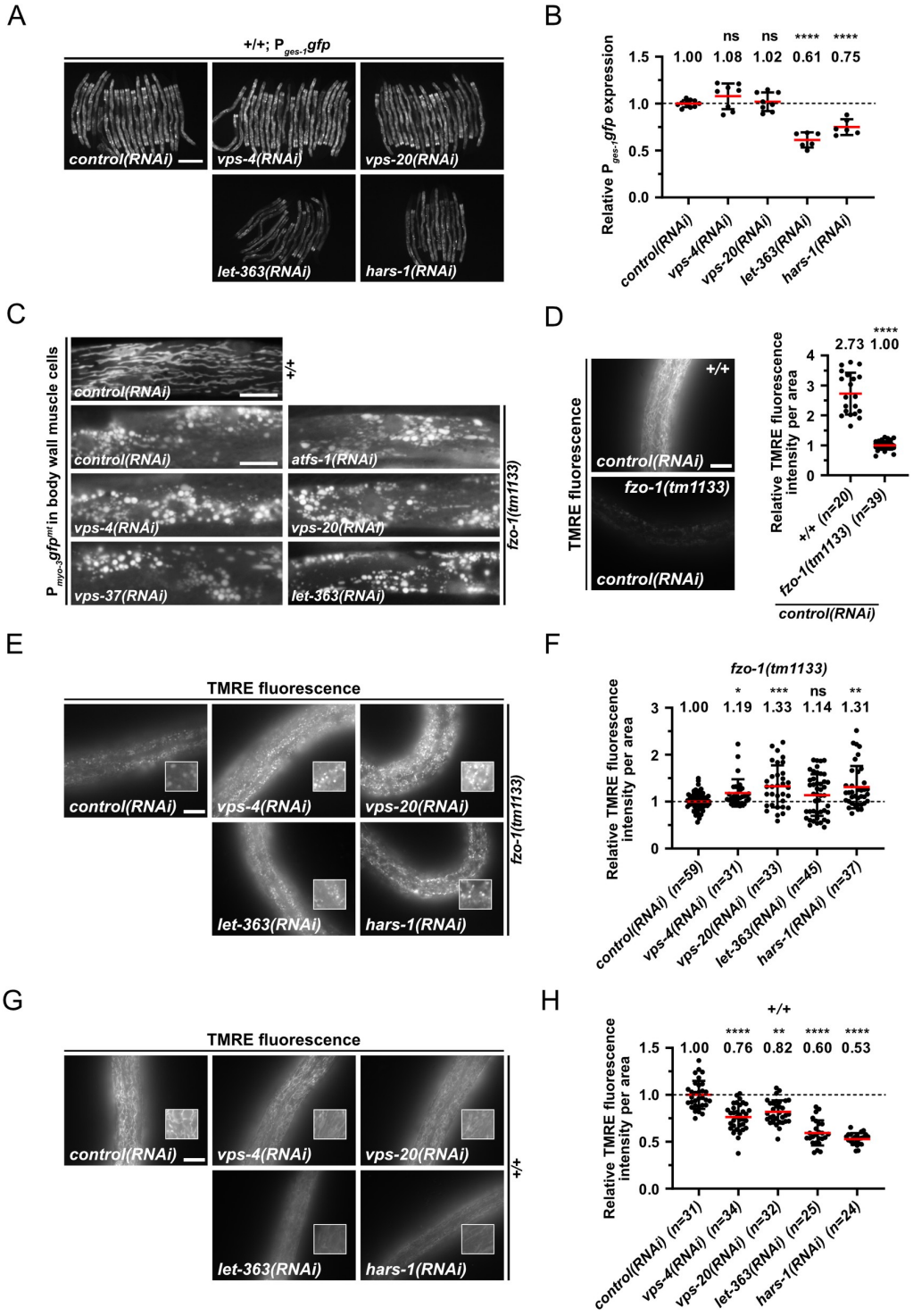

Fig 2. Induction of autophagy increases mitochondrial membrane potential and suppresses *fzo-1(tm1133)*-induced UPR^{mt}. **(A)** Fluorescence images of L4 larvae expressing P$_{ges-1}$*gfp* in wild type (+/+). L4 larvae were subjected to *control(RNAi)*, *vps-4 (RNAi)*, *vps-20(RNAi)*, *let-363(RNAi)* or *hars-1(RNAi)* and the F1 generation was imaged. Scale bar: 200 μm. **(B)** Quantifications of fluorescence images from panel A. The values were normalized to *control(RNAi)* and each dot represents the quantification of

fluorescence intensity of 15–20 L4 larvae. Values indicate means ± SD of 3 independent experiments in duplicates. ns: not significant, $^{****}P<0.0001$ using one-way ANOVA with Dunnett's multiple comparison test to *control(RNAi)*. **(C)** Fluorescence images of L4 larvae expressing $P_{myo\text{-}3}gfp^{mt}$ in wild type (+/+) or *fzo-1(tm1133)*. L4 larvae were subjected to *control(RNAi)*, *atfs-1 (RNAi)*, *vps-4(RNAi)*, *vps-20(RNAi)*, *vps-37(RNAi)* or *let-363(RNAi)* and the F1 generation was imaged. Scale bar: 10 μm. **(D)** Fluorescence images and quantifications of L4 larvae stained with TMRE in wild type (+/+) or *fzo-1(tm1133)*. L4 larvae were subjected to *control(RNAi)* and the F1 generation was stained with TMRE overnight and imaged. Scale bar: 10 μm. Values indicate means ± SD of 3 independent experiments in duplicates. $^{****}P<0.0001$ using unpaired two-tailed t-test with Welch's correction. **(E)** Fluorescence images of L4 larvae stained with TMRE in *fzo-1(tm1133)*. L4 larvae were subjected to *control(RNAi)*, *vps-4(RNAi)*, *vps-20(RNAi)*, *let-363(RNAi)* or *hars-1(RNAi)* and the F1 generation was stained with TMRE overnight and imaged. Scale bar: 10 μm. **(F)** Quantifications of fluorescence images from panel E. The values were normalized to *fzo-1(tm1133)* on *control(RNAi)* and each dot represents the quantification of fluorescence intensity per area from one L4 larvae. Values indicate means ± SD of 3 independent experiments in duplicates. ns: not significant, $^{*}P<0.05$, $^{**}P<0.01$, $^{***}P<0.001$ using Kruskal-Wallis test with Dunn's multiple comparison test to *control(RNAi)*. **(G)** Fluorescence images of wild-type L4 larvae stained with TMRE. L4 larvae were subjected to *control(RNAi)*, *vps-4(RNAi)*, *vps-20(RNAi)*, *let-363(RNAi)* or *hars-1(RNAi)* and the F1 generation was stained with TMRE overnight and imaged. Scale bar: 10 μm. **(H)** Quantifications of fluorescence images from panel G. The values were normalized to wild type on *control(RNAi)* and each dot represents the quantification of fluorescence intensity per area from one L4 larvae. Values indicate means ± SD of 3 independent experiments in duplicates. $^{**}P<0.01$, $^{****}P<0.0001$ using Kruskal-Wallis test with Dunn's multiple comparison test to *control(RNAi)*.

https://doi.org/10.1371/journal.pgen.1008638.g002

fluorescence intensity is proportional to mitochondrial membrane potential [47]. Therefore, *ESCRT(RNAi)* results in an increase in mitochondrial membrane potential in *fzo-1(tm1133)* mutants. Hence, our data suggests that the suppression of *fzo-1(tm1133)*-induced UPR^{mt} upon ESCRT depletion is due to rescue of the decreased mitochondrial membrane potential and not the fragmented mitochondria phenotype.

Depletion of ESCRT components increases autophagic flux in *fzo-1 (tm1133)* animals

Previous studies have shown that in *C. elegans*, the depletion of ESCRT components leads to the induction of autophagy [39,40]. We confirmed this in wild-type animals (S2B Fig) and tested whether ESCRT depletion also induces autophagy in *fzo-1(tm1133)* animals. First, we determined the basal level of autophagy in *fzo-1(tm1133)* animals using three different assays that utilize the reporters $P_{lgg\text{-}1\ \mathrm{GABARAP}}gfp$::*lgg-1* and $P_{sqst\text{-}1\ \mathrm{p62}}$*sqst-1*::*gfp*, which are widely used to monitor autophagy in *C. elegans* [40,48–52]. Specifically, we determined the number of GFP::LGG-$1^{GABARAP}$ foci in hypodermal seam cells of animals of the fourth larval stage (L4 larvae) and found that the average number of GFP::LGG-$1^{GABARAP}$ foci increases from ~4 on average in wild-type animals (+/+) to ~23 on average in *fzo-1(tm1133)* animals (Fig 3A and 3B). As a positive control, we used RNAi against the gene *let-363*^{mTOR}, which induces autophagy when knocked-down [19]. As expected, *let-363(RNAi)* animals show an increase in the number of GFP::LGG-$1^{GABARAP}$ foci in hypodermal seam cells (~15 on average) (Fig 3A and 3B). To determine whether the increase in the number of GFP::LGG-$1^{GABARAP}$ foci is caused by a block in autophagy, we analyzed the expression of the reporter $P_{sqst\text{-}1\ \mathrm{p62}}$*sqst-1*::*gfp*. (The accumulation of SQST-1^{p62}::GFP is indicative of defective autophagic clearance [51].) Whereas embryos homozygous for a lf mutation of *unc-51*^{ULK}, *e369*, a gene required for autophagy [26], show strong accumulation of SQST-1^{p62}::GFP, we found that *fzo-1(tm1133)* embryos do not accumulate SQST-1^{p62}::GFP (Fig 3C). To further verify an increase in autophagic flux in *fzo-1 (tm1133)* animals, we used an immunoblotting assay based on the cleavage of the GFP::LGG-$1^{GABARAP}$ fusion protein (in autolysosomes) to generate a 'free GFP' fragment, referred to as 'cleaved GFP' [50,53,54]. As shown in Fig 3D, compared to wild type, *fzo-1(tm1133)* mutants exhibit a ~2.7-fold increase on average in the level of cleaved GFP. This confirms that autophagic flux is increased in animals lacking *fzo-1*^{MFN}.

To test whether depletion of ESCRT components can further increase autophagy in *fzo-1 (tm1133)* animals, we knocked-down *vps-4*^{VPS4}, *vps-20*^{CHMP6}, *hgrs-1*^{HGS} or *vps-37*^{VPS37} in *fzo-*

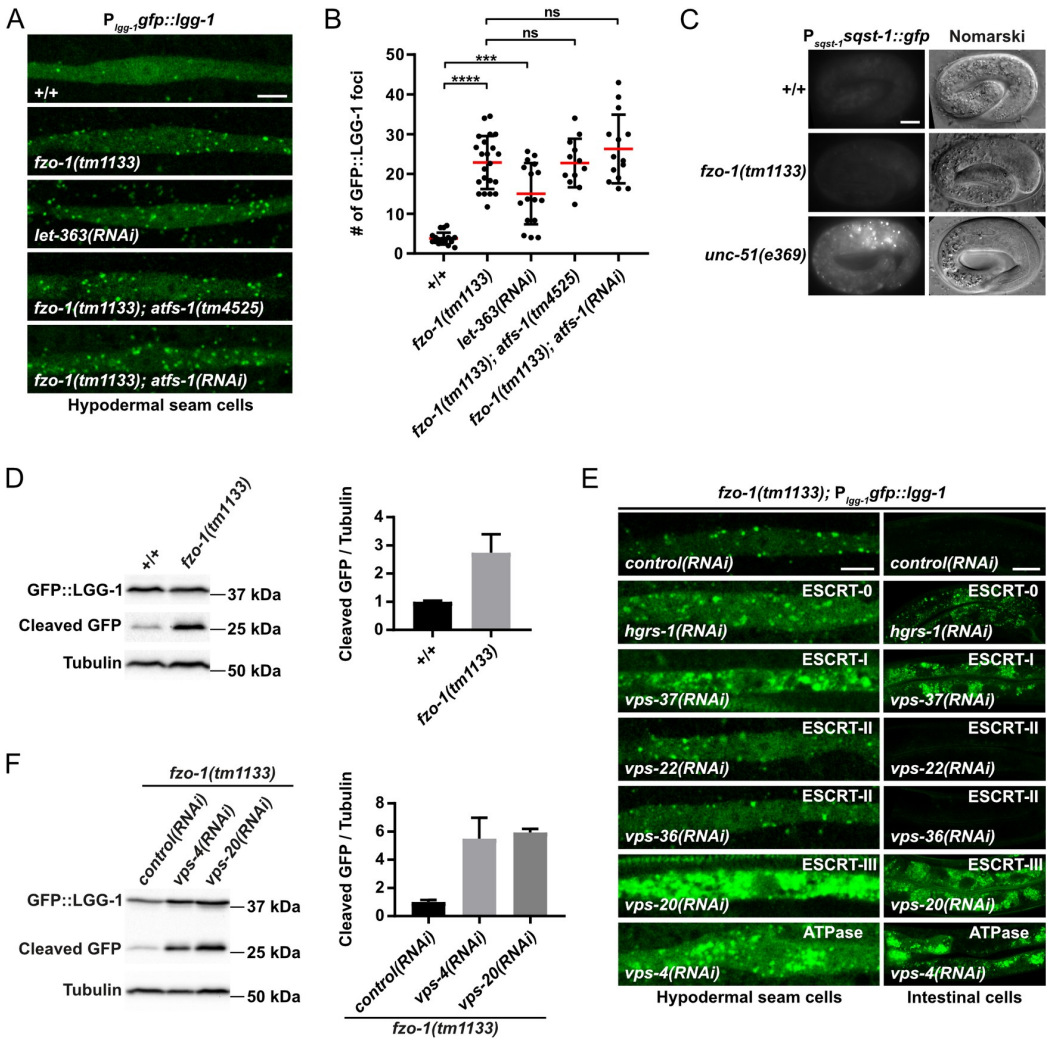

Fig 3. Autophagy is induced independently of ATFS-1^{ATF4,5} in *fzo-1(tm1133)* animals and further increased after ESCRT depletion. **(A)** P$_{lgg-1}$*gfp::lgg-1* expression in hypodermal seam cells of wild type (+/+), *fzo-1(tm1133)* or *fzo-1(tm1133); atfs-1 (tm4525)* L4 larvae. For RNAi against *let-363* and *atfs-1*, L4 larvae were subjected to the respective RNAi and the F1 generation was imaged. Scale bar: 5 μm. **(B)** Quantification of GFP::LGG-1 foci in hypodermal seam cells from panel A. Each dot represents the average amount of GFP::LGG-1 foci counted from 2–5 seam cells in one animal. n≥12 for each genotype; values indicate means ± SD; ns: not significant, $^{***}P<0.001$, $^{****}P<0.0001$ using Kruskal-Wallis test with Dunn's multiple comparison to wild type (+/+) or *fzo-1(tm1133)*, respectively. **(C)** Nomarski and fluorescent images of the P$_{sqst-1}$*sqst-1*::*gfp* translational reporter in embryos of wild type (+/+) or *fzo-1(tm1133)*. As a positive control for a block in autophagy, *unc-51(e369)* was used. Representative images of >60 embryos are shown. Scale bar: 10 μm. **(D)** Western blot analysis of cleaved GFP levels in wild type (+/+) or *fzo-1(tm1133)* using anti-GFP antibodies. Quantification of three independent experiments is shown. Values indicate means ± SD. **(E)** P$_{lgg-1}$*gfp*::*lgg-1* expression of *fzo-1(tm1133)* L4 larvae in hypodermal seam cells and intestinal cells upon *control(RNAi)*, *vps-4(RNAi)*, *vps-20(RNAi)*, *vps-22(RNAi)*, *hgrs-1(RNAi)*, *vps-36(RNAi)* or *vps-37(RNAi)*. Representative images of >80 animals from four independent biological replicates are shown. Scale bar hypodermal seam cells: 5 μm. Scale bar intestinal cells: 20 μm. **(F)** Western blot analysis of cleaved GFP levels in *fzo-1(tm1133)* upon *control(RNAi)*, *vps-4(RNAi)* or *vps-20(RNAi)* using anti-GFP antibodies. Quantification of four independent experiments is shown. Values indicate means ± SD.

https://doi.org/10.1371/journal.pgen.1008638.g003

1(tm1133) animals and analyzed GFP::LGG-1^{GABARAP} foci using the P$_{lgg-1\ GABARAP}$*gfp*::*lgg-1* reporter. We found that RNAi knock-down of each of these four genes in *fzo-1(tm1133)* animals causes a dramatic increase in the accumulation of GFP::LGG-1^{GABARAP} foci in

hypodermal seam cells as well as intestinal cells (Fig 3E). Furthermore, compared to *control (RNAi)*-treated animals, we found increased levels of cleaved GFP in *fzo-1(tm1133)* animals treated with *vps-4(RNAi)* (~5.5-fold) or *vps-20(RNAi)* (~5.9-fold) (Fig 3F). However, RNAi against the ESCRT-II components *vps-22*^{SNF8} or *vps-36*^{VPS36} (which fail to suppress *fzo-1 (tm1133)*-induced UPR^{mt} when knocked-down (Fig 1A–1D)) has no effect on the formation of GFP::LGG-1^{GABARAP} foci in hypodermal seam cells or intestinal cells (Fig 3E), probably due to an inefficient knock-down. In summary, our findings demonstrate that the depletion of components of ESCRT-0, -I, -III or the VPS-4 ATPase increases autophagic flux in *fzo-1 (tm1133)* animals.

Induction of autophagy suppresses *fzo-1(tm1133)*-induced UPR^{mt}

To determine whether increasing autophagy through means other than knock-down of ESCRT components also suppresses *fzo-1(tm1133)*-induced UPR^{mt}, we knocked-down *let-363*^{mTOR} by RNAi and examined the expression of P$_{hsp-6\ mtHSP70}$*gfp (bcSi9)* and P$_{hsp-60\ HSP60}$*gfp (zcIs9)* in *fzo-1(tm1133)* animals. We found that compared to controls, the expression of both reporters is significantly suppressed upon *let-363(RNAi)* in *fzo-1(tm1133)* animals (Fig 1A–1D). Specifically, on average, the expression of P$_{hsp-6\ mtHSP70}$*gfp* is suppressed by 40% and that of P$_{hsp-60\ HSP60}$*gfp* by 45%, which is comparable to the level of suppression observed upon RNAi knock-down of either *atfs-1*^{ATF4,5} or *vps-4*^{VPS4}. As shown for the depletion of ESCRT components, mitochondrial morphology upon *let-363(RNAi)* was found not to be altered in *fzo-1(tm1133)* or wild-type animals (Fig 2C, 2E and 2G and S3A and S3B Fig).

To obtain further evidence that induction of autophagy leads to suppression of *fzo-1 (tm1133)*-induced UPR^{mt}, we searched for additional genes with a regulatory role in autophagy in our dataset of 299 suppressors. We found 17 additional genes that were previously identified in a genome-wide RNAi screen for regulators of autophagy in *C. elegans* [40] (Fig 4A). Moreover, we used a database of autophagy-related genes and their orthologs (http://www.tanpaku.org/autophagy/index.html) [55], results from two screens for regulators of autophagy in mammals [56,57], three interaction databases (wormbase.org, genemania.org and string-db.org) followed by literature searches and identified 13 additional genes in our dataset that potentially induce autophagy upon knock-down (Fig 4A) [58–74]. Therefore, including the three genes encoding components of the ESCRT (*vps-4*^{VPS4}, *vps-20*^{CHMP6}, *vps-37*^{VPS37}), 33 of the 299 suppressors have previously been shown to induce autophagy when knocked-down.

Finally, we knocked-down all 299 suppressors in an otherwise wild-type background and tested for an increase in autophagy. Using this approach, we found that 126 genes encode negative regulators of autophagy (16 of which were among the 33 genes identified through our literature search; indicated by $^{\$}$ in Fig 4A), since they result in the accumulation of GFP::LGG-1^{GABARAP} foci in hypodermal seam cells and/or intestinal cells of larvae but not in the accumulation of SQST-1^{p62}::GFP in embryos when knocked-down (S1 Table). Adding the 17 genes that we identified through literature searches, which were not found in this 'autophagy' screen (Fig 4A), we, in total, found 143 out of 299 suppressors (~48%) of *fzo-1(tm1133)*-induced UPR^{mt} to negatively regulate autophagy.

To confirm that the additionally identified genes enhance autophagy also in the *fzo-1 (tm1133)* background, we knocked-down six of them (*cogc-2*^{COG2}, *cogc-4*^{COG4}, *hars-1*^{HARS}, *rpt-3*^{PSMC4}, *smgl-1*^{NBAS} and *ins-7*) and tested them for increased autophagic flux in *fzo-1 (tm1133)* animals. We found that the knock-down of each gene causes an increase in autophagic flux in *fzo-1(tm1133)* animals, most prominently in the intestine (Fig 4B). We also determined the level of cleaved GFP in these animals and found that, compared to *fzo-1(tm1133)*

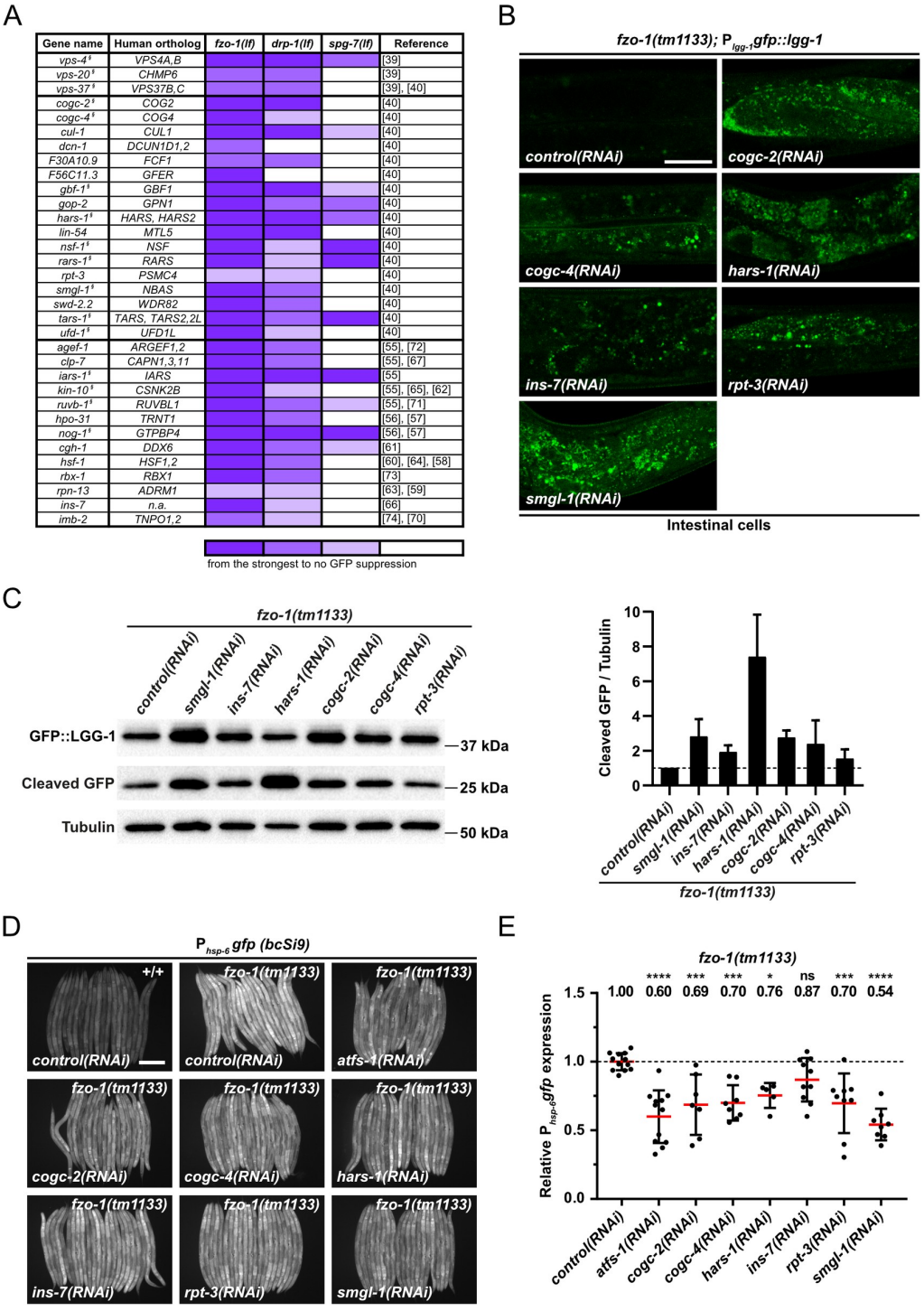

Fig 4. Additional candidates identified in RNAi screen that suppress *fzo-1(tm1133)*- and *drp-1(tm1108)*-induced UPR^{mt} through activation of autophagy. (A) List of candidate genes identified in the primary screen with *fzo-1(tm1133);* P$_{hsp-6}$*gfp (zcIs13)* by RNAi. L4 larvae were subjected to the respective RNAi and the F1 generation was imaged. Candidate genes were screened three times in technical duplicates with the same reporter in two different mutant backgrounds: *drp-1(tm1108)* and *spg-7(ad2249)*. Fluorescence intensity was scored and classified from very strong suppression to weak suppression (gradual violet

coloring) or no suppression (white). § indicates genes that, upon knock-down in our experiments, showed accumulation of GFP::LGG-1 dots in hypodermal seam cells or intestinal cells. **(B)** $P_{lgg\text{-}1}$*gfp::lgg-1* expression of *fzo-1(tm1133)* L4 larvae in intestinal cells upon *control(RNAi)*, *cogc-2(RNAi)*, *cogc-4(RNAi)*, *hars-1(RNAi)*, *ins-7(RNAi)*, *rpt-3(RNAi)* or *smgl-1(RNAi)*. Representative images of >60 animals from four independent biological replicates are shown. Scale bar: 20 μm. **(C)** Western blot analysis of cleaved GFP levels in *fzo-1(tm1133)* upon *control(RNAi)*, *smgl-1(RNAi)*, *ins-7(RNAi)*, *hars-1(RNAi)*, *cogc-2(RNAi)*, *cogc-4(RNAi)* or *rpt-3(RNAi)* using anti-GFP antibodies. Quantification of three independent experiments is shown. Values indicate means ± SD. **(D)** Fluorescence images of L4 larvae expressing $P_{hsp\text{-}6}$*gfp (bcSi9)* in wild type (+/+) or *fzo-1(tm1133)*. L4 larvae were subjected to *control(RNAi)*, *atfs-1(RNAi)*, *cogc-2(RNAi)*, *cogc-4(RNAi)*, *hars-1(RNAi)*, *ins-7(RNAi)*, *rpt-3(RNAi)* or *smgl-1(RNAi)* and the F1 generation was imaged. Scale bar: 200 μm. **(E)** Quantifications of fluorescence images from panel D. After subtracting the mean fluorescence intensity of wild type (+/+) on *control(RNAi)*, the values were normalized to *fzo-1(tm1133)* on *control (RNAi)*. Each dot represents the quantification of fluorescence intensity of 15–20 L4 larvae. Values indicate means ± SD of at least 3 independent experiments in duplicates. ns: not significant, $^{*}P<0.05$, $^{***}P<0.001$, $^{****}P<0.0001$ using one-way ANOVA with Dunnett's multiple comparison test to *control(RNAi)*.

https://doi.org/10.1371/journal.pgen.1008638.g004

animals on *control(RNAi)*, the level is increased ranging from ~1.5-fold upon *rpt-3(RNAi)* to ~7.4-fold upon *hars-1(RNAi)* (Fig 4C). Using the single-copy $P_{hsp\text{-}6\ \mathrm{mtHSP70}}$*gfp* transgene *bcSi9*, we confirmed that the knock-down of *cogc-2*$^{\mathrm{COG2}}$, *cogc-4*$^{\mathrm{COG4}}$, *hars-1*$^{\mathrm{HARS}}$, *rpt-3*$^{\mathrm{PSMC4}}$, *smgl-1*$^{\mathrm{NBAS}}$ or *ins-7* suppresses *fzo-1(tm1133)*-induced UPR$^{\mathrm{mt}}$ (Fig 4D and 4E). Therefore, we propose that it is the increase in autophagic flux that suppresses *fzo-1(tm1133)*-induced UPR$^{\mathrm{mt}}$.

Since *let-363*$^{\mathrm{mTOR}}$ as well as some of the additionally identified candidates (such as *hars-1*$^{\mathrm{HARS}}$, *rars-1*$^{\mathrm{RARS}}$, *tars-1*$^{\mathrm{TARS}}$ or *iars-1*$^{\mathrm{IARS}}$) have roles in translation [19], we tested the effects of the depletion of *let-363*$^{\mathrm{mTOR}}$ or *hars-1*$^{\mathrm{HARS}}$ on $P_{ges\text{-}1\ \mathrm{GES2}}$*gfp* expression in order to exclude that their depletion simply attenuates synthesis of GFP protein. We found that *let-363(RNAi)* or *hars-1(RNAi)* leads to suppression of $P_{ges\text{-}1\ \mathrm{GES2}}$*gfp* expression by 39% or 25%, respectively (Fig 2A and 2B). However, we found that depletion of *let-363*$^{\mathrm{mTOR}}$ or *hars-1*$^{\mathrm{HARS}}$ also has a beneficial effect on mitochondrial membrane potential in *fzo-1(tm1133)* mutants since TMRE fluorescence intensity per mitochondrial area is increased by 14% or 31%, respectively while having the opposite effect in wild-type animals, in which it is decreased by 40% or 47%, respectively (Fig 2E–2H). This suggests that the suppression of *fzo-1(tm1133)*-induced UPR$^{\mathrm{mt}}$ upon depletion of *let-363*$^{\mathrm{mTOR}}$ or *hars-1*$^{\mathrm{HARS}}$ is the result of a combination of an increase in mitochondrial membrane potential and the attenuation of cytosolic translation.

The induction of autophagy is not *per se* beneficial for organismal fitness

Since mitochondrial membrane potential is increased in *fzo-1(tm1133)* animals upon induction of autophagy, we tested whether this has a beneficial effect at the organismal level. Using the 'thrashing' assay [75,76], we tested whether the motility of *fzo-1(tm1133)* animals is improved. As previously shown [77], thrashing rates are decreased in *fzo-1(tm1133)* mutants when compared to wild type (S5A Fig). We found that thrashing rates do not change upon *vps-4(RNAi)* or *vps-20(RNAi)* in either *fzo-1(tm1133)* or wild-type animals (S5B and S5C Fig). Therefore, increasing autophagic flux does not *per se* have beneficial effects on organismal fitness. In contrast, we found that thrashing rates are significantly increased upon *let-363(RNAi)* or *hars-1(RNAi)* in both *fzo-1(tm1133)* and wild-type animals (S5B and S5C Fig). Thus, the induction of autophagy can lead to increased motility under certain circumstances, but this effect may be covered upon depletion of ESCRT.

Depletion of ESCRT components in *fzo-1(tm1133)* animals with a block in autophagy results in embryonic lethality

To test the hypothesis that increased autophagic flux is necessary for the suppression of *fzo-1 (tm1133)*-induced UPR$^{\mathrm{mt}}$ in ESCRT-depleted animals, we generated a *fzo-1(tm1133); unc-51 (e369)* double mutant in the $P_{hsp\text{-}6\ \mathrm{mtHSP70}}$*gfp (bcSi9)* reporter background and subjected it to

RNAi against either *vps-4*^{VPS4} or *vps-20*^{CHMP6}. However, we found that either RNAi treatment results in progeny that undergoes embryonic arrest. To circumvent this problem, we subjected *fzo-1(tm1133)* mutants to double-RNAi against *unc-51*^{ULK} and *ESCRT* but failed to detect suppression of UPR^{mt} upon *ESCRT(RNAi)* diluted with *control(RNAi)* (S6A Fig). Next, we depleted ESCRT components by RNAi starting from the second larval stage (L2) (rather than in the parental generation and throughout development) and examined reporter expression once the animals had reached the fourth larval stage (L4). Interestingly, we found that subjecting *fzo-1 (tm1133)* L2 larvae to *vps-4(RNAi)* or *vps-20(RNAi)* does not increase autophagic flux and fails to suppress UPR^{mt}, while *atfs-1(RNAi)* is able to suppress UPR^{mt} under these conditions (S6B and S6C Fig). We repeated this experiment in the background of an RNAi-sensitizing mutation, *rrf-3(pk1426)*, but again were unable to detect suppression of the P$_{hsp\text{-}6\ \mathrm{mtHSP70}}$*gfp (bcSi9)* reporter upon *ESCRT(RNAi)* while *atfs-1(RNAi)* suppressed (S6D Fig). Based on these results, we conclude that *ESCRT(RNAi)* does not directly act on ATFS-1^{ATF4,5} to suppress UPR^{mt}. Instead, we propose that it affects UPR^{mt} indirectly through the induction of autophagy.

Blocking mitophagy does not prevent suppression in *fzo-1*(*tm1133*) animals of UPR^{mt} by ESCRT depletion

Since we were unable to test whether blocking autophagy blocks the suppression of *fzo-1 (tm1133)*-induced UPR^{mt} by depletion of ESCRT components, we tested the role of *pdr-1*^{Parkin}- and *fndc-1*^{FUNDC1,2}-dependent mitophagy in this context [78,79]. First, we used *fzo-1(tm1133); pdr-1(lg103)* double mutants, carrying the P$_{hsp\text{-}6\ \mathrm{mtHSP70}}$*gfp* (*bcSi9*) reporter, to test whether *pdr-1*^{Parkin}-dependent mitophagy is required for ESCRT-dependent suppression of *fzo-1(tm1133)*-induced UPR^{mt}. We found that knock-down of *vps-4*^{VPS4}, *vps-20*^{CHMP6} or *hgrs-1*^{HGS} still suppresses *fzo-1(tm1133)*-induced UPR^{mt} in the *pdr-1(lg103)* background (Fig 5A and 5B). Furthermore, compared to the level of suppression in *fzo-1(tm1133)* animals alone, the level of UPR^{mt} suppression in *fzo-1(tm1133); pdr-1(lg103)* animals is similar upon *vps-4(RNAi)* or *vps-20(RNAi)* and even higher upon *hgrs-1(RNAi)* (Figs 1A, 1C, 5A and 5B). Second, we tested whether depletion of ESCRT components suppresses UPR^{mt} in *fzo-1(tm1133) fndc-1(rny14)* double mutants and found that it does so to a similar extent (Fig 5C and 5D). Therefore, *pdr-1*^{Parkin}- and *fndc-1*^{FUNDC1,2}-dependent mitophagy are not required for the suppression of *fzo-1 (tm1133)*-induced UPR^{mt} upon ESCRT depletion.

Blocking autophagy in the absence of mitochondrial stress induces UPR^{mt}, but neither blocking nor inducing UPR^{mt} affects autophagy

Increasing autophagic flux suppresses *fzo-1(tm1133)*-induced UPR^{mt}. To test whether decreasing autophagic flux, conversely, induces UPR^{mt}, we analyzed *unc-51(e369)* animals (in which autophagy is blocked) and found that compared to wild-type animals, the P$_{hsp\text{-}6\ \mathrm{mtHSP70}}$*gfp* reporter is induced by 41% on average (Fig 5E and 5F). To determine whether the P$_{hsp\text{-}6\ \mathrm{mtHSP70}}$*gfp* reporter is also induced under conditions where UPR^{mt} is already activated, we analyzed *fzo-1(tm1133)*; *unc-51(e369)* double mutant animals. We found that, in the *fzo-1 (tm1133)* background, the loss of *unc-51*^{ULK} does not result in a significant increase in the expression of P$_{hsp\text{-}6\ \mathrm{mtHSP70}}$*gfp* (Fig 5E and 5F). Thus, blocking autophagy induces UPR^{mt} in the absence of mitochondrial stress but not under conditions where UPR^{mt} is already activated.

Next, we analyzed whether blocking or inducing UPR^{mt} affects autophagy. Therefore, we analyzed autophagy in animals homozygous for either the *atfs-1*^{ATF4,5} lf mutation *tm4525* or the *atfs-1*^{ATF4,5} gain-of-function (gf) mutation *et15*gf [11,80]. *atfs-1(tm4525)* has been shown to suppress the expression of the P$_{hsp\text{-}6\ \mathrm{mtHSP70}}$*gfp* and P$_{hsp\text{-}60\ \mathrm{HSP60}}$*gfp* reporters upon *spg-7*

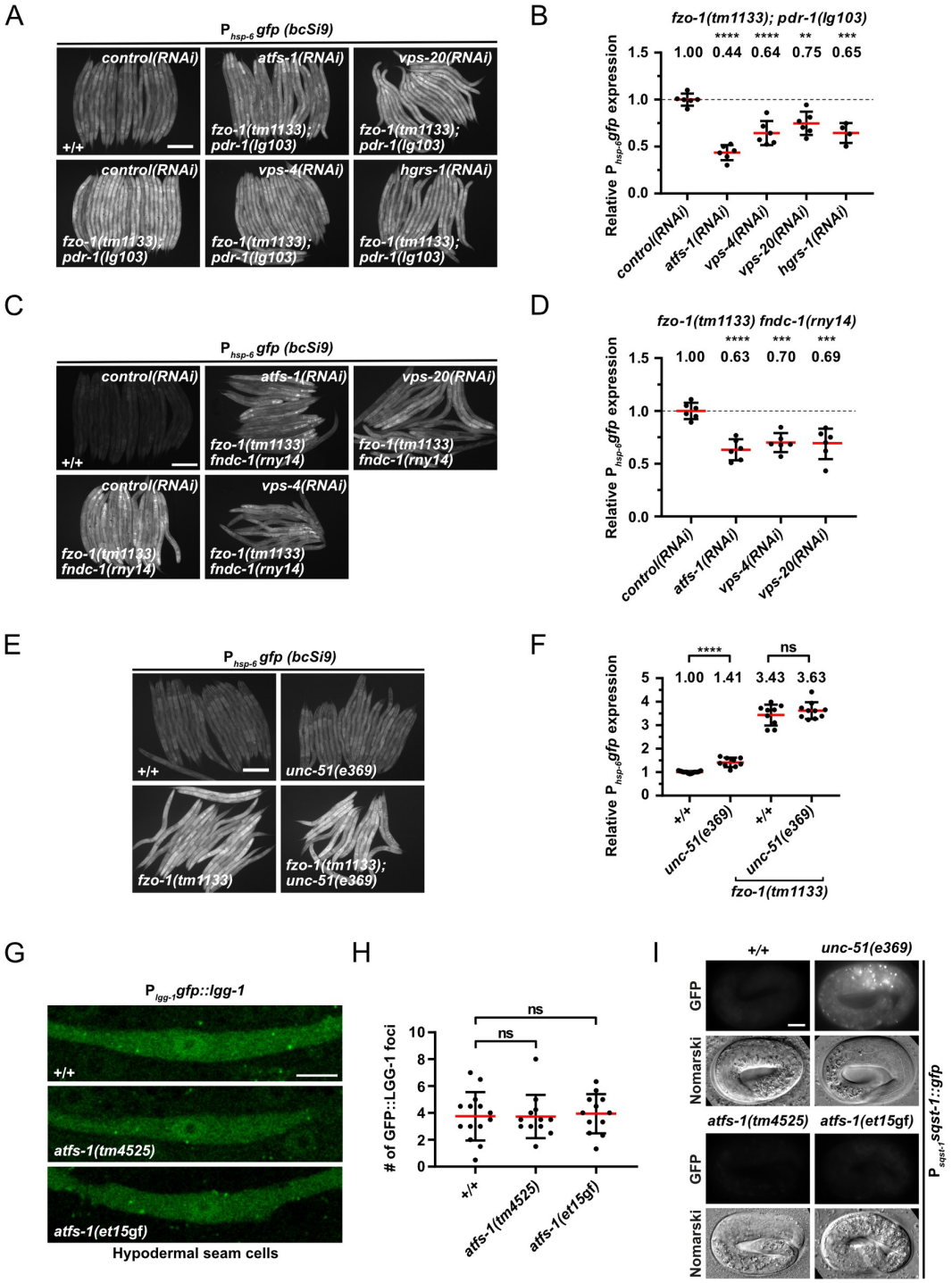

Fig 5. Functional interactions between mitophagy, autophagy and UPR^{mt}. (A) L4 larvae of *fzo-1(tm1133); pdr-1(lg103)* expressing P*hsp-6gfp (bcSi9)* were subjected to *control(RNAi)*, *atfs-1(RNAi)*, *vps-4(RNAi)*, *vps-20(RNAi)* or *hgrs-1(RNAi)* and the F1 generation was imaged. Scale bar: 200 μm. **(B)** Quantifications of fluorescence images from panel A. After subtracting the mean fluorescence intensity of wild type (+/+) on *control(RNAi)*, the values were normalized to *fzo-1(tm1133); pdr-1(lg103)* on *control(RNAi)*. Each dot represents the quantification of fluorescence intensity of 15–20 L4 larvae. Values indicate means ± SD of 3 independent experiments in

duplicates. $^{**}P<0.01$, $^{***}P<0.001$, $^{****}P<0.0001$ using one-way ANOVA with Dunnett's multiple comparison test to *control(RNAi)*. **(C)** L4 larvae of *fzo-1(tm1133) fndc-1(rny14)* expressing P_{hsp-6}*gfp (bcSi9)* were subjected to *control(RNAi)*, *atfs-1(RNAi)*, *vps-4(RNAi)* or *vps-20(RNAi)* and the F1 generation was imaged. Scale bar: 200 μm. **(D)** Quantifications of fluorescence images from panel C. After subtracting the mean fluorescence intensity of wild type (+/+) on *control(RNAi)*, the values were normalized to *fzo-1(tm1133) fndc-1 (rny-14)* on *control(RNAi)*. Each dot represents the quantification of fluorescence intensity of 15–20 L4 larvae. Values indicate means ± SD of 3 independent experiments in duplicates. $^{***}P<0.001$, $^{****}P<0.0001$ using one-way ANOVA with Dunnett's multiple comparison test to *control(RNAi)*. **(E)** Fluorescence images of L4 larvae expressing P_{hsp-6}*gfp (bcSi9)* in wild type (+/+), *unc-51(e369)*, *fzo-1(tm1133)* or *fzo-1(tm1133); unc-51(e369)*. Scale bar: 200 μm. **(F)** Quantifications of fluorescence images from panel E. Each dot represents the quantification of fluorescence intensity of 15–20 L4 larvae. Values indicate means ± SD of at least 4 independent experiments in duplicates. ns: not significant, $^{****}P<0.0001$ using two-tailed t-test. **(G)** P_{lgg-1}*gfp::lgg-1* expression in hypodermal seam cells of wild type (+/+), *atfs-1(tm4525)* or *atfs-1(et15*gf*)* L4 larvae. Scale bar: 5 μm. **(H)** Quantification of GFP::LGG-1 foci in hypodermal seam cells from panel G. Each dot represents the average amount of GFP::LGG-1 foci counted from 2–5 seam cells in one animal. n≥12 for each genotype; values indicate means ± SD; ns: not significant using one-way ANOVA with Dunnett's multiple comparison test to wild type (+/+). **(I)** Nomarski and fluorescent images of the P_{sqst-1}*sqst-1::gfp* translational reporter in embryos of wild type (+/+), *atfs-1(tm4525)* or *atfs-1(et15*gf*)* animals. As a positive control for a block in autophagy, *unc-51(e369)* was used. Representative images of >60 embryos are shown. Scale bar: 10 μm.

https://doi.org/10.1371/journal.pgen.1008638.g005

(RNAi) and of the endogenous *hsp-6*$^{\text{mtHSP70}}$ and *hsp-60*$^{\text{HSP60}}$ loci upon *cco-1(RNAi)* [11,81]. Conversely, *atfs-1(et15*gf*)* has been shown to constitutively activate UPR$^{\text{mt}}$ [80]. We found that compared to wild-type animals, hypodermal seam cells of *atfs-1(tm4525)* or *atfs-1(et15*gf*)* animals show no significant changes in the number of GFP::LGG-1$^{\text{GABARAP}}$ foci (Fig 5G and 5H). In addition, *atfs-1(tm4525)* or *atfs-1(et15*gf*)* embryos do not accumulate SQST-1$^{\text{p62}}$::GFP foci (Fig 5I). Since it has previously been reported that mitochondrial stress induces autophagy in an *atfs-1*$^{\text{ATF4,5}}$-dependent manner [40], we also tested whether the loss of *atfs-1*$^{\text{ATF4,5}}$ suppresses autophagy in *fzo-1(tm1133)* animals. We found that the number of GFP::LGG-1$^{\text{GABARAP}}$ foci remains unchanged both in *fzo-1(tm1133)* animals upon *atfs-1(RNAi)* as well as *fzo-1(tm1133); atfs-1(tm4525)* double mutants (Fig 3A and 3B), demonstrating that the induction of autophagy in *fzo-1(tm1133)* mutants is ATFS-1$^{\text{ATF4,5}}$-independent. Finally, we tested whether increasing UPR$^{\text{mt}}$ in *fzo-1(tm1133)* mutants by introducing *atfs-1(et15*gf*)* affects autophagic flux. However, we found that *fzo-1(tm1133); atfs-1(et15*gf*)* double mutants are not viable. Therefore, blocking or inducing UPR$^{\text{mt}}$ by manipulating ATFS-1$^{\text{ATF4,5}}$ activity does not affect autophagic flux in wild type and blocking UPR$^{\text{mt}}$ does not affect autophagy in *fzo-1(tm1133)* animals.

The induction of autophagy suppresses UPR$^{\text{mt}}$ induced by a block in mitochondrial dynamics but not by the loss of *spg-7*$^{\text{AFG3L2}}$

To determine whether the suppression of UPR$^{\text{mt}}$ by increased autophagic flux is specific to *fzo-1(tm1133)*-induced UPR$^{\text{mt}}$, we tested all 143 suppressors of *fzo-1(tm1133)*-induced UPR$^{\text{mt}}$ with a role in autophagy for their ability to suppress *drp-1(tm1108)*- or *spg-7(ad2249)*-induced UPR$^{\text{mt}}$ using the multi-copy $P_{hsp-6\ \text{mtHSP70}}$*gfp* transgene *zcIs13*. As shown in Fig 4A and S1 Table, we found that the knock-down of 138 of the genes (~97%) also suppresses *drp-1 (tm1108)*-induced UPR$^{\text{mt}}$. In contrast, the knock-down of 90 of the genes (~63%) suppresses *spg-7(ad2249)*-induced UPR$^{\text{mt}}$. Among these 90 genes, 41 belong to the GO categories 'Translation' or 'Ribosome Biogenesis'. Hence, their depletion may interfere with synthesis of GFP.

Interestingly, we found that knock-down of *vps-4*$^{\text{VPS4}}$ but not *vps-20*$^{\text{CHMP6}}$ or *vps-37*$^{\text{VPS37}}$ also suppresses *spg-7(ad2249)*-induced UPR$^{\text{mt}}$ (Fig 4A). Therefore, we tested whether the knock-down of *vps-4*$^{\text{VPS4}}$ or *vps-20*$^{\text{CHMP6}}$ leads to increased autophagic flux in *spg-7(ad2249)* animals. We first analyzed the basal level of autophagy in *spg-7(ad2249)* animals using the $P_{lgg-1\ \text{GABARAP}}$*gfp::lgg-1* reporter and found that compared to wild type, the number of GFP::LGG-1$^{\text{GABARAP}}$ foci is increased 2-fold (from ~4 on average in wild-type animals to ~8 on average in *spg-7(ad2249)* animals) (S7A and S7B Fig). To determine whether this increase in autophagosomes is due to a block in autophagy, we analyzed the accumulation of SQST-1$^{\text{p62}}$::GFP using

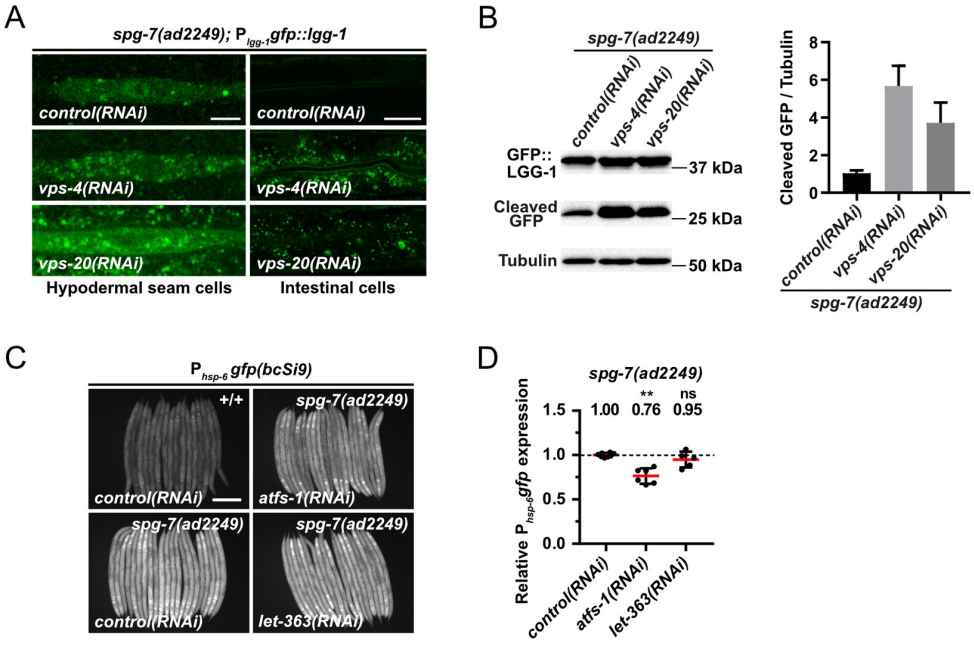

Fig 6. Induction of autophagy is not sufficient to suppress *spg-7(ad2249)*-induced UPR^{mt}. **(A)** P_{lgg-1}*gfp::lgg-1* expression of *spg-7(ad2249)* L4 larvae in hypodermal seam cells and intestinal cells upon *control(RNAi)*, *vps-4(RNAi)* or *vps-20(RNAi)*. Representative images of >80 animals from three independent biological replicates are shown. Scale bar hypodermal seam cells: 5 μm. Scale bar intestinal cells: 20 μm. **(B)** Western blot analysis of cleaved GFP levels in *spg-7(ad2249)* upon *control (RNAi)*, *vps-4(RNAi)* or *vps-20(RNAi)* using anti-GFP antibodies. Quantification of three independent experiments is shown. Values indicate means ± SD. **(C)** Fluorescence images of L4 larvae expressing P_{hsp-6}*gfp (bcSi9)* in wild type (+/+) or *spg-7(ad2249)*. L4 larvae were subjected to *control(RNAi)*, *atfs-1(RNAi)* or *let-363(RNAi)* and the F1 generation was imaged. Scale bar: 200 μm. **(D)** Quantifications of fluorescence images from panel C. After subtracting the mean fluorescence intensity of wild type (+/+) on *control(RNAi)*, the values were normalized to *spg-7(ad2249)* on *control(RNAi)*. Each dot represents the quantification of fluorescence intensity of 15–20 L4 larvae. Values indicate means ± SD of 3 independent experiments in duplicates. ns: not significant, $^{**}P<0.01$ using Kruskal-Wallis test with Dunn's multiple comparison test to *control(RNAi)*.

https://doi.org/10.1371/journal.pgen.1008638.g006

the $P_{sqst-1\ p62}$*sqst-1::gfp* reporter. We did not observe SQST-1^{p62}::GFP accumulation in *spg-7 (ad2249)* animals, thus indicating that autophagic flux is increased in *spg-7(ad2249)* mutants (S7C Fig). Next, we tested whether *vps-4(RNAi)* or *vps-20(RNAi)* further induces autophagy in the *spg-7(ad2249)* background and found that knock-down of *vps-4*^{VPS4} and also *vps-20*^{CHMP6} leads to an increase in the average number of GFP::LGG-1^{GABARAP} foci in hypodermal seam cells and intestinal cells (Fig 6A). Confirming an increase in autophagic flux, immunoblotting of GFP::LGG-1^{GABARAP} in *spg-7(ad2249)* animals revealed increased levels of cleaved GFP upon *vps-4(RNAi)* or *vps-20(RNAi)* (~5.7-fold and ~3.7-fold, respectively; Fig 6B). Finally, we tested whether the loss of *let-363*^{mTOR}, which induces autophagy and suppresses *fzo-1 (tm1133)*-induced UPR^{mt} (Fig 1A–1D), can suppress *spg-7(ad2249)*-induced UPR^{mt}. Using the single-copy $P_{hsp-6\ mtHSP70}$*gfp* transgene *bcSi9*, we found that RNAi knock-down of *let-363*^{mTOR} fails to suppress *spg-7(ad2249)*-induced UPR^{mt} (Fig 6C and 6D). In summary, these results indicate that UPR^{mt} induced by the loss of *spg-7*^{AFG3L2} is not suppressed by increasing autophagic flux. Based on these findings we propose that the induction of autophagy is sufficient to suppress UPR^{mt} induced by a block in mitochondrial dynamics but not by the loss of *spg-7*^{AFG3L2}.

Defects in mitochondrial dynamics lead to changes in the levels of certain types of triacylglyerols, which can partially be reverted by induction of autophagy

To elucidate how the induction of autophagy leads to suppression of UPR^{mt} in *fzo-1(tm1133)* and *drp-1(tm1108)* animals, we determined potential differences in metabolism in these genetic backgrounds. Since mitochondria and autophagy are known to regulate specific aspects of lipid metabolism, we performed non-targeted lipid profiling in *fzo-1(tm1133)*, *drp-1 (tm1108)* and *spg-7(ad2249)* mutant backgrounds and compared them to wild type.

Of the 5284 lipid 'features' detected, the levels of 3819 are changed in at least one of the three pairwise comparisons (*fzo-1(tm1133)* vs. wild type, *drp-1(tm1108)* vs. wild type, *spg-7 (ad2249)* vs. wild type) (S8A Fig). Among the 3819 lipid features that are changed, 1774 are currently annotated as lipids. Interestingly, a third of the annotated lipids, whose levels were changed, are triacylglycerols (TGs). TGs are storage lipids and make up a major part of lipid droplets, which are broken down into fatty acids and subsequently oxidized in mitochondria upon energy demand [82–84]. We initially determined the total amounts of TGs in the mutant backgrounds and compared them to that of wild type. Whereas *drp-1(tm1108)* mutants show an increase in the total amount of TGs, no changes are observed in *fzo-1(tm1133)* mutants and a decrease is detected in *spg-7(ad2249)* mutants (S8B Fig). To determine whether the amounts of TG species with a specific length of acyl chains and/or number of double bonds are altered, we plotted all 659 detected TGs and subsequently marked TGs that are specifically up- (red) or downregulated (blue) in *fzo-1(tm1133)*, *drp-1(tm1108)* or *spg-7(ad2249)* animals (S8C Fig and S2 Table). Consistent with the observed decrease in the total amount of TGs, most of the individual TG species are downregulated in *spg-7(ad2249)* mutants (S8B and S8C Fig). In the *drp-1(tm1108)* background, TG species with altered levels initially showed no distinct pattern regarding length of acyl chains or degree of desaturation (S8C Fig and S2 Table). However, in the *fzo-1(tm1133)* background, these TG species can be separated into two clusters. Whereas TGs with shorter acyl chains are downregulated in *fzo-1(tm1133)* mutants, 'longer' TGs with a higher degree of unsaturation are increased (S8C Fig and S2 Table). Interestingly, when looking at the overlap between *fzo-1(tm1133)* and *drp-1(tm1108)*, we observed a similar trend regarding changes in acyl length and desaturation for *drp-1(tm1108)* as well (S8D Fig and S2 Table).

Next, we tested whether the induction of autophagy can revert the specific changes in TG pattern observed in *fzo-1(tm1133)* mutants. Therefore, we knocked-down *vps-4*^{VPS4} or *cogc-2*^{COG2} to induce autophagy in *fzo-1(tm1133)* and wild-type animals and again, performed lipid profiling. We used principal component analysis (PCA) in order to show how distinct or similar the lipid profiles upon *vps-4(RNAi)* or *cogc-2(RNAi)* are. Interestingly, knock-down of *vps-4*^{VPS4} in either genotype was distinct from controls, which indicates major changes in the lipidome due to an efficient RNAi knock-down (Fig 7A). Moreover, we found that RNAi against *cogc-2*^{COG2} has only mild effects, since the samples cluster with controls in both genotypes. This might be attributed to a weak knock-down and most probably a weak induction of autophagy.

Subsequently, we specifically analyzed the TGs in *fzo-1(tm1133)* mutants on *control(RNAi)* and, consistent with our previous results (S8C Fig (left panel) and S2 Table), detected a decrease in the levels of TGs with shorter acyl chains while levels of TGs with longer chains increase, compared to wild type on *control(RNAi)* (Fig 7B (left panel) and S2 Table). The levels of TGs that are downregulated in the *fzo-1(tm1133)* background are either unchanged or further decreased upon depletion of *vps-4*^{VPS4} and the concomitant induction of autophagy (Fig 7B (middle panel) and S2 Table). In contrast, the levels of TGs that are upregulated in *fzo-1*

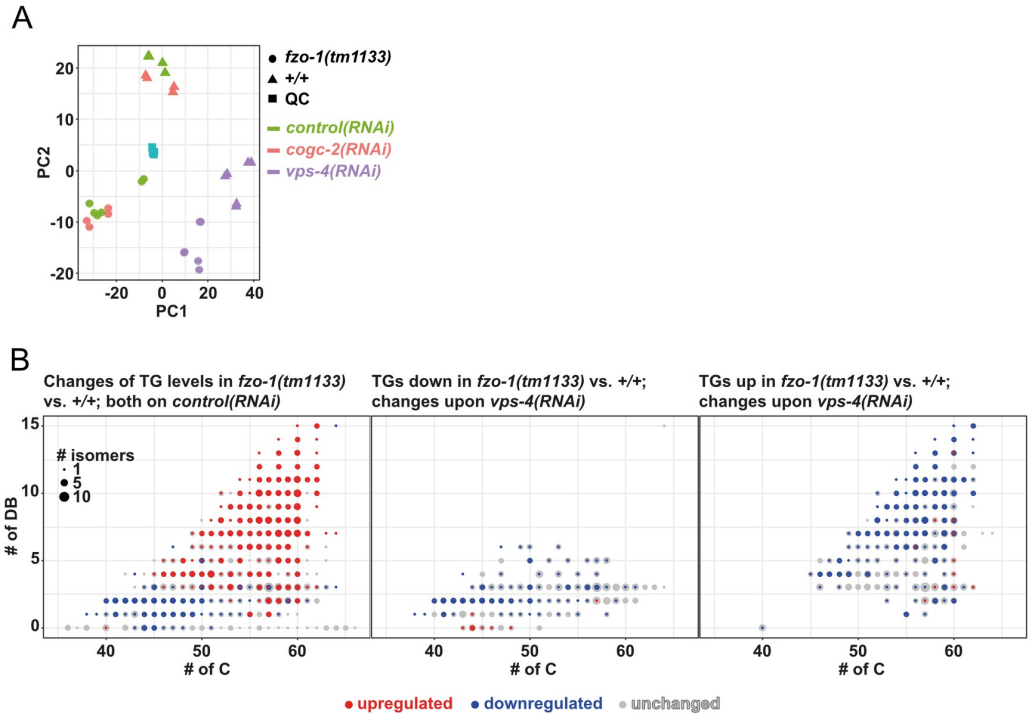

Fig 7. Induction of autophagy upon *vps-4(RNAi)* changes the levels of specific TGs in *fzo-1(tm1133)* mutants. (A) Principal component analysis (PCA) scores plot of wild-type (+/+) and *fzo-1(tm1133)* animals subjected to *control(RNAi)*, *cogc-2(RNAi)* or *vps-4(RNAi)*. Turquois squares indicate internal quality controls (QC). **(B)** Scatterplot indicating the distribution and changes in the levels of TG species in *fzo-1(tm1133)* mutants in comparison to wild type (+/+). The x-axis labels the number of carbons (# of C) and the y-axis the number of double bonds (DB) in the acyl sidechains. The size of a dot indicates the number of detected isomers for a specific sum composition. Grey dots represent all detected TGs species and blue and red dots indicate down- (blue) or upregulation (red).

https://doi.org/10.1371/journal.pgen.1008638.g007

(tm1133) animals are reduced upon induction of autophagy by knock-down of *vps-4*^{VPS4}, although not always to the levels of wild type (Fig 7B (right panel) and S2 Table). Upon *cogc-2 (RNAi)*, we detected only minor effects on the levels of TGs in *fzo-1(tm1133)* (S9A Fig and S2 Table), which is consistent with the relatively small changes in the lipid profile as assessed by PCA (Fig 7A). However, the levels of most TGs that are decreased upon *cogc-2(RNAi)* are also decreased upon depletion of *vps-4*^{VPS4} (S9B Fig), suggesting that the induction of autophagy caused by the two different knock-downs leads to partially overlapping changes in the levels of TGs. Taken together, we find that the levels of specific TGs are changed in a similar manner in mutants with defects in mitochondrial dynamics. Moreover, we show that some of these changes can be reverted by the induction of autophagy in *fzo-1(tm1133)* animals.

Discussion

Induction of autophagy increases mitochondrial membrane potential and suppresses UPR^{mt} in *fzo-1(tm1133)* mutants

We propose that the induction of autophagy partially restores membrane potential and thereby suppresses *fzo-1(tm1133)*-induced UPR^{mt}. Interestingly, a decrease in mitochondrial membrane potential has recently been shown to be the signal for UPR^{mt} induction [10]. Therefore, some aspect of mitochondrial stress that leads to both decreased membrane potential and the

induction of UPR^{mt} in *fzo-1(tm1133)* mutants can be rescued by the induction of autophagy in these animals. We were unable to verify our hypothesis since ESCRT-depleted *fzo-1(tm1133); unc-51(e369)* double mutants arrest during embryogenesis. This is in agreement with a study from Djeddi *et al*., which reported that induction of autophagy is a pro-survival mechanism in ESCRT-depleted animals [39]. Moreover, our data suggests that clearance of defective and depolarized mitochondria by *pdr-1*^{Parkin}- or *fndc-1*^{FUNDC1,2}-dependent mitophagy does not play a role in the suppression of *fzo-1(tm1133)*-induced UPR^{mt}. In addition, we propose that the induction of autophagy may lead to increased organismal fitness, but that this effect is masked by pleiotropic effects upon knock-down of certain genes such as the *ESCRT* genes.

Increased autophagic flux compensates for a block in mitochondrial dynamics

We provide evidence that the induction of autophagy can also compensate for a block in mitochondrial fission and, hence, for defects in mitochondrial dynamics. In contrast, induction of autophagy does not suppress *spg-7(ad2249)*-induced UPR^{mt}. Among the genes that suppress *spg-7(ad2249)*-induced UPR^{mt} almost half have roles in translation or ribosome biogenesis, the knock-down of which may impair GFP synthesis by compromising cytosolic translation. Furthermore, we speculate that the knock-down of the remaining genes suppresses *spg-7 (ad2249)*-induced UPR^{mt} through mechanisms other than the induction of autophagy. This supports the notion that UPR^{mt} induced by different types of mitochondrial stress are distinct in their mechanisms of induction and also in their mechanisms of suppression. In line with this, we found that different mitochondrial stresses have different impacts on the lipidome. Although FZO-1 and DRP-1 play different roles in mitochondrial dynamics, they have similar effects on the levels of many TGs when mutated. In contrast, the levels of these TGs are distinct in *spg-7(ad2249)* animals. The role of mitochondria in the metabolism of TGs is diverse. First, mitochondria are using fatty acids released from TGs upon lipolysis for energy production. Second, lipid droplet associated mitochondria deliver building blocks and energy for the synthesis of fatty acids and TGs. Fatty acids derived from this pathway typically show lower chain length and a higher degree of saturation [85]. Since we see a decrease in TGs with shorter chain length in *fzo-1(tm1133)* mutants, it is plausible that contact sites between lipid droplets and mitochondria are affected. Consistent with this, Benador *et al*. found high levels of MFN2 in lipid droplet associated mitochondria in brown adipose tissue of mice [85]. Furthermore, Rambold *et al*. reported that altered mitochondrial morphology in mouse embryonic fibroblasts lacking either *Opa1* or *Mfn1* affects fatty acid transfer from lipid droplets to mitochondria, thereby causing heterogeneous fatty acid distribution across the mitochondrial population [86]. Therefore, we speculate that the loss of *fzo-1*^{MFN} or *drp-1*^{DRP1} but not *spg-7*^{AFG3L2} leads to alterations in contact sites between lipid droplets and mitochondria and that these alterations lead to specific changes in metabolism.

Interestingly, we found that increasing autophagic flux in *fzo-1(tm1133)* animals reverts some of the changes in the levels of TGs. Consistent with these results, autophagy has been shown to have a role in the breakdown of TGs from lipid droplets, which ensures a constant fatty acid supply to mitochondria for β-oxidation [87], highlighting the importance of autophagy in fatty acid metabolism. More recently, autophagy has also been shown to directly affect the levels of enzymes involved in β-oxidation by causing the degradation of the co-repressor of PPARα, a master regulator of lipid metabolism [88]. Therefore, we propose that the induction of autophagy in mutants with defects in mitochondrial dynamics results in elevated breakdown of specific TGs that are used to fuel mitochondrial metabolism, thereby leading to increased mitochondrial membrane potential and suppression of UPR^{mt}.

Functional interactions between autophagy and UPR^{mt}

Protection of mitochondrial and ultimately cellular homeostasis was previously proposed to be dependent on the integration of different mitochondrial and cellular stress pathways but experimental data so far was limited [89]. The first evidence that autophagy can affect UPR^{mt} was the finding by Haynes *et al.* that knock-down of *rheb-1*^{RHEB}, a known positive regulator of TOR [90], suppresses the $P_{hsp\text{-}60\ HSP60}$*gfp* reporter [13]. Two more recent studies reported contradictory results with respect to the effect of blocking mitophagy on UPR^{mt} induction [7,91]. We demonstrate that a block in autophagy in the absence of mitochondrial stress induces UPR^{mt}. Blocking autophagy results in major changes in metabolism [92,93] which may, to some extent, be caused by decreased delivery of lipids into mitochondria. This could consequently lead to the activation of UPR^{mt} and thereby to a metabolic shift towards glycolysis [94]. Thus, *fzo-1(tm1133)* mutants, in which UPR^{mt} is already activated, are less dependent on their mitochondria with regard to energy production and this might explain why blocking autophagy in these animals does not further increase UPR^{mt}. Interestingly, based on our results, altering autophagy can influence UPR^{mt}, but changes in UPR^{mt} do not affect autophagy. In contrast, Guo *et al.* reported that upon mitochondrial stress, upregulation of both UPR^{mt} and autophagy is dependent on ATFS-1^{ATF4,5} [40] and Nargund *et al.* showed that a small subset of autophagy related genes are upregulated via ATFS-1^{ATF4,5} upon mitochondrial stress (induced by *spg-7(RNAi)*) [11]. However, we show that import of ATFS-1^{ATF4,5} into the nucleus under conditions where mitochondrial stress is absent, is not sufficient to induce autophagy. Taken together, we found a previously undescribed functional connection between autophagy and UPR^{mt}. We propose that the two pathways do not interact directly but that the induction of autophagy leads to improved mitochondrial function by affecting lipid metabolism and ameliorating cellular homeostasis, thereby suppressing UPR^{mt} in mutants with defects in mitochondrial dynamics (Fig 8).

Genome-wide RNAi screen identifies a new autophagy network

In our dataset of 299 suppressors of *fzo-1(tm1133)*-induced UPR^{mt} we found 143 genes that negatively regulate autophagy. Interestingly, 94% of these candidates (135/143) have orthologs in humans. We identified several components of the ubiquitin-proteasome system (UPS) (*rpt-3*^{PSMC4}, *rpn-13*^{ADRM1}, *ufd-1*^{UFD1}, *rbx-1*^{RBX1}, *cul-1*^{CUL1}) [73,95,96] and found evidence in the literature that activation of autophagy compensates for the loss of the UPS [59,63]. Additionally, we identified several genes that are involved in cell signaling, e.g. *ruvb-1*^{RUVBL1}, a

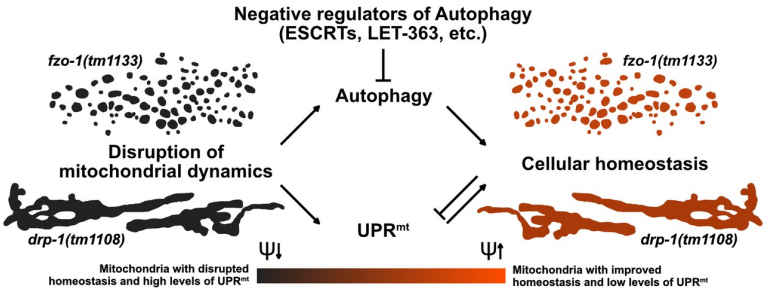

Fig 8. Autophagy compensates for defects in mitochondrial dynamics. The disruption of mitochondrial dynamics leads to altered mitochondrial morphology and to activation of UPR^{mt} and autophagy. We propose that in animals with compromised mitochondrial dynamics, the induction of autophagy fuels mitochondrial metabolism, thereby leading to increased mitochondrial membrane potential (ψ) and improved cellular homeostasis, which consequently results in suppression of UPR^{mt}.

https://doi.org/10.1371/journal.pgen.1008638.g008

component of the TOR pathway in *C. elegans* that induces autophagy when knocked-down [71]. Among the genes with roles in cellular trafficking, we found *imb-2*^{TNPO1,2}, a regulator of the nuclear transport of DAF-16^{FOXO} [70], which has been implicated in the regulation of autophagy [74]. Approximately one third of the candidates identified (44/143) are genes that regulate protein biosynthesis (S1 Table, GO categories 'Ribosome Biogenesis' and 'Translation'), which was shown to be protective against mitochondrial stress when impaired [97]. Baker and colleagues showed that knock-down of protein kinases involved in translation, such as *let-363*^{mTOR}, specifically suppress P$_{hsp-60\ HSP60}$*gfp (zcIs9)* expression. Based on our results, we propose that this effect could, to some extent, be due to the induction of autophagy. Taken together, we identified a broad range of cellular components and processes that all impact autophagy when deregulated, demonstrating the diverse and critical roles of autophagy in cellular homeostasis.

Conclusions

A block in mitochondrial dynamics leads to decreased mitochondrial membrane potential and the induction of UPR^{mt}. Lipid profiling indicates that a block in mitochondrial dynamics also causes an increase in the levels of certain types of TGs, which is reversed by induction of autophagy. We propose that the breakdown of these TGs through an autophagy-dependent process leads to elevated metabolic activity and that this causes an increase in mitochondrial membrane potential and the suppression of UPR^{mt}.

Methods

General *C. elegans* methods and strains

C. elegans strains were cultured as previously described [98]. Bristol N2 was used as the wild-type strain and the following alleles and transgenes were used: LGI: *spg-7(ad2249)* [41]; LGII: *fzo-1(tm1133)* (National BioResource Project), *rrf-3(pk1426)* [99], *fndc-1(rny14)* [78]; LGIII: *pdr-1(lg103)* [100]; LGIV: *drp-1(tm1108)* (National BioResource Project), *bcSi9* (P$_{hsp-6}$::*gfp*::*unc-54 3'UTR*) (this study), *frIs7 (nlp-29p*::*GFP + col-12p*::*DsRed)* [101]; LGV: *unc-51(e369)* [23], *atfs-1(tm4525)* (National BioResource Project), *atfs-1(et15*gf) [80]. Additionally, the following multi-copy integrated transgenes were used: *adIs2122(lgg-1p*::*GFP*::*lgg-1 + rol-6 (su1006))* [102], *bpIs151 (sqst-1p*::*sqst-1*::*GFP + unc-76(+))* [51], *zcIs9* (P$_{hsp-60}$::*gfp*::*unc-54 3'UTR)* [14], *zcIs13* (P$_{hsp-6}$::*gfp*::*unc-54 3'UTR)* [14], *zcIs18* (P$_{ges-1}$::*gfp(cyt))* [103], *bcIs79* (P$_{let-858}$::*gfp*^{mt}::*let-858 3'UTR + rol-6(su1006))*, *bcIs78* (P$_{myo-3}$::*gfp*^{mt}::*unc-54 3'UTR + rol-6(su1006)*) [46]. The strains MOC92 *bicIs10(hsp-1*::*tagRFP*::*unc-54 3'UTR)* and MOC119 *bicIs12(ttr-45p*::*tagRFP*::*ttr-45 3'UTR)* were generated in the Casanueva lab by gonadal microinjection of plasmids pMOC1 and pMOC2, respectively followed by genome integration via UV irradiation using a Stratagene UV Crosslinker (Stratalinker) [104]. The irradiation dose was 35mJ/cm^2 corresponding to Stratalinker power set up at 350. The single-copy integration allele *bcSi9* was generated using MosSCI [105] of the plasmid pBC1516. The strain EG8081 (*unc-119(ed3) III; oxTi177 IV*) was used for targeted insertion on LGIV [106]. The strain MD2988 (P$_{let-858}$*gfp*^{mt}) was generated by gonadal microinjection of the plasmid pBC938 followed by genome integration via EMS mutagenesis.

Plasmid construction

The plasmid pBC1516 was constructed using Gibson assembly [107]. The vector pCFJ350 (a gift from Erik Jorgensen; Addgene plasmid no. 34866) [108] was digested using AvrII. The putative *hsp-6* promoter (1695bp upstream of the start codon of *hsp-6*) + 30 bp of the *hsp-6*

gene were PCR amplified from gDNA using overhang primers to pCFJ350 5'- acgtcaccggttctagatacTCGAGTCCATACAAGCACTC -3' and *gfp*::*unc-54 3'UTR* 5'- ctttactcatGGAAGACAAGAATGATCGTG -3' (lower case letters indicating overhangs). *gfp*::*unc-54 3'UTR* was PCR amplified from pPD95.77 using overhang primers to P_{hsp-6} 5'- cttgtcttccATGAGTAAAGGAGAAGAACTTTTC -3' and pCFJ350 5'- tagagggtaccagagctcacAAACAGTTATGTTTGGTATATTGG -3' (lower case letters indicating overhangs).

The plasmid pBC938 was constructed using a classical cloning approach. Therefore, gfp^{mt} was amplified by PCR from pBC307 ($P_{hs}gfp^{mt}$) [109] using the following primers carrying a NheI or KpnI restriction site, respectively:

mitogfpFKpnI: 5'- GGTACCATGGCACTCCTGCAATCAC -3'

mitogfpRNheI: 5'- GCTAGCCTATTTGTATAGTTCATCCATGC -3'

The amplified fragment was then digested with KpnI and NheI and subsequently ligated into the NheI and KpnI digested backbone L3786 ($P_{let-858}$*NLS-GFP*) (L3786 was a gift from Andrew Fire (Addgene plasmid # 1593; http://n2t.net/addgene:1593; RRID:Addgene_1593)).

The plasmids pMOC1 and pMOC2 were generated by Gibson cloning, using Gibson Assembly Master Mix (New England Biolabs E2611) according to standard protocol using the vector pTagRFP-C as backbone (Evrogen). For the plasmid pMOC1 *(hsp-1p*::*tagRFP*::*unc-54 3'UTR))*, the 1.3 kb intergenic region upstream *hsp-1* was amplified and inserted at ScaI site, using the following primers:

hsp-1p fwd: 5'- GCCTCTAGAGTTACTTCGGCTCTATTACTG -3'

hsp-1p rev: 5'- tatcgcgagtTTTTACTGTAAAAAATAATTTAAAAATCAAGAAATAG -3'

The 3'UTR of *unc-54* was amplified and inserted at XhoI site using the primers:

unc54UTR RFP fwd: 5'- CTTAATTaaAGGACTCAGATCgtccaattactcttcaacatc -3'

unc54UTR RFP rev: 5'- CAGAATTCGAAGCTTGAGCttcaaaaaaatttatcagaag -3'

For the plasmid pMOC2 *(ttr-45p*::*tagRFP*::*ttr45 3'UTR)*, the 1.85 kb intergenic region upstream *ttr-45* was amplified and inserted at XbaI site, using the following primers:

ttr-45p fwd: 5'- GCCTGCAGGCGCGCCTctgaaaaaaaatcatattacaaatcag -3'

ttr-45p rev: 5'- AGATATCGCGAGTACTtgaaattttaaattttgaattttagtc -3'

The 3'UTR of *ttr-45*, contained in the following primer (lower case) was inserted at the XhoI site:

ttr-45UTR:

5'- TTaaAGGACTCAGATCaataattttgattttatgtataataaagactttatctcggGCTCAAGCTTCGAATT -3'

RNA-mediated interference

RNAi by feeding was performed using the Ahringer RNAi library [45]. *sorb-1(RNAi)* was used as a negative control (referred to as '*control(RNAi)*') in all RNAi experiments. For all experiments, except for the screens in *fzo-1(tm1133)*, *drp-1(tm1108)* and *spg-7(ad2249)*, RNAi clones were cultured overnight in 2 mL of LB carbenicillin (100 μg/mL) at 37˚C and 200 rpm. The RNAi cultures were adjusted to 0.5 OD and 50 μL were used to seed 30 mm RNAi plates containing 6 mM IPTG. The plates were incubated at 20˚C in the dark. 24 hours later, two L4 larvae of all wild-type strains or 16 L4 larvae of all strains carrying the *fzo-1(tm1133)* allele were inoculated onto the RNAi plates. L4 larvae of the F1 generation were collected after 4 days (wild-type strains) or 6–7 days (*fzo-1(tm1133)* mutants). *hars-1(RNAi)* was diluted 1:5 with *sorb-1(RNAi)* in all experiments. Larvae were imaged using M9 buffer with 150 mM sodium azide.

For the screens with the multi-copy *zcIs13* transgene in *fzo-1(tm1133)*, *drp-1(tm1108)* and *spg-7(ad2249)*, RNAi clones were cultured overnight in 100 μL of LB carbenicillin (100 μg/mL)

in a 96 well plate format at 37˚C and 200 rpm. 10 μL of the RNAi cultures was used to seed 24 well RNAi plates containing 0.25% Lactose (w/v). The plates were incubated at 20˚C in the dark. 24 hours later, 3 L4 larvae of all strains carrying the *fzo-1(tm1133)* and *spg-7(ad2249)* allele, and 2 L4 larvae of *drp-1(tm1108)* were inoculated onto the RNAi plates. The F1 generation was scored by eye for fluorescence intensity after 4–7 days.

Image acquisition, processing and analysis

For each RNAi condition, 10–20 animals were immobilized with M9 buffer containing 150 mM sodium azide on 2% agarose pads and imaged at 100x using a Leica GFP dissecting microscope (M205 FA) and the software Leica Application Suite (3.2.0.9652).

For image analysis, we used a Fiji-implemented macro using the IJ1 Macro language to automate the intensity measurement within defined areas of 2-dimensional images. An automated threshold using the Triangle method was applied to the fluorescence microscopy image, in order to generate a binary mask (The Triangle method was selected among the 16 available auto threshold methods of ImageJ as it provided the best results.). The mask was then inverted and the Particle Analyzer of ImageJ was used to remove noise by setting a minimum size (10 pixels) for objects to be included in the mask. After manually removing any remaining unwanted objects, the mask was applied to the corresponding fluorescent microscopy image and mean fluorescent intensity was measured. The mean fluorescent intensity outside the mask was defined as the background.

Mitochondrial morphology was assessed in a strain carrying *bcIs78* and *bcIs79* using a Zeiss Axioskop 2 and MetaMorph software (Molecular Devices).

TMRE staining and quantification

TMRE staining was performed with the F1 generation of respective RNAi treatments. L2 larvae were inoculated onto plates containing 0.1 μM TMRE (Thermo Life Sciences T669) and imaged in L4 stage using a 63x objective on Zeiss Axioskop 2 and MetaMorph software (Molecular Devices). Thereby TMRE is used in non-quenching mode and therefore suitable for quantifications and direct correlations to mitochondrial membrane potential.

The image is first converted to an 8-bit image, after which the continuous background signal is removed through background subtraction using the "rolling ball" algorithm with a ball radius of 15 pixels [110]. To remove remaining noise, two filters are applied. The first being a minimum filter with a value of 1, therefore replacing each pixel in the image with the smallest pixel value in a particular pixel's neighborhood. This is followed by a mean filter with a radius of 2, which replaces each pixel with the neighborhood mean. Next, the Tubeness plugin is run with a sigma value of 1.0, which generates a score of how tube-like each point in the image is by using the eigenvalues of the Hessian matrix to calculate the measure of "tubeness" [111]. The resulting 32-bit image is converted back to 8-bit and an automatic threshold (using the IsoData algorithm) generates a binary mask. The final step involves the removal of any particles that are smaller than 10 pixels in size for they are assumed to be noise.

Raw image files are opened in parallel to their appendant binary masks (generated by the segmentation macro) and a mask-based selection is created in the raw image. Within this selection measurements are obtained in the raw image and collected for subsequent analysis.

Western blot analysis

Mixed-stage populations of worms were harvested, washed three times in M9 buffer, and the pellets were lysed in 2x Laemmli buffer. For analysis of the additional candidates (Fig 4) 60–80 L4 stage animals were picked for western blotting. For analysis of endogenous HSP-6, 100 L4

larvae were harvested per genotype. The protein extracts were separated by 10% SDS-PAGE and transferred to a PVDF membrane (0.45 μm pore, Merck Millipore). To detect GFP and Tubulin, we used primary anti-GFP (1:1000, Roche 11814460001) and primary anti-α-Tubulin (1:5000, Abcam ab7291) antibodies and secondary horseradish peroxidase-conjugated goat anti-mouse antibodies (BioRad #1706516). To detect endogenous HSP-6, we used anti-HSP-6 (1:10,000) as described previously [42] and secondary horseradish peroxidase-conjugated goat anti-rabbit antibodies (BioRad #1706515). Blots were developed using ECL (Amersham) or ECL Prime (Amersham) according to manufacturer's protocol and images were quantified using the ChemiDoc XRS+ System (BioRad).

Analysis of autophagy and quantification of GFP::LGG-1 foci

L4 stage animals (except otherwise mentioned) were immobilized with M9 buffer containing 150 mM sodium azide on 2% agarose pads. Animals were imaged using a Leica TCS SP5 II confocal microscope (Leica Application Suite LAS software) with a 63x objective. GFP fluorescence was detected by excitation at 488 nm and emission at 507–518 nm. GFP::LGG-1 foci were counted in hypodermal seam cells on single images where the nucleus could clearly be seen. The amount of GFP::LGG-1 foci was counted in 2–5 seam cells per animal and the average number of GFP::LGG-1 foci per hypodermal seam cell was plotted for graphical representation and statistical analysis. SQST-1::GFP was imaged using Zeiss Axioskop 2 and MetaMorph software (Molecular Devices).

Analysis of thrashing rate

Body bends of L4 larvae were counted as previously described [75]. Briefly, the animals were transferred from the RNAi plates onto an empty NGM plate to get rid of all bacteria and then subsequently transferred into an empty petri dish filled with M9 buffer. After letting the L4 larvae adjust for one minute, they were recorded using a Samsung Galaxy S8 attached to a Leica MS5 stereomicroscope. The videos were played back at reduced speed using VLC media player (v3.0.8) and the number of body bends was counted manually for 1 minute.

Statistics

For experiments where two groups were compared, datasets were first tested for normality using Shapiro-Wilk normality test. If all samples of one dataset were found to be normally distributed, we conducted an unpaired two-tailed t-test. If samples were found to have non-equal variance, we conducted an unpaired tow-tailed t-test with Welch's correction. For experiments where more than two groups were compared, datasets were first tested for normal distribution using Shapiro-Wilk normality test and then tested for equal variance using Brown-Forsythe test. If samples of one dataset were found to be normally distributed and to have equal variance, one-way ANOVA with Dunnett's post hoc test was used to test for statistical significance with multiple comparisons to controls. If the dataset was not found to have normal distribution and/or have equal variance, Kruskal-Wallis test with Dunn's post hoc test for multiple comparisons to controls was used.

Lipid profiling using UPLC-UHR-ToF-MS

RNAi in lipidomic experiments was performed using *OP50(xu363)*, which is compatible for dsRNA production and delivery [112]. The L4440 plasmids containing the coding sequence of *sorb-1*, *cogc-2* or *vps-4* were purified from HT115 bacteria of the Ahringer library [45] using Qiagen Plasmid Mini Kit (Cat. No. 12125) and subsequently transformed into chemically

competent *OP50(xu363)*. Single clones were picked, sequenced and glycerol stocks were made for subsequent experiments. Bacterial clones were grown as described in section 'RNA-mediated interference' and 1 mL bacterial culture (OD_{600} = 0.5) was seeded onto 92 mm RNAi plates containing 1 mM IPTG. For *sorb-1(RNAi)* 120 L4 larvae, for *vps-4(RNAi)* 240 L4 larvae and for *cogc-2(RNAi)* 200 L4 larvae were transferred onto RNAi plates. Worms were collected in L4 stage after 6 days by washing the plates with MPEG. Worm pellets were subsequently washed using M9 and shock-frozen using liquid nitrogen and kept at -80˚C until extraction.

Lipids were extracted using the BUME method [113]. Briefly, worms were resuspended in 50 μL MeOH and transferred to custom made bead beating tubes. Samples were homogenized at 8000 rpm in a Precellys Bead Beater for 3 times 10 seconds with 20 seconds breaks in between. The additional Cryolys module was used with liquid nitrogen to prevent excessive heating of samples during disruption. 150 μL butanol and 200 μL heptane-ethyl acetate (3:1) was added to each sample sequentially which were then incubated for 1 h at 500 rpm / RT. 200 μL 1% acetic acid was added to each sample followed by centrifugation for 15 min at 13000 rpm / 4˚C. The upper organic phase was transferred to a fresh Eppendorf tube and the lower aqueous phase was re-extracted by the addition of 200 μL heptane-ethyl acetate followed by incubation and centrifugation as described above. The upper organic phase was transferred to the already obtained organic phase. The lower phase was transferred to a new Eppendorf tube and used for metabolomic analyses. Samples were evaporated to dryness and stored at -20˚C. For lipidomics, samples were re-dissolved in 50 μL 65% isopropanol / 35% acetonitrile / 5% H_2O, vortexed and 40 μL were transferred to an autosampler vial. The remaining 10 μL were pooled to form a QC sample for the entire study. The precipitated proteins in the aqueous phase were used for determination of protein content using a Bicinchoninic Acid Protein Assay Kit (Sigma-Aldrich, Taufkirchen, Germany).

Lipids were analyzed as previously described [114]. Briefly, lipids were separated on a Waters Acquity UPLC (Waters, Eschborn, Germany) using a Waters Cortecs C18 column (150 mm x 2.1 mm ID, 1.6 μm particle size, Waters, Eschborn Germany) and a linear gradient from 68% eluent A (40% H_2O / 60% acetonitrile, 10 mM ammonium formate and 0.1% formic acid) to 97% eluent B (10% acetonitrile / 90% isopropanol, 10 mM ammonium formate and 0.1% formic acid). Mass spectrometric detection was performed using a Bruker maXis UHR-ToF-MS (Bruker Daltonic, Bremen, Germany) in positive ionization mode using data dependent acquisition to obtain MS^1 and MS^2 information. Every ten samples, a pooled QC was injected to check performance of the UPLC-UHR-ToF-MS system and used for normalization.

Raw data was processed with Genedata Expressionist for MS 13.0 (Genedata AG, Basel, Switzerland). Preprocessing steps included noise subtraction, m/z recalibration, chromatographic alignment and peak detection and grouping. Data was exported for Genedata Expressionist for MS 13.0 Analyst statistical analysis software and as .xlxs for further investigation. Maximum peak intensities were used for statistical analysis and data was normalized on the protein content of the sample and an intensity drift normalization based on QC samples was used to normalize for the acquisition sequence.

Lipid features that were detected in all pooled QC samples and had a relative standard deviation (RSD) $< 30\%$ were further investigated by statistical analysis. 5284 features passed this filter and the different mutants were compared against the wild-type control using Welch test. Lipids with a p-value < 0.05 were considered to be significantly changed.

Lipids were putatively annotated on the MS^1 level using an in-house developed database for *C. elegans* lipids and bulk composition from LipidMaps [115], when available. Matching of MS^2 spectra against an in-silico database of *C. elegans* lipids and LipidBlast was performed using the masstrixR package [116] (https://github.com/michaelwitting/masstrixR) and only

hits with a forward and reverse matching score > 0.75 were considered. Annotations of interesting biological peaks were manually verified and corrected if necessary.

High throughput qRT-PCR on single worms using the Biomark system

cDNA from single worms was analyzed on the biomark system using Flex Six IFC. This nanofluidic chip allows the comparison of 12 target genes across 36 individual worms per genotype. We monitored biological variability in gene expression of targets: endogenous *hsp-6*, *hsp-60* and either *bcSi9* single-copy or *zcIs13* multi-copy transgenes. In addition, we monitored variability in gene expression of three "gold standard" control genes: either non-variable (*hsp-1*), medium variable (*ttr-45*) or highly variable (*nlp-29*). Ct values for all targets were normalized to the average of three housekeeping genes (*cdc-42*, *ire-1* and *pmp-3*).

Design of qRT-PCR primers. Primers sets were designed to quantify *C. elegans* post-spliced transcripts. Primer sets were designed to span exon-exon junctions using NCBI Primer Blast software and subsequently blasted against the *C. elegans* genome to test for off-target complementarity. The list of qRT-PCR primers used with their PCR efficiency and coefficient of determination (R^2) is shown in S3 Table.

Quantification of primer efficiency and specificity. Primers were selected for high PCR efficiency between 90 and 115%. To estimate primer efficiencies, a comprehensive titration of cDNA obtained from 500 ng of Trizol-extracted RNA was prepared within the range of linear amplification using a 1:2 series dilution. Each qRT-PCR reaction contained 1.5 μL of primer mix forward and reverse at 1.6 μM each, 3.5 μL of nuclease free water, 6 μL of 2X Platinum® SYBR® Green qPCR Supermix-UDG (Thermo Fisher Scientific PN 11744–500) and 1 μL of worm DNA lysate diluted or not. The qRT-PCR reactions were run on an iCycler system (Bio-Rad). PCR efficiencies were calculated by plotting the results of the titration of cDNA (Ct values versus log dilution) within the range of linear amplification. The efficiency was defined by the formula 100 x (10 ($^{-1/slope}$)/2) with an optimal slope defined as -3.3 ($^{1/3.3}$) = 2.

Worm synchronization. Worms were grown at 20˚C and bleach synchronized. 36 worms per genotype were harvested at the L4.8/L4.9 stage based on vulval development [117], at about 48h post L1 plating for WT and about 65h post L1 plating for *fzo-1(tm1133)*.

Worm lysis for total RNA preparation of single worm RNA. During harvesting, synchronized worms were individually picked into 10 μL lysis buffer (Power SYBR® Green Cells-to-C_T™ kit, Thermo Fisher Scientific) in 8 strip PCR tubes. After harvesting the worms, the 8 strip PCR tubes were freeze-thawed 10 times by transferring tubes from a liquid nitrogen bath into a warm water bath (about 40ºC). Samples were vortexed during 20 minutes on a thermoblock set up at 4ºC. The samples were then quickly spun down and 1 μL of stop solution (Power SYBR Green Cells-to-C_T kit, Thermo Fisher scientific) was added in each tube. The samples were then stored at -80ºC before further processing. Storage time was no more than one week before proceeding to reverse transcription.

Reverse transcription. Reverse Transcription PCR (RT-PCR) was performed by adding 5 μL of lysis mix (lysis buffer and stop solution) to 1.25 μL of Reverse Transcription Master Mix (Fluidigm PN 100–6297) into 96 well plates. We included one minus RT control per plate, containing 5 μL of lysis mix and 1.25 μL of RNase free water. Reverse Transcription cycling conditions were 25ºC for 5 min, 42ºC for 30 min and 85ºC for 5 min.

Pre-amplification. Pre-amplification was performed according to Fluidigm instruction manual: for every nano-fluidic chip, a pooled primer mix was prepared by adding 1 μL of primer stock (for every target gene to be tested on the chip) to water up to a final volume of 100 μL. Every primer stock contained both reverse and forward primers at a concentration of 50 μM each. A pre-amplification mix was prepared containing for each sample: 1 μL of

PreAmp Master mix (Fluidigm PN 100–5744), 0.5 μL of pooled primer mix and 2.25 μL of nuclease free water. 3.75 μL of pre-amplification mix was then aliquoted in a 96 well-plate. 1.25 μL of cDNA was then added in each well. The samples were mixed by quick vortexing and centrifuged. Pre amplification conditions were the following: 95°C for 2 min, 10 cycles of denaturation at 95°C for 15 s followed by annealing/extension at 60°C for 4 min.

Exo I treatment and sample dilution. To remove unincorporated primers, 2 μL of Exonuclease I mix was added to each pre-amplification reaction. The Exonuclease I mix contained 0.2 μL of Exonuclease I reaction buffer (New England BioLabs), 0.4 μL Exonuclease I at 20 Units/μL (New England BioLabs), and 1.4 μL of nuclease free water. The samples were incubated at 37°C for 30 min followed by 15 min at 80°C. The samples were finally diluted 1:5 by adding 18 μL of DNA suspension buffer (10 mM Tris, 0.1 mM EDTA, pH = 8.0, TEKnova PN-T0021).

Assay Mix preparation. For every pair of primers to be tested on the Fluidigm nano-fluidic chip, an assay mix was individually prepared on a 384 well PCR plate (for easier transfer to the Fluidigm nano-fluidic chips), typically the day before the experiment. Each assay mix (for 36 samples) contained 6.25 μL of 2X Assay loading reagent (Fluidigm PN 100–5359), 5 μL of DNA suspension buffer (10 mM Tris, 0.1 mM EDTA, pH = 8.0, TEKnova PN T0021), and 1.25 μL of primer stock (reverse and forward primers at a concentration of 50 μM each). Assay mixes were vortexed during 30 s minimum on a thermoblock set up at 4 °C and centrifuged for 30 s minimum. 3 μL of each assay mix were loaded onto Flex Six Gene Expression IFC chips (Fluidigm PN 100–6308).

Sample Mix preparation. The samples mixes were prepared at the day of the experiment. 1.8 μL of diluted PreAmp and Exo I treated samples were added to a sample mix containing 2 μL of 2X SsoFast EvaGreen Supermix with Low ROX (Bio-Rad, PN 172–5211) and 0.2 μL of Flex Six Delta Gene Sample Reagent (Fluidigm PN 100–7673). 3 μL of each sample mix was loaded onto Flex Six IFC chips.

Biomark Run and data clean-up. Assay and sample mixes of Flex Six IFCs were loaded using a HX IFC controller (Fluidigm). The nano-fluidic chips were then run on a Biomark HD using the FlexSix Fast PCR+melt protocols. After the run, the data from every well on the plate was checked and cleaned up as following: samples for which all PCRs failed were eliminated. Any well, in which the melting peak temperature of a particular pair of primers was not as expected, was eliminated. It would happen occasionally, presumably when pairs of primers form dimers when target gene concentrations are very low, or from interactions of target primers with other primers in the pooled primer mix. Ct values were then normalized to the average of housekeeping genes and relative mRNA expression levels were calculated using the delta Ct method.

Determination of "Gold Standard" stable and variable transcripts. To validate our single-worm high throughput qRT-PCR method to monitor inter-individual variability in gene expression, we measured the coefficient of variation CV (CV = standard deviation/mean) for fluorescent transcriptional reporters of a stable gene MOC92 *bicIs10(hsp-1p*::*tagRFP*::*unc-54 3'UTR)* and of two variable transgenes MOC119 *bicls12(ttr-45p*::*tagRFP*::*ttr45 3'UTR)* (medium variable) and IG274 *frIs7(nlp-29p*::*GFP; col-12p*::*DsRed)* (highly variable). We verified that it matches the coefficient of variation calculated from normalized Ct values of endogenous transcripts *hsp-1*, *ttr-45* and *nlp-29* measured in our high-throughput single worm qPCR assay. Synchronized MOC92 and MOC119 transgenic worms were immobilized in M9 containing 3 mM Levamisole and imaged on a Nikon SMZ18 stereo epi-fluorescence microscope, while synchronized IG274 transgenic animals were mounted in 3 mM levamisole on a 2% agarose pad and imaged on a Nikon Ti Eclipse inverted microscope, as the fluorescence levels of the *nlp-29* reporter in IG274 were too low to be imaged on the Nikon SMZ18. The

fluorescence of each individual transgenic worm was quantified using Fiji software, by subtracting the background measurement from fluorescence measurements. The coefficient of variation was determined for synchronized population of day 2 animals (day 2 of adulthood: 74h post L1 plating at 20˚C) for *nlp-29* and *ttr-45* reporters, while it was determined in day 1 synchronized animals (50h post L1 plating at 20˚C) for *hsp-1* reporter. The coefficient of variation is measured as follows:

- *bicIs10(hsp-1p*::*tagRFP*::*unc-54 3'UTR)*: 0.09< CV <0.14 (3 biological replicates)
- *bicls12(ttr-45p*::*tagRFP*::*ttr45 3'UTR)*: 0.31<CV<0.45 (3 biological replicates)
- *frIs7(nlp-29p*::*GFP; col-12p*::*DsRed)*: CV = 1.0 (1 biological replicate)

We observed a good correlation between the coefficient of variation for *hsp-1*, *ttr-45* and *nlp-29* transgenic reporters and the coefficient of variation for endogenous transcripts *hsp-1*, *ttr-45* and *nlp-29* measured by single worm qRT-PCR (S1F Fig).

Supporting information

S1 Fig. Comparison of expression levels and inter-individual variability of multi-copy $P_{hsp\text{-}6\ mtHSP70}$*gfp (zcIs13)* and single-copy integrated $P_{hsp\text{-}6\ mtHSP70}$*gfp (bcSi9)* transgenes. **(A)** Brightfield (upper panel) and fluorescence images (lower panel) of L4 larvae expressing $P_{hsp\text{-}6}$*gfp (zcIs13)* in wild type (+/+), *spg-7(ad2249)*, *fzo-1(tm1133) or drp-1(tm1108)*. Scale bar: 200 μm. **(B)** Brightfield (upper panel) and fluorescence images (lower panel) of L4 larvae expressing $P_{hsp\text{-}6}$*gfp (bcSi9)* in wild type (+/+), *spg-7(ad2249)*, *fzo-1(tm1133)* or *drp-1(tm1108)*. Scale bar: 200 μm. **(C)** Quantifications of fluorescence images of panel A ($P_{hsp\text{-}6}$*gfp (zcIs13)*) are shown. Each dot represents quantification of 15–20 L4 larvae. Values indicate means ± SD of ≥5 independent measurements. **(D)** Quantifications of fluorescence images of panel B ($P_{hsp\text{-}6}$*gfp (bcSi9)*) are shown. Each dot represents quantification of 15–20 L4 larvae. Values indicate means ± SD of ≥4 independent measurements. **(E)** Quantifications of western blot analysis of endogenous HSP-6 levels in wild-type (+/+), *spg-7(ad2249)*, *fzo-1(tm1133)* or *drp-1 (tm1108)* using anti-HSP-6 antibodies. For each genotype, 100 L4 larvae were harvested per experiment for western blot analysis. Values indicate means of relative HSP-6 expression (HSP-6/TUB) ± SD, n = 2. **(F)** Inter-individual variability in gene expression of target genes in *bcSi9* and *zcIs13* in both wild type (+/+) and *fzo-1(tm1133)*. To estimate inter-individual variability in gene expression, the coefficient of variation was calculated from individual mRNA levels obtained from normalized Ct values using the delta Ct method. Inter-individual variability values were normalized such that variability values for *nlp-29* in wild type = 1 *(bcSi9* or *zcIs13)*. Number of individual worms: n = 35 *(bcSi9)*, n = 32 (*bcSi9; fzo-1(tm1133))*, n = 31 *(zcIs13)*, n = 31 *(zcIs13; fzo-1(tm1133))*.
(TIF)

S2 Fig. RNAi against *vps-4*^{VPS4} and *vps-20*^{CHMP6} suppresses expression of *bcSi9* and induces autophagy in wild type (+/+). **(A)** L4 larvae were subjected to *control(RNAi)*, *atfs-1 (RNAi)*, *vps-4(RNAi)* or *vps-20(RNAi)* and the F1 generation was imaged. Each dot represents the quantification of fluorescence intensity of 15–20 L4 larvae. Values indicate means ± SD of 5 independent experiments in duplicates. $^{*}P<0.05$, $^{***}P<0.001$ using one-way ANOVA with Dunnett's multiple comparison test to *control(RNAi)*. **(B)** $P_{lgg\text{-}1}$*gfp*::*lgg-1* expression of L4 larvae in hypodermal seam cells and intestinal cells upon *control(RNAi)*, *vps-4(RNAi)* or *vps-20 (RNAi)*. Representative images of >30 animals from two independent biological replicates are shown. Scale bar hypodermal seam cells: 5 μm. Scale bar intestinal cells: 20 μm.
(TIF)

S3 Fig. Knock-down of ESCRT components in body wall muscle cells of wild type and intestinal cells in *fzo-1(tm1133)* does not change mitochondrial morphology. (A) Fluorescence images of L4 larvae expressing $P_{myo-3}gfp^{mt}$ in wild type (+/+). L4 larvae were subjected to *control(RNAi)*, *atfs-1(RNAi)*, *vps-4(RNAi)*, *vps-20(RNAi)* or *let-363(RNAi)* and the F1 generation was imaged. Scale bar: 10 μm. **(B)** Fluorescence images of L4 larvae expressing $P_{let-858}gfp^{mt}$ in wild type (+/+) or *fzo-1(tm1133)*. L4 larvae were subjected to *control(RNAi)*, *atfs-1 (RNAi)*, *vps-4(RNAi)*, *vps-20(RNAi)* or *let-363(RNAi)* and the F1 generation was imaged. Scale bar: 10 μm.
(TIF)

S4 Fig. Image segmentation and intensity measurement workflow. A raw 16-bit image (1) is converted to 8-bit, followed by a background subtraction using the rolling ball algorithm (2). This is followed by the successive application of a minimum (3) and average filter (4). The ImageJ Tubeness plugin generates an image with object curvature scores (5), after which the IsoData autothresholding is applied to generate the binary mask (6). Noise is removed by filtering out particles below a certain size (7) and the final mask is used to define the area in which intensity measurements are obtained (8). Scale bar: 5 μm.
(TIF)

S5 Fig. Thrashing assay in wild-type and *fzo-1(tm1133)* animals upon induction of autophagy. Thrashing rate was analyzed by counting body bends of animals swimming for 1 minute in M9 buffer in 3 independent experiments. Each dot represents one L4 larvae. **(A)** Thrashing rates of wild-type (+/+) or *fzo-1(tm1133)* L4 larvae. $^{****}P<0.0001$ using unpaired two-tailed t-test. n = 30. **(B)** Thrashing rates in wild-type animals upon induction of autophagy. L4 larvae were subjected to *control(RNAi)*, *vps-4(RNAi)*, *vps-20(RNAi)*, *let-363(RNAi)* or *hars-1(RNAi)* and the F1 generation was analyzed. ns: not significant, $^{****}P<0.0001$ using Kruskal-Wallis test with Dunn's multiple comparison test to *control(RNAi)*. n = 30. **(C)** Thrashing rates in *fzo-1(tm1133)* animals upon induction of autophagy. L4 larvae were subjected to *control(RNAi)*, *vps-4(RNAi)*, *vps-20(RNAi)*, *let-363(RNAi)* or *hars-1(RNAi)* and the F1 generation was analyzed. ns: not significant, $^{***}P<0.001$ using Kruskal-Wallis test with Dunn's multiple comparison test to *control(RNAi)*. n = 30.
(TIF)

S6 Fig. RNAi against *vps-4*^{VPS4} and *vps-20*^{CHMP6} does not suppress *fzo-1(tm1133)*-induced UPR^{mt} when diluted with *control(RNAi)* or carried out in one generation from L2 to L4 larvae. (A) Quantifications of fluorescence images of L4 larvae expressing $P_{hsp-6}gfp$ *(bcSi9)* in *fzo-1(tm1133)*. Each *ESCRT(RNAi)* was diluted 1:1 with *control(RNAi)*. After subtracting the mean fluorescence intensity of wild type (+/+) on *control(RNAi)*, the values were normalized to *fzo-1(tm1133)* on *control(RNAi)*. Each dot represents the quantification of fluorescence intensity of 15–20 L4 larvae. Values indicate means ± SD of 3 independent experiments in duplicates. ns: not significant, using one-way ANOVA with Dunnett's multiple comparison test to *control(RNAi)*. **(B)** Quantifications of fluorescence images of L4 larvae expressing $P_{hsp-6}gfp$ *(bcSi9)* in *fzo-1(tm1133)*. L2 larvae were subjected to *control(RNAi)*, *atfs-1(RNAi)*, *vps-4 (RNAi)* or *vps-20(RNAi)* and the same animals were imaged in L4 stage. After subtracting the mean fluorescence intensity of wild type (+/+) on *control(RNAi)*, the values were normalized to *fzo-1(tm1133)* on *control(RNAi)*. Each dot represents the quantification of fluorescence intensity of 15–20 L4 larvae. Values indicate means ± SD of 4 independent experiments in duplicates. ns: not significant, $^{**}P<0.01$ using Kruskal-Wallis test with Dunn's multiple comparison test to *control(RNAi)*. **(C)** $P_{lgg-1}gfp$::*lgg-1* expression of *fzo-1(tm1133)* L4 larvae in

hypodermal seam cells and intestinal cells. L2 larvae were subjected to *control(RNAi)*, *vps-4 (RNAi)* or *vps-20(RNAi)* and the same animals were imaged in L4 stage. Representative images of >60 animals from two independent biological replicates are shown. Scale bar hypodermal seam cells: 5 μm. Scale bar intestinal cells: 20 μm. **(D)** Quantifications of fluorescence images of L4 larvae expressing P_{hsp-6}*gfp (bcSi9)* in *fzo-1(tm1133) rrf-3(pk1426)*. L2 larvae were subjected to *control(RNAi)*, *atfs-1(RNAi)*, *vps-4(RNAi)* or *vps-20(RNAi)* and the same animals were imaged in L4 stage. After subtracting the mean fluorescence intensity of wild type (+/+) on *control(RNAi)*, the values were normalized to *fzo-1(tm1133)* on *control(RNAi)*. Each dot represents the quantification of fluorescence intensity of 15–20 L4 larvae. Values indicate means ± SD of 4 independent experiments in duplicates. ns: not significant, $^{****}P<0.0001$ using one-way ANOVA with Dunnett's multiple comparison test to *control(RNAi)*.
(TIF)

S7 Fig. Autophagy is induced in *spg-7(ad2249)* animals. (A) P_{lgg-1}*gfp*::*lgg-1* expression in hypodermal seam cells of wild type (+/+) or *spg-7(ad2249)* L4 larvae. Scale bar: 5 μm. **(B)** Quantification of GFP::LGG-1 foci in hypodermal seam cells from panel A. Each dot represents the average amount of GFP::LGG-1 foci counted from 2–5 seam cells in one animal. n≥18 for each genotype; values indicate means ± SD; $^{**}P<0.01$ using unpaired two-tailed t-test with Welch's correction. **(C)** Nomarski and fluorescent images of the P_{sqst-1}*sqst-1*::*gfp* translational reporter in embryos of wild type (+/+) and *spg-7(ad2249)* animals. As a positive control for a block in autophagy, *unc-51(e369)* was used. Representative images of >60 embryos are shown. Scale bar: 10 μm.
(TIF)

S8 Fig. Defects in mitochondrial homeostasis lead to major changes in lipid metabolism. (A) Venn diagrams showing the overlap of lipids up- or downregulated in *fzo-1(tm1133)*, *drp-1(tm1108)* and *spg-7(ad2249)* in comparison to wild type (+/+). **(B)** Total amount of TGs in wild type (+/+), *fzo-1(tm1133)*, *drp-1(tm1108)* and *spg-7(ad2249)* backgrounds. Means ± SD are shown; ns: not significant, $^{*}P<0.05$, $^{****}P<0.0001$ using Welch test. **(C)** Scatterplot indicating the distribution and changes in the levels of TG species in the different mutants in comparison to wild type (+/+). **(D))** Scatterplot indicating the overlap of the changes in the levels of TG species of *fzo-1(tm1133)* and *drp-1(tm1108)* mutants in comparison to wild type (+/+). **(C)** and **(D)** The x-axis labels the number of carbons (# of C) and the y-axis the number of double bonds (DB) in the acyl sidechains. The size of a dot indicates the number of detected isomers for a specific sum composition. Grey dots represent all detected TGs species and blue and red dots indicate down- (blue) or upregulation (red).
(TIF)

S9 Fig. Induction of autophagy upon *cogc-2(RNAi)* changes the levels of specific TGs in *fzo-1(tm1133)* mutants. (A) Scatterplot indicating the distribution and changes in the level of TG species in *fzo-1(tm1133)* mutants in comparison to wild type (+/+). The x-axis labels the number of carbons (# of C) and the y-axis the number of double bonds (DB) in the acyl sidechains. The size of a dot indicates the number of detected isomers for a specific sum composition. Grey dots represent all detected TGs species and blue and red dots indicate down- (blue) or upregulation (red). **(B)** Venn diagram indicating the overlap of TG species downregulated (left panel) or upregulated (right panel) in *fzo-1(tm1133)* and downregulated upon *vps-4 (RNAi)* or *cogc-2(RNAi)*.
(TIF)

S1 Table. List of genes that suppress *fzo-1(lf)*-induced UPR^{mt} and induce autophagy in wild-type animals upon knock-down. Candidate genes were identified in the primary RNAi-

screen using *fzo-1(tm1133)*, subsequently knocked-down and tested for induction of autophagy and re-screened for UPR^{mt} suppression in two different mutant backgrounds: *drp-1 (tm1108)* and *spg-7(ad2249)*.
(XLSX)

S2 Table. Numerical data of lipidomic experiments. Significantly up- or downregulated lipids in *fzo-1(tm1133)*, *drp-1(tm1108)* or *spg-7(ad2249)* mutants (Sheet 1), significantly up- or downregulated TGs in *fzo-1(tm1133)*, *drp-1(tm1108)* or *spg-7(ad2249)* mutants (Sheet 2) and significantly up- or downregulated TGs in *fzo-1(tm1133)* upon induction of autophagy by *vps-4(RNAi)* or *cogc-2(RNAi)* (Sheet 3). MS^1 annotations, *P*-values and fold change are indicated.
(XLSX)

S3 Table. List of qRT-PCR primers. Primers used for qRT-PCR including PCR efficiency and coefficient of determination (R^2).
(XLSX)

Acknowledgments

We thank Eric Lambie, Dejana Mokranjac, the 'Mito Club' and members of the Conradt lab for discussion and comments on the manuscript. We thank M. Bauer, L. Jocham, N. Lebedeva and M. Schwarz for excellent technical support and S. Mitani (National BioResource Project, Tokyo, Japan) for *fzo-1*(*tm1133*), *drp-1(tm1108)* and *atfs-1(tm4525)*. We thank Keith Nehrke and Vincent Galy for *fndc-1(rny-14)*. Some strains were provided by the CGC, which is funded by NIH Office of Research Infrastructure Programs (P40 OD010440).

Author Contributions

Conceptualization: Simon Haeussler, Fabian Köhler, Michael Witting, Stéphane G. Rolland, Laetitia Chauve, Olivia Casanueva, Barbara Conradt.

Data curation: Simon Haeussler, Fabian Köhler, Michael Witting.

Formal analysis: Simon Haeussler, Fabian Köhler, Michael Witting, Madeleine F. Premm, Christian Fischer, Laetitia Chauve.

Funding acquisition: Barbara Conradt.

Investigation: Simon Haeussler, Fabian Köhler.

Methodology: Simon Haeussler, Fabian Köhler, Michael Witting.

Project administration: Barbara Conradt.

Resources: Simon Haeussler, Fabian Köhler, Michael Witting.

Software: Christian Fischer.

Validation: Simon Haeussler, Fabian Köhler, Madeleine F. Premm.

Visualization: Simon Haeussler, Fabian Köhler, Michael Witting, Christian Fischer, Laetitia Chauve.

Writing – original draft: Simon Haeussler, Fabian Köhler, Michael Witting, Barbara Conradt.

Writing – review & editing: Simon Haeussler, Fabian Köhler, Michael Witting, Barbara Conradt.

References

1. Youle RJ, van der Bliek AM. Mitochondrial fission, fusion, and stress. Science (New York, NY). 2012; 337(6098):1062–5.
2. van der Bliek AM, Shen Q, Kawajiri S. Mechanisms of Mitochondrial Fission and Fusion. Cold Spring Harbor Perspectives in Biology. 2013;5(6).
3. Labrousse AM, Zappaterra MD, Rube DA, van der Bliek AM. *C. elegans* Dynamin-Related Protein DRP-1 Controls Severing of the Mitochondrial Outer Membrane. Molecular cell. 1999; 4(5):815–26. https://doi.org/10.1016/s1097-2765(00)80391-3 PMID: 10619028
4. Ingerman E, Perkins EM, Marino M, Mears JA, McCaffery JM, Hinshaw JE, et al. Dnm1 forms spirals that are structurally tailored to fit mitochondria. The Journal of cell biology. 2005; 170(7):1021–7. https://doi.org/10.1083/jcb.200506078 PMID: 16186251
5. Ichishita R, Tanaka K, Sugiura Y, Sayano T, Mihara K, Oka T. An RNAi Screen for Mitochondrial Proteins Required to Maintain the Morphology of the Organelle in *Caenorhabditis elegans*. The Journal of Biochemistry. 2008; 143(4):449–54. https://doi.org/10.1093/jb/mvm245 PMID: 18174190
6. Kanazawa T, Zappaterra MD, Hasegawa A, Wright AP, Newman-Smith ED, Buttle KF, et al. The *C. elegans* Opa1 Homologue EAT-3 Is Essential for Resistance to Free Radicals. PLoS genetics. 2008; 4 (2):e1000022. https://doi.org/10.1371/journal.pgen.1000022 PMID: 18454199
7. Kim S, Sieburth D. Sphingosine Kinase Activates the Mitochondrial Unfolded Protein Response and Is Targeted to Mitochondria by Stress. Cell reports. 2018; 24(11):2932–45.e4. https://doi.org/10.1016/j.celrep.2018.08.037 PMID: 30208318
8. Zhang Q, Wu X, Chen P, Liu L, Xin N, Tian Y, et al. The Mitochondrial Unfolded Protein Response Is Mediated Cell-Non-autonomously by Retromer-Dependent Wnt Signaling. Cell. 2018; 174(4):870–83. e17. https://doi.org/10.1016/j.cell.2018.06.029 PMID: 30057120
9. Haynes CM, Yang Y, Blais SP, Neubert TA, Ron D. The matrix peptide exporter HAF-1 signals a mitochondrial UPR by activating the transcription factor ZC376.7 in *C. elegans*. Molecular cell. 2010; 37 (4):529–40. https://doi.org/10.1016/j.molcel.2010.01.015 PMID: 20188671
10. Rolland SG, Schneid S, Schwarz M, Rackles E, Fischer C, Haeussler S, et al. Compromised Mitochondrial Protein Import Acts as a Signal for UPR^{mt}. Cell reports. 2019; 28(7):1659–69.e5. https://doi.org/10.1016/j.celrep.2019.07.049 PMID: 31412237
11. Nargund AM, Pellegrino MW, Fiorese CJ, Baker BM, Haynes CM. Mitochondrial import efficiency of ATFS-1 regulates mitochondrial UPR activation. Science (New York, NY). 2012; 337(6094):587–90. https://doi.org/10.1126/science.1223560 PMID: 22700657
12. Benedetti C, Haynes CM, Yang Y, Harding HP, Ron D. Ubiquitin-like protein 5 positively regulates chaperone gene expression in the mitochondrial unfolded protein response. Genetics. 2006; 174 (1):229–39. https://doi.org/10.1534/genetics.106.061580 PMID: 16816413
13. Haynes CM, Petrova K, Benedetti C, Yang Y, Ron D. ClpP mediates activation of a mitochondrial unfolded protein response in *C. elegans*. Developmental cell. 2007; 13(4):467–80. https://doi.org/10.1016/j.devcel.2007.07.016 PMID: 17925224
14. Yoneda T, Benedetti C, Urano F, Clark SG, Harding HP, Ron D. Compartment-specific perturbation of protein handling activates genes encoding mitochondrial chaperones. Journal of cell science. 2004; 117(Pt 18):4055–66.
15. Levine B, Klionsky DJ. Development by Self-Digestion. Developmental cell. 2004; 6(4):463–77. https://doi.org/10.1016/s1534-5807(04)00099-1 PMID: 15068787
16. Mizushima N. Autophagy: process and function. Genes Dev. 2007; 21(22):2861–73. https://doi.org/10.1101/gad.1599207 PMID: 18006683
17. Feng Y, He D, Yao Z, Klionsky DJ. The machinery of macroautophagy. Cell Res. 2014; 24(1):24–41. https://doi.org/10.1038/cr.2013.168 PMID: 24366339
18. Nakatogawa H, Suzuki K, Kamada Y, Ohsumi Y. Dynamics and diversity in autophagy mechanisms: lessons from yeast. Nature reviews Molecular cell biology. 2009; 10(7):458–67. https://doi.org/10.1038/nrm2708 PMID: 19491929
19. Long X, Spycher C, Han ZS, Rose AM, Müller F, Avruch J. TOR Deficiency in *C. elegans* Causes Developmental Arrest and Intestinal Atrophy by Inhibition of mRNA Translation. Current Biology. 2002; 12(17):1448–61. https://doi.org/10.1016/s0960-9822(02)01091-6 PMID: 12225660
20. Hansen M, Chandra A, Mitic LL, Onken B, Driscoll M, Kenyon C. A role for autophagy in the extension of lifespan by dietary restriction in *C. elegans*. PLoS genetics. 2008; 4(2):e24. https://doi.org/10.1371/journal.pgen.0040024 PMID: 18282106

21. Jia K, Chen D, Riddle DL. The TOR pathway interacts with the insulin signaling pathway to regulate *C. elegans* larval development, metabolism and life span. Development. 2004; 131(16):3897–906. https://doi.org/10.1242/dev.01255 PMID: 15253933

22. Kuroyanagi H, Yan J, Seki N, Yamanouchi Y, Suzuki Y, Takano T, et al. Human ULK1, a novel serine/threonine kinase related to UNC-51 kinase of *Caenorhabditis elegans*: cDNA cloning, expression, and chromosomal assignment. Genomics. 1998; 51(1):76–85. https://doi.org/10.1006/geno.1998.5340 PMID: 9693035

23. Ogura K, Wicky C, Magnenat L, Tobler H, Mori I, Müller F, et al. *Caenorhabditis elegans* unc-51 gene required for axonal elongation encodes a novel serine/threonine kinase. Genes & Development. 1994; 8(20):2389–400.

24. Wullschleger S, Loewith R, Hall MN. TOR signaling in growth and metabolism. Cell. 2006; 124 (3):471–84. https://doi.org/10.1016/j.cell.2006.01.016 PMID: 16469695

25. Tsukada M, Ohsumi Y. Isolation and characterization of autophagy-defective mutants of *Saccharomyces cerevisiae*. FEBS Letters. 1993; 333(1–2):169–74. https://doi.org/10.1016/0014-5793(93)80398-e PMID: 8224160

26. Sato M, Sato K. Degradation of Paternal Mitochondria by Fertilization-Triggered Autophagy in *C. elegans* Embryos. Science (New York, NY). 2011; 334(6059):1141–4.

27. Christ L, Raiborg C, Wenzel EM, Campsteijn C, Stenmark H. Cellular Functions and Molecular Mechanisms of the ESCRT Membrane-Scission Machinery. Trends in biochemical sciences. 2017; 42 (1):42–56. https://doi.org/10.1016/j.tibs.2016.08.016 PMID: 27669649

28. Katzmann DJ, Babst M, Emr SD. Ubiquitin-Dependent Sorting into the Multivesicular Body Pathway Requires the Function of a Conserved Endosomal Protein Sorting Complex, ESCRT-I. Cell. 2001; 106 (2):145–55. https://doi.org/10.1016/s0092-8674(01)00434-2 PMID: 11511343

29. Raiborg C, Bache KG, Gillooly DJ, Madshus IH, Stang E, Stenmark H. Hrs sorts ubiquitinated proteins into clathrin-coated microdomains of early endosomes. Nature cell biology. 2002; 4(5):394–8. https://doi.org/10.1038/ncb791 PMID: 11988743

30. Sachse M, Urbe S, Oorschot V, Strous GJ, Klumperman J. Bilayered clathrin coats on endosomal vacuoles are involved in protein sorting toward lysosomes. Mol Biol Cell. 2002; 13(4):1313–28. https://doi.org/10.1091/mbc.01-10-0525 PMID: 11950941

31. Amit I, Yakir L, Katz M, Zwang Y, Marmor MD, Citri A, et al. Tal, a Tsg101-specific E3 ubiquitin ligase, regulates receptor endocytosis and retrovirus budding. Genes Dev. 2004; 18(14):1737–52. https://doi.org/10.1101/gad.294904 PMID: 15256501

32. Carlton JG, Martin-Serrano J. Parallels between cytokinesis and retroviral budding: a role for the ESCRT machinery. Science (New York, NY). 2007; 316(5833):1908–12.

33. Filimonenko M, Stuffers S, Raiborg C, Yamamoto A, Malerod L, Fisher EM, et al. Functional multivesicular bodies are required for autophagic clearance of protein aggregates associated with neurodegenerative disease. The Journal of cell biology. 2007; 179(3):485–500. https://doi.org/10.1083/jcb.200702115 PMID: 17984323

34. Lee JA, Beigneux A, Ahmad ST, Young SG, Gao FB. ESCRT-III dysfunction causes autophagosome accumulation and neurodegeneration. Curr Biol. 2007; 17(18):1561–7. https://doi.org/10.1016/j.cub.2007.07.029 PMID: 17683935

35. Rusten TE, Vaccari T, Lindmo K, Rodahl LM, Nezis IP, Sem-Jacobsen C, et al. ESCRTs and *Fab1* regulate distinct steps of autophagy. Curr Biol. 2007; 17(20):1817–25. https://doi.org/10.1016/j.cub.2007.09.032 PMID: 17935992

36. Tamai K, Tanaka N, Nara A, Yamamoto A, Nakagawa I, Yoshimori T, et al. Role of Hrs in maturation of autophagosomes in mammalian cells. Biochem Biophys Res Commun. 2007; 360(4):721–7. https://doi.org/10.1016/j.bbrc.2007.06.105 PMID: 17624298

37. Takahashi Y, He H, Tang Z, Hattori T, Liu Y, Young MM, et al. An autophagy assay reveals the ESCRT-III component CHMP2A as a regulator of phagophore closure. Nature communications. 2018; 9(1):2855. https://doi.org/10.1038/s41467-018-05254-w PMID: 30030437

38. Zhou F, Wu Z, Zhao M, Murtazina R, Cai J, Zhang A, et al. Rab5-dependent autophagosome closure by ESCRT. The Journal of cell biology. 2019; 218(6):1908–27. https://doi.org/10.1083/jcb.201811173 PMID: 31010855

39. Djeddi A, Michelet X, Culetto E, Alberti A, Barois N, Legouis R. Induction of autophagy in ESCRT mutants is an adaptive response for cell survival in *C. elegans*. Journal of cell science. 2012; 125 (3):685–94.

40. Guo B, Huang X, Zhang P, Qi L, Liang Q, Zhang X, et al. Genome-wide screen identifies signaling pathways that regulate autophagy during *Caenorhabditis elegans* development. EMBO reports. 2014; 15(6):705–13. https://doi.org/10.1002/embr.201338310 PMID: 24764321

41. Zubovych IO, Straud S, Roth MG, Newmeyer DD. Mitochondrial Dysfunction Confers Resistance to Multiple Drugs in *Caenorhabditis elegans*. Molecular Biology of the Cell. 2010; 21(6):956–69. https://doi.org/10.1091/mbc.E09-08-0673 PMID: 20089839

42. Köhler F, Müller-Rischart AK, Conradt B, Rolland SG. The loss of *LRPPRC* function induces the mitochondrial unfolded protein response. Aging. 2015; 7(9):701–12. https://doi.org/10.18632/aging.100812 PMID: 26412102

43. Liu Y, Samuel BS, Breen PC, Ruvkun G. *Caenorhabditis elegans* pathways that surveil and defend mitochondria. Nature. 2014; 508(7496):406–10. https://doi.org/10.1038/nature13204 PMID: 24695221

44. Runkel ED, Liu S, Baumeister R, Schulze E. Surveillance-activated defenses block the ROS-induced mitochondrial unfolded protein response. PLoS genetics. 2013; 9(3):e1003346. https://doi.org/10.1371/journal.pgen.1003346 PMID: 23516373

45. Kamath RS, Ahringer J. Genome-wide RNAi screening in *Caenorhabditis elegans*. Methods (San Diego, Calif). 2003; 30(4):313–21.

46. Rolland SG, Motori E, Memar N, Hench J, Frank S, Winklhofer KF, et al. Impaired complex IV activity in response to loss of LRPPRC function can be compensated by mitochondrial hyperfusion. Proceedings of the National Academy of Sciences of the United States of America. 2013; 110(32):E2967–76. https://doi.org/10.1073/pnas.1303872110 PMID: 23878239

47. Loew LM, Tuft RA, Carrington W, Fay FS. Imaging in five dimensions: time-dependent membrane potentials in individual mitochondria. Biophysical Journal. 1993; 65(6):2396–407. https://doi.org/10.1016/S0006-3495(93)81318-3 PMID: 8312478

48. Chen Y, Scarcelli V, Legouis R. Approaches for Studying Autophagy in *Caenorhabditis elegans*. Cells. 2017; 6(3).

49. Jenzer C, Simionato E, Legouis R. Tools and methods to analyze autophagy in *C. elegans*. Methods (San Diego, Calif). 2015; 75:162–71.

50. Klionsky DJ, Abdelmohsen K, Abe A, Abedin MJ, Abeliovich H, Acevedo Arozena A, et al. Guidelines for the use and interpretation of assays for monitoring autophagy (3rd edition). Autophagy. 2016; 12(1):1–222. https://doi.org/10.1080/15548627.2015.1100356 PMID: 26799652

51. Tian Y, Li Z, Hu W, Ren H, Tian E, Zhao Y, et al. *C. elegans* Screen Identifies Autophagy Genes Specific to Multicellular Organisms. Cell. 2010; 141(6):1042–55. https://doi.org/10.1016/j.cell.2010.04.034 PMID: 20550938

52. Zhang H, Chang JT, Guo B, Hansen M, Jia K, Kovacs AL, et al. Guidelines for monitoring autophagy in *Caenorhabditis elegans*. Autophagy. 2015; 11(1):9–27. https://doi.org/10.1080/15548627.2014.1003478 PMID: 25569839

53. Chapin HC, Okada M, Merz AJ, Miller DL. Tissue-specific autophagy responses to aging and stress in *C. elegans*. Aging (Albany NY). 2015; 7(6):419–34.

54. Mizushima N, Yoshimori T, Levine B. Methods in Mammalian Autophagy Research. Cell. 2010; 140(3):313–26. https://doi.org/10.1016/j.cell.2010.01.028 PMID: 20144757

55. Homma K, Suzuki K, Sugawara H. The Autophagy Database: an all-inclusive information resource on autophagy that provides nourishment for research. Nucleic Acids Research. 2011; 39(suppl_1):D986–D90.

56. Lipinski MM, Hoffman G, Ng A, Zhou W, Py BF, Hsu E, et al. A genome-wide siRNA screen reveals multiple mTORC1 independent signaling pathways regulating autophagy under normal nutritional conditions. Developmental cell. 2010; 18(6):1041–52. https://doi.org/10.1016/j.devcel.2010.05.005 PMID: 20627085

57. Strohecker AM, Joshi S, Possemato R, Abraham RT, Sabatini DM, White E. Identification of 6-phosphofructo-2-kinase/fructose-2,6-bisphosphatase as a novel autophagy regulator by high content shRNA screening. Oncogene. 2015; 34(45):5662–76. https://doi.org/10.1038/onc.2015.23 PMID: 25772235

58. Dayalan Naidu S, Dikovskaya D, Gaurilcikaite E, Knatko EV, Healy ZR, Mohan H, et al. Transcription factors NRF2 and HSF1 have opposing functions in autophagy. Sci Rep. 2017; 7(1):11023. https://doi.org/10.1038/s41598-017-11262-5 PMID: 28887499

59. Demishtein A, Fraiberg M, Berko D, Tirosh B, Elazar Z, Navon A. SQSTM1/p62-mediated autophagy compensates for loss of proteasome polyubiquitin recruiting capacity. Autophagy. 2017; 13(10):1697–708. https://doi.org/10.1080/15548627.2017.1356549 PMID: 28792301

60. Dokladny K, Zuhl MN, Mandell M, Bhattacharya D, Schneider S, Deretic V, et al. Regulatory coordination between two major intracellular homeostatic systems: heat shock response and autophagy. The Journal of biological chemistry. 2013; 288(21):14959–72. https://doi.org/10.1074/jbc.M113.462408 PMID: 23576438

61. Hu G, McQuiston T, Bernard A, Park YD, Qiu J, Vural A, et al. A conserved mechanism of TOR-dependent RCK-mediated mRNA degradation regulates autophagy. Nature cell biology. 2015; 17(7):930–42. https://doi.org/10.1038/ncb3189 PMID: 26098573

62. Hwang DW, So KS, Kim SC, Park KM, Lee YJ, Kim SW, et al. Autophagy Induced by CX-4945, a Casein Kinase 2 Inhibitor, Enhances Apoptosis in Pancreatic Cancer Cell Lines. Pancreas. 2017; 46 (4):575–81. https://doi.org/10.1097/MPA.0000000000000780 PMID: 28196025

63. Keith SA, Maddux SK, Zhong Y, Chinchankar MN, Ferguson AA, Ghazi A, et al. Graded Proteasome Dysfunction in *Caenorhabditis elegans* Activates an Adaptive Response Involving the Conserved SKN-1 and ELT-2 Transcription Factors and the Autophagy-Lysosome Pathway. PLoS genetics. 2016; 12(2):e1005823. https://doi.org/10.1371/journal.pgen.1005823 PMID: 26828939

64. Kumsta C, Chang JT, Schmalz J, Hansen M. Hormetic heat stress and HSF-1 induce autophagy to improve survival and proteostasis in *C. elegans*. Nature communications. 2017; 8:14337. https://doi.org/10.1038/ncomms14337 PMID: 28198373

65. Lee SW, Song YS, Lee SY, Yoon YG, Lee SH, Park BS, et al. Downregulation of protein kinase CK2 activity facilitates tumor necrosis factor-alpha-mediated chondrocyte death through apoptosis and autophagy. PloS one. 2011; 6(4):e19163. https://doi.org/10.1371/journal.pone.0019163 PMID: 21559479

66. Meléndez A, Tallóczy Z, Seaman M, Eskelinen E-L, Hall DH, Levine B. Autophagy Genes Are Essential for Dauer Development and Life-Span Extension in *C. elegans*. Science (New York, NY). 2003; 301(5638):1387–91.

67. Menzies FM, Garcia-Arencibia M, Imarisio S, O'Sullivan NC, Ricketts T, Kent BA, et al. Calpain inhibition mediates autophagy-dependent protection against polyglutamine toxicity. Cell death and differentiation. 2015; 22(3):433–44. https://doi.org/10.1038/cdd.2014.151 PMID: 25257175

68. Murphy CT, McCarroll SA, Bargmann CI, Fraser A, Kamath RS, Ahringer J, et al. Genes that act downstream of DAF-16 to influence the lifespan of *Caenorhabditis elegans*. Nature. 2003; 424:277. https://doi.org/10.1038/nature01789 PMID: 12845331

69. Pierce SB, Costa M, Wisotzkey R, Devadhar S, Homburger SA, Buchman AR, et al. Regulation of DAF-2 receptor signaling by human insulin and ins-1, a member of the unusually large and diverse C. elegans insulin gene family. Genes & Development. 2001; 15(6):672–86.

70. Putker M, Madl T, Vos Harmjan R, de Ruiter H, Visscher M, van den Berg Maaike CW, et al. Redox-Dependent Control of FOXO/DAF-16 by Transportin-1. Molecular cell. 2013; 49(4):730–42. https://doi.org/10.1016/j.molcel.2012.12.014 PMID: 23333309

71. Sheaffer KL, Updike DL, Mango SE. The Target of Rapamycin pathway antagonizes *pha-4/FoxA* to control development and aging. Curr Biol. 2008; 18(18):1355–64. https://doi.org/10.1016/j.cub.2008.07.097 PMID: 18804378

72. Tang L, Fares H, Zhao X, Du W, Liu BF. Different endocytic functions of AGEF-1 in *C. elegans* coelomocytes. Biochimica et biophysica acta. 2012; 1820(7):829–40. https://doi.org/10.1016/j.bbagen.2012.03.004 PMID: 22446376

73. Yang D, Li L, Liu H, Wu L, Luo Z, Li H, et al. Induction of autophagy and senescence by knockdown of ROC1 E3 ubiquitin ligase to suppress the growth of liver cancer cells. Cell death and differentiation. 2013; 20(2):235–47. https://doi.org/10.1038/cdd.2012.113 PMID: 22935614

74. Zhao Y, Yang J, Liao W, Liu X, Zhang H, Wang S, et al. Cytosolic FoxO1 is essential for the induction of autophagy and tumour suppressor activity. Nature cell biology. 2010; 12:665. https://doi.org/10.1038/ncb2069 PMID: 20543840

75. Nawa M, Kage-Nakadai E, Aiso S, Okamoto K, Mitani S, Matsuoka M. Reduced expression of BTBD10, an Akt activator, leads to motor neuron death. Cell Death & Differentiation. 2012; 19 (8):1398–407.

76. Nawa M, Matsuoka M. The Method of the Body Bending Assay Using Caenorhabditis elegans. Bio Protoc. 2012; 2(17):e253.

77. Johnson D, Nehrke K. Mitochondrial Fragmentation Leads to Intracellular Acidification in Caenorhabditis elegans and Mammalian Cells. Molecular Biology of the Cell. 2010; 21(13):2191–201. https://doi.org/10.1091/mbc.E09-10-0874 PMID: 20444981

78. Lim Y, Rubio-Peña K, Sobraske PJ, Molina PA, Brookes PS, Galy V, et al. Fndc-1 contributes to paternal mitochondria elimination in C. elegans. Developmental Biology. 2019; 454(1):15–20. https://doi.org/10.1016/j.ydbio.2019.06.016 PMID: 31233739

79. Palikaras K, Lionaki E, Tavernarakis N. Coordination of mitophagy and mitochondrial biogenesis during ageing in *C. elegans*. Nature. 2015.

80. Rauthan M, Ranji P, Aguilera Pradenas N, Pitot C, Pilon M. The mitochondrial unfolded protein response activator ATFS-1 protects cells from inhibition of the mevalonate pathway. Proceedings of

the National Academy of Sciences of the United States of America. 2013; 110(15):5981–6. https://doi.org/10.1073/pnas.1218778110 PMID: 23530189

81. Bennett CF, Vander Wende H, Simko M, Klum S, Barfield S, Choi H, et al. Activation of the mitochondrial unfolded protein response does not predict longevity in *Caenorhabditis elegans*. Nature communications. 2014; 5:3483. https://doi.org/10.1038/ncomms4483 PMID: 24662282

82. Buis A, Bellemin S, Goudeau J, Monnier L, Loiseau N, Guillou H, et al. Coelomocytes Regulate Starvation-Induced Fat Catabolism and Lifespan Extension through the Lipase LIPL-5 in Caenorhabditis elegans. Cell reports. 2019; 28(4):1041–9.e4. https://doi.org/10.1016/j.celrep.2019.06.064 PMID: 31340142

83. Harvald EB, Sprenger RR, Dall KB, Ejsing CS, Nielsen R, Mandrup S, et al. Multi-omics Analyses of Starvation Responses Reveal a Central Role for Lipoprotein Metabolism in Acute Starvation Survival in *C.elegans*. Cell Systems. 2017; 5(1):38–52.e4. https://doi.org/10.1016/j.cels.2017.06.004 PMID: 28734827

84. Vrablik TL, Petyuk VA, Larson EM, Smith RD, Watts JL. Lipidomic and proteomic analysis of Caenorhabditis elegans lipid droplets and identification of ACS-4 as a lipid droplet-associated protein. Biochimica et Biophysica Acta (BBA)—Molecular and Cell Biology of Lipids. 2015; 1851(10):1337–45.

85. Benador IY, Veliova M, Mahdaviani K, Petcherski A, Wikstrom JD, Assali EA, et al. Mitochondria Bound to Lipid Droplets Have Unique Bioenergetics, Composition, and Dynamics that Support Lipid Droplet Expansion. Cell metabolism. 2018; 27(4):869–85.e6. https://doi.org/10.1016/j.cmet.2018.03.003 PMID: 29617645

86. Rambold Angelika S, Cohen S, Lippincott-Schwartz J. Fatty Acid Trafficking in Starved Cells: Regulation by Lipid Droplet Lipolysis, Autophagy, and Mitochondrial Fusion Dynamics. Developmental cell. 2015; 32(6):678–92. https://doi.org/10.1016/j.devcel.2015.01.029 PMID: 25752962

87. Singh R, Kaushik S, Wang Y, Xiang Y, Novak I, Komatsu M, et al. Autophagy regulates lipid metabolism. Nature. 2009; 458:1131. https://doi.org/10.1038/nature07976 PMID: 19339967

88. Saito T, Kuma A, Sugiura Y, Ichimura Y, Obata M, Kitamura H, et al. Autophagy regulates lipid metabolism through selective turnover of NCoR1. Nature communications. 2019; 10(1):1567. https://doi.org/10.1038/s41467-019-08829-3 PMID: 30952864

89. Pellegrino MW, Nargund AM, Haynes CM. Signaling the mitochondrial unfolded protein response. Biochimica et Biophysica Acta (BBA)—Molecular Cell Research. 2013; 1833(2):410–6.

90. Honjoh S, Yamamoto T, Uno M, Nishida E. Signalling through RHEB-1 mediates intermittent fasting-induced longevity in *C. elegans*. Nature. 2008; 457:726. https://doi.org/10.1038/nature07583 PMID: 19079239

91. Cooper JF, Machiela E, Dues DJ, Spielbauer KK, Senchuk MM, Van Raamsdonk JM. Activation of the mitochondrial unfolded protein response promotes longevity and dopamine neuron survival in Parkinson's disease models. Scientific Reports. 2017; 7(1):16441. https://doi.org/10.1038/s41598-017-16637-2 PMID: 29180793

92. Kim KH, Lee M-S. Autophagy—a key player in cellular and body metabolism. Nature Reviews Endocrinology. 2014; 10:322. https://doi.org/10.1038/nrendo.2014.35 PMID: 24663220

93. Rabinowitz JD, White E. Autophagy and Metabolism. Science (New York, NY). 2010; 330 (6009):1344–8.

94. Lin Y-F, Haynes CM. Metabolism and the UPR^{mt}. Molecular cell. 2016; 61(5):677–82. https://doi.org/10.1016/j.molcel.2016.02.004 PMID: 26942672

95. Mouysset J, Kähler C, Hoppe T. A conserved role of *Caenorhabditis elegans* CDC-48 in ER-associated protein degradation. Journal of Structural Biology. 2006; 156(1):41–9. https://doi.org/10.1016/j.jsb.2006.02.015 PMID: 16647269

96. Takahashi M, Iwasaki H, Inoue H, Takahashi K. Reverse Genetic Analysis of the *Caenorhabditis elegans* 26S Proteasome Subunits by RNA Interference. Biological Chemistry2002. p. 1263. https://doi.org/10.1515/BC.2002.140 PMID: 12437114

97. Baker BM, Nargund AM, Sun T, Haynes CM. Protective coupling of mitochondrial function and protein synthesis via the eIF2alpha kinase GCN-2. PLoS genetics. 2012; 8(6):e1002760. https://doi.org/10.1371/journal.pgen.1002760 PMID: 22719267

98. Brenner S. The Genetics of *Caenorhabditis Elegans*. Genetics. 1974; 77(1):71–94. PMID: 4366476

99. Simmer F, Tijsterman M, Parrish S, Koushika SP, Nonet ML, Fire A, et al. Loss of the Putative RNA-Directed RNA Polymerase RRF-3 Makes *C. elegans* Hypersensitive to RNAi. Current Biology. 2002; 12(15):1317–9. https://doi.org/10.1016/s0960-9822(02)01041-2 PMID: 12176360

100. Springer W, Hoppe T, Schmidt E, Baumeister R. A *Caenorhabditis elegans* Parkin mutant with altered solubility couples α-synuclein aggregation to proteotoxic stress. Human Molecular Genetics. 2005; 14 (22):3407–23. https://doi.org/10.1093/hmg/ddi371 PMID: 16204351

101. Pujol N, Cypowyj S, Ziegler K, Millet A, Astrain A, Goncharov A, et al. Distinct Innate Immune Responses to Infection and Wounding in the *C. elegans* Epidermis. Current Biology. 2008; 18(7):481–9. https://doi.org/10.1016/j.cub.2008.02.079 PMID: 18394898

102. Kang C, You Y-j, Avery L. Dual roles of autophagy in the survival of *Caenorhabditis elegans* during starvation. Genes & Development. 2007; 21(17):2161–71.

103. Urano F, Calfon M, Yoneda T, Yun C, Kiraly M, Clark SG, et al. A survival pathway for Caenorhabditis elegans with a blocked unfolded protein response. The Journal of cell biology. 2002; 158(4):639–46. https://doi.org/10.1083/jcb.200203086 PMID: 12186849

104. Mariol M-C, Walter L, Bellemin S, Gieseler K. A rapid protocol for integrating extrachromosomal arrays with high transmission rate into the *C. elegans* genome. Journal of visualized experiments: JoVE. 2013(82):e50773–e. https://doi.org/10.3791/50773 PMID: 24379027

105. Frøkjær-Jensen C, Wayne Davis M, Hopkins CE, Newman BJ, Thummel JM, Olesen S-P, et al. Single-copy insertion of transgenes in *Caenorhabditis elegans*. Nature Genetics. 2008; 40:1375. https://doi.org/10.1038/ng.248 PMID: 18953339

106. Frøkjær-Jensen C, Davis MW, Sarov M, Taylor J, Flibotte S, LaBella M, et al. Random and targeted transgene insertion in *Caenorhabditis elegans* using a modified Mos1 transposon. Nature Methods. 2014; 11:529. https://doi.org/10.1038/nmeth.2889 PMID: 24820376

107. Gibson DG, Young L, Chuang R-Y, Venter JC, Hutchison Iii CA, Smith HO. Enzymatic assembly of DNA molecules up to several hundred kilobases. Nature Methods. 2009; 6:343. https://doi.org/10.1038/nmeth.1318 PMID: 19363495

108. Frøkjær-Jensen C, Davis MW, Ailion M, Jorgensen EM. Improved Mos1-mediated transgenesis in *C. elegans*. Nature Methods. 2012; 9:117. https://doi.org/10.1038/nmeth.1865 PMID: 22290181

109. Jagasia R, Grote P, Westermann B, Conradt B. DRP-1-mediated mitochondrial fragmentation during EGL-1-induced cell death in C. elegans. Nature. 2005; 433(7027):754–60. https://doi.org/10.1038/nature03316 PMID: 15716954

110. Sternberg SR. Biomedical Image Processing. Computer. 1983; 16(1):22–34.

111. Sato Y, Nakajima S, Shiraga N, Atsumi H, Yoshida S, Koller T, et al. Three-dimensional multi-scale line filter for segmentation and visualization of curvilinear structures in medical images. Medical Image Analysis. 1998; 2(2):143–68. https://doi.org/10.1016/s1361-8415(98)80009-1 PMID: 10646760

112. Xiao R, Chun L, Ronan Elizabeth A, Friedman David I, Liu J, Xu XZS. RNAi Interrogation of Dietary Modulation of Development, Metabolism, Behavior, and Aging in *C. elegans*. Cell reports. 2015; 11(7):1123–33. https://doi.org/10.1016/j.celrep.2015.04.024 PMID: 25959815

113. Löfgren L, Forsberg G-B, Ståhlman M. The BUME method: a new rapid and simple chloroform-free method for total lipid extraction of animal tissue. Scientific Reports. 2016; 6(1):27688.

114. Witting M, Maier TV, Garvis S, Schmitt-Kopplin P. Optimizing a ultrahigh pressure liquid chromatography-time of flight-mass spectrometry approach using a novel sub-2μm core–shell particle for in depth lipidomic profiling of Caenorhabditis elegans. Journal of Chromatography A. 2014; 1359:91–9. https://doi.org/10.1016/j.chroma.2014.07.021 PMID: 25074420

115. O'Donnell VB, Dennis EA, Wakelam MJO, Subramaniam S. LIPID MAPS: Serving the next generation of lipid researchers with tools, resources, data, and training. Science Signaling. 2019; 12(563):eaaw2964. https://doi.org/10.1126/scisignal.aaw2964 PMID: 30622195

116. Kind T, Liu K-H, Lee DY, DeFelice B, Meissen JK, Fiehn O. LipidBlast in silico tandem mass spectrometry database for lipid identification. Nature Methods. 2013; 10(8):755–8. https://doi.org/10.1038/nmeth.2551 PMID: 23817071

117. Mok DZL, Sternberg PW, Inoue T. Morphologically defined sub-stages of *C. elegans* vulval development in the fourth larval stage. BMC developmental biology. 2015; 15:26–. https://doi.org/10.1186/s12861-015-0076-7 PMID: 26066484

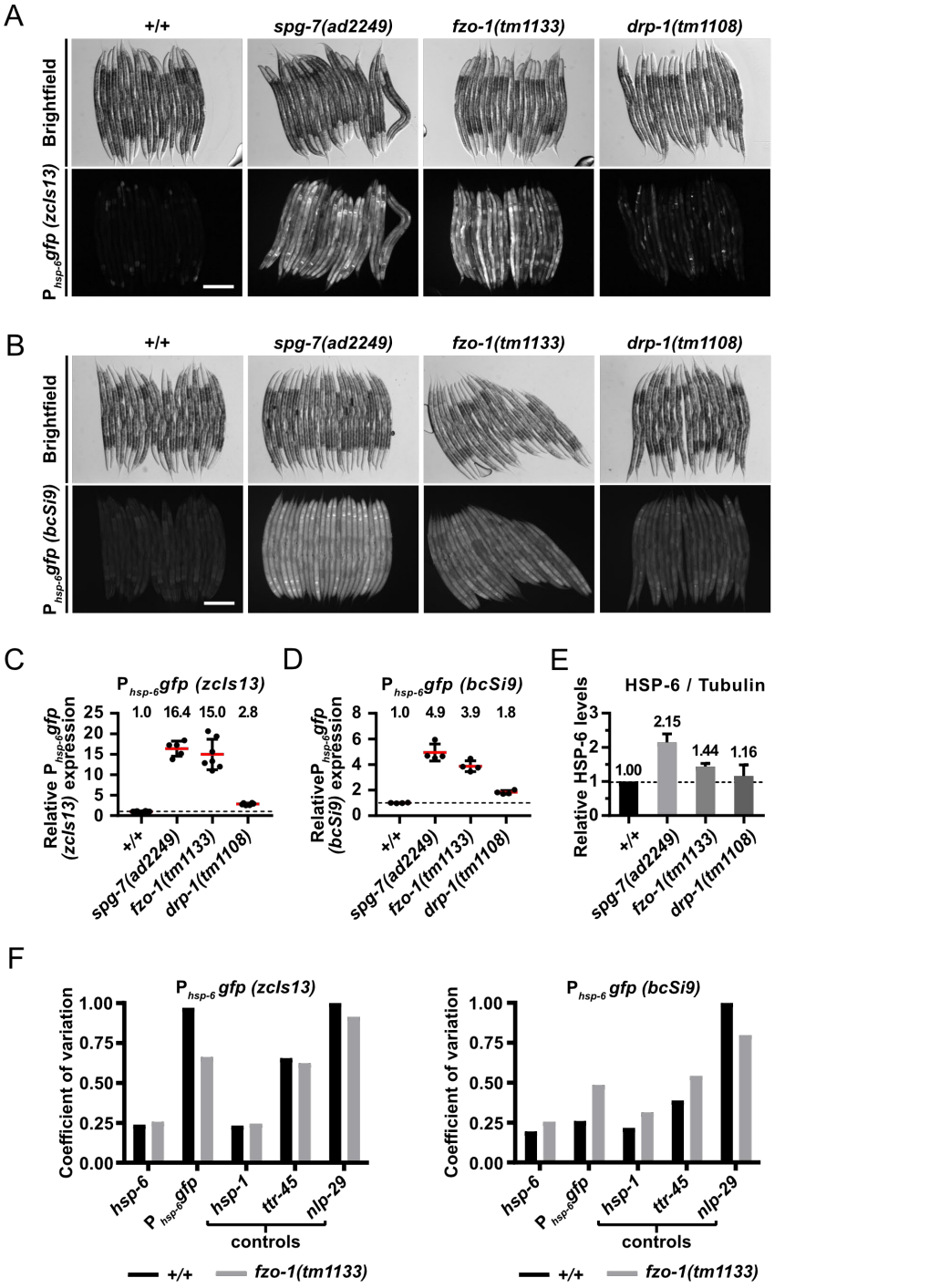

S1 Fig. Comparison of expression levels and inter-individual variability of multi-copy P$_{hsp\text{-}6\ mtHSP70}$*gfp (zcIs13)* and single-copy integrated P$_{hsp\text{-}6\ mtHSP70}$*gfp (bcSi9)* transgenes. (A) Brightfield (upper panel) and fluorescence images (lower panel) of L4 larvae expressing P$_{hsp\text{-}6}$*gfp (zcIs13)* in wild type (+/+), *spg-7(ad2249)*, *fzo-1(tm1133) or drp-1(tm1108)*. Scale bar: 200 μm. **(B)** Brightfield (upper panel) and fluorescence images (lower panel) of L4 larvae expressing P$_{hsp\text{-}6}$*gfp (bcSi9)* in wild type (+/+), *spg-7(ad2249)*, *fzo-1(tm1133)* or *drp-1(tm1108)*. Scale bar: 200 μm. **(C)** Quantifications of fluorescence images of panel A (P$_{hsp\text{-}6}$*gfp (zcIs13)*) are shown. Each dot represents quantification of 15–20 L4 larvae. Values indicate means ± SD of ≥5 independent measurements. **(D)** Quantifications of fluorescence images of panel B (P$_{hsp\text{-}6}$*gfp (bcSi9)*) are shown. Each dot represents quantification of 15–20 L4 larvae. Values indicate means ± SD of ≥4 independent measurements. **(E)** Quantifications of western blot analysis of endogenous HSP-6 levels in wild-type (+/+), *spg-7(ad2249)*, *fzo-1(tm1133)* or *drp-1(tm1108)* using anti-HSP-6 antibodies. For each genotype, 100 L4 larvae were harvested per experiment for western blot analysis. Values indicate means of relative HSP-6 expression (HSP-6/TUB) ± SD, n = 2. **(F)** Inter-individual variability in gene expression of target genes in *bcSi9* and *zcIs13* in both wild type (+/+) and *fzo-1(tm1133)*. To estimate inter-individual variability in gene expression, the coefficient of variation was calculated from individual mRNA levels obtained from normalized Ct values using the delta Ct method. Inter-individual variability values were normalized such that variability values for *nlp-29* in wild type = 1 *(bcSi9* or *zcIs13)*. Number of individual worms: n = 35 *(bcSi9)*, n = 32 (*bcSi9; fzo-1(tm1133)*), n = 31 *(zcIs13)*, n = 31 *(zcIs13; fzo-1(tm1133)*).

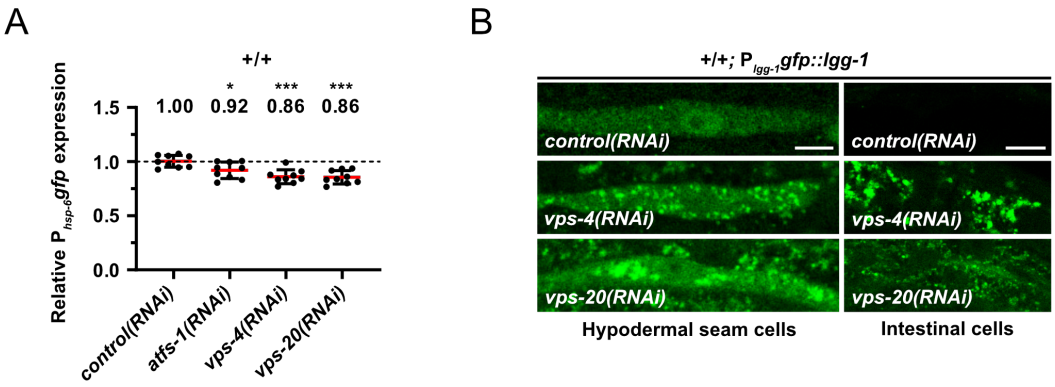

S2 Fig. RNAi against *vps-4*^{VPS4} and *vps-20*^{CHMP6} suppresses expression of *bcSi9* and induces autophagy in wild type (+/+). (A) L4 larvae were subjected to *control(RNAi)*, *atfs-1(RNAi)*, *vps-4(RNAi)* or *vps-20(RNAi)* and the F1 generation was imaged. Each dot represents the quantification of fluorescence intensity of 15–20 L4 larvae. Values indicate means ± SD of 5 independent experiments in duplicates. **P*<0.05, ****P*<0.001 using one-way ANOVA with Dunnett's multiple comparison test to *control(RNAi)*. **(B)** P*lgg-1gfp::lgg-1* expression of L4 larvae in hypodermal seam cells and intestinal cells upon *control(RNAi)*, *vps-4(RNAi)* or *vps-20(RNAi)*. Representative images of >30 animals from two independent biological replicates are shown. Scale bar hypodermal seam cells: 5 μm. Scale bar intestinal cells: 20 μm.

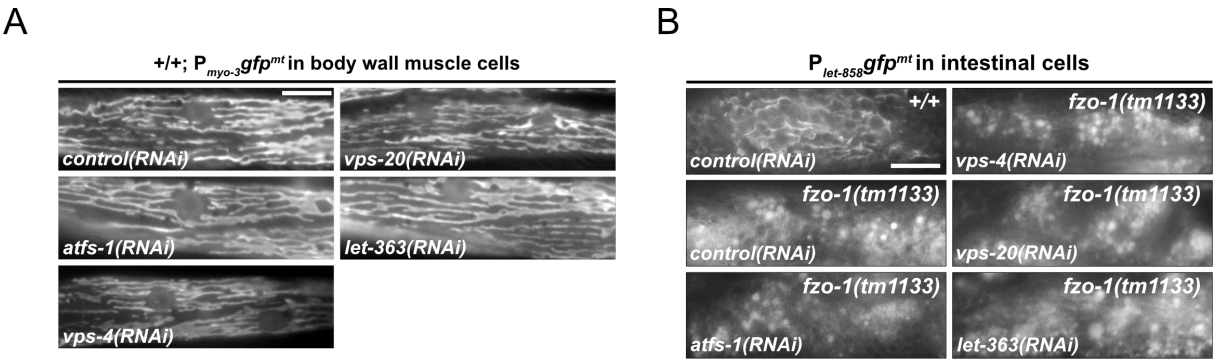

S3 Fig. Knock-down of ESCRT components in body wall muscle cells of wild type and intestinal cells in *fzo-1(tm1133)* does not change mitochondrial morphology. (A) Fluorescence images of L4 larvae expressing $P_{myo\text{-}3}gfp^{mt}$ in wild type (+/+). L4 larvae were subjected to *control(RNAi)*, *atfs-1(RNAi)*, *vps-4(RNAi)*, *vps-20(RNAi)* or *let-363(RNAi)* and the F1 generation was imaged. Scale bar: 10 μm. **(B)** Fluorescence images of L4 larvae expressing $P_{let\text{-}858}gfp^{mt}$ in wild type (+/+) or *fzo-1(tm1133)*. L4 larvae were subjected to *control(RNAi)*, *atfs-1(RNAi)*, *vps-4(RNAi)*, *vps-20(RNAi)* or *let-363(RNAi)* and the F1 generation was imaged. Scale bar: 10 μm.

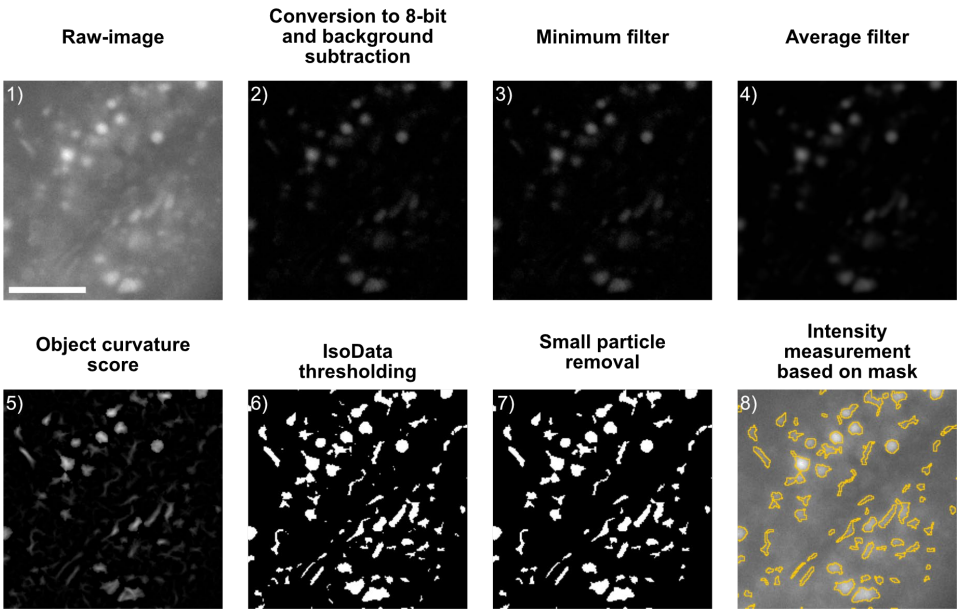

S4 Fig. Image segmentation and intensity measurement workflow. A raw 16-bit image (1) is converted to 8-bit, followed by a background subtraction using the rolling ball algorithm (2). This is followed by the successive application of a minimum (3) and average filter (4). The ImageJ Tubeness plugin generates an image with object curvature scores (5), after which the IsoData autothresholding is applied to generate the binary mask (6). Noise is removed by filtering out particles below a certain size (7) and the final mask is used to define the area in which intensity measurements are obtained (8). Scale bar: 5 μm.

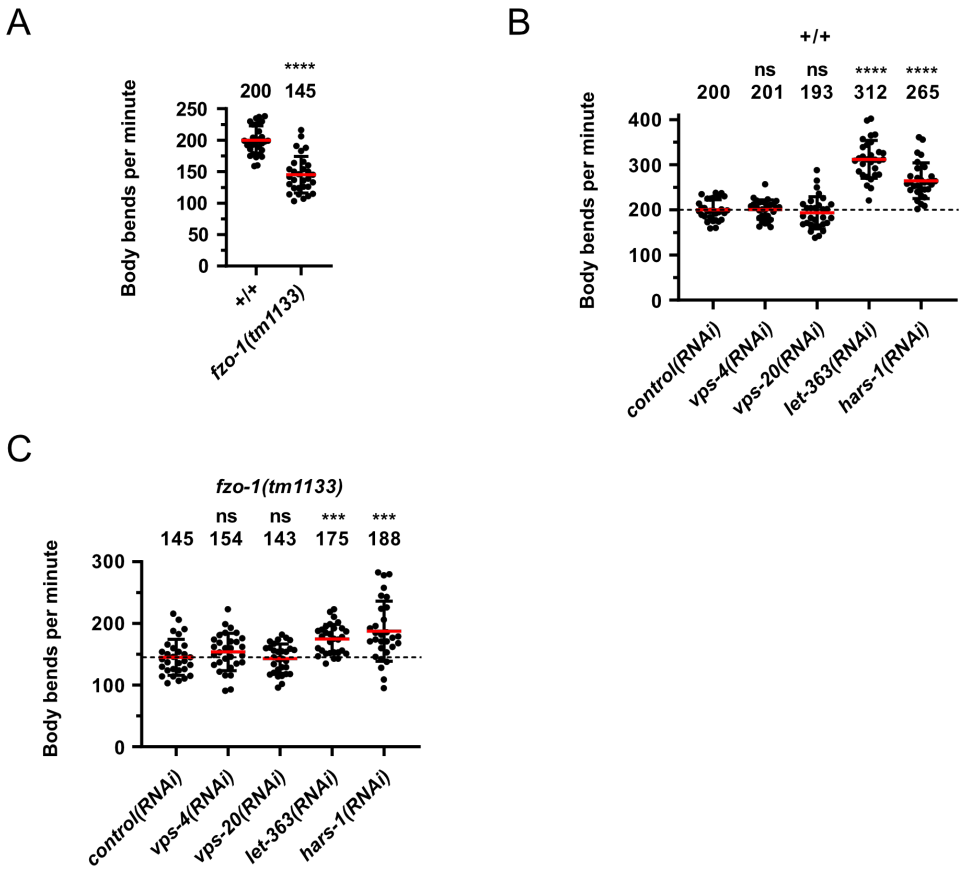

S5 Fig. Thrashing assay in wild-type and *fzo-1(tm1133)* animals upon induction of autophagy. Thrashing rate was analyzed by counting body bends of animals swimming for 1 minute in M9 buffer in 3 independent experiments. Each dot represents one L4 larvae. **(A)** Thrashing rates of wild-type (+/+) or *fzo-1(tm1133)* L4 larvae. *****P*<0.0001 using unpaired two-tailed t-test. n = 30. **(B)** Thrashing rates in wild-type animals upon induction of autophagy. L4 larvae were subjected to *control(RNAi)*, *vps-4(RNAi)*, *vps-20(RNAi)*, *let-363(RNAi)* or *hars-1(RNAi)* and the F1 generation was analyzed. ns: not significant, *****P*<0.0001 using Kruskal-Wallis test with Dunn's multiple comparison test to *control(RNAi)*. n = 30. **(C)** Thrashing rates in *fzo-1(tm1133)* animals upon induction of autophagy. L4 larvae were subjected to *control(RNAi)*, *vps-4(RNAi)*, *vps-20(RNAi)*, *let-363(RNAi)* or *hars-1(RNAi)* and the F1 generation was analyzed. ns: not significant, ****P*<0.001 using Kruskal-Wallis test with Dunn's multiple comparison test to *control(RNAi)*. n = 30.

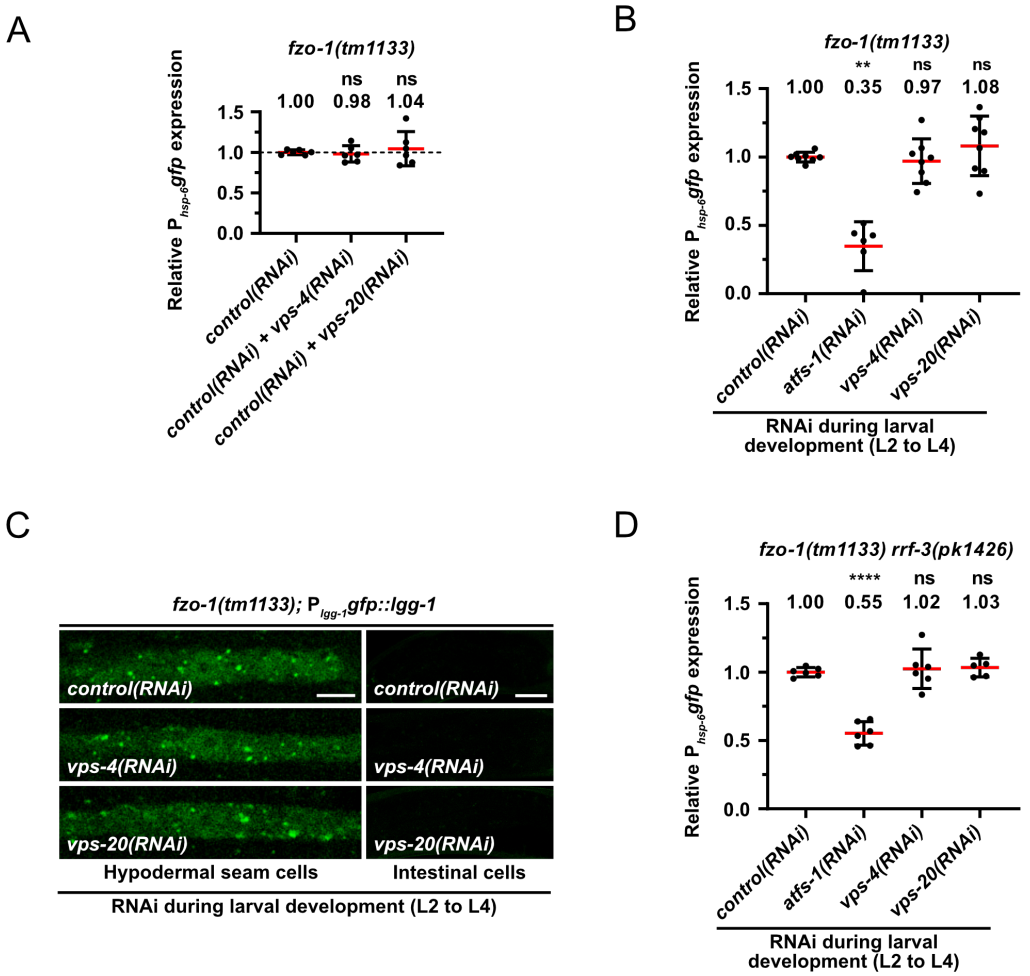

S6 Fig. RNAi against *vps-4*^{VPS4} and *vps-20*^{CHMP6} does not suppress *fzo-1(tm1133)*-induced UPR^{mt} when diluted with *control(RNAi)* or carried out in one generation from L2 to L4 larvae. (A) Quantifications of fluorescence images of L4 larvae expressing P$_{hsp-6}$*gfp (bcSi9)* in *fzo-1(tm1133)*. Each *ESCRT(RNAi)* was diluted 1:1 with *control(RNAi)*. After subtracting the mean fluorescence intensity of wild type (+/+) on *control(RNAi)*, the values were normalized to *fzo-1(tm1133)* on *control(RNAi)*. Each dot represents the quantification of fluorescence intensity of 15–20 L4 larvae. Values indicate means ± SD of 3 independent experiments in duplicates. ns: not significant, using one-way ANOVA with Dunnett's multiple comparison test to *control(RNAi)*. **(B)** Quantifications of fluorescence images of L4 larvae expressing P$_{hsp-6}$*gfp (bcSi9)* in *fzo-1(tm1133)*. L2 larvae were subjected to *control(RNAi)*, *atfs-1(RNAi)*, *vps-4(RNAi)* or *vps-20(RNAi)* and the same animals were imaged in L4 stage. After subtracting the mean fluorescence intensity of wild type (+/+) on *control(RNAi)*, the values were normalized to *fzo-1(tm1133)* on *control(RNAi)*. Each dot represents the quantification of fluorescence intensity of 15–20 L4 larvae. Values indicate means ± SD of 4 independent experiments in duplicates. ns: not significant, $^{**}P<0.01$ using Kruskal-Wallis test with Dunn's multiple comparison test to *control(RNAi)*. **(C)** P$_{lgg-1}$*gfp::lgg-1* expression of *fzo-1(tm1133)* L4 larvae in hypodermal seam cells and intestinal cells. L2 larvae were subjected to *control(RNAi)*, *vps-4(RNAi)* or *vps-20(RNAi)* and the same animals were imaged in L4 stage. Representative images of >60 animals from two independent biological replicates are shown. Scale bar hypodermal seam cells: 5 μm. Scale bar intestinal cells: 20 μm. **(D)** Quantifications of fluorescence images of L4 larvae expressing P$_{hsp-6}$*gfp (bcSi9)* in *fzo-1(tm1133) rrf-3(pk1426)*. L2 larvae were subjected to *control(RNAi)*, *atfs-1(RNAi)*, *vps-4(RNAi)* or *vps-20(RNAi)* and the same animals were imaged in L4 stage. After subtracting the mean fluorescence intensity of wild type (+/+) on *control(RNAi)*, the values were normalized to *fzo-1(tm1133)* on *control(RNAi)*. Each dot represents the quantification of fluorescence intensity of 15–20 L4 larvae. Values indicate means ± SD of 4 independent experiments in duplicates. ns: not significant, $^{****}P<0.0001$ using one-way ANOVA with Dunnett's multiple comparison test to *control(RNAi)*.

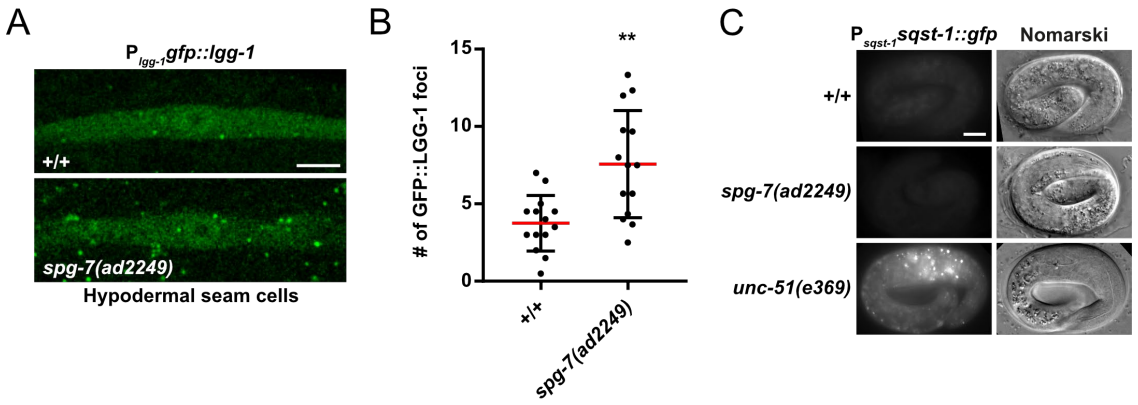

S7 Fig. Autophagy is induced in *spg-7(ad2249)* animals. (A) P*lgg-1*::*gfp*::*lgg-1* expression in hypodermal seam cells of wild type (+/+) or *spg-7(ad2249)* L4 larvae. Scale bar: 5 μm. **(B)** Quantification of GFP::LGG-1 foci in hypodermal seam cells from panel A. Each dot represents the average amount of GFP::LGG-1 foci counted from 2–5 seam cells in one animal. n≥18 for each genotype; values indicate means ± SD; ** $P<0.01$ using unpaired two-tailed t-test with Welch's correction. **(C)** Nomarski and fluorescent images of the P*sqst-1*::*sqst-1*::*gfp* translational reporter in embryos of wild type (+/+) and *spg-7(ad2249)* animals. As a positive control for a block in autophagy, *unc-51(e369)* was used. Representative images of >60 embryos are shown. Scale bar: 10 μm.

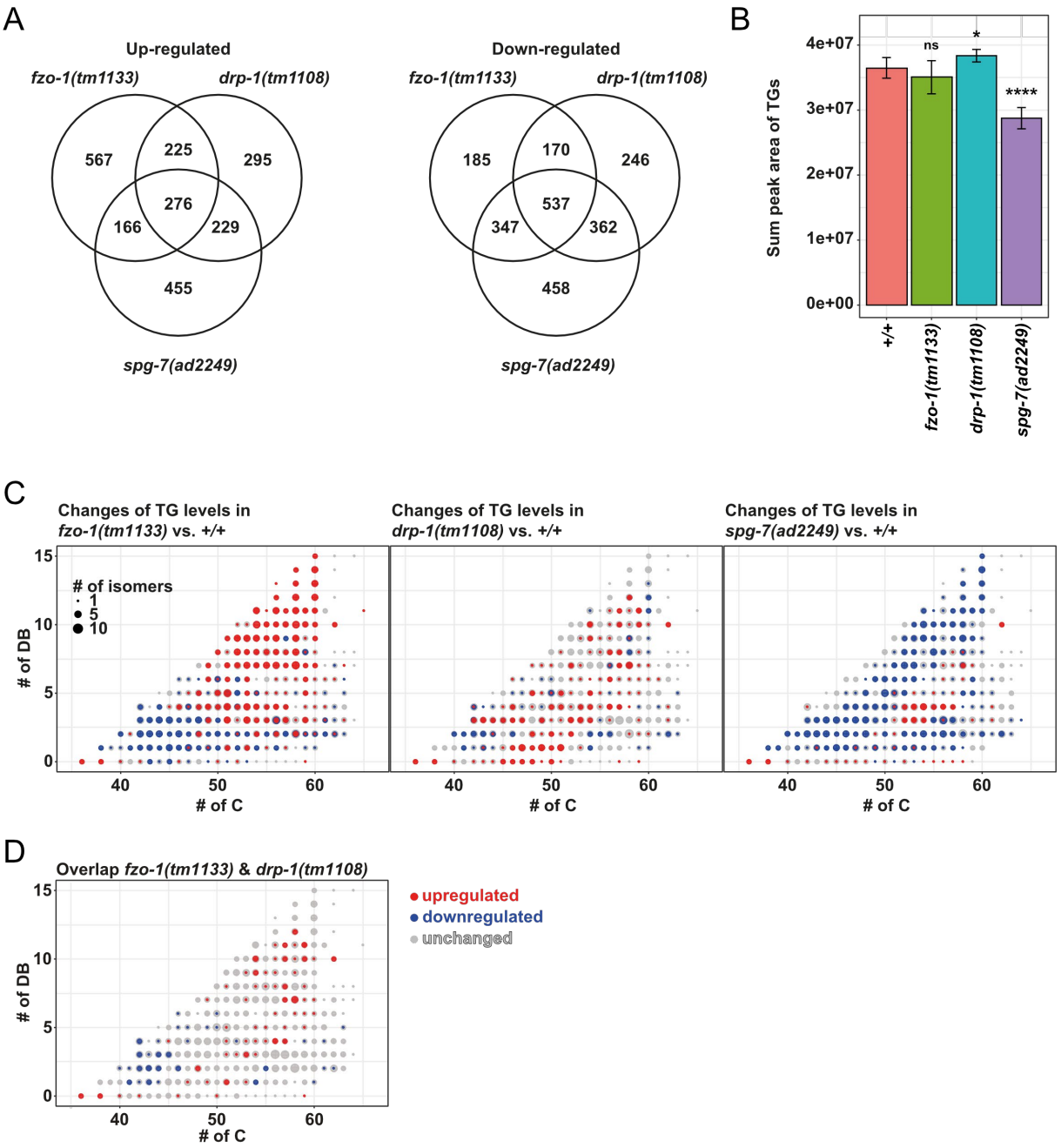

S8 Fig. Defects in mitochondrial homeostasis lead to major changes in lipid metabolism. (A) Venn diagrams showing the overlap of lipids up- or downregulated in *fzo-1(tm1133)*, *drp-1(tm1108)* and *spg-7(ad2249)* in comparison to wild type (+/+). **(B)** Total amount of TGs in wild type (+/+), *fzo-1(tm1133)*, *drp-1(tm1108)* and *spg-7(ad2249)* backgrounds. Means ± SD are shown; ns: not significant, **P*<0.05, *****P*<0.0001 using Welch test. **(C)** Scatterplot indicating the distribution and changes in the levels of TG species in the different mutants in comparison to wild type (+/+). **(D))** Scatterplot indicating the overlap of the changes in the levels of TG species of *fzo-1(tm1133)* and *drp-1(tm1108)* mutants in comparison to wild type (+/+). **(C)** and **(D)** The x-axis labels the number of carbons (# of C) and the y-axis the number of double bonds (DB) in the acyl sidechains. The size of a dot indicates the number of detected isomers for a specific sum composition. Grey dots represent all detected TGs species and blue and red dots indicate down- (blue) or upregulation (red).

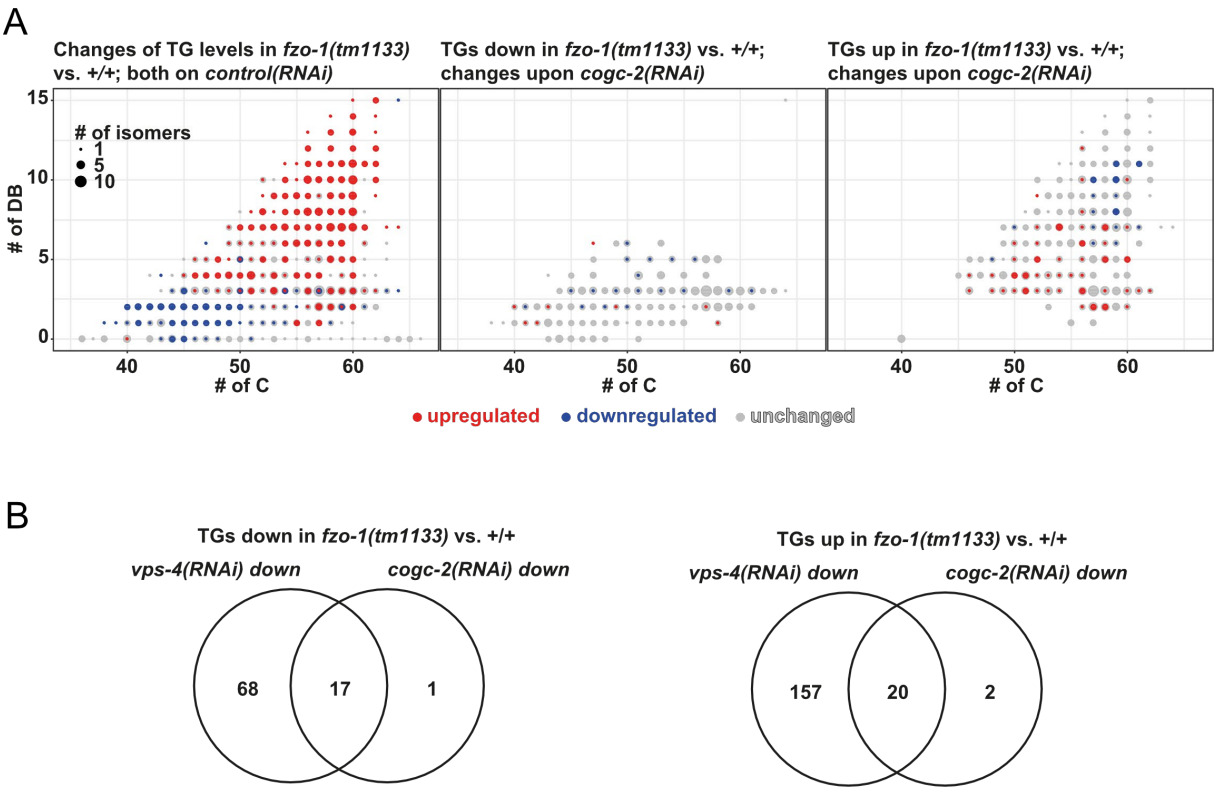

S9 Fig. Induction of autophagy upon *cogc-2(RNAi)* changes the levels of specific TGs in *fzo-1(tm1133)* mutants. (A) Scatterplot indicating the distribution and changes in the level of TG species in *fzo-1(tm1133)* mutants in comparison to wild type (+/+). The x-axis labels the number of carbons (# of C) and the y-axis the number of double bonds (DB) in the acyl sidechains. The size of a dot indicates the number of detected isomers for a specific sum composition. Grey dots represent all detected TGs species and blue and red dots indicate down- (blue) or upregulation (red). **(B)** Venn diagram indicating the overlap of TG species downregulated (left panel) or upregulated (right panel) in *fzo-1(tm1133)* and downregulated upon *vps-4(RNAi)* or *cogc-2(RNAi)*.

S1 Table. List of genes that suppress *fzo-1(lf)*-induced UPR^{mt} and induce autophagy in wild-type animals upon knock-down. Candidate genes were identified in the primary RNAi-screen using *fzo-1(tm1133)*, subsequently knocked-down and tested for induction of autophagy and re-screened for UPR^{mt} suppression in two different mutant backgrounds: *drp-1(tm1108)* and *spg-7(ad2249)*.

Category	Sequence	Gene name	Human ortholog	*fzo-1(lf)*	*drp-1(lf)*	*spg-7(lf)*
Cell Architecture	K07C5.1	*arx-2*	*ACTR2*			
	D2024.6	*cap-1*	*CAPZA1,2*			
	M106.5	*cap-2*	*CAPZB*			
	C53A5.6	*C53A5.6*	*IPP*			
	C17H12.1	*dyci-1*	*DYNC1I1,2*			
Cell Signaling	W03H9.4	*cacn-1*	*CACTIN*			
	H25P06.2	*cdk-9*	*CDK9*			
	C24H11.7	*gbf-1**	*GBF1*			
	T01G9.6	*kin-10**	*CSNK2B*			
	C27H6.2	*ruvb-1**	*RUVBL1*			
Cellular Trafficking	C06G3.10	*cogc-2**	*COG2*			
	Y51H7C.6	*cogc-4**	*COG4*			
	F23F1.5	*F23F1.5*	*SNUPN*			
	F38A1.8	*F38A1.8*	*SRPRA*			
	F32E10.4	*ima-3*	*KPNA3,4*			
	C53D5.6	*imb-3*	*IPO5, RANBP6*			
	Y59E9AL.7	*nbet-1*	*BET1*			
	Y77E11A.13	*npp-20*	*SEC13*			
	H15N14.2	*nsf-1**	*NSF*			
	R186.3	*R186.3*	*SRPRB*			
	F20G4.1	*smgl-1**	*NBAS*			
	F55C5.8	*srpa-68*	*SRP68*			
	T10H9.3	*syx-18*	*STX18*			
	Y63D3A.5	*tfg-1*	*TFG*			
	Y34D9A.10	*vps-4**	*VPS4A,B*			
	Y65B4A.3	*vps-20**	*CHMP6*			
	CD4.4	*vps-37**	*VPS37B,C*			
	Y48G1A.5	*xpo-2/imb-5*	*CSE1L*			
Chromatin Structure	ZK1251.1	*htas-1*	*H2AFY, H2AFY2*			
	F26F12.7	*let-418*	*CHD4*			
	F55A3.3	*spt-16*	*SUPT16H*			
Metabolism	C33H5.18	*cdgs-1*	*CDS2*			
	C06E4.6	*C06E4.6*	*HSD17B14*			
	F25B4.6	*hmgs-1*	*HMGCS1,2*			
	H37A05.1	*lpin-1*	*LPIN1,2,3*			
	W09B6.1	*pod-2*	*ACACB*			
	C47E12.4	*pyp-1*	*PPA1,2*			
PTM	T17E9.2	*nmt-1*	*NMT1,2*			
	W02A11.4	*uba-2*	*UBA2*			
Proteostasis	T21B10.7	*cct-2*	*CCT2*			
	C04A2.7	*dnj-5*	*DNAJC14*			

Proteostasis	C56C10.8	*icd-1*	*BTF3,L4*			
	F21C3.5	*pfd-6*	*PFDN6*			
	F54C9.2	*stc-1*	*HSPA13*			
	F19B6.2	*ufd-1**	*UFD1L*			
RNA Processing	B0511.6	*B0511.6*	*DDX18*			
	C14A4.4	*crn-3*	*EXOSC10*			
	C55B7.8	*dbr-1*	*DBR1*			
	F42H10.7	*ess-2*	*ESS2*			
	F59C6.4	*exos-3*	*EXOSC3*			
	F10B5.8	*F10B5.8*	*INTS11*			
	C17E4.5	*pabp-2*	*PABPN1*			
	C06E1.10	*rha-2*	*DHX37*			
	C47E12.7	*rrp-1*	*RRP1B, RRP1*			
	Y116A8C.32	*sfa-1*	*SF1*			
	T28D9.10	*snr-3*	*SNRPD1*			
	Y49E10.15	*snr-6*	*SNRPE*			
	K02F2.3	*teg-4*	*SF3B3*			
	W04A4.5	*W04A4.5*	*INTS4*			
Transcription	B0261.1	*B0261.1*	*BDP1*			
	F10E9.4	*F10E9.4*	*TWISTNB*			
	C48E7.2	*let-611*	*POLR3C*			
	Y113G7B.18	*mdt-17*	*MED17*			
	F28F8.5	*mdt-28*	*MED28*			
	F58A4.9	*rpac-19*	*POLR1D*			
	H43I07.2	*rpac-40*	*POLR1C*			
	C42D4.8	*rpc-1*	*POLR3A*			
	F09F7.3	*rpc-2*	*POLR3B*			
	ZK856.10	*rpc-25*	*POLR3H*			
	R119.6	*taf-4*	*TAF4B, TAF4*			
	F30F8.8	*taf-5*	*TAF5*			
	ZK1320.12	*taf-8*	*TAF8*			
	K03B4.3	*taf-10*	*TAF10*			
	Y50D7A.2	*xpd-1*	*ERCC2*			
Miscellaneous	W07B3.2	*gei-4*	*n.a.*			
	Y46G5A.6	*phi-3*	*n.a.*			
	ZK637.8	*unc-32*	*ATP6V0A1,4*			
Uncharacterized	C23G10.8	*C23G10.8*	*n.a.*			
	K02E2.7	*K02E2.7*	*n.a.*			
	K10G6.5	*K10G6.5*	*n.a.*			
	K10H10.4	*K10H10.4*	*n.a.*			
	Y82E9BR.13	*pals-17*	*n.a.*			
Ribosome Biogenesis	E02H1.1	*E02H1.1*	*DIMT1*			
	T01C3.7	*fib-1*	*FBLL1*			
	K12H4.3	*K12H4.3*	*BRIX1*			
	R13A5.12	*lpd-7*	*PES1*			

Ribosome Biogenesis	T07A9.9	*nog-1**	*GTPBP4*			
	R151.3	*rpl-6*	*RPL6*			
	F53G12.10	*rpl-7*	*RPL7*			
	Y24D9A.4	*rpl-7A*	*RPL7A*			
	JC8.3	*rpl-12*	*RPL12*			
	C04F12.4	*rpl-14*	*RPL14*			
	Y45F10D.12	*rpl-18*	*RPL18*			
	E04A4.8	*rpl-20*	*RPL18A*			
	C14B9.7	*rpl-21*	*RPL21*			
	C27A2.2	*rpl-22*	*RPL22*			
	B0336.10	*rpl-23*	*RPL23*			
	F28C6.7	*rpl-26*	*RPL26*			
	C53H9.1	*rpl-27*	*RPL27*			
	W09C5.6	*rpl-31*	*RPL31*			
	ZK652.4	*rpl-35*	*RPL35*			
	B0393.1	*rps-0*	*RPSA*			
	C23G10.3	*rps-3*	*RPS3*			
	Y71A12B.1	*rps-6*	*RPS6*			
	F40F11.1	*rps-11*	*RPS11*			
	Y41D4B.5	*rps-28*	*RPS28*			
	F10G7.1	*tag-151*	*TSR1*			
Translation	F17C11.9	*eef-1G*	*EEF1G*			
	H06H21.3	*eif-1.A*	*EIF1AX,Y*			
	F11A3.2	*eif-2Bδ*	*EIF2B4*			
	D2085.3	*eif-2Bε*	*EIF2B5*			
	Y54E2A.11	*eif-3.B*	*EIF3B*			
	B0511.10	*eif-3.E*	*EIF3E*			
	H19N07.1	*erfa-3*	*GSPT1,2*			
	F28H1.3	*aars-2*	*AARS*			
	T08B2.9	*fars-1*	*FARSA*			
	T10F2.1	*gars-1*	*GARS*			
	T11G6.1	*hars-1**	*HARS, HARS2*			
	R11A8.6	*iars-1**	*IARS*			
	F22D6.3	*nars-1*	*NARS*			
	Y41E3.4	*qars-1*	*QARS*			
	F26F4.10	*rars-1**	*RARS*			
	C47D12.6	*tars-1**	*TARS, TARS2,2L*			
	Y80D3A.1	*wars-1*	*WARS*			
	R08D7.4	*R08D7.4*	*EEF2KMT, FAM86B1,2*			
	Y65B4A.6	*Y65B4A.6*	*EIF4A3*			

* Genes that are already implemented in Fig 4A

from the strongest to no GFP suppression

Candidate genes were screened for UPR^{mt} suppression three times in technical duplicates with the same reporter *(zcIs13)* in two different mutant backgrounds: *drp-1(tm1108)* and *spg-7(ad2249)*. Fluorescence intensity was scored and classified

from very strong suppression to weak suppression (gradual violet coloring) or no suppression (white).
PTM: Post-translational modification.

S2 Table is a .xlsx file that contains all numerical data of the lipidomic experiments. To view please visit https://doi.org/10.1371/journal.pgen.1008638

S3 Table. List of qRT-PCR primers. Primers used for qRT-PCR including PCR efficiency and coefficient of determination (R^2).

Gene	Sequence Forward Primer	Sequence Reverse Primer	PCR Efficiency (%)	R^2
cdc-42	TCCACAGACCGACGTGTTTC	AGGCACCCATTTTTCTCGGA	100.3	0.99
gfp	TGTTCCATGGCCAACACTTG	CCTGTACATAACCTTCGGGCA	99.1	0.99
hsp-1	CACTGTTTTCGATGCCAAACG	TCCTTCGGCAGAGATGACCT	107.8	0.99
hsp-6	GATTGGATAAGGACGCTGGAGA	CCGTTGGTGGACTTGACCTC	101	0.99
hsp-60	CCAAGGACGTCAAGTTCGGA	TCACGTTTCTTCCTTTTGGGC	106	0.99
ire-1	TACTTGCCACCACGGAGACC	CGTTGCCATCGTCATCATTG	110.3	0.99
nlp-29	AGGATATGGAAGAGGATATGGAGG	CTCCGTACATTCCACGTCCA	114.8	0.99
pmp-3	GTTCCCGTGTTCATCACTCAT	ACACCGTCGAGAAGCTGTAGA	109.3	0.99
ttr-45	CGACGGGCAAGGAATGTTCA	CGGAGTCCTGGCTTCAACTT	114.2	0.99

4 Discussion

Various stressors that impact mitochondria lead to activation of certain stress response pathways in order to maintain mitochondrial homeostasis. Among these are the UPR^{mt}, autophagy/mitophagy and mitochondrial hyperfusion (reviewed in Friedman and Nunnari, 2014; Pellegrino et al., 2013). The results presented in chapter I provide evidence that depletion of LRPPRC or MMA-1 not only leads to mitochondrial hyperfusion but also to the induction of UPR^{mt}. The functional interactions between UPR^{mt} and autophagy are the focus of chapter II, in which it is shown that the induction of autophagy suppresses UPR^{mt} induced by a block in mitochondrial dynamics.

4.1 Loss of *LRPPRC* function induces the mitochondrial unfolded protein response

Mitochondrial hyperfusion is triggered upon starvation or inhibition of cytosolic protein synthesis and it has been proposed that this acts as a prosurvival mechanism because it ensures the ATP supply in the cell (Gomes et al., 2011; Rambold et al., 2011; Tondera et al., 2009). This is in line with a study showing that the loss of *LRPPRC* or *mma-1* function, which results in impaired complex IV activity, is transiently compensated by mitochondrial hyperfusion since cellular ATP levels are maintained (Rolland et al., 2013). The impaired complex IV activity upon knock-down of *LRPPRC* or *mma-1* is due to a decrease in mitochondria-encoded subunits of complex IV (Rolland et al., 2013; Ruzzenente et al., 2012; Sasarman et al., 2010). Consequently, loss of *LRPPRC* or *mma-1* function also leads to an imbalance between mitochondria-encoded and nuclear-encoded complex IV subunits and our data shown in chapter I provide evidence that the UPR^{mt} is activated under these conditions. Initially, the disruption in mitochondrial proteostasis was thought to be the signal for UPR^{mt} activation, however, it has recently been demonstrated that, in *C. elegans*, it is rather the decrease in mitochondrial membrane potential that acts as the signal since it regulates mitochondrial import efficiency of ATFS-1 (Rolland et al., 2019). Thus, the loss of *mma-1* function most likely decreases mitochondrial membrane potential and thereby activates the UPR^{mt}, which is in accordance with the finding that the impairment of the mitochondrial respiratory chain generally induces UPR^{mt} in *C. elegans* (Benedetti et al., 2006; Durieux et al., 2011; Yoneda et al., 2004). Because depletion of *mma-1* leads to activation of UPR^{mt} while ATP levels are maintained, this also

suggests that mitochondrial hyperfusion does not primarily locally increase mitochondrial membrane potential but rather increases the total surface area for OXHPOS to ensure maintenance of global ATP levels. Notably, a decrease in OXPHOS capacity and mitochondrial membrane potential has been confirmed in fibroblasts from patients suffering from French Canadian Leigh Syndrome (Burelle et al., 2015). However, UPR^{mt} regulation in mammalian systems is more complex and also involves the ISR. Hence, it requires further research in order to unravel the exact role of mitochondrial membrane potential in ISR and UPR^{mt} activation in mammals.

We show that UPR^{mt} is transiently activated upon depletion of LRPPRC until mitochondrial proteostasis is restored. Hence, UPR^{mt} participates in restoring the imbalance between mitochondria- and nuclear-encoded subunits of complex IV. Since COX IV, a nuclear-encoded encoded protein of complex IV, is down-regulated in response to the loss of *LRPPRC* function, this suggests that not only proteases and chaperones act to restore this imbalance but that also the inhibition of general protein synthesis plays an important role in this regard. It would be interesting to test if COX IV downregulation is dependent on GCN2 and phosphorylation of eIF2α and, if so, whether this is also true upon *mma-1* knock-down in *C. elegans* since this branch of UPR^{mt} activation seems not to be conserved in nematodes (see 1.2.4).

Remarkably, UPR^{mt} and mitochondrial hyperfusion induced by the loss of LRPPRC are coordinated and follow similar kinetics. Nevertheless, these two responses are likely mediated by distinct genetic pathways because depletion of ATFS-1 or HAF-1 does not affect the mitochondrial hyperfusion phenotype in *C. elegans*. This is supported by the fact that mild depletion of MMA-1 solely leads to UPR^{mt} while strong depletion of MMA-1 leads to both UPR^{mt} and mitochondrial hyperfusion. Noteworthy, this also shows that, depending on the severity of a stress, different stress response pathways can be activated. Upon weak stress levels, UPR^{mt} is sufficient to restore mitochondrial homeostasis. If the stress persists or when the stress level is high, UPR^{mt} activation is not enough to cope with the stress, which additionally results in the stimulation of mitochondrial hyperfusion. Interestingly, the induction of UPR^{mt} goes along with a metabolic shift towards glycolysis (reviewed in Lin and Haynes, 2016). Hence, the UPR^{mt} potentially compensates for decreased OXHPOS activity upon mild depletion of MMA-1 or LRPPRC. However, this compensation may fail when OXPHOS is more severely affected and this may then be counteracted by mitochondrial hyperfusion. In line with this, it has been shown that, under conditions where hyperfusion is present, increased glycolysis does not play a role in the compensation of ATP levels upon *LRPPRC* knock-down

since cells grown in low glucose medium still display stable amounts of ATP (Rolland et al., 2013). Taken together, this indicates that mitochondrial hyperfusion may be more vital for cellular homeostasis as compared to UPR^{mt} and this could explain why mitochondrial hyperfusion (Rolland et al., 2013) but not ATFS-1-dependent UPR^{mt} is essential for viability in response to knock-down of *mma-1*. Nonetheless, it is worth mentioning that there still could be ATFS-1-independent UPR^{mt} that plays an important role for organismal viability since more than 40% of genes upregulated upon *spg-7(RNAi)* were found to be still upregulated in an *atfs-1*(lf) background (Nargund et al., 2012).

How the loss of *LRPPRC* or *mma-1* function results in mitochondrial hyperfusion stills needs to be determined, however, it has been shown that the mitochondrial hyperfusion phenotype is likely the results of increased mitochondrial fusion rather than defective fission (Rolland et al., 2013). Furthermore, it was speculated that complex IV may directly affect mitochondrial fusion since it has already been shown that mammalian OPA1 can interact with some subunits of complex IV (Agier et al., 2012; Rolland et al., 2013). Another idea could be that the AMPK signaling pathway is involved in mediating mitochondrial hyperfusion as it is the major energy sensing pathway and has been shown to be able to promote mitochondrial fusion (Kang et al., 2016; Wu et al., 2020).

Upon *LRPPRC* knock-down, both UPR^{mt} and mitochondrial hyperfusion are transient responses and prolonged inactivation of *LRPPRC* has been shown to results in mitochondrial fragmentation (Rolland et al., 2013). This is in accordance with studies showing that defects in the mitochondrial respiratory chain complexes generally cause mitochondrial fragmentation (Guillery et al., 2008; Koopman et al., 2005; Liot et al., 2009; Moran et al., 2010). Hence, mitochondrial hyperfusion can only compensate for complex IV defects in short-term conditions. Moreover, fibroblasts of patients suffering from French Canadian Leigh Syndrome exhibit mitochondrial fragmentation as well as reduced OXPHOS capacity, which both most likely contributes to the pathophysiology of the disease (Burelle et al., 2015; Sasarman et al., 2010). Noteworthy, it has also been shown that, despite the fragmented mitochondria phenotype, ATP levels remain constant in fibroblasts of patients suffering from French Canadian Leigh Syndrome and it has been proposed that this is due to mTOR-mediated re-programming of metabolism (Burelle et al., 2015; Mukaneza et al., 2019). Whether UPR^{mt} is induced in French Canadian Leigh Syndrome patient cells remains to be determined, however, since mitochondrial membrane potential is decreased in fibroblasts derived from patients, it could well be that the UPR^{mt} is active. If not, this could indicate that UPR^{mt} already failed and

this would suggest that the two stress response pathways cannot restore mitochondrial and cellular homeostasis upon severe and long-term impairment of complex IV activity.

Interestingly, LRPPRC has also been implicated in the regulation of autophagy. More precisely, LRPPRC associates with Bcl-2 and Beclin-1 in a ternary complex and it has been shown that the binding of LRPPRC specifically increases Bcl-2 stability, which results in the enhanced sequestration of the autophagy inducer Beclin-1 and the suppression of basal levels of autophagy (Zou et al., 2013). Upon depletion of LRPPRC, Bcl-2 levels are decreased and Beclin-1 is released, thus leading to autophagy induction via the PI3K/Akt/mTOR signaling pathway (Zou et al., 2013). Similarly, LRPPRC was shown to suppress mitophagy through interaction with Parkin (Zou et al., 2014). The same study also showed that short-term exposure of cells with CCCP, a mitochondrial uncoupler, leads to activation of mitophagy/autophagy while long-term CCCP treatment finally impairs autophagic flux due to the depletion of ATG proteins (Zou et al., 2014). Hence, it would be interesting to test whether long-term depletion of LRPPRC potentially impairs autophagy. If so, this would indicate that autophagy induction upon knock-down of *LRPPRC* is also a transient response that potentially follows the same kinetics as mitochondrial hyperfusion and the activation of the UPR^{mt}. Since the deregulation of mitophagy/autophagy has been implicated in neurodegenerative diseases (Hara et al., 2006; reviewed in Shefa et al., 2019), studies in cells derived from French Canadian Leigh Syndrome patients will help to unravel whether mitophagy/autophagy also plays a role in the pathogenesis of this neurodegenerative disease. This could in the long run help to develop new therapeutic approaches in order to alleviate the set of symptoms associated with the disease. Whether LRPPRC's function in autophagy regulation is conserved and whether it involves the Bcl-2-like protein CED-9 in *C. elegans* remains to be elucidated. Noteworthy, LRPPRC not only affects autophagy but also vice versa. Specifically, mTOR inhibition by rapamycin as well as long-term mitophagy stress by CCCP treatment results in decreased levels of LRPPRC (Mukaneza et al., 2019; Zou et al., 2014).

4.2 Induction of autophagy suppresses *fzo-1(tm1133)*-induced UPR^{mt} through increasing mitochondrial membrane potential

The data presented in chapter II provide evidence that increased autophagic flux suppresses *fzo-1(tm1133)*-induced UPR^{mt}. Increased autophagic flux has previously been shown to result in mitochondrial hyperfusion (Gomes et al., 2011; Morita et al., 2017; Rambold et al., 2011),

however, we did not detect a change in mitochondrial morphology in the case of *fzo-1(tm1133)* animals but instead observed that mitochondrial membrane potential is partially restored. Noteworthy, mitochondrial membrane potential was recently found to be the signal for UPR^{mt} induction in *C. elegans* (Rolland et al., 2019), wherefore we propose that it is the increase in mitochondrial membrane potential that leads to suppression of *fzo-1(tm1133)*-induced UPR^{mt}. Whether UPR^{mt} is similarly regulated in other organisms remains to be determined, however, the loss of Mfn1 or Mfn2 in mammalian cells has been shown to result in decreased mitochondrial membrane potential, too (Bach et al., 2003; Pich et al., 2005). Moreover, recent evidence indicates that both the UPR^{mt} as well as the ISR are activated in response to malfunctioning or depletion of Mfn2 (Chung et al., 2019; Kowaltowski et al., 2019; Rocha et al., 2017; Xin et al., 2019). Thus, it would be interesting to test whether the induction of autophagy is also able to suppress UPR^{mt} induced by the loss of mitochondrial fusion in mammalian systems and, if so, whether this is also regulated through changes in mitochondrial membrane potential. Remarkably, increased autophagic flux has already been indicated to lead to increased mitochondrial membrane potential in yeast as well as in mammalian cells, suggesting that this functional connection may be conserved (Bonawitz et al., 2007; Lerner et al., 2013; Pan et al., 2011; Zhu et al., 2020). Surprisingly, we found that the induction of autophagy in wild-type animals results in decreased mitochondrial membrane potential and further research will be necessary to elucidate why autophagy induction in *C. elegans* affects mitochondrial membrane potential in opposite ways under different circumstances.

Interestingly, autophagy induction upon knock-down of most if not all candidate genes is predominantly observed in the intestine. Since autophagy in *fzo-1(tm1133)* animals alone (without additional knock-down of genes) is largely present in hypodermal seam cells but not the intestine, this indicates that the induction of autophagy specifically in this tissue is crucial for suppression of UPR^{mt}. Therefore, it would be worth testing whether the intestine-specific induction of autophagy is sufficient to suppress *fzo-1(tm1133)*-induced UPR^{mt}. Conversely, intestine-specific knock-down of autophagy genes (e.g., *lgg-1* or *unc-51*) could be used to test if this mitigates UPR^{mt} suppression. Notably, it has previously been shown that intestinal autophagy is critical for increased health- and lifespan in *C. elegans* during dietary restriction (Gelino et al., 2016), however, whether this effect is also the consequence of improved mitochondrial homeostasis and elevated respiration capacity remains to be determined. We propose that the induction of autophagy can lead to increased motility; however, further analysis of knock-down of candidate genes should be performed in order to corroborate this statement. Moreover, this effect is probably masked upon depletion of ESCRT components due to

pleiotropic effects. Although the induction of autophagy in wild-type animals results in decreased membrane potential, we observed that motility is increased. Thus, a compensatory energy-providing pathway may be activated in these animals.

The approach to ultimately confirm that autophagy induction is the cause for UPR^{mt} suppression was unsuccessful since ESCRT depletion in *fzo-1(tm1133)* animals with a block in autophagy results in embryonic lethality, which is in accordance with a previous study showing that autophagy is a pro-survival mechanism in response to loss of ESCRT (Djeddi et al., 2012). Moreover, neither diluted *ESCRT(RNAi)* nor *ESCRT(RNAi)* during larval development suffices to suppress *fzo-1(tm1133)*-induced UPR^{mt}, suggesting that efficient knock-down for a certain minimum period of time is necessary for autophagy induction and, hence, UPR^{mt} suppression. Furthermore, our data indicate that UPR^{mt} suppression is not due to *pdr-1*-dependent mitophagic degradation of defective and depolarized mitochondria. Additionally, we show that *fndc-1* receptor-mediated mitophagy does not affect the suppression of *fzo-1(tm1133)*-induced UPR^{mt}, which altogether suggests that autophagy rather than mitophagy is the underlying process that facilitates UPR^{mt} suppression. Nevertheless, autophagy may also be able to degrade some defective mitochondria in an unspecific manner.

4.3 Autophagy compensates for defects in mitochondrial dynamics

Increased autophagic flux not only suppresses UPR^{mt} induced by a block in mitochondrial fusion but also by a block in mitochondrial fission. Hence, autophagy compensates for defects in mitochondrial dynamics. Interestingly, compromised mitochondrial fission has been shown to impair mitophagy (Lee et al., 2011; Parone et al., 2008; Twig et al., 2008; Wu et al., 2016), again pointing towards autophagy and not the selective degradation of mitochondria being responsible for UPR^{mt} suppression. Since *spg-7(ad2249)*-induced UPR^{mt} is not suppressed by the induction of autophagy, this may not be a general effect. Almost half of the genes that suppress *spg-7(ad2249)*-induced UPR^{mt} are assigned to the GO categories ‘Ribosome Biogenesis’ or ‘Translation’ and we speculate that at least some of them are false positive candidates since the knock-down of these genes likely interferes with GFP synthesis by compromising cytosolic translation. Furthermore, inactivation of the remaining genes may suppress *spg-7(ad2249)*-induced UPR^{mt} by other means than the induction of autophagy. The fact that UPR^{mt} induced by a block in mitochondrial dynamics but not by the loss of SPG-7 is suppressed by increased autophagic flux also indicates that different mitochondrial stressors

may activate UPR^{mt} in a dissimilar manner. The reason for this could, for example, be that SPG-7 is an intramitochondrial protein while FZO-1 and DRP-1 are not. Hence, the loss of SPG-7 largely leads to defects within mitochondria whereas the loss of FZO-1 or DRP-1 specifically affects mitochondrial morphology. Noteworthy, the two components of the mitochondrial *m*-AAA protease complex, SPG-7 and PPGN-1, have recently also been associated with mitochondrial dynamics. More precisely, they have been proposed to inhibit mitochondrial fusion through negatively regulating EAT-3 levels (Chaudhari and Kipreos, 2017). However, *spg-7* single mutants only display minor changes in mitochondrial morphology while more prominent changes are visible in *spg-7; ppgn-1* double mutants (Chaudhari and Kipreos, 2017).

Lipid profiling revealed that a block in mitochondrial fusion leads to changes in the levels of specific triacylglycerols (TGs). Interestingly, a block in mitochondrial fission results in similar changes albeit playing an opposing role with regard to mitochondrial morphology. The changes observed in response to the loss of SPG-7 are very distinct, indicating that different mitochondrial stressors can affect the lipidome in a diverse manner. TGs are the major component of lipid droplets and mitochondria associated with lipid droplets have been shown to play an important role in TG synthesis through delivering building blocks and energy (Benador et al., 2018). We therefore speculate that similar changes in the levels of specific TGs observed in *fzo-1(tm1133)* and *drp-1(tm1108)* are due to alterations in contact sites between lipid droplets and mitochondria. In line with this, mitochondrial fusion has previously been reported to be critical for the distribution of fatty acids across the mitochondrial network since the loss of OPA1 or Mfn1 greatly affects the transfer of fatty acids from lipid droplets to mitochondria in mouse embryonic fibroblasts (Rambold et al., 2015). Moreover, lipid droplet-associated mitochondria were found to possess high levels of Mfn2 in brown adipose tissue of mice (Benador et al., 2018).

Importantly, certain changes in the levels of specific TGs observed in *fzo-1(tm1133)* mutants are, to some extent, reverted by increased autophagic flux and our results indicate that autophagy facilitates the degradation of most TGs. This is in accordance with a study showing that autophagy mediates the breakdown of TGs from lipid droplets for fatty acid supply, which is also referred to as ‘lipophagy’ (Singh et al., 2009). Since mitochondria can use these free fatty acids released from TGs for energy production via β-oxidation, this suggests that increased autophagic flux in mutants with defects in mitochondrial dynamics leads to elevated metabolic activity, increased mitochondrial membrane potential and, thereby, consequently to attenuation

of UPR^{mt}. Interestingly, autophagy has recently also been shown to cause degradation of NCoR1, a repressor of the major lipid metabolism regulator PPARα, in order to upregulate the expression of enzymes involved in β-oxidation (Saito et al., 2019). Unfortunately, it is to date not possible to specifically block lipophagy in *C. elegans* due to the lack of understanding of how lipid droplets are recognized and sequestered by autophagic membranes. Apart from lipophagy, cytosolic lipolysis is another process that is involved in the breakdown of TGs. In mammals, it is executed by the action of the cytoplasmic lipases ATGL, HSL and MGL (reviewed in Zechner, 2015). To underpin that it is specifically the degradation of TGs that suppresses UPR^{mt}, it would be interesting to test whether the activation of cytosolic lipolysis in *fzo-1(tm1133)* or *drp-1(tm1108)* animals results in UPR^{mt} suppression as well. Noteworthy, it has lately been shown that overexpression of ATGL-1, the nematode ortholog of ATGL, increases basal and maximum oxygen consumption rate, arguing for enhanced mitochondrial metabolic activity (Zaarur et al., 2019). However, recent evidence indicates that cytosolic lipolysis and lipophagy are not distinct lipolytic processes but rather functionally linked and coordinated through commonly shared proteins since, for example, ATGL has been shown to be required and sufficient for induction of both lipophagy and autophagy in mice (Martinez-Lopez et al., 2016; Sathyanarayan et al., 2017). Another way to corroborate our model could be to look at lipid droplets. Specifically, it is worth assessing whether lipid droplets are enriched and/or enlarged in mutants with defects in mitochondrial dynamics. Yet, since the total amount of TGs is not altered in *fzo-1(tm1133)* animals and only slightly increased in *drp-1(tm1108)* mutants, this may not be the case. Nevertheless, it could be tested if increased autophagic flux in these animals may lead to reduction in the abundance and/or size of lipid droplets. In *C. elegans*, lipid droplets can, for example, be visualized using DGAT-2::GFP, PLIN1::GFP or ATGL-1::GFP (Liu et al., 2014b; reviewed in Mak, 2013). Because the knock-down of candidate genes especially increases autophagic flux in the intestine, the analysis of lipid droplets should be performed in this tissue. The fact that *spg-7(ad2249)* mutants display a reduced number of total TGs may imply that lipid droplets in these animals are less abundant and/or smaller. Moreover, this indicates that autophagy is potentially not able to access enough TGs from degradation of lipid droplets in order to properly fuel mitochondrial metabolism and, hence, suppress UPR^{mt}. Thus, it could be tested if *spg-7(ad2249)*-induced UPR^{mt} may be suppressed through increased autophagic flux when animals are fed a high fat diet.

Future experiments will reveal whether the attenuation of UPR^{mt} upon induction of autophagy is specific to a block in mitochondrial dynamics or whether further UPR^{mt}s can be suppressed

in a similar manner. Moreover, it remains to be determined whether autophagy may generally suppress all UPR^{mt}s that are associated with a certain threshold of total TGs.

4.4 Functional interactions between UPR^{mt} and autophagy

The question of whether and how different stress response pathways influence each other has become the focus of recent attention in the field of cell biology. A first hint that the induction of autophagy may affect UPR^{mt} in *C. elegans* was the discovery that the loss of *rheb-1*, a positive regulator of *let-363* (Honjoh et al., 2008), suppresses the induction of P$_{hsp-60}$*gfp* (Haynes et al., 2007). Moreover, the knock-down of *let-363* itself has previously been reported to be able to suppress the expression of P$_{hsp-60}$*gfp* in *clk-1(qm30)* mutants (Baker et al., 2012). Whether UPR^{mt} is induced in response to compromised mitophagy remains controversial since one study showed that UPR^{mt} is upregulated in animals lacking *pdr-1* or *pink-1* function (Cooper et al., 2017) whereas two other studies did not observe any effect on P$_{hsp-6}$*gfp* expression (Kim and Sieburth, 2018; Rolland et al., 2019). Our data presented in chapter II provide evidence that blocking autophagy in the absence of mitochondrial stress leads to activation of UPR^{mt}. This could be explained by the fact that the loss of autophagy is known to largely impact metabolism since it provides the cell, and especially mitochondria, with building blocks for energy production (reviewed in Kim and Lee, 2014; Rabinowitz and White, 2010). Because the activation of UPR^{mt} is accompanied by a metabolic shift towards glycolysis (reviewed in Lin and Haynes, 2016), UPR^{mt} may therefore compensate for decreased OXPHOS activity. Hence, mutants with a block in mitochondrial fusion, in which UPR^{mt} is already active, are less dependent on mitochondrial energy production, which potentially explains why UPR^{mt} is not further increased upon a block of autophagy in these animals. Further analysis in different mutants should be performed in order to substantiate this hypothesis.

It has previously been shown that RNAi against *spg-7* upregulates both UPR^{mt} and autophagy (Guo et al., 2014), which we confirm in *spg-7(ad2249)* mutants and also observe in *fzo-1(tm1133)* animals. Interestingly, our results show that the induction of autophagy in animals with a block in mitochondrial fusion is not dependent on ATFS-1, which is in conflict with the study of Guo et al. since they propose that, upon mitochondrial stress, the upregulation of both UPR^{mt} and autophagy is mediated via ATFS-1 (Guo et al., 2014). Moreover, it has been reported that ATFS-1 upregulates the expression of a small subset of autophagy related genes in response to *spg-7(RNAi)* (Nargund et al., 2012). Thus, some mitochondrial stresses may

activate both UPR^{mt} and autophagy via ATFS-1 while others may activate autophagy in an ATFS-1-independent manner. However, we additionally show that *atfs-1(et15*gf*)* does not affect autophagy in an otherwise wild-type background, indicating that nuclear import of ATFS-1 in the absence of mitochondrial stress does not suffice to induce autophagy. Since *fzo-1(tm1133)*; *atfs-1(et15*gf*)* double mutants are not viable, this suggests that an excessive level of UPR^{mt} in animals suffering of mitochondrial stress is detrimental to organismal health. The reason for this could be that a minimum amount of ATFS-1 inside mitochondria is necessary to maintain cellular homeostasis, which may be due to ATFS-1's role in limiting expression of mtDNA-encoded mRNAs in order to coordinate nuclear and mitochondrial genome-encoded OXPHOS components (Nargund et al., 2015).

Taken together, altering autophagy can affect UPR^{mt}, but changes in UPR^{mt} do not influence autophagy in our experiments. Moreover, our results indicate that autophagy and UPR^{mt} do not interact directly but rather influence each other via changes in lipid metabolism. It would be interesting to test if the induction of autophagy can also affect other organellar or cellular stress response pathways and, if so, if this is mediated by changes in metabolism as well. Another open question that remains to be answered is the role of mitophagy in *C. elegans*. Specifically, the recent understanding of how UPR^{mt} is regulated via changes in mitochondrial membrane potential (Rolland et al., 2019) raises the question whether, upon reduction of mitochondrial membrane potential, UPR^{mt} and mitophagy are activated in a simultaneous or sequential manner. One idea that has been postulated is that UPR^{mt} is activated first while mitophagy is only triggered if mitochondrial stress persists for a certain period of time (Pellegrino et al., 2013). However, whether this is true in *C. elegans* and whether this is regulated via distinct thresholds of mitochondrial membrane potential remains to be determined.

4.5 Identification of an autophagy network

We first hypothesized that increased autophagic flux may suppress UPR^{mt} when we knocked-down ESCRT components in *fzo-1(tm1133)* animals. Interestingly, ESCRT has been shown to be required for autophagy in mammalian cells whereas compromising ESCRT function in *C. elegans* induces autophagy (see 1.4). One possible explanation for this phenomenon could be that, in mammalian cells, most of the autophagosomes fuse with endosomes (thereby forming amphisomes) prior to fusion with lysosomes, whereas, in *C. elegans*, most of the autophagosomes may directly fuse with lysosomes. Future investigations should be performed

in order to unravel why exactly the loss of ESCRT affects autophagy in opposing ways in different organisms. Furthermore, ESCRT depletion in *C. elegans* may induce autophagy not necessarily due to the presence of enlarged endosomes (Djeddi et al., 2012) but impaired degradation of endosomal cargo may potentially mimic nutrient starvation and thereby induce autophagy.

Including the ESCRT components, we, in total, identified 143 genes that induce autophagy when inactivated. Among these are several other genes that are involved in cellular trafficking, one of them being *imb-2*, a regulator of the nuclear transport of DAF-16 (Putker et al., 2013), whose mammalian homolog FOXO has previously been shown to be involved in the regulation of autophagy (Zhao et al., 2010). In addition, we found the DAF-16 target gene *ins-7*, which is one of around 40 insulin-like genes in *C. elegans* and an agonist of the insulin/IGF-1-like signaling (IIS) receptor *daf-2* (Kawano et al., 2000; Meléndez et al., 2003; Murphy et al., 2003; Pierce et al., 2001; Zheng et al., 2014). Moreover, we identified several genes with a role in transcription, for example *rpac-19* and *rpac-40*. Both encode for subunits of RNA polymerase I and the inhibition of RNA polymerase I transcription in mammalian cells has already been demonstrated to result in the induction of autophagy (Katagiri et al., 2015). Among the genes that are classified into the GO category 'Cell Signaling', we found *ruvb-1*, a component of the TOR pathway in *C. elegans* (Sheaffer et al., 2008). Furthermore, we identified a number of genes that encode for proteins that are involved in the ubiquitin-proteasome system (UPS), namely *rpt-3*, *rpn-13*, *ufd-1*, *rbx-1* and *cul-1* (Mouysset et al., 2006; Takahashi et al., 2002; Yang et al., 2013). In line with this observation, it has recently been shown that compromising proteasomal function leads to induction of autophagy (Demishtein et al., 2017; Keith et al., 2016). Interestingly, it was also found that the inhibition of mTOR in mammalian cells not only activates autophagy but stimulates the ubiquitination and proteasomal degradation of long-lived proteins, however, this was shown to be independent of the autophagic machinery (Zhao et al., 2015). More than 30% of all genes found to induce autophagy when inactivated belong to the GO category 'Ribosome Biogenesis' or 'Translation' and are involved in the global regulation of protein biosynthesis. Thus, impairing translation potentially mimics nutrient starvation and thereby activates autophagy. Interestingly, attenuation of translation has previously been shown to be beneficial for mitochondrial function during stress conditions and it has been proposed that this is due to the reduced protein load into mitochondria (Baker et al., 2012; Wang et al., 2008). Based on our results, we propose that this effect may, at least to some extent, also be due to increased autophagic flux.

Taken together, we found a multitude of genes that are involved in many different cellular processes and that share one common feature, i.e., the induction of autophagy upon inactivation. Our work not only highlights the importance of autophagy in maintaining cellular homeostasis, it also reemphasizes the need for studies into this process in the context of animal health and disease.

4.6 Conclusions

Data presented in the first chapter provide evidence that the loss of *LRPPRC* function leads to an imbalance between mitochondria- and nuclear-encoded subunits of complex IV and triggers UPR^{mt}. Moreover, this response is conserved since inactivation of the *LRPPRC*-like gene *mma-1* in *C. elegans* leads to UPR^{mt} activation, too. In addition, our results show that UPR^{mt} and mitochondrial hyperfusion induced by depletion of LRPPRC are transient responses and follow similar kinetics. Whether UPR^{mt} is also induced in cells derived from French Canadian Leigh Syndrome patients remains to be answered.

Data presented in the second chapter show that the induction of autophagy suppresses UPR^{mt} induced by a block in mitochondrial dynamics by increasing mitochondrial membrane potential. Interestingly, blocking mitochondrial fusion or fission leads to an increase in the levels of certain types of TGs, which is partially reverted by the induction of autophagy. Thus, we propose that the autophagy-dependent breakdown of these TGs is used to fuel mitochondrial metabolism, resulting in increased mitochondrial membrane potential and, hence, suppression of UPR^{mt}. Future investigations will shed light on whether UPR^{mt} induced by other means may also be suppressed in a similar manner. Furthermore, studies in mammalian cell culture may reveal if this mechanism of UPR^{mt} suppression is evolutionary conserved.

5 References

Agier, V., Oliviero, P., Laine, J., L'Hermitte-Stead, C., Girard, S., Fillaut, S., Jardel, C., Bouillaud, F., Bulteau, A.L., and Lombes, A. (2012). Defective mitochondrial fusion, altered respiratory function, and distorted cristae structure in skin fibroblasts with heterozygous OPA1 mutations. Biochimica et biophysica acta *1822*, 1570-1580.

Akram, M. (2014). Citric acid cycle and role of its intermediates in metabolism. Cell Biochem Biophys *68*, 475-478.

Anand, R., Wai, T., Baker, M.J., Kladt, N., Schauss, A.C., Rugarli, E., and Langer, T. (2014). The i-AAA protease YME1L and OMA1 cleave OPA1 to balance mitochondrial fusion and fission. The Journal of cell biology *204*, 919-929.

Arun, V., Wiley, J.C., Kaur, H., Kaplan, D.R., and Guha, A. (2013). A novel neurofibromin (NF1) interaction with the leucine-rich pentatricopeptide repeat motif-containing protein links neurofibromatosis type 1 and the French Canadian variant of Leigh's syndrome in a common molecular complex. J Neurosci Res *91*, 494-505.

Autret, A., and Martin, S.J. (2010). Bcl-2 family proteins and mitochondrial fission/fusion dynamics. Cell Mol Life Sci *67*, 1599-1606.

Avery, L. (1993). The genetics of feeding in *Caenorhabditis elegans*. Genetics *133*, 897-917.

Axe, E.L., Walker, S.A., Manifava, M., Chandra, P., Roderick, H.L., Habermann, A., Griffiths, G., and Ktistakis, N.T. (2008). Autophagosome formation from membrane compartments enriched in phosphatidylinositol 3-phosphate and dynamically connected to the endoplasmic reticulum. The Journal of cell biology *182*, 685-701.

Bach, D., Pich, S., Soriano, F.X., Vega, N., Baumgartner, B., Oriola, J., Daugaard, J.R., Lloberas, J., Camps, M., Zierath, J.R.*, et al.* (2003). Mitofusin-2 determines mitochondrial network architecture and mitochondrial metabolism. A novel regulatory mechanism altered in obesity. The Journal of biological chemistry *278*, 17190-17197.

Baker, B.M., Nargund, A.M., Sun, T., and Haynes, C.M. (2012). Protective coupling of mitochondrial function and protein synthesis via the eIF2α kinase GCN-2. PLoS genetics *8*, e1002760.

Barbosa, C., Peixeiro, I., and Romao, L. (2013). Gene expression regulation by upstream open reading frames and human disease. PLoS genetics *9*, e1003529.

Benador, I.Y., Veliova, M., Mahdaviani, K., Petcherski, A., Wikstrom, J.D., Assali, E.A., Acin-Perez, R., Shum, M., Oliveira, M.F., Cinti, S.*, et al.* (2018). Mitochondria Bound to Lipid Droplets Have Unique Bioenergetics, Composition, and Dynamics that Support Lipid Droplet Expansion. Cell metabolism *27*, 869-885 e866.

Benard, G., Bellance, N., Jose, C., and Rossignol, R. (2011). Relationships Between Mitochondrial Dynamics and Bioenergetics. In Mitochondrial Dynamics and Neurodegeneration, pp. 47-68.

Benedetti, C., Haynes, C.M., Yang, Y., Harding, H.P., and Ron, D. (2006). Ubiquitin-like protein 5 positively regulates chaperone gene expression in the mitochondrial unfolded protein response. Genetics *174*, 229-239.

Berg, T.O., Fengsrud, M., Stromhaug, P.E., Berg, T., and Seglen, P.O. (1998). Isolation and characterization of rat liver amphisomes. Evidence for fusion of autophagosomes with both early and late endosomes. The Journal of biological chemistry *273*, 21883-21892.

Berry, E.A., Guergova-Kuras, M., Huang, L.S., and Crofts, A.R. (2000). Structure and function of cytochrome bc complexes. Annual review of biochemistry *69*, 1005-1075.

Billingsley, K.J., Bandres-Ciga, S., Saez-Atienzar, S., and Singleton, A.B. (2018). Genetic risk factors in Parkinson's disease. Cell and Tissue Research *373*, 9-20.

Bjorkoy, G., Lamark, T., Brech, A., Outzen, H., Perander, M., Overvatn, A., Stenmark, H., and Johansen, T. (2005). p62/SQSTM1 forms protein aggregates degraded by autophagy and has a protective effect on huntingtin-induced cell death. The Journal of cell biology *171*, 603-614.

Bleazard, W., McCaffery, J.M., King, E.J., Bale, S., Mozdy, A., Tieu, Q., Nunnari, J., and Shaw, J.M. (1999). The dynamin-related GTPase Dnm1 regulates mitochondrial fission in yeast. Nature cell biology *1*, 298-304.

Bock, F.J., and Tait, S.W.G. (2020). Mitochondria as multifaceted regulators of cell death. Nature Reviews Molecular Cell Biology *21*, 85-100.

Bogenhagen, D.F. (2012). Mitochondrial DNA nucleoid structure. Biochimica et biophysica acta *1819*, 914-920.

Bonawitz, N.D., Chatenay-Lapointe, M., Pan, Y., and Shadel, G.S. (2007). Reduced TOR signaling extends chronological life span via increased respiration and upregulation of mitochondrial gene expression. Cell metabolism *5*, 265-277.

Bota, D.A., and Davies, K.J. (2002). Lon protease preferentially degrades oxidized mitochondrial aconitase by an ATP-stimulated mechanism. Nature cell biology *4*, 674-680.

Braymer, J.J., and Lill, R. (2017). Iron-sulfur cluster biogenesis and trafficking in mitochondria. The Journal of biological chemistry *292*, 12754-12763.

Breckenridge, D.G., Kang, B.H., Kokel, D., Mitani, S., Staehelin, L.A., and Xue, D. (2008). *Caenorhabditis elegans drp-1* and *fis-2* regulate distinct cell-death execution pathways downstream of *ced-3* and independent of *ced-9*. Molecular cell *31*, 586-597.

Breda, C.N.d.S., Davanzo, G.G., Basso, P.J., Saraiva Câmara, N.O., and Moraes-Vieira, P.M.M. (2019). Mitochondria as central hub of the immune system. Redox biology *26*, 101255.

Burelle, Y., Bemeur, C., Rivard, M.E., Thompson Legault, J., Boucher, G., Consortium, L., Morin, C., Coderre, L., and Des Rosiers, C. (2015). Mitochondrial vulnerability and

increased susceptibility to nutrient-induced cytotoxicity in fibroblasts from leigh syndrome French canadian patients. PloS one *10*, e0120767.

Byrne, J.J., Soh, M.S., Chandhok, G., Vijayaraghavan, T., Teoh, J.S., Crawford, S., Cobham, A.E., Yapa, N.M.B., Mirth, C.K., and Neumann, B. (2019). Disruption of mitochondrial dynamics affects behaviour and lifespan in *Caenorhabditis elegans*. Cell Mol Life Sci *76*, 1967-1985.

Calhoun, M.W., Thomas, J.W., and Gennis, R.B. (1994). The cytochrome oxidase superfamily of redox-driven proton pumps. Trends in biochemical sciences *19*, 325-330.

Carlton, J.G., and Martin-Serrano, J. (2007). Parallels between cytokinesis and retroviral budding: a role for the ESCRT machinery. Science (New York, NY) *316*, 1908-1912.

Cecchini, G. (2003). Function and structure of complex II of the respiratory chain. Annual review of biochemistry *72*, 77-109.

Chacinska, A., Koehler, C.M., Milenkovic, D., Lithgow, T., and Pfanner, N. (2009). Importing mitochondrial proteins: machineries and mechanisms. Cell *138*, 628-644.

Chakravorty, A., Jetto, C.T., and Manjithaya, R. (2019). Dysfunctional Mitochondria and Mitophagy as Drivers of Alzheimer's Disease Pathogenesis. Front Aging Neurosci *11*, 311.

Chan, D.C. (2012). Fusion and fission: interlinked processes critical for mitochondrial health. Annu Rev Genet *46*, 265-287.

Chaudhari, S.N., and Kipreos, E.T. (2017). Increased mitochondrial fusion allows the survival of older animals in diverse *C. elegans* longevity pathways. Nature communications *8*, 182.

Chen, H., Chomyn, A., and Chan, D.C. (2005). Disruption of fusion results in mitochondrial heterogeneity and dysfunction. The Journal of biological chemistry *280*, 26185-26192.

Chen, H., Detmer, S.A., Ewald, A.J., Griffin, E.E., Fraser, S.E., and Chan, D.C. (2003). Mitofusins Mfn1 and Mfn2 coordinately regulate mitochondrial fusion and are essential for embryonic development. The Journal of cell biology *160*, 189-200.

Chen, Y., Scarcelli, V., and Legouis, R. (2017). Approaches for Studying Autophagy in *Caenorhabditis elegans*. Cells *6*.

Cheng, M.Y., Hartl, F.U., Martin, J., Pollock, R.A., Kalousek, F., Neupert, W., Hallberg, E.M., Hallberg, R.L., and Horwich, A.L. (1989). Mitochondrial heat-shock protein hsp60 is essential for assembly of proteins imported into yeast mitochondria. Nature *337*, 620-625.

Choi, A.M., Ryter, S.W., and Levine, B. (2013). Autophagy in human health and disease. N Engl J Med *368*, 651-662.

Chujo, T., Ohira, T., Sakaguchi, Y., Goshima, N., Nomura, N., Nagao, A., and Suzuki, T. (2012). LRPPRC/SLIRP suppresses PNPase-mediated mRNA decay and promotes polyadenylation in human mitochondria. Nucleic Acids Res *40*, 8033-8047.

Chung, H.K., Ryu, D., Kim, K.S., Chang, J.Y., Kim, Y.K., Yi, H.S., Kang, S.G., Choi, M.J., Lee, S.E., Jung, S.B.*, et al.* (2017). Growth differentiation factor 15 is a myomitokine governing systemic energy homeostasis. The Journal of cell biology *216*, 149-165.

Chung, K.P., Hsu, C.L., Fan, L.C., Huang, Z., Bhatia, D., Chen, Y.J., Hisata, S., Cho, S.J., Nakahira, K., Imamura, M.*, et al.* (2019). Mitofusins regulate lipid metabolism to mediate the development of lung fibrosis. Nature communications *10*, 3390.

Cooper, J.F., Machiela, E., Dues, D.J., Spielbauer, K.K., Senchuk, M.M., and Van Raamsdonk, J.M. (2017). Activation of the mitochondrial unfolded protein response promotes longevity and dopamine neuron survival in Parkinson's disease models. Scientific Reports *7*, 16441.

Cooper, M.P., Qu, L., Rohas, L.M., Lin, J., Yang, W., Erdjument-Bromage, H., Tempst, P., and Spiegelman, B.M. (2006). Defects in energy homeostasis in Leigh syndrome French Canadian variant through PGC-1alpha/LRP130 complex. Genes Dev *20*, 2996-3009.

Cuervo, A.M., and Wong, E. (2014). Chaperone-mediated autophagy: roles in disease and aging. Cell Res *24*, 92-104.

Cummins, N., Tweedie, A., Zuryn, S., Bertran-Gonzalez, J., and Gotz, J. (2019). Disease-associated tau impairs mitophagy by inhibiting Parkin translocation to mitochondria. The EMBO journal *38*.

D'Silva, P.D., Schilke, B., Walter, W., Andrew, A., and Craig, E.A. (2003). J protein cochaperone of the mitochondrial inner membrane required for protein import into the mitochondrial matrix. Proceedings of the National Academy of Sciences of the United States of America *100*, 13839-13844.

De Duve, C., and Wattiaux, R. (1966). Functions of lysosomes. Annu Rev Physiol *28*, 435-492.

Demishtein, A., Fraiberg, M., Berko, D., Tirosh, B., Elazar, Z., and Navon, A. (2017). SQSTM1/p62-mediated autophagy compensates for loss of proteasome polyubiquitin recruiting capacity. Autophagy *13*, 1697-1708.

Desautels, M., and Goldberg, A.L. (1982). Liver mitochondria contain an ATP-dependent, vanadate-sensitive pathway for the degradation of proteins. Proceedings of the National Academy of Sciences of the United States of America *79*, 1869-1873.

Dever, T.E. (2002). Gene-specific regulation by general translation factors. Cell *108*, 545-556.

Dice, J.F. (1990). Peptide sequences that target cytosolic proteins for lysosomal proteolysis. Trends in biochemical sciences *15*, 305-309.

Ding, W.X., Ni, H.M., Li, M., Liao, Y., Chen, X., Stolz, D.B., Dorn, G.W., 2nd, and Yin, X.M. (2010). Nix is critical to two distinct phases of mitophagy, reactive oxygen species-

mediated autophagy induction and Parkin-ubiquitin-p62-mediated mitochondrial priming. The Journal of biological chemistry *285*, 27879-27890.

Djeddi, A., Michelet, X., Culetto, E., Alberti, A., Barois, N., and Legouis, R. (2012). Induction of autophagy in ESCRT mutants is an adaptive response for cell survival in *C. elegans*. Journal of cell science *125*, 685-694.

Durieux, J., Wolff, S., and Dillin, A. (2011). The cell-non-autonomous nature of electron transport chain-mediated longevity. Cell *144*, 79-91.

Egan, D.F., Shackelford, D.B., Mihaylova, M.M., Gelino, S., Kohnz, R.A., Mair, W., Vasquez, D.S., Joshi, A., Gwinn, D.M., Taylor, R.*, et al.* (2011). Phosphorylation of ULK1 (hATG1) by AMP-activated protein kinase connects energy sensing to mitophagy. Science (New York, NY) *331*, 456-461.

Fang, E.F., Hou, Y., Palikaras, K., Adriaanse, B.A., Kerr, J.S., Yang, B., Lautrup, S., Hasan-Olive, M.M., Caponio, D., Dan, X.*, et al.* (2019). Mitophagy inhibits amyloid-β and tau pathology and reverses cognitive deficits in models of Alzheimer's disease. Nat Neurosci *22*, 401-412.

Feng, Y., He, D., Yao, Z., and Klionsky, D.J. (2014). The machinery of macroautophagy. Cell Res *24*, 24-41.

Filimonenko, M., Stuffers, S., Raiborg, C., Yamamoto, A., Malerod, L., Fisher, E.M., Isaacs, A., Brech, A., Stenmark, H., and Simonsen, A. (2007). Functional multivesicular bodies are required for autophagic clearance of protein aggregates associated with neurodegenerative disease. The Journal of cell biology *179*, 485-500.

Fiorese, C.J., Schulz, A.M., Lin, Y.F., Rosin, N., Pellegrino, M.W., and Haynes, C.M. (2016). The Transcription Factor ATF5 Mediates a Mammalian Mitochondrial UPR. Curr Biol *26*, 2037-2043.

Fire, A., Xu, S., Montgomery, M.K., Kostas, S.A., Driver, S.E., and Mello, C.C. (1998). Potent and specific genetic interference by double-stranded RNA in *Caenorhabditis elegans*. Nature *391*, 806-811.

Frank, S., Gaume, B., Bergmann-Leitner, E.S., Leitner, W.W., Robert, E.G., Catez, F., Smith, C.L., and Youle, R.J. (2001). The role of dynamin-related protein 1, a mediator of mitochondrial fission, in apoptosis. Developmental cell *1*, 515-525.

Frezza, C., Cipolat, S., Martins de Brito, O., Micaroni, M., Beznoussenko, G.V., Rudka, T., Bartoli, D., Polishuck, R.S., Danial, N.N., De Strooper, B.*, et al.* (2006). OPA1 controls apoptotic cristae remodeling independently from mitochondrial fusion. Cell *126*, 177-189.

Friedman, J.R., Lackner, L.L., West, M., DiBenedetto, J.R., Nunnari, J., and Voeltz, G.K. (2011). ER Tubules Mark Sites of Mitochondrial Division. Science (New York, NY) *334*, 358-362.

Friedman, J.R., and Nunnari, J. (2014). Mitochondrial form and function. Nature *505*, 335-343.

Fusakio, M.E., Willy, J.A., Wang, Y., Mirek, E.T., Al Baghdadi, R.J., Adams, C.M., Anthony, T.G., and Wek, R.C. (2016). Transcription factor ATF4 directs basal and stress-induced gene expression in the unfolded protein response and cholesterol metabolism in the liver. Mol Biol Cell *27*, 1536-1551.

Galluzzi, L., Baehrecke, E.H., Ballabio, A., Boya, P., Bravo-San Pedro, J.M., Cecconi, F., Choi, A.M., Chu, C.T., Codogno, P., Colombo, M.I.*, et al.* (2017). Molecular definitions of autophagy and related processes. The EMBO journal *36*, 1811-1836.

Gandre-Babbe, S., and van der Bliek, A.M. (2008). The novel tail-anchored membrane protein Mff controls mitochondrial and peroxisomal fission in mammalian cells. Mol Biol Cell *19*, 2402-2412.

Gao, K., Li, Y., Hu, S., and Liu, Y. (2019). SUMO peptidase ULP-4 regulates mitochondrial UPR-mediated innate immunity and lifespan extension. Elife *8*.

Gatta, A.T., and Carlton, J.G. (2019). The ESCRT-machinery: closing holes and expanding roles. Current opinion in cell biology *59*, 121-132.

Gaume, B., Klaus, C., Ungermann, C., Guiard, B., Neupert, W., and Brunner, M. (1998). Unfolding of preproteins upon import into mitochondria. The EMBO journal *17*, 6497-6507.

Gaweda-Walerych, K., Mohagheghi, F., Zekanowski, C., and Buratti, E. (2016). Parkinson's disease-related gene variants influence pre-mRNA splicing processes. Neurobiol Aging *47*, 127-138.

Gelino, S., Chang, J.T., Kumsta, C., She, X., Davis, A., Nguyen, C., Panowski, S., and Hansen, M. (2016). Intestinal Autophagy Improves Healthspan and Longevity in *C. elegans* during Dietary Restriction. PLoS genetics *12*, e1006135.

Giorgi, C., Marchi, S., and Pinton, P. (2018). The machineries, regulation and cellular functions of mitochondrial calcium. Nature Reviews Molecular Cell Biology *19*, 713-730.

Gomes, L.C., Di Benedetto, G., and Scorrano, L. (2011). During autophagy mitochondria elongate, are spared from degradation and sustain cell viability. Nature cell biology *13*, 589-598.

Gordon, P.B., and Seglen, P.O. (1988). Prelysosomal convergence of autophagic and endocytic pathways. Biochem Biophys Res Commun *151*, 40-47.

Griparic, L., Kanazawa, T., and van der Bliek, A.M. (2007). Regulation of the mitochondrial dynamin-like protein Opa1 by proteolytic cleavage. The Journal of cell biology *178*, 757-764.

Guillery, O., Malka, F., Frachon, P., Milea, D., Rojo, M., and Lombes, A. (2008). Modulation of mitochondrial morphology by bioenergetics defects in primary human fibroblasts. Neuromuscul Disord *18*, 319-330.

Guo, B., Huang, X., Zhang, P., Qi, L., Liang, Q., Zhang, X., Huang, J., Fang, B., Hou, W., Han, J.*, et al.* (2014). Genome-wide screen identifies signaling pathways that regulate autophagy during *Caenorhabditis elegans* development. EMBO reports *15*, 705-713.

Guo, X., Disatnik, M.-H., Monbureau, M., Shamloo, M., Mochly-Rosen, D., and Qi, X. (2013). Inhibition of mitochondrial fragmentation diminishes Huntington's disease–associated neurodegeneration. The Journal of clinical investigation *123*, 5371-5388.

Gwinn, D.M., Shackelford, D.B., Egan, D.F., Mihaylova, M.M., Mery, A., Vasquez, D.S., Turk, B.E., and Shaw, R.J. (2008). AMPK phosphorylation of raptor mediates a metabolic checkpoint. Molecular cell *30*, 214-226.

Hales, K.G., and Fuller, M.T. (1997). Developmentally regulated mitochondrial fusion mediated by a conserved, novel, predicted GTPase. Cell *90*, 121-129.

Hammerling, B.C., Najor, R.H., Cortez, M.Q., Shires, S.E., Leon, L.J., Gonzalez, E.R., Boassa, D., Phan, S., Thor, A., Jimenez, R.E.*, et al.* (2017). A Rab5 endosomal pathway mediates Parkin-dependent mitochondrial clearance. Nature communications *8*, 14050.

Hansen, M., Rubinsztein, D.C., and Walker, D.W. (2018). Autophagy as a promoter of longevity: insights from model organisms. Nature reviews Molecular cell biology *19*, 579-593.

Hara, T., Nakamura, K., Matsui, M., Yamamoto, A., Nakahara, Y., Suzuki-Migishima, R., Yokoyama, M., Mishima, K., Saito, I., Okano, H.*, et al.* (2006). Suppression of basal autophagy in neural cells causes neurodegenerative disease in mice. Nature *441*, 885-889.

Harding, T.M., Morano, K.A., Scott, S.V., and Klionsky, D.J. (1995). Isolation and characterization of yeast mutants in the cytoplasm to vacuole protein targeting pathway. The Journal of cell biology *131*, 591-602.

Hartl, F.U., Pfanner, N., Nicholson, D.W., and Neupert, W. (1989). Mitochondrial protein import. Biochimica et biophysica acta *988*, 1-45.

Hatch, A.L., Gurel, P.S., and Higgs, H.N. (2014). Novel roles for actin in mitochondrial fission. Journal of cell science *127*, 4549-4560.

Hayashi-Nishino, M., Fujita, N., Noda, T., Yamaguchi, A., Yoshimori, T., and Yamamoto, A. (2009). A subdomain of the endoplasmic reticulum forms a cradle for autophagosome formation. Nature cell biology *11*, 1433-1437.

Haynes, C.M., Petrova, K., Benedetti, C., Yang, Y., and Ron, D. (2007). ClpP mediates activation of a mitochondrial unfolded protein response in *C. elegans*. Developmental cell *13*, 467-480.

Haynes, C.M., Yang, Y., Blais, S.P., Neubert, T.A., and Ron, D. (2010). The matrix peptide exporter HAF-1 signals a mitochondrial UPR by activating the transcription factor ZC376.7 in *C. elegans*. Molecular cell *37*, 529-540.

Herlan, M., Vogel, F., Bornhovd, C., Neupert, W., and Reichert, A.S. (2003). Processing of Mgm1 by the rhomboid-type protease Pcp1 is required for maintenance of mitochondrial morphology and of mitochondrial DNA. The Journal of biological chemistry *278*, 27781-27788.

Hermann, G.J., Thatcher, J.W., Mills, J.P., Hales, K.G., Fuller, M.T., Nunnari, J., and Shaw, J.M. (1998). Mitochondrial fusion in yeast requires the transmembrane GTPase Fzo1p. The Journal of cell biology *143*, 359-373.

Hinnebusch, A.G., Ivanov, I.P., and Sonenberg, N. (2016). Translational control by 5'-untranslated regions of eukaryotic mRNAs. Science (New York, NY) *352*, 1413-1416.

Hirst, J. (2005). Energy transduction by respiratory complex I--an evaluation of current knowledge. Biochem Soc Trans *33*, 525-529.

Hodgkin, J., and Doniach, T. (1997). Natural variation and copulatory plug formation in *Caenorhabditis elegans*. Genetics *146*, 149-164.

Hodgkin, J., Horvitz, H.R., and Brenner, S. (1979). Nondisjunction Mutants of the Nematode *CAENORHABDITIS ELEGANS*. Genetics *91*, 67-94.

Honjoh, S., Yamamoto, T., Uno, M., and Nishida, E. (2008). Signalling through RHEB-1 mediates intermittent fasting-induced longevity in *C. elegans*. Nature *457*, 726.

Hoppins, S., Lackner, L., and Nunnari, J. (2007). The machines that divide and fuse mitochondria. Annual review of biochemistry *76*, 751-780.

Horibe, T., and Hoogenraad, N.J. (2007). The chop gene contains an element for the positive regulation of the mitochondrial unfolded protein response. PloS one *2*, e835.

Houten, S.M., Violante, S., Ventura, F.V., and Wanders, R.J. (2016). The Biochemistry and Physiology of Mitochondrial Fatty Acid β-Oxidation and Its Genetic Disorders. Annu Rev Physiol *78*, 23-44.

Houtkooper, R.H., Mouchiroud, L., Ryu, D., Moullan, N., Katsyuba, E., Knott, G., Williams, R.W., and Auwerx, J. (2013). Mitonuclear protein imbalance as a conserved longevity mechanism. Nature *497*, 451-457.

Huang, W.P., Scott, S.V., Kim, J., and Klionsky, D.J. (2000). The itinerary of a vesicle component, Aut7p/Cvt5p, terminates in the yeast vacuole via the autophagy/Cvt pathways. The Journal of biological chemistry *275*, 5845-5851.

Ichimura, Y., Kirisako, T., Takao, T., Satomi, Y., Shimonishi, Y., Ishihara, N., Mizushima, N., Tanida, I., Kominami, E., Ohsumi, M.*, et al.* (2000). A ubiquitin-like system mediates protein lipidation. Nature *408*, 488-492.

Ichishita, R., Tanaka, K., Sugiura, Y., Sayano, T., Mihara, K., and Oka, T. (2008). An RNAi Screen for Mitochondrial Proteins Required to Maintain the Morphology of the Organelle in *Caenorhabditis elegans*. The Journal of Biochemistry *143*, 449-454.

Inoki, K., Li, Y., Zhu, T., Wu, J., and Guan, K.L. (2002). TSC2 is phosphorylated and inhibited by Akt and suppresses mTOR signalling. Nature cell biology *4*, 648-657.

Ishihara, N., Eura, Y., and Mihara, K. (2004). Mitofusin 1 and 2 play distinct roles in mitochondrial fusion reactions via GTPase activity. Journal of cell science *117*, 6535-6546.

Issman-Zecharya, N., and Schuldiner, O. (2014). The PI3K class III complex promotes axon pruning by downregulating a Ptc-derived signal via endosome-lysosomal degradation. Developmental cell *31*, 461-473.

Jagasia, R., Grote, P., Westermann, B., and Conradt, B. (2005). DRP-1-mediated mitochondrial fragmentation during EGL-1-induced cell death in *C. elegans*. Nature *433*, 754-760.

Jiang, X., Li, X., Huang, H., Jiang, F., Lin, Z., He, H., Chen, Y., Yue, F., Zou, J., He, Y.*, et al.* (2014). Elevated levels of mitochondrion-associated autophagy inhibitor LRPPRC are associated with poor prognosis in patients with prostate cancer. Cancer *120*, 1228-1236.

Jimenez, A.J., Maiuri, P., Lafaurie-Janvore, J., Divoux, S., Piel, M., and Perez, F. (2014). ESCRT machinery is required for plasma membrane repair. Science (New York, NY) *343*, 1247136.

Jin, S.M., Lazarou, M., Wang, C., Kane, L.A., Narendra, D.P., and Youle, R.J. (2010). Mitochondrial membrane potential regulates PINK1 import and proteolytic destabilization by PARL. The Journal of cell biology *191*, 933-942.

Johansen, T., and Lamark, T. (2011). Selective autophagy mediated by autophagic adapter proteins. Autophagy *7*, 279-296.

Jousse, C., Bruhat, A., Carraro, V., Urano, F., Ferrara, M., Ron, D., and Fafournoux, P. (2001). Inhibition of CHOP translation by a peptide encoded by an open reading frame localized in the chop 5'UTR. Nucleic Acids Res *29*, 4341-4351.

Jovaisaite, V., Mouchiroud, L., and Auwerx, J. (2014). The mitochondrial unfolded protein response, a conserved stress response pathway with implications in health and disease. J Exp Biol *217*, 137-143.

Junge, W., and Nelson, N. (2015). ATP synthase. Annual review of biochemistry *84*, 631-657.

Kanazawa, T., Zappaterra, M.D., Hasegawa, A., Wright, A.P., Newman-Smith, E.D., Buttle, K.F., McDonald, K., Mannella, C.A., and van der Bliek, A.M. (2008). The *C. elegans* Opa1 Homologue EAT-3 Is Essential for Resistance to Free Radicals. PLoS genetics *4*, e1000022.

Kane, L.A., Lazarou, M., Fogel, A.I., Li, Y., Yamano, K., Sarraf, S.A., Banerjee, S., and Youle, R.J. (2014). PINK1 phosphorylates ubiquitin to activate Parkin E3 ubiquitin ligase activity. The Journal of cell biology *205*, 143-153.

Kang, S.G., Ortega, J., Singh, S.K., Wang, N., Huang, N.N., Steven, A.C., and Maurizi, M.R. (2002). Functional proteolytic complexes of the human mitochondrial ATP-dependent protease, hClpXP. The Journal of biological chemistry *277*, 21095-21102.

Kang, S.W., Haydar, G., Taniane, C., Farrell, G., Arias, I.M., Lippincott-Schwartz, J., and Fu, D. (2016). AMPK Activation Prevents and Reverses Drug-Induced Mitochondrial and Hepatocyte Injury by Promoting Mitochondrial Fusion and Function. PloS one *11*, e0165638.

Katagiri, N., Kuroda, T., Kishimoto, H., Hayashi, Y., Kumazawa, T., and Kimura, K. (2015). The nucleolar protein nucleophosmin is essential for autophagy induced by inhibiting Pol I transcription. Scientific Reports *5*, 8903.

Katzmann, D.J., Babst, M., and Emr, S.D. (2001). Ubiquitin-Dependent Sorting into the Multivesicular Body Pathway Requires the Function of a Conserved Endosomal Protein Sorting Complex, ESCRT-I. Cell *106*, 145-155.

Kawano, T., Ito, Y., Ishiguro, M., Takuwa, K., Nakajima, T., and Kimura, Y. (2000). Molecular cloning and characterization of a new insulin/IGF-like peptide of the nematode *Caenorhabditis elegans*. Biochem Biophys Res Commun *273*, 431-436.

Keith, S.A., Maddux, S.K., Zhong, Y., Chinchankar, M.N., Ferguson, A.A., Ghazi, A., and Fisher, A.L. (2016). Graded Proteasome Dysfunction in *Caenorhabditis elegans* Activates an Adaptive Response Involving the Conserved SKN-1 and ELT-2 Transcription Factors and the Autophagy-Lysosome Pathway. PLoS genetics *12*, e1005823.

Kim, J., Kundu, M., Viollet, B., and Guan, K.L. (2011). AMPK and mTOR regulate autophagy through direct phosphorylation of Ulk1. Nature cell biology *13*, 132-141.

Kim, K.H., and Lee, M.-S. (2014). Autophagy—a key player in cellular and body metabolism. Nature Reviews Endocrinology *10*, 322.

Kim, S., and Sieburth, D. (2018). Sphingosine Kinase Activates the Mitochondrial Unfolded Protein Response and Is Targeted to Mitochondria by Stress. Cell reports *24*, 2932-2945.e2934.

Kirisako, T., Baba, M., Ishihara, N., Miyazawa, K., Ohsumi, M., Yoshimori, T., Noda, T., and Ohsumi, Y. (1999). Formation process of autophagosome is traced with Apg8/Aut7p in yeast. The Journal of cell biology *147*, 435-446.

Kirisako, T., Ichimura, Y., Okada, H., Kabeya, Y., Mizushima, N., Yoshimori, T., Ohsumi, M., Takao, T., Noda, T., and Ohsumi, Y. (2000). The reversible modification regulates the membrane-binding state of Apg8/Aut7 essential for autophagy and the cytoplasm to vacuole targeting pathway. The Journal of cell biology *151*, 263-276.

Kitada, T., Asakawa, S., Hattori, N., Matsumine, H., Yamamura, Y., Minoshima, S., Yokochi, M., Mizuno, Y., and Shimizu, N. (1998). Mutations in the parkin gene cause autosomal recessive juvenile parkinsonism. Nature *392*, 605-608.

Klionsky, D.J., Abdelmohsen, K., Abe, A., Abedin, M.J., Abeliovich, H., Acevedo Arozena, A., Adachi, H., Adams, C.M., Adams, P.D., Adeli, K.*, et al.* (2016). Guidelines for the use and interpretation of assays for monitoring autophagy (3rd edition). Autophagy *12*, 1-222.

Klionsky, D.J., Cregg, J.M., Dunn, W.A., Jr., Emr, S.D., Sakai, Y., Sandoval, I.V., Sibirny, A., Subramani, S., Thumm, M., Veenhuis, M.*, et al.* (2003). A unified nomenclature for yeast autophagy-related genes. Developmental cell *5*, 539-545.

Kondapalli, C., Kazlauskaite, A., Zhang, N., Woodroof, H.I., Campbell, D.G., Gourlay, R., Burchell, L., Walden, H., Macartney, T.J., Deak, M.*, et al.* (2012). PINK1 is activated by mitochondrial membrane potential depolarization and stimulates Parkin E3 ligase activity by phosphorylating Serine 65. Open Biol *2*, 120080.

Koopman, W.J., Visch, H.J., Verkaart, S., van den Heuvel, L.W., Smeitink, J.A., and Willems, P.H. (2005). Mitochondrial network complexity and pathological decrease in complex I activity are tightly correlated in isolated human complex I deficiency. Am J Physiol Cell Physiol *289*, C881-890.

Korobova, F., Gauvin, T.J., and Higgs, H.N. (2014). A role for myosin II in mammalian mitochondrial fission. Curr Biol *24*, 409-414.

Korobova, F., Ramabhadran, V., and Higgs, H.N. (2013). An actin-dependent step in mitochondrial fission mediated by the ER-associated formin INF2. Science (New York, NY) *339*, 464-467.

Koshiba, T., Detmer, S.A., Kaiser, J.T., Chen, H., McCaffery, J.M., and Chan, D.C. (2004). Structural basis of mitochondrial tethering by mitofusin complexes. Science (New York, NY) *305*, 858-862.

Kowaltowski, A.J., Menezes-Filho, S.L., Assali, E.A., Goncalves, I.G., Cabral-Costa, J.V., Abreu, P., Miller, N., Nolasco, P., Laurindo, F.R.M., Bruni-Cardoso, A.*, et al.* (2019). Mitochondrial morphology regulates organellar Ca^{2+} uptake and changes cellular Ca^{2+} homeostasis. FASEB J *33*, 13176-13188.

Koyano, F., Okatsu, K., Kosako, H., Tamura, Y., Go, E., Kimura, M., Kimura, Y., Tsuchiya, H., Yoshihara, H., Hirokawa, T.*, et al.* (2014). Ubiquitin is phosphorylated by PINK1 to activate parkin. Nature *510*, 162-166.

Kraus, F., and Ryan, M.T. (2017). The constriction and scission machineries involved in mitochondrial fission. Journal of cell science *130*, 2953-2960.

Kukat, C., Wurm, C.A., Spahr, H., Falkenberg, M., Larsson, N.G., and Jakobs, S. (2011). Super-resolution microscopy reveals that mammalian mitochondrial nucleoids have a uniform size and frequently contain a single copy of mtDNA. Proceedings of the National Academy of Sciences of the United States of America *108*, 13534-13539.

Kulawiak, B., Hopker, J., Gebert, M., Guiard, B., Wiedemann, N., and Gebert, N. (2013). The mitochondrial protein import machinery has multiple connections to the respiratory chain. Biochimica et biophysica acta *1827*, 612-626.

Kwak, S.H., Park, K.S., Lee, K.-U., and Lee, H.K. (2010). Mitochondrial metabolism and diabetes. J Diabetes Investig *1*, 161-169.

Labieniec-Watala, M., Siewiera, K., Gierszewski, S., and Watal, C. (2012). Mitochondria Function in Diabetes – From Health to Pathology – New Perspectives for Treatment of Diabetes-Driven Disorders. In Biomedical Science, Engineering and Technology.

Labrousse, A.M., Zappaterra, M.D., Rube, D.A., and van der Bliek, A.M. (1999). *C. elegans* Dynamin-Related Protein DRP-1 Controls Severing of the Mitochondrial Outer Membrane. Molecular cell *4*, 815-826.

Lagouge, M., Mourier, A., Lee, H.J., Spahr, H., Wai, T., Kukat, C., Silva Ramos, E., Motori, E., Busch, J.D., Siira, S.*, et al.* (2015). SLIRP Regulates the Rate of Mitochondrial Protein Synthesis and Protects LRPPRC from Degradation. PLoS genetics *11*, e1005423.

Lazarou, M., Sliter, D.A., Kane, L.A., Sarraf, S.A., Wang, C., Burman, J.L., Sideris, D.P., Fogel, A.I., and Youle, R.J. (2015). The ubiquitin kinase PINK1 recruits autophagy receptors to induce mitophagy. Nature *524*, 309-314.

Lee, J.A., Beigneux, A., Ahmad, S.T., Young, S.G., and Gao, F.B. (2007). ESCRT-III dysfunction causes autophagosome accumulation and neurodegeneration. Curr Biol *17*, 1561-1567.

Lee, J.W., Park, S., Takahashi, Y., and Wang, H.G. (2010). The association of AMPK with ULK1 regulates autophagy. PloS one *5*, e15394.

Lee, Y., Lee, H.Y., Hanna, R.A., and Gustafsson, A.B. (2011). Mitochondrial autophagy by Bnip3 involves Drp1-mediated mitochondrial fission and recruitment of Parkin in cardiac myocytes. Am J Physiol Heart Circ Physiol *301*, H1924-1931.

Lee, Y.K., and Lee, J.A. (2016). Role of the mammalian ATG8/LC3 family in autophagy: differential and compensatory roles in the spatiotemporal regulation of autophagy. BMB Rep *49*, 424-430.

Lerner, C., Bitto, A., Pulliam, D., Nacarelli, T., Konigsberg, M., Van Remmen, H., Torres, C., and Sell, C. (2013). Reduced mammalian target of rapamycin activity facilitates mitochondrial retrograde signaling and increases life span in normal human fibroblasts. Aging cell *12*, 966-977.

Levine, B., and Klionsky, D.J. (2004). Development by Self-Digestion. Developmental cell *6*, 463-477.

Li, X., Lv, L., Zheng, J., Zhou, J., Liu, B., Chen, H., Liang, C., Wang, R., Su, L., Li, X.*, et al.* (2014). The significance of LRPPRC overexpression in gastric cancer. Med Oncol *31*, 818.

Lim, Y., Rubio-Peña, K., Sobraske, P.J., Molina, P.A., Brookes, P.S., Galy, V., and Nehrke, K. (2019). *Fndc-1* contributes to paternal mitochondria elimination in *C. elegans*. Developmental Biology *454*, 15-20.

Lin, W., and Kang, U.J. (2008). Characterization of PINK1 processing, stability, and subcellular localization. J Neurochem *106*, 464-474.

Lin, Y.-F., and Haynes, C.M. (2016). Metabolism and the UPR^{mt}. Molecular cell *61*, 677-682.

Lin, Y.F., Schulz, A.M., Pellegrino, M.W., Lu, Y., Shaham, S., and Haynes, C.M. (2016). Maintenance and propagation of a deleterious mitochondrial genome by the mitochondrial unfolded protein response. Nature *533*, 416-419.

Liot, G., Bossy, B., Lubitz, S., Kushnareva, Y., Sejbuk, N., and Bossy-Wetzel, E. (2009). Complex II inhibition by 3-NP causes mitochondrial fragmentation and neuronal cell death via an NMDA- and ROS-dependent pathway. Cell death and differentiation *16*, 899-909.

Liu, L., Sakakibara, K., Chen, Q., and Okamoto, K. (2014a). Receptor-mediated mitophagy in yeast and mammalian systems. Cell Res *24*, 787-795.

Liu, Z., Li, X., Ge, Q., Ding, M., and Huang, X. (2014b). A lipid droplet-associated GFP reporter-based screen identifies new fat storage regulators in *C. elegans*. J Genet Genomics *41*, 305-313.

Loson, O.C., Song, Z., Chen, H., and Chan, D.C. (2013). Fis1, Mff, MiD49, and MiD51 mediate Drp1 recruitment in mitochondrial fission. Mol Biol Cell *24*, 659-667.

Lu, P.D., Harding, H.P., and Ron, D. (2004). Translation reinitiation at alternative open reading frames regulates gene expression in an integrated stress response. The Journal of cell biology *167*, 27-33.

Lu, Y., Rolland, S.G., and Conradt, B. (2011). A molecular switch that governs mitochondrial fusion and fission mediated by the BCL2-like protein CED-9 of *Caenorhabditis elegans*. Proceedings of the National Academy of Sciences of the United States of America *108*, E813-822.

Mak, H.Y. (2013). Visualization of lipid droplets in *C. elegans* by light and electron microscopy. Methods Cell Biol *116*, 39-51.

Manil-Segalen, M., Lefebvre, C., Jenzer, C., Trichet, M., Boulogne, C., Satiat-Jeunemaitre, B., and Legouis, R. (2014). The *C. elegans* LC3 acts downstream of GABARAP to degrade autophagosomes by interacting with the HOPS subunit VPS39. Developmental cell *28*, 43-55.

Manor, U., Bartholomew, S., Golani, G., Christenson, E., Kozlov, M., Higgs, H., Spudich, J., and Lippincott-Schwartz, J. (2015). A mitochondria-anchored isoform of the actin-nucleating spire protein regulates mitochondrial division. Elife *4*.

Martin, J., Mahlke, K., and Pfanner, N. (1991). Role of an energized inner membrane in mitochondrial protein import. $\Delta\Psi$ drives the movement of presequences. The Journal of biological chemistry *266*, 18051-18057.

Martinez-Lopez, N., Garcia-Macia, M., Sahu, S., Athonvarangkul, D., Liebling, E., Merlo, P., Cecconi, F., Schwartz, G.J., and Singh, R. (2016). Autophagy in the CNS and Periphery Coordinate Lipophagy and Lipolysis in the Brown Adipose Tissue and Liver. Cell metabolism *23*, 113-127.

Martinez-Reyes, I., Sanchez-Arago, M., and Cuezva, J.M. (2012). AMPK and GCN2-ATF4 signal the repression of mitochondria in colon cancer cells. Biochem J *444*, 249-259.

Martinus, R.D., Garth, G.P., Webster, T.L., Cartwright, P., Naylor, D.J., Hoj, P.B., and Hoogenraad, N.J. (1996). Selective induction of mitochondrial chaperones in response to loss of the mitochondrial genome. Eur J Biochem *240*, 98-103.

Mattie, S., Riemer, J., Wideman, J.G., and McBride, H.M. (2018). A new mitofusin topology places the redox-regulated C terminus in the mitochondrial intermembrane space. The Journal of cell biology *217*, 507-515.

McQuibban, G.A., Saurya, S., and Freeman, M. (2003). Mitochondrial membrane remodelling regulated by a conserved rhomboid protease. Nature *423*, 537-541.

Meeusen, S., DeVay, R., Block, J., Cassidy-Stone, A., Wayson, S., McCaffery, J.M., and Nunnari, J. (2006). Mitochondrial inner-membrane fusion and crista maintenance requires the dynamin-related GTPase Mgm1. Cell *127*, 383-395.

Meeusen, S., McCaffery, J.M., and Nunnari, J. (2004). Mitochondrial fusion intermediates revealed in vitro. Science (New York, NY) *305*, 1747-1752.

Melber, A., and Haynes, C.M. (2018). UPR^{mt} regulation and output: a stress response mediated by mitochondrial-nuclear communication. Cell Research *28*, 281.

Melendez, A., and Levine, B. (2009). Autophagy in *C. elegans*. WormBook, 1-26.

Meléndez, A., Tallóczy, Z., Seaman, M., Eskelinen, E.-L., Hall, D.H., and Levine, B. (2003). Autophagy Genes Are Essential for Dauer Development and Life-Span Extension in *C. elegans*. Science (New York, NY) *301*, 1387-1391.

Merkwirth, C., Jovaisaite, V., Durieux, J., Matilainen, O., Jordan, S.D., Quiros, P.M., Steffen, K.K., Williams, E.G., Mouchiroud, L., Tronnes, S.U*., et al.* (2016). Two Conserved Histone Demethylases Regulate Mitochondrial Stress-Induced Longevity. Cell *165*, 1209-1223.

Michel, S., Canonne, M., Arnould, T., and Renard, P. (2015). Inhibition of mitochondrial genome expression triggers the activation of CHOP-10 by a cell signaling dependent on the integrated stress response but not the mitochondrial unfolded protein response. Mitochondrion *21*, 58-68.

Mijaljica, D., Prescott, M., and Devenish, R.J. (2011). Microautophagy in mammalian cells: revisiting a 40-year-old conundrum. Autophagy *7*, 673-682.

Mili, S., and Pinol-Roma, S. (2003). LRP130, a pentatricopeptide motif protein with a noncanonical RNA-binding domain, is bound in vivo to mitochondrial and nuclear RNAs. Mol Cell Biol *23*, 4972-4982.

Mishra, P., Carelli, V., Manfredi, G., and Chan, D.C. (2014). Proteolytic cleavage of Opa1 stimulates mitochondrial inner membrane fusion and couples fusion to oxidative phosphorylation. Cell metabolism *19*, 630-641.

Mishra, P., and Chan, D.C. (2016). Metabolic regulation of mitochondrial dynamics. The Journal of cell biology *212*, 379-387.

Mizushima, N. (2007). Autophagy: process and function. Genes Dev *21*, 2861-2873.

Mizzen, L.A., Chang, C., Garrels, J.I., and Welch, W.J. (1989). Identification, characterization, and purification of two mammalian stress proteins present in mitochondria, grp 75, a member of the hsp 70 family and hsp 58, a homolog of the bacterial groEL protein. The Journal of biological chemistry *264*, 20664-20675.

Mootha, V.K., Lepage, P., Miller, K., Bunkenborg, J., Reich, M., Hjerrild, M., Delmonte, T., Villeneuve, A., Sladek, R., Xu, F.*, et al.* (2003). Identification of a gene causing human cytochrome c oxidase deficiency by integrative genomics. Proceedings of the National Academy of Sciences of the United States of America *100*, 605-610.

Moran, M., Marin-Buera, L., Gil-Borlado, M.C., Rivera, H., Blazquez, A., Seneca, S., Vazquez-Lopez, M., Arenas, J., Martin, M.A., and Ugalde, C. (2010). Cellular pathophysiological consequences of BCS1L mutations in mitochondrial complex III enzyme deficiency. Hum Mutat *31*, 930-941.

Morita, M., Prudent, J., Basu, K., Goyon, V., Katsumura, S., Hulea, L., Pearl, D., Siddiqui, N., Strack, S., McGuirk, S.*, et al.* (2017). mTOR Controls Mitochondrial Dynamics and Cell Survival via MTFP1. Molecular cell *67*, 922-935 e925.

Mouysset, J., Kähler, C., and Hoppe, T. (2006). A conserved role of *Caenorhabditis elegans* CDC-48 in ER-associated protein degradation. Journal of Structural Biology *156*, 41-49.

Mozdy, A.D., McCaffery, J.M., and Shaw, J.M. (2000). Dnm1p GTPase-mediated mitochondrial fission is a multi-step process requiring the novel integral membrane component Fis1p. The Journal of cell biology *151*, 367-380.

Mozdy, A.D., and Shaw, J.M. (2003). A fuzzy mitochondrial fusion apparatus comes into focus. Nature reviews Molecular cell biology *4*, 468-478.

Mukaneza, Y., Cohen, A., Rivard, M.E., Tardif, J., Deschenes, S., Ruiz, M., Consortium, L., Laprise, C., Des Rosiers, C., and Coderre, L. (2019). mTORC1 is required for expression of LRPPRC and cytochrome-c oxidase but not HIF-1α in Leigh syndrome French Canadian type patient fibroblasts. Am J Physiol Cell Physiol *317*, C58-C67.

Murphy, C.T., McCarroll, S.A., Bargmann, C.I., Fraser, A., Kamath, R.S., Ahringer, J., Li, H., and Kenyon, C. (2003). Genes that act downstream of DAF-16 to influence the lifespan of *Caenorhabditis elegans*. Nature *424*, 277.

Nair, U., Yen, W.L., Mari, M., Cao, Y., Xie, Z., Baba, M., Reggiori, F., and Klionsky, D.J. (2012). A role for Atg8-PE deconjugation in autophagosome biogenesis. Autophagy *8*, 780-793.

Nakatogawa, H., Suzuki, K., Kamada, Y., and Ohsumi, Y. (2009). Dynamics and diversity in autophagy mechanisms: lessons from yeast. Nature reviews Molecular cell biology *10*, 458-467.

Narendra, D.P., Jin, S.M., Tanaka, A., Suen, D.F., Gautier, C.A., Shen, J., Cookson, M.R., and Youle, R.J. (2010). PINK1 is selectively stabilized on impaired mitochondria to activate Parkin. PLoS Biol *8*, e1000298.

Naresh, N.U., and Haynes, C.M. (2019). Signaling and Regulation of the Mitochondrial Unfolded Protein Response. Cold Spring Harb Perspect Biol *11*.

Nargund, A.M., Fiorese, C.J., Pellegrino, M.W., Deng, P., and Haynes, C.M. (2015). Mitochondrial and Nuclear Accumulation of the Transcription Factor ATFS-1 Promotes OXPHOS Recovery during the UPR^{mt}. Molecular cell *58*, 123-133.

Nargund, A.M., Pellegrino, M.W., Fiorese, C.J., Baker, B.M., and Haynes, C.M. (2012). Mitochondrial import efficiency of ATFS-1 regulates mitochondrial UPR activation. Science (New York, NY) *337*, 587-590.

Nezich, C.L., and Youle, R.J. (2013). Make or break for mitochondria. Elife *2*, e00804.

Nguyen, T.N., Padman, B.S., and Lazarou, M. (2016a). Deciphering the Molecular Signals of PINK1/Parkin Mitophagy. Trends in cell biology *26*, 733-744.

Nguyen, T.N., Padman, B.S., Usher, J., Oorschot, V., Ramm, G., and Lazarou, M. (2016b). Atg8 family LC3/GABARAP proteins are crucial for autophagosome-lysosome fusion but not autophagosome formation during PINK1/Parkin mitophagy and starvation. The Journal of cell biology *215*, 857-874.

Okatsu, K., Oka, T., Iguchi, M., Imamura, K., Kosako, H., Tani, N., Kimura, M., Go, E., Koyano, F., Funayama, M.*, et al.* (2012). PINK1 autophosphorylation upon membrane potential dissipation is essential for Parkin recruitment to damaged mitochondria. Nature communications *3*, 1016.

Okimoto, R., Macfarlane, J.L., Clary, D.O., and Wolstenholme, D.R. (1992). The mitochondrial genomes of two nematodes, *Caenorhabditis elegans* and *Ascaris suum*. Genetics *130*, 471-498.

Olichon, A., Baricault, L., Gas, N., Guillou, E., Valette, A., Belenguer, P., and Lenaers, G. (2003). Loss of OPA1 perturbates the mitochondrial inner membrane structure and integrity, leading to cytochrome c release and apoptosis. The Journal of biological chemistry *278*, 7743-7746.

Olichon, A., Elachouri, G., Baricault, L., Delettre, C., Belenguer, P., and Lenaers, G. (2007). OPA1 alternate splicing uncouples an evolutionary conserved function in mitochondrial fusion from a vertebrate restricted function in apoptosis. Cell death and differentiation *14*, 682-692.

Ono, T., Isobe, K., Nakada, K., and Hayashi, J.-I. (2001). Human cells are protected from mitochondrial dysfunction by complementation of DNA products in fused mitochondria. Nature Genetics *28*, 272-275.

Ordureau, A., Sarraf, S.A., Duda, D.M., Heo, J.M., Jedrychowski, M.P., Sviderskiy, V.O., Olszewski, J.L., Koerber, J.T., Xie, T., Beausoleil, S.A., *et al.* (2014). Quantitative proteomics reveal a feedforward mechanism for mitochondrial PARKIN translocation and ubiquitin chain synthesis. Molecular cell *56*, 360-375.

Osellame, L.D., Singh, A.P., Stroud, D.A., Palmer, C.S., Stojanovski, D., Ramachandran, R., and Ryan, M.T. (2016). Cooperative and independent roles of the Drp1 adaptors Mff, MiD49 and MiD51 in mitochondrial fission. Journal of cell science *129*, 2170-2181.

Otera, H., Wang, C., Cleland, M.M., Setoguchi, K., Yokota, S., Youle, R.J., and Mihara, K. (2010). Mff is an essential factor for mitochondrial recruitment of Drp1 during mitochondrial fission in mammalian cells. The Journal of cell biology *191*, 1141-1158.

Pakos-Zebrucka, K., Koryga, I., Mnich, K., Ljujic, M., Samali, A., and Gorman, A.M. (2016). The integrated stress response. EMBO Rep *17*, 1374-1395.

Palade, G.E. (1952). The fine structure of mitochondria. Anat Rec *114*, 427-451.

Palade, G.E. (1953). An electron microscope study of the mitochondrial structure. J Histochem Cytochem *1*, 188-211.

Palikaras, K., Lionaki, E., and Tavernarakis, N. (2018). Mechanisms of mitophagy in cellular homeostasis, physiology and pathology. Nature cell biology *20*, 1013-1022.

Palmer, C.S., Elgass, K.D., Parton, R.G., Osellame, L.D., Stojanovski, D., and Ryan, M.T. (2013). Adaptor proteins MiD49 and MiD51 can act independently of Mff and Fis1 in Drp1 recruitment and are specific for mitochondrial fission. The Journal of biological chemistry *288*, 27584-27593.

Palmer, C.S., Osellame, L.D., Laine, D., Koutsopoulos, O.S., Frazier, A.E., and Ryan, M.T. (2011). MiD49 and MiD51, new components of the mitochondrial fission machinery. EMBO Rep *12*, 565-573.

Palmisano, N.J., and Melendez, A. (2019). Autophagy in *C. elegans* development. Dev Biol *447*, 103-125.

Pan, Y., Schroeder, E.A., Ocampo, A., Barrientos, A., and Shadel, G.S. (2011). Regulation of yeast chronological life span by TORC1 via adaptive mitochondrial ROS signaling. Cell metabolism *13*, 668-678.

Pankiv, S., Clausen, T.H., Lamark, T., Brech, A., Bruun, J.A., Outzen, H., Overvatn, A., Bjorkoy, G., and Johansen, T. (2007). p62/SQSTM1 binds directly to Atg8/LC3 to facilitate degradation of ubiquitinated protein aggregates by autophagy. The Journal of biological chemistry *282*, 24131-24145.

Parone, P.A., Da Cruz, S., Tondera, D., Mattenberger, Y., James, D.I., Maechler, P., Barja, F., and Martinou, J.C. (2008). Preventing mitochondrial fission impairs mitochondrial function and leads to loss of mitochondrial DNA. PloS one *3*, e3257.

Pellegrino, M.W., Nargund, A.M., and Haynes, C.M. (2013). Signaling the mitochondrial unfolded protein response. Biochimica et Biophysica Acta (BBA) - Molecular Cell Research *1833*, 410-416.

Perez Ortiz, J.M., and Swerdlow, R.H. (2019). Mitochondrial dysfunction in Alzheimer's disease: Role in pathogenesis and novel therapeutic opportunities. British Journal of Pharmacology *176*, 3489-3507.

Pich, S., Bach, D., Briones, P., Liesa, M., Camps, M., Testar, X., Palacin, M., and Zorzano, A. (2005). The Charcot-Marie-Tooth type 2A gene product, Mfn2, up-regulates fuel oxidation through expression of OXPHOS system. Hum Mol Genet *14*, 1405-1415.

Pickles, S., Vigie, P., and Youle, R.J. (2018). Mitophagy and Quality Control Mechanisms in Mitochondrial Maintenance. Curr Biol *28*, R170-R185.

Pierce, S.B., Costa, M., Wisotzkey, R., Devadhar, S., Homburger, S.A., Buchman, A.R., Ferguson, K.C., Heller, J., Platt, D.M., Pasquinelli, A.A.*, et al.* (2001). Regulation of DAF-2 receptor signaling by human insulin and ins-1, a member of the unusually large and diverse *C. elegans* insulin gene family. Genes & Development *15*, 672-686.

Putker, M., Madl, T., Vos, Harmjan R., de Ruiter, H., Visscher, M., van den Berg, Maaike C.W., Kaplan, M., Korswagen, Hendrik C., Boelens, R., Vermeulen, M.*, et al.* (2013). Redox-Dependent Control of FOXO/DAF-16 by Transportin-1. Molecular cell *49*, 730-742.

Quiros, P.M., Prado, M.A., Zamboni, N., D'Amico, D., Williams, R.W., Finley, D., Gygi, S.P., and Auwerx, J. (2017). Multi-omics analysis identifies ATF4 as a key regulator of the mitochondrial stress response in mammals. The Journal of cell biology *216*, 2027-2045.

Rabinowitz, J.D., and White, E. (2010). Autophagy and Metabolism. Science (New York, NY) *330*, 1344-1348.

Rambold, Angelika S., Cohen, S., and Lippincott-Schwartz, J. (2015). Fatty Acid Trafficking in Starved Cells: Regulation by Lipid Droplet Lipolysis, Autophagy, and Mitochondrial Fusion Dynamics. Developmental cell *32*, 678-692.

Rambold, A.S., Kostelecky, B., Elia, N., and Lippincott-Schwartz, J. (2011). Tubular network formation protects mitochondria from autophagosomal degradation during nutrient starvation. Proceedings of the National Academy of Sciences of the United States of America *108*, 10190-10195.

Rhee, H.W., Zou, P., Udeshi, N.D., Martell, J.D., Mootha, V.K., Carr, S.A., and Ting, A.Y. (2013). Proteomic mapping of mitochondria in living cells via spatially restricted enzymatic tagging. Science (New York, NY) *339*, 1328-1331.

Rich, P.R., and Marechal, A. (2010). The mitochondrial respiratory chain. Essays Biochem *47*, 1-23.

Rizzuto, R., De Stefani, D., Raffaello, A., and Mammucari, C. (2012). Mitochondria as sensors and regulators of calcium signalling. Nature Reviews Molecular Cell Biology *13*, 566-578.

Robin, E.D., and Wong, R. (1988). Mitochondrial DNA molecules and virtual number of mitochondria per cell in mammalian cells. J Cell Physiol *136*, 507-513.

Rocha, N., Bulger, D.A., Frontini, A., Titheradge, H., Gribsholt, S.B., Knox, R., Page, M., Harris, J., Payne, F., Adams, C.*, et al.* (2017). Human biallelic MFN2 mutations induce mitochondrial dysfunction, upper body adipose hyperplasia, and suppression of leptin expression. Elife *6*.

Rogov, V., Dotsch, V., Johansen, T., and Kirkin, V. (2014). Interactions between autophagy receptors and ubiquitin-like proteins form the molecular basis for selective autophagy. Molecular cell *53*, 167-178.

Rolland, S.G., Motori, E., Memar, N., Hench, J., Frank, S., Winklhofer, K.F., and Conradt, B. (2013). Impaired complex IV activity in response to loss of LRPPRC function can be compensated by mitochondrial hyperfusion. Proceedings of the National Academy of Sciences of the United States of America *110*, E2967-2976.

Rolland, S.G., Schneid, S., Schwarz, M., Rackles, E., Fischer, C., Haeussler, S., Regmi, S.G., Yeroslaviz, A., Habermann, B., Mokranjac, D.*, et al.* (2019). Compromised Mitochondrial Protein Import Acts as a Signal for UPR^{mt}. Cell reports *28*, 1659-1669.e1655.

Rossignol, R., Gilkerson, R., Aggeler, R., Yamagata, K., Remington, S.J., and Capaldi, R.A. (2004). Energy substrate modulates mitochondrial structure and oxidative capacity in cancer cells. Cancer Res *64*, 985-993.

Rusten, T.E., Vaccari, T., Lindmo, K., Rodahl, L.M., Nezis, I.P., Sem-Jacobsen, C., Wendler, F., Vincent, J.P., Brech, A., Bilder, D.*, et al.* (2007). ESCRTs and *Fab1* regulate distinct steps of autophagy. Curr Biol *17*, 1817-1825.

Ruzzenente, B., Metodiev, M.D., Wredenberg, A., Bratic, A., Park, C.B., Camara, Y., Milenkovic, D., Zickermann, V., Wibom, R., Hultenby, K.*, et al.* (2012). LRPPRC is necessary for polyadenylation and coordination of translation of mitochondrial mRNAs. The EMBO journal *31*, 443-456.

Ryu, D., Mouchiroud, L., Andreux, P.A., Katsyuba, E., Moullan, N., Nicolet-Dit-Felix, A.A., Williams, E.G., Jha, P., Lo Sasso, G., Huzard, D.*, et al.* (2016). Urolithin A induces mitophagy and prolongs lifespan in *C. elegans* and increases muscle function in rodents. Nat Med *22*, 879-888.

Saha, S., Panigrahi, D.P., Patil, S., and Bhutia, S.K. (2018). Autophagy in health and disease: A comprehensive review. Biomed Pharmacother *104*, 485-495.

Saito, T., Kuma, A., Sugiura, Y., Ichimura, Y., Obata, M., Kitamura, H., Okuda, S., Lee, H.-C., Ikeda, K., Kanegae, Y.*, et al.* (2019). Autophagy regulates lipid metabolism through selective turnover of NCoR1. Nature communications *10*, 1567.

Sasarman, F., Brunel-Guitton, C., Antonicka, H., Wai, T., Shoubridge, E.A., and Consortium, L. (2010). LRPPRC and SLIRP interact in a ribonucleoprotein complex that regulates posttranscriptional gene expression in mitochondria. Mol Biol Cell *21*, 1315-1323.

Sathyanarayan, A., Mashek, M.T., and Mashek, D.G. (2017). ATGL Promotes Autophagy/Lipophagy via SIRT1 to Control Hepatic Lipid Droplet Catabolism. Cell reports *19*, 1-9.

Satoh, M., and Kuroiwa, T. (1991). Organization of multiple nucleoids and DNA molecules in mitochondria of a human cell. Exp Cell Res *196*, 137-140.

Sesaki, H., and Jensen, R.E. (1999). Division versus fusion: Dnm1p and Fzo1p antagonistically regulate mitochondrial shape. The Journal of cell biology *147*, 699-706.

Shadel, G.S., and Horvath, T.L. (2015). Mitochondrial ROS signaling in organismal homeostasis. Cell *163*, 560-569.

Shao, L.W., Niu, R., and Liu, Y. (2016). Neuropeptide signals cell non-autonomous mitochondrial unfolded protein response. Cell Res *26*, 1182-1196.

Shaye, D.D., and Greenwald, I. (2011). OrthoList: a compendium of *C. elegans* genes with human orthologs. PloS one *6*, e20085.

Sheaffer, K.L., Updike, D.L., and Mango, S.E. (2008). The Target of Rapamycin pathway antagonizes *pha-4/FoxA* to control development and aging. Curr Biol *18*, 1355-1364.

Shefa, U., Jeong, N.Y., Song, I.O., Chung, H.J., Kim, D., Jung, J., and Huh, Y. (2019). Mitophagy links oxidative stress conditions and neurodegenerative diseases. Neural Regen Res *14*, 749-756.

Shen, Q., Yamano, K., Head, B.P., Kawajiri, S., Cheung, J.T., Wang, C., Cho, J.H., Hattori, N., Youle, R.J., and van der Bliek, A.M. (2014). Mutations in Fis1 disrupt orderly disposal of defective mitochondria. Mol Biol Cell *25*, 145-159.

Shlevkov, E., Kramer, T., Schapansky, J., LaVoie, M.J., and Schwarz, T.L. (2016). Miro phosphorylation sites regulate Parkin recruitment and mitochondrial motility. Proceedings of the National Academy of Sciences of the United States of America *113*, E6097-E6106.

Siira, S.J., Spahr, H., Shearwood, A.J., Ruzzenente, B., Larsson, N.G., Rackham, O., and Filipovska, A. (2017). LRPPRC-mediated folding of the mitochondrial transcriptome. Nature communications *8*, 1532.

Singh, R., Kaushik, S., Wang, Y., Xiang, Y., Novak, I., Komatsu, M., Tanaka, K., Cuervo, A.M., and Czaja, M.J. (2009). Autophagy regulates lipid metabolism. Nature *458*, 1131.

Sjostrand, F.S. (1953). Electron microscopy of mitochondria and cytoplasmic double membranes. Nature *171*, 30-32.

Slobodkin, M.R., and Elazar, Z. (2013). The Atg8 family: multifunctional ubiquitin-like key regulators of autophagy. Essays Biochem *55*, 51-64.

Smirnova, E., Griparic, L., Shurland, D.L., and van der Bliek, A.M. (2001). Dynamin-related protein Drp1 is required for mitochondrial division in mammalian cells. Mol Biol Cell *12*, 2245-2256.

Song, Z., Chen, H., Fiket, M., Alexander, C., and Chan, D.C. (2007). OPA1 processing controls mitochondrial fusion and is regulated by mRNA splicing, membrane potential, and Yme1L. The Journal of cell biology *178*, 749-755.

Sousa, J.S., D'Imprima, E., and Vonck, J. (2018). Mitochondrial Respiratory Chain Complexes. Subcell Biochem *87*, 167-227.

Sterky, F.H., Ruzzenente, B., Gustafsson, C.M., Samuelsson, T., and Larsson, N.G. (2010). LRPPRC is a mitochondrial matrix protein that is conserved in metazoans. Biochem Biophys Res Commun *398*, 759-764.

Sulston, J.E., and Horvitz, H.R. (1977). Post-embryonic cell lineages of the nematode, *Caenorhabditis elegans*. Dev Biol *56*, 110-156.

Sulston, J.E., Schierenberg, E., White, J.G., and Thomson, J.N. (1983). The embryonic cell lineage of the nematode *Caenorhabditis elegans*. Dev Biol *100*, 64-119.

Taguchi, N., Ishihara, N., Jofuku, A., Oka, T., and Mihara, K. (2007). Mitotic phosphorylation of dynamin-related GTPase Drp1 participates in mitochondrial fission. The Journal of biological chemistry *282*, 11521-11529.

Takahashi, M., Iwasaki, H., Inoue, H., and Takahashi, K. (2002). Reverse Genetic Analysis of the *Caenorhabditis elegans* 26S Proteasome Subunits by RNA Interference. In Biological Chemistry, pp. 1263.

Takahashi, Y., He, H., Tang, Z., Hattori, T., Liu, Y., Young, M.M., Serfass, J.M., Chen, L., Gebru, M., Chen, C.*, et al.* (2018). An autophagy assay reveals the ESCRT-III component CHMP2A as a regulator of phagophore closure. Nature communications *9*, 2855.

Tamai, K., Tanaka, N., Nara, A., Yamamoto, A., Nakagawa, I., Yoshimori, T., Ueno, Y., Shimosegawa, T., and Sugamura, K. (2007). Role of Hrs in maturation of autophagosomes in mammalian cells. Biochem Biophys Res Commun *360*, 721-727.

Tatsuta, T., and Langer, T. (2017). Intramitochondrial phospholipid trafficking. Biochim Biophys Acta Mol Cell Biol Lipids *1862*, 81-89.

Teske, B.F., Fusakio, M.E., Zhou, D., Shan, J., McClintick, J.N., Kilberg, M.S., and Wek, R.C. (2013). CHOP induces activating transcription factor 5 (ATF5) to trigger apoptosis in response to perturbations in protein homeostasis. Mol Biol Cell *24*, 2477-2490.

Thumm, M., Egner, R., Koch, B., Schlumpberger, M., Straub, M., Veenhuis, M., and Wolf, D.H. (1994). Isolation of autophagocytosis mutants of *Saccharomyces cerevisiae*. FEBS Lett *349*, 275-280.

Tian, T., Ikeda, J., Wang, Y., Mamat, S., Luo, W., Aozasa, K., and Morii, E. (2012). Role of leucine-rich pentatricopeptide repeat motif-containing protein (LRPPRC) for anti-apoptosis and tumourigenesis in cancers. Eur J Cancer *48*, 2462-2473.

Tian, Y., Garcia, G., Bian, Q., Steffen, K.K., Joe, L., Wolff, S., Meyer, B.J., and Dillin, A. (2016). Mitochondrial Stress Induces Chromatin Reorganization to Promote Longevity and UPR^{mt}. Cell *165*, 1197-1208.

Tian, Y., Li, Z., Hu, W., Ren, H., Tian, E., Zhao, Y., Lu, Q., Huang, X., Yang, P., Li, X.*, et al.* (2010). *C. elegans* Screen Identifies Autophagy Genes Specific to Multicellular Organisms. Cell *141*, 1042-1055.

Tondera, D., Grandemange, S., Jourdain, A., Karbowski, M., Mattenberger, Y., Herzig, S., Da Cruz, S., Clerc, P., Raschke, I., Merkwirth, C.*, et al.* (2009). SLP-2 is required for stress-induced mitochondrial hyperfusion. The EMBO journal *28*, 1589-1600.

Tooze, J., Hollinshead, M., Ludwig, T., Howell, K., Hoflack, B., and Kern, H. (1990). In exocrine pancreas, the basolateral endocytic pathway converges with the autophagic pathway immediately after the early endosome. The Journal of cell biology *111*, 329-345.

Tsukada, M., and Ohsumi, Y. (1993). Isolation and characterization of autophagy-defective mutants of *Saccharomyces cerevisiae*. FEBS Lett *333*, 169-174.

Twig, G., Elorza, A., Molina, A.J., Mohamed, H., Wikstrom, J.D., Walzer, G., Stiles, L., Haigh, S.E., Katz, S., Las, G.*, et al.* (2008). Fission and selective fusion govern mitochondrial segregation and elimination by autophagy. The EMBO journal *27*, 433-446.

Valente, E.M., Abou-Sleiman, P.M., Caputo, V., Muqit, M.M., Harvey, K., Gispert, S., Ali, Z., Del Turco, D., Bentivoglio, A.R., Healy, D.G.*, et al.* (2004). Hereditary early-onset Parkinson's disease caused by mutations in PINK1. Science (New York, NY) *304*, 1158-1160.

van der Bliek, A.M., Sedensky, M.M., and Morgan, P.G. (2017). Cell Biology of the Mitochondrion. Genetics *207*, 843-871.

Vattem, K.M., and Wek, R.C. (2004). Reinitiation involving upstream ORFs regulates ATF4 mRNA translation in mammalian cells. Proceedings of the National Academy of Sciences of the United States of America *101*, 11269-11274.

Vietri, M., Radulovic, M., and Stenmark, H. (2020). The many functions of ESCRTs. Nature reviews Molecular cell biology *21*, 25-42.

Villa, E., Marchetti, S., and Ricci, J.E. (2018). No Parkin Zone: Mitophagy without Parkin. Trends in cell biology *28*, 882-895.

Voisine, C., Craig, E.A., Zufall, N., von Ahsen, O., Pfanner, N., and Voos, W. (1999). The protein import motor of mitochondria: unfolding and trapping of preproteins are distinct and separable functions of matrix Hsp70. Cell *97*, 565-574.

Wai, T., Garcia-Prieto, J., Baker, M.J., Merkwirth, C., Benit, P., Rustin, P., Ruperez, F.J., Barbas, C., Ibanez, B., and Langer, T. (2015). Imbalanced OPA1 processing and mitochondrial fragmentation cause heart failure in mice. Science (New York, NY) *350*, aad0116.

Wang, N., Gottesman, S., Willingham, M.C., Gottesman, M.M., and Maurizi, M.R. (1993). A human mitochondrial ATP-dependent protease that is highly homologous to bacterial Lon protease. Proceedings of the National Academy of Sciences of the United States of America *90*, 11247-11251.

Wang, S.F., Chen, M.S., Chou, Y.C., Ueng, Y.F., Yin, P.H., Yeh, T.S., and Lee, H.C. (2016). Mitochondrial dysfunction enhances cisplatin resistance in human gastric cancer cells via the ROS-activated GCN2-eIF2alpha-ATF4-xCT pathway. Oncotarget *7*, 74132-74151.

Wang, X., Liu, Z., Fan, F., Hou, Y., Yang, H., Meng, X., Zhang, Y., and Ren, F. (2019). Microfluidic chip and its application in autophagy detection. TrAC Trends in Analytical Chemistry *117*.

Wang, X., Zuo, X., Kucejova, B., and Chen, X.J. (2008). Reduced cytosolic protein synthesis suppresses mitochondrial degeneration. Nature cell biology *10*, 1090-1097.

Webster, B.M., Colombi, P., Jager, J., and Lusk, C.P. (2014). Surveillance of nuclear pore complex assembly by ESCRT-III/Vps4. Cell *159*, 388-401.

Wiesner, R.J., Ruegg, J.C., and Morano, I. (1992). Counting target molecules by exponential polymerase chain reaction: copy number of mitochondrial DNA in rat tissues. Biochem Biophys Res Commun *183*, 553-559.

Wong, E.D., Wagner, J.A., Gorsich, S.W., McCaffery, J.M., Shaw, J.M., and Nunnari, J. (2000). The dynamin-related GTPase, Mgm1p, is an intermembrane space protein required for maintenance of fusion competent mitochondria. The Journal of cell biology *151*, 341-352.

Wong, E.D., Wagner, J.A., Scott, S.V., Okreglak, V., Holewinske, T.J., Cassidy-Stone, A., and Nunnari, J. (2003). The intramitochondrial dynamin-related GTPase, Mgm1p, is a component of a protein complex that mediates mitochondrial fusion. The Journal of cell biology *160*, 303-311.

Wu, F., Watanabe, Y., Guo, X.Y., Qi, X., Wang, P., Zhao, H.Y., Wang, Z., Fujioka, Y., Zhang, H., Ren, J.Q.*, et al.* (2015). Structural Basis of the Differential Function of the Two *C. elegans* Atg8 Homologs, LGG-1 and LGG-2, in Autophagy. Molecular cell *60*, 914-929.

Wu, W., Lin, C., Wu, K., Jiang, L., Wang, X., Li, W., Zhuang, H., Zhang, X., Chen, H., Li, S.*, et al.* (2016). FUNDC1 regulates mitochondrial dynamics at the ER-mitochondrial contact site under hypoxic conditions. The EMBO journal *35*, 1368-1384.

Wu, X., Luo, J., Liu, H., Cui, W., Feng, D., and Qu, Y. (2020). SIRT3 protects against early brain injury following subarachnoid hemorrhage via promoting mitochondrial fusion in an AMPK dependent manner. Chinese Neurosurgical Journal *6*, 1.

Xie, Z., Nair, U., and Klionsky, D.J. (2008). Atg8 controls phagophore expansion during autophagosome formation. Mol Biol Cell *19*, 3290-3298.

Xin, Y., Wu, W., Qu, J., Wang, X., Lei, S., Yuan, L., and Liu, X. (2019). Inhibition of Mitofusin-2 Promotes Cardiac Fibroblast Activation via the PERK/ATF4 Pathway and Reactive Oxygen Species. Oxid Med Cell Longev *2019*, 3649808.

Xu, F., Morin, C., Mitchell, G., Ackerley, C., and Robinson, B.H. (2004). The role of the LRPPRC (leucine-rich pentatricopeptide repeat cassette) gene in cytochrome oxidase assembly: mutation causes lowered levels of COX (cytochrome c oxidase) I and COX III mRNA. Biochem J *382*, 331-336.

Yamano, K., and Youle, R.J. (2013). PINK1 is degraded through the N-end rule pathway. Autophagy *9*, 1758-1769.

Yang, D., Li, L., Liu, H., Wu, L., Luo, Z., Li, H., Zheng, S., Gao, H., Chu, Y., Sun, Y.*, et al.* (2013). Induction of autophagy and senescence by knockdown of ROC1 E3 ubiquitin ligase to suppress the growth of liver cancer cells. Cell death and differentiation *20*, 235-247.

Yla-Anttila, P., Vihinen, H., Jokitalo, E., and Eskelinen, E.L. (2009). 3D tomography reveals connections between the phagophore and endoplasmic reticulum. Autophagy *5*, 1180-1185.

Yoneda, T., Benedetti, C., Urano, F., Clark, S.G., Harding, H.P., and Ron, D. (2004). Compartment-specific perturbation of protein handling activates genes encoding mitochondrial chaperones. Journal of cell science *117*, 4055-4066.

Yoshikawa, S., Muramoto, K., Shinzawa-Itoh, K., Aoyama, H., Tsukihara, T., Shimokata, K., Katayama, Y., and Shimada, H. (2006). Proton pumping mechanism of bovine heart cytochrome c oxidase. Biochimica et biophysica acta *1757*, 1110-1116.

Youle, R.J., and van der Bliek, A.M. (2012). Mitochondrial fission, fusion, and stress. Science (New York, NY) *337*, 1062-1065.

Young, S.K., and Wek, R.C. (2016). Upstream Open Reading Frames Differentially Regulate Gene-specific Translation in the Integrated Stress Response. The Journal of biological chemistry *291*, 16927-16935.

Zaarur, N., Desevin, K., Mackenzie, J., Lord, A., Grishok, A., and Kandror, K.V. (2019). ATGL-1 mediates the effect of dietary restriction and the insulin/IGF-1 signaling pathway on longevity in *C. elegans*. Mol Metab *27*, 75-82.

Zechner, R. (2015). FAT FLUX: enzymes, regulators, and pathophysiology of intracellular lipolysis. EMBO Mol Med *7*, 359-362.

Zhang, H., Chang, J.T., Guo, B., Hansen, M., Jia, K., Kovacs, A.L., Kumsta, C., Lapierre, L.R., Legouis, R., Lin, L.*, et al.* (2015). Guidelines for monitoring autophagy in *Caenorhabditis elegans*. Autophagy *11*, 9-27.

Zhang, Q., Wu, X., Chen, P., Liu, L., Xin, N., Tian, Y., and Dillin, A. (2018). The Mitochondrial Unfolded Protein Response Is Mediated Cell-Non-autonomously by Retromer-Dependent Wnt Signaling. Cell *174*, 870-883.e817.

Zhao, J., Zhai, B., Gygi, S.P., and Goldberg, A.L. (2015). mTOR inhibition activates overall protein degradation by the ubiquitin proteasome system as well as by autophagy. Proceedings of the National Academy of Sciences of the United States of America *112*, 15790-15797.

Zhao, Q., Wang, J., Levichkin, I.V., Stasinopoulos, S., Ryan, M.T., and Hoogenraad, N.J. (2002). A mitochondrial specific stress response in mammalian cells. The EMBO journal *21*, 4411-4419.

Zhao, Y., Yang, J., Liao, W., Liu, X., Zhang, H., Wang, S., Wang, D., Feng, J., Yu, L., and Zhu, W.-G. (2010). Cytosolic FoxO1 is essential for the induction of autophagy and tumour suppressor activity. Nature cell biology *12*, 665.

Zhen, Y., Spangenberg, H., Munson, M.J., Brech, A., Schink, K.O., Tan, K.W., Sorensen, V., Wenzel, E.M., Radulovic, M., Engedal, N.*, et al.* (2019). ESCRT-mediated phagophore sealing during mitophagy. Autophagy, 1-16.

Zheng, S., Liao, S., Zou, Y., Qu, Z., and Liu, F. (2014). *ins-7* Gene expression is partially regulated by the DAF-16/IIS signaling pathway in *Caenorhabditis elegans* under celecoxib intervention. PloS one *9*, e100320.

Zhou, D., Palam, L.R., Jiang, L., Narasimhan, J., Staschke, K.A., and Wek, R.C. (2008). Phosphorylation of eIF2 directs ATF5 translational control in response to diverse stress conditions. The Journal of biological chemistry *283*, 7064-7073.

Zhou, F., Wu, Z., Zhao, M., Murtazina, R., Cai, J., Zhang, A., Li, R., Sun, D., Li, W., Zhao, L.*, et al.* (2019). Rab5-dependent autophagosome closure by ESCRT. The Journal of cell biology *218*, 1908-1927.

Zhu, N., Cao, X., Hao, P., Zhang, Y., Chen, Y., Zhang, J., Li, J., Gao, C., and Li, L. (2020). Berberine attenuates mitochondrial dysfunction by inducing autophagic flux in myocardial hypoxia/reoxygenation injury. Cell Stress Chaperones.

Zorova, L.D., Popkov, V.A., Plotnikov, E.Y., Silachev, D.N., Pevzner, I.B., Jankauskas, S.S., Babenko, V.A., Zorov, S.D., Balakireva, A.V., Juhaszova, M.*, et al.* (2018). Mitochondrial membrane potential. Analytical biochemistry *552*, 50-59.

Zorzano, A., and Pich, S. (2006). What is the biological significance of the two mitofusin proteins present in the outer mitochondrial membrane of mammalian cells? IUBMB Life *58*, 441-443.

Zou, J., Yue, F., Jiang, X., Li, W., Yi, J., and Liu, L. (2013). Mitochondrion-associated protein LRPPRC suppresses the initiation of basal levels of autophagy via enhancing Bcl-2 stability. Biochem J *454*, 447-457.

Zou, J., Yue, F., Li, W., Song, K., Jiang, X., Yi, J., and Liu, L. (2014). Autophagy inhibitor LRPPRC suppresses mitophagy through interaction with mitophagy initiator Parkin. PloS one *9*, e94903.

Zuchner, S., Mersiyanova, I.V., Muglia, M., Bissar-Tadmouri, N., Rochelle, J., Dadali, E.L., Zappia, M., Nelis, E., Patitucci, A., Senderek, J.*, et al.* (2004). Mutations in the mitochondrial GTPase mitofusin 2 cause Charcot-Marie-Tooth neuropathy type 2A. Nat Genet *36*, 449-451.

Acknowledgements

First and foremost, I want to express my deepest thanks to my PhD supervisor Barbara Conradt for giving me the opportunity to do my PhD in her lab and for the excellent mentoring and support during the past years. I would also like to express my sincere thanks to Stéphane Rolland. Thank you for all your time, all the discussions and for teaching me so many things in the lab. Many thanks to our technicians Nadja Lebedeva, Linda Jocham, Melanie Schwarz and Michaela Bauer for their excellent technical support.

Special thanks to Simon for being a good friend and lab buddy. It was great working on a project with you. Thanks to all the members of the Conradt, Lambie, Zanin, Wagener, Mikeladze-Dvali and Rolland group whom I had the opportunity to meet during the past years. It has been a real pleasure with all of you and I really had a wonderful time (inside and outside the lab)! Many thanks to Ryan Sherrard, who taught me how to make nice figures in Affinity Designer.

I also want to thank the people of the 'Mito Club' for all the suggestions and helpful discussions.

Even though we only met at the very end of my PhD, I want to thank Tanja and Marcel for the discussions and their support.

Nicht zuletzt möchte ich meinen Eltern dafür danken, dass sie mich über die Jahre immer unterstützt und an mich geglaubt haben. Ohne Sie wäre ich nie so weit gekommen.